STRUCTURAL AND CHEMICAL PROPERTIES OF SOLID ORGANIC INCLUSION COMPOUNDS

Ian James Shannon

A Thesis Submitted for the Degree of PhD
at the
University of St Andrews

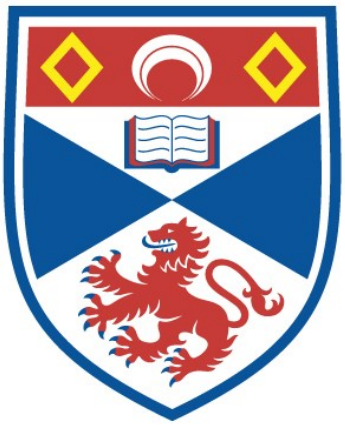

1995

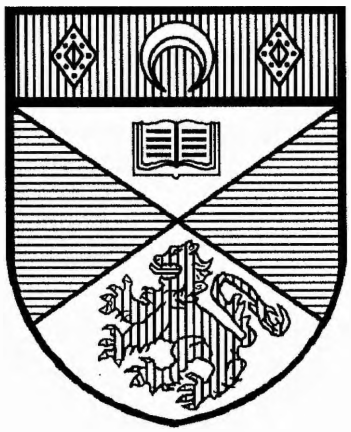

Structural and Chemical Properties of Solid Organic Inclusion Compounds

A thesis presented for the degree of

Doctor of Philosophy

in the Faculty of Science of the University of St. Andrews

by Ian James Shannon, B.Sc.(Hons.)

February 1995

Department of Chemistry,

St. Andrews

ProQuest LLC.
789 East Eisenhower Parkway
P.O. Box 1346
Ann Arbor, MI 48106 – 1346

Declaration

I, Ian James Shannon, certify that this thesis has been composed by myself, that it is a record of my own work, and has not been submitted in any previous application for a higher degree.

Signed: Date: 7TH FEB 1995

I was admitted to the Faculty of Science in the University of St. Andrews under Ordinance General No. 12 on 1 October, 1991 and as a candidate for the degree of Doctor of Philosophy on 1 October, 1992.

Signed: Date: 7TH FEB 1995

Certification

I hereby certify that Ian James Shannon, B.Sc. has spent twelve terms of research work under my supervision, and that he has fulfilled the conditions of the Resolution and Regulations appropriate to the degree of Doctor of Philosophy.

February 1995 Signed:

K.D.M. Harris

Library Declaration

In submitting this thesis to the University of St. Andrews, I understand that I am giving permission for it to be made available for use in accordance with regulations of the University Library for the time being in force, subject to any copyright vested in the work not being affected thereby. I also understand that the title and abstract will be published, and that a copy of the work may be made and supplied to any bona fide library or research worker.

Signed:

To Mum and Dad,

and My Wife, Maryjane

Acknowledgements

I would like to express my thanks to all the people who have worked with me during my PhD studies, for two years at St. Andrews, and for the final year at University College London. Special thanks go to all members of the Harris research group, past and present, with whom I have had the pleasure of sharing these last three years – in chronological order, Sharon Smart, Ali Mahdyarfar, Abil Aliev, Matthew Jones, Patricia Schofield, Elizabeth MacLean, Ashley George and Stephanie Camus.

Particular thanks must go to those from other institutions who have collaborated on specific aspects of the work presented here, and whose knowledge and input has helped enormously:

The EXAFS studies described in this thesis were carried out in collaboration with Professor R.W. Joyner and Dr M.R.H. Siddiqui (Leverhulme Centre for Innovative Catalysis, University of Liverpool). The single crystal X-ray diffractometric studies were carried out in conjunction with Professor M.B. Hursthouse (University of Wales in Cardiff). The work carried out on perhydrotriphenylene inclusion compounds was undertaken at Indiana University, U.S.A. under the supervision of Professor M.D. Hollingsworth and with help from Mr M.E. Brown.

Thanks must also go to Dr S. Arumugam for his help with the solid state NMR studies, Mr I.L.J. Patterson for synthesising some of the guest molecules studied, and Miss P.A. Schofield for collaboration on the modelling of the chlorocyclohexane/thiourea inclusion compound.

Lastly, and most importantly, I would like to save my greatest thanks for my supervisor, Dr K.D.M. Harris, for his endless knowledge, help and enthusiasm throughout my three years under his tutelage, and for introducing me to such interesting and stimulating research in solid state chemistry.

Abstract

Urea and thiourea form inclusion compounds in which organic and organometallic guest molecules are confined within non-intersecting, unidirectional tunnels within a solid urea or thiourea host structure.

In this thesis, studies have been undertaken using a variety of techniques to examine the properties of urea and thiourea inclusion compounds, with a view to improving the understanding of the forces controlling the ordering of these systems on a molecular scale.

From single crystal X-ray diffraction studies of urea inclusion compounds carried out at room temperature, different modes of ordering between guest molecules in adjacent tunnels, dependent on the guest species present, have been observed. Extension of these studies to low temperature, in conjunction with powder X-ray diffraction, has revealed information on phase transitions in both the host and guest substructures of urea inclusion compounds.

Computer modelling, using a mathematical model developed for application to one-dimensional inclusion compounds, has been applied to model properties of n-alkane/urea and dimethylketone/urea inclusion compounds. The model has also been applied to the chlorocyclohexane/thiourea inclusion compound.

EXAFS spectroscopy has been carried out on α,ω-dibromoalkane/urea inclusion compounds to examine the local structural properties of the guest molecules. Halogenocyclohexane/thiourea and halogenocyclohexanes included within the pores of several zeolite-type hosts have also been investigated to determine the conformation of the guest molecules when constrained to occupy a confined environment.

Additional studies have examined the potential for the polymerisation of monomeric guest molecules within the tunnels of the organic host structure of perhydrotriphenylene, and a solid state NMR investigation on the effect of magic angle spinning on the observed NMR spectrum for metallocenes.

Table of Contents

Contents **Page**

Chapter 1

Inclusion Compounds

1.1 Introduction

The structural and dynamic properties of crystalline organic inclusion compounds of urea and thiourea have been of great interest since Bengen discovered, in 1940, that urea would form a crystalline adduct with octanol [1]. Their accidental discovery broadened the range of host molecules already being utilised, as well as introducing a plethora of new guest species. Due to the properties of some of these organic inclusion compounds, such as the non-linear optics of the thiourea inclusion compound formed with benzenechromiumtricarbonyl [2], interest has continued to be stimulated up to the present day. In particular, steps have been taken towards attaining a greater understanding of the structural characteristics of these materials, as it is only when these are fully understood that the true potential of the systems for materials applications will be realised.

It is with this aim that the present research is being carried out, into the physico-chemical properties of crystalline inclusion compounds. The majority of the research described in this thesis is dedicated to the study of systems containing urea as the host structure, and involving a range of different guest species. The primary aim is towards a greater understanding of the guest substructure, particularly in relation to the factors controlling the modes of ordering and packing of the guest molecules within the host structure, by making as full use as possible of the wide range of experimental techniques currently available to the solid state chemist.

1.2 What are Inclusion Compounds?

Inclusion compounds can be defined as systems in which one species (referred to as the "guest") is spatially confined within another species (known as the "host").

This broad definition, which covers a diverse range of compounds can be refined to categorise more specifically all the different types encountered [Fig. 1.1].

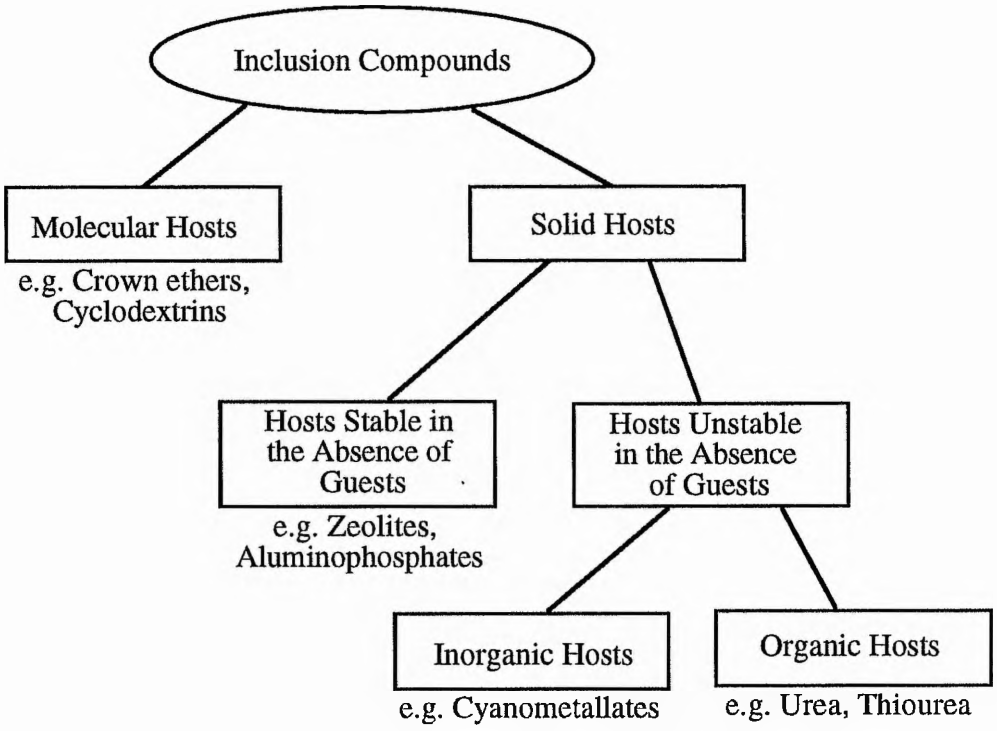

Fig. 1.1: Flowchart showing how inclusion compounds may be categorised into different types.

Inclusion compounds may be initially split into those systems which contain a molecular host, and those in which the host is a crystalline material. An example of the former is the crown ethers, for which Pedersen was awarded the Nobel Prize for Chemistry in 1987. These compounds, and other similar hosts such as cyclodextrins and cryptands, are able to selectively incarcerate specific shapes of guest molecule or types of ion. Many of these molecular inclusion compounds are stable in both the solid and liquid states. The field of solid hosts covers those in which the guest molecules are located within cavities found within a crystalline host matrix. The solid hosts can be further subdivided into structures in which the host structure remains stable upon

removal of the guest species (e.g. zeolites and aluminophosphates), and those in which the host structure is unstable in the absence of guests, and collapses to a more compact and more stable structure which does not contain cavities. Of these compounds, both organic hosts (such as urea, thiourea and cholic acids) and inorganic hosts (e.g. cyanometallates) are known.

Within the solid hosts there are a wide range different topologies of inclusion cavities such as layered structure (e.g. clays), networks of intersecting or non-intersecting tunnels, and cages, in which a wide variety of shapes and sizes of guest may be selectively accommodated. Zeolites are the most versatile of these hosts, as different zeolites can be synthesised encompassing a wide range of topologies, and are able to include both molecular and atomic (ionic) guests. As a consequence of their stability and selectivity for guests, zeolites have found widespread uses in selective synthesis, catalysis and as molecular sieves.

Urea and thiourea can be classified as examples of unstable, organic, solid hosts, containing non-intersecting unidirectional tunnels, and in many respects represent organic analogues of zeolites.

1.3 Urea Inclusion Compounds

Urea inclusion compounds are crystalline "host-guest" systems; the host structure is constructed from an extensively hydrogen bonded arrangement of urea (H_2N-CO-NH_2) molecules and contains essentially infinite, uni-directional tunnels, within which the guest molecules are located [1,3]. The crystal structure of the host was first solved by Smith in 1952 [4]. The space group in the conventional urea inclusion compounds is $P6_122$, and the unit cell dimensions, $|\boldsymbol{a}_h| = |\boldsymbol{b}_h| \approx 8.2$ Å, $|\boldsymbol{c}_h| \approx 11.0$ Å [Fig. 1.2]. Due to the comparatively small internal diameter of the tunnels (*ca.* 5.1–5.9 Å), suitable guest molecules are straight chain alkanes and their derivatives, although some guest molecules containing a small degree of branching can be accommodated within the urea tunnel [1,5]. These guests must be of sufficient length

for the inclusion compound to be stable – for instance, n-hexane forms an inclusion compound at room temperature, but n-pentane does not.

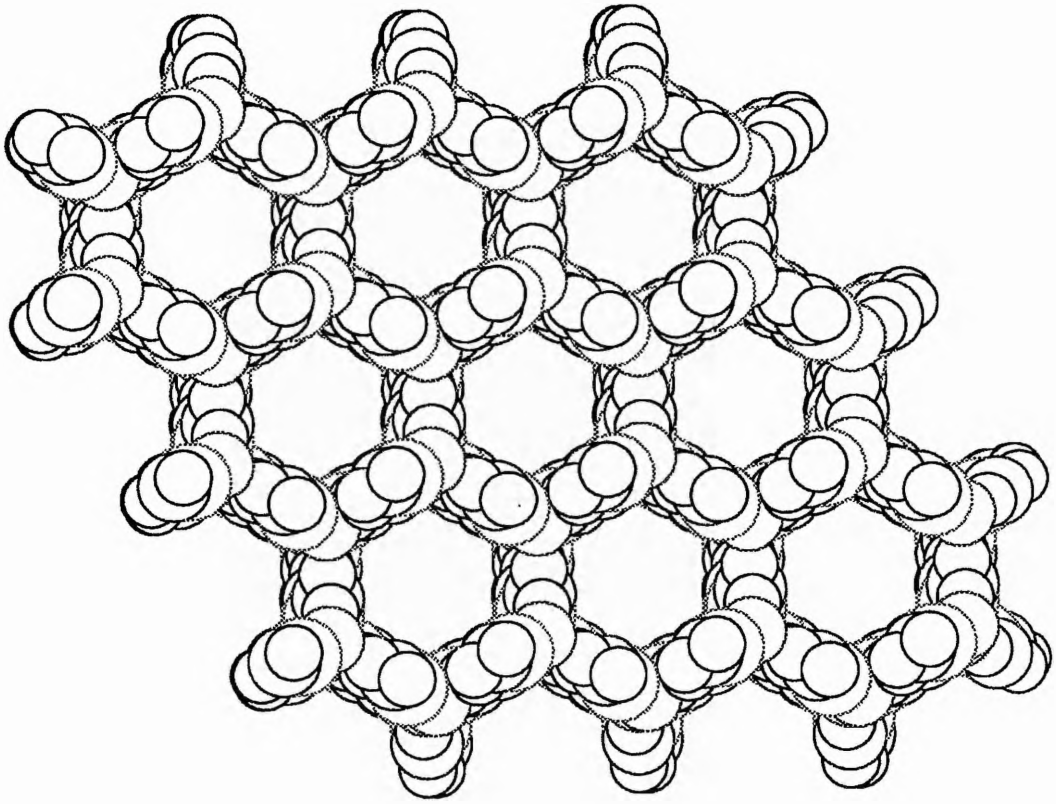

Fig. 1.2: Diagram showing nine complete tunnels of the host structure in the conventional urea inclusion compounds at room temperature, viewed down the *c*-axis. Conventional van der Waals radii for the atoms are represented. In practice, this urea tunnel structure is stable only in the presence of the guest molecules. The distance between the centres of adjacent tunnels is *ca*. 8.2 Å.

Upon heating crystals of urea inclusion compounds, the guest molecules are removed from the tunnels [6,7]. The temperature of decomposition increases linearly with the length of the guest within each family of guest molecules, up to the melting point of urea. On removal of the guest molecules, the urea host structure collapses to give tetragonal prisms of pure urea [Space group $P\bar{4}2_1m$, cell dimensions $|\boldsymbol{a}| = |\boldsymbol{b}| = 5.67$

Å, |*c*| = 4.73 Å] [8]. This decomposition has also been modelled by computer simulation [9].

The structural constraints imposed by the host can have a crucial influence on the conformational characteristics of the guest molecules. For example, in n-alkane/urea inclusion compounds, the n-alkane guest molecules exist predominantly in the "all-trans" conformation [10], in contrast to the multitude of conformations that exist for the same molecules in dispersed phases; the n-alkane/urea inclusion compounds therefore provide an ideal system for investigation and characterisation of the properties of n-alkanes in the "all-trans" conformation.

It is worth noting that the urea molecules form a chiral host structure, while the component urea molecules are themselves achiral; within any single crystal the urea molecules constructing the tunnel walls are arranged in either a right or left handed screw. This chiral nature of the tunnels is of great importance, as it leads to the possibility of carrying out selective synthesis, and separating enantiomers from a racemic mixture. The 2-chlorooctane/urea inclusion compound represents an example in which, within each crystal, one of the enantiomers is in excess due to chiral recognition [11]. Another example of selective synthesis is the photodecomposition of alkanones in urea [12], in which 5-nonanone has been shown to preferentially decompose to give the products 2-hexanone and selectively the *cis*-1-butyl-2-methylcyclobutanol isomer in preference to the *trans*-1-butyl-2-methylcyclobutanol isomer. This is attributed to less geometric rearrangement of the reactive intermediate being required to take place inside the confined environment within the tunnel. Urea inclusion compounds have also been used as a means to extract n-alkanes from light crude oils, to the exclusion of branched hydrocarbons [13]. It has also been demonstrated, through experiments on urea inclusion compounds with decane and 1,8-dichlorooctane guests, that it is possible for exchange of guest molecules to occur in the tunnels without the urea host matrix being destroyed [14], similar to zeolites.

While the structural features of the host are relatively well understood, considerably less is known about the guest substructure. This is due to the fact that at

ambient temperature the guest molecules are known to undergo rotation about the tunnel axis and translation along this axis, and so the structure cannot be solved in the conventional sense from X-ray diffraction studies. Sufficient ordering is present, however, that an average periodicity may be defined, and measured, for the guest substructure. In many cases, it has been shown that the host and guest substructures are incommensurate with respect to each other – i.e. the host and guest components are not in structural registry along the tunnel axis.

Thus, if the host periodicity along the tunnel axis is defined as c_h, and the guest periodicity along the tunnel axis as c_g, then the inclusion compound is said to be commensurate if there exist sufficiently "small" integers, p and q, such that:

$$pc_h \approx qc_g \qquad \text{Eq. 1.1}$$

and the compound is said to be incommensurate if sufficiently small p and q do not exist.

More recent work [15–17], has defined the incommensurate versus commensurate behaviour of urea inclusion compounds on the basis of energetic criteria. Modelling of the structures of urea inclusion compounds, with different guest molecules, has enabled predictions of the nature of the structural relationship between the host and guest components to be made.

The consequence of an incommensurate relationship is that, in theory, no two guest molecules, within the same tunnel, are in the same environment with respect to the host structure, and that the interaction between the host and guest substructures is insensitive to the position of the guest substructure along the tunnel. Experimental observation of incommensurate behaviour may be made using Brillouin scattering, in which the observation of a fourth acoustic mode (known as a sliding mode) is indicative of an incommensurate structure [18,19].

Almost all known urea inclusion compounds are incommensurate. An example of a commensurate urea inclusion compound, which crystallises in the hexagonal tunnel structure is the 5-undecanone/urea inclusion compound [20].

In most cases, the formation of a commensurate structure involves distortion of the host structure. In the case of α,ω-dinitrile/urea inclusion compounds, there is a change in the structural properties of the compounds as the length of the guest molecules increases. For the guests $NC(CH_2)_rCN$ with r = 3–5, strong hydrogen bonding favours a 1:1 layered structure of alternating sheets of urea and α,ω-dinitrile molecules [21]. For longer guest molecules (r > 5), inefficiency of packing of the alkyl chains dictates a change to a tunnel structure. The host structure is the conventional hexagonal host structure with the exception of the sebaconitrile/urea inclusion compound (r = 8), which possesses a tunnel structure in which the host is distorted significantly from the hexagonal host structure [22]. This arises as a result of strong hydrogen bonding between the nitrile groups of the guest and the host urea. The 1,6-dibromohexane/urea inclusion compound is another example in which the host tunnels are distorted from the hexagonal tunnel structure due to the length of the guest being very close to being commensurate [23] – it is also relevant that the 1,6-dibromohexane molecule is the shortest α,ω-dibromoalkane which forms a stable inclusion compound with urea at room temperature.

Other examples include the polyethylene oxide/urea inclusion compound, in which the guests possess a helical structure, and the host forms a hydrogen bonded structure containing larger tunnels. In addition to the polyethylene oxide guest, extra urea molecules are found inside the tunnels, which form hydrogen bonds to both the host and the guest [24]. In the trioxane/urea inclusion compound, the molar ratio of host to guest is 3:1 [25], though the cell dimensions are different from those normally encountered in the hexagonal host ($|\boldsymbol{a}_h| = |\boldsymbol{b}_h| = 14.3$ Å, $|\boldsymbol{c}_h| = 11.0$ Å) and the space group is rhombohedral.

In addition to the incommensurate relationship between the host and guest substructures, X-ray diffraction studies have revealed different modes of three-

dimensional ordering between guest molecules in adjacent tunnels. Different modes of ordering are found for the n-alkane/urea inclusion compounds [26,27], the diacyl peroxide/urea inclusion compounds [28] and the α,ω-dibromoalkane/urea inclusion compounds [29]. These properties are discussed more fully in Chapter 2.

Most studies of the structural properties of urea inclusion compounds have been carried out at room temperature and have revealed the interesting properties, such as the incommensurateness of the host and guest substructures and the different types of intertunnel ordering of the guests, discussed above.

There have, however, been several studies which have extended this work to subambient temperatures. Calorimetric studies, carried out on the n-alkane/urea systems [30,31] revealed that low temperature phase transitions occur in many urea inclusion compounds. For n-alkane/urea inclusion compounds, the transition temperature increases as the length of the guest molecule increases, and the transition was attributed to the onset of guest rotation in the tunnels. Variance in intensity with temperature of the guest reflections in the X-ray diffraction patterns for n-alkane/urea inclusion compounds has been explained in terms of anharmonic oscillations of the centres of mass of adjacent guests [26]. The disorder generated by thermal vibration increases greatly at high temperature. Other X-ray diffraction studies have shown that the low temperature phase transitions observed for the n-alkane/urea inclusion compounds in the calorimetric studies are associated with a change in symmetry of the urea host structure in conjunction with a substantial increase in the ordering of the guest molecules below the transition [32,33]. Several attempts to solve the low temperature host structure in the hexadecane/urea inclusion compound, from both single crystal [34,35] and powder [36] X-ray diffraction, have failed to produce satisfactory results, though it has been ascertained that the host structure is orthorhombic in the low temperature phase.

A great deal of research has also focused on the conformational characteristics and dynamics of the guest molecules when incarcerated within the urea host tunnel structure and how these properties differ from those in the pure crystalline solid of the

same molecules. The most widely used techniques for conformational analysis have been Raman and infrared spectroscopy. Independent studies have agreed that, in n-alkane/urea inclusion compounds, the guest molecules are in a predominantly all-trans conformation, though there are widely differing views as to the degree of gauche end-groups in n-alkanes, with estimates ranging from less than 3 % to around 40 % [10,37–39]. Molecular dynamics simulations for the n-alkane/urea inclusion compounds have also thrown up differing values from 3 % [40] to 22 % [41]. In α,ω-dibromoalkane/urea inclusion compounds, the percentage of gauche end-groups has been predicted to be 7–13 % [42], though for 1,8-dichlorooctane/urea this has been found to rise to 50 % [43]. Stearic acid has been shown to be almost exclusively in the all-trans conformation [44].

The dynamic properties of guest molecules in their urea inclusion compounds have been studied extensively by ^{2}H NMR spectroscopy and incoherent quasi-elastic neutron scattering. Again this work has focused mainly on n-alkane, carboxylic acid and α,ω-dibromoalkane guest molecules. From the ^{2}H NMR studies on n-alkane/urea inclusion compounds, a rotational diffusion model (rates of 10^{11} to 10^{12} s^{-1}) for motion of the guest molecules in the high temperature phase has been proposed [45,46], while below the phase transition a jump model has been suggested for the guest motion [47]. It is not possible to derive information about translatory motion from ^{2}H NMR. The incoherent quasi-elastic neutron scattering work has found the guest motions in the tunnels to be on a timescale of 10^{11} to 10^{12} s^{-1} for translation (oscillation) along the tunnel and diffusive rotation about the tunnel axis in the high temperature phase, but the data does not fit to a jump model, even in the low temperature phase [39,48]. It is possible that the translation and diffusive rotation of guest are correlated, but this has not yet been examined. The results on α,ω-dibromoalkane/urea inclusion compounds [49,50] have shown that replacing the terminal substituent -CH_3 groups with bromine has no significant mechanistic effect on the dynamics – direct comparisons of rates cannot be made because the lengths of the guest molecules in these studies are different. The oscillation amplitudes of the guests has been found to be *ca.* 2 Å.

Other dynamic studies have revealed that the host urea molecules undergo 180° rotational jumps about the C=O axis at a rate of 2 x 10^6 s^{-1} at 303 K in the hexadecane/urea inclusion compound [51]. A ^2H NMR study of host motion in α,ω-dibromoalkane/urea inclusion compounds has shown similar dynamics for the urea molecules, though significantly for the shorter guest molecules the jump rate of the urea molecules was slower, indicating possibly a hindrance to rotation on account of the greater proportion of bromine atoms in the tunnels [52]. The difference in rates observed for the host motion and the guest motions described above suggests that they are uncorrelated [53].

1.4 Thiourea Inclusion Compounds

Thiourea also forms a crystalline hydrogen bonded host structure in the presence of suitable guest molecules [Fig. 1.3], within which there are parallel one-dimensional tunnels [1,54,55]. The crystal structure of the host has been solved at room temperature (for the chlorocyclohexane/thiourea inclusion compound) and found to have space group $R\bar{3}c$, $|a_R| \approx 10.1$ Å, $\alpha = 104.27°$ [56]. The minimum diameter of the tunnels varies between 5.8 Å to 7.1 Å (depending upon the position along the tunnel axis) [57], and this larger diameter allows for larger guest molecules to be included within the tunnels. Linear alkanes do not form inclusion compounds with thiourea, but branched alkanes (e.g. 2,2,4-trimethylpentane) do.

Unlike the urea inclusion compounds discussed above, the thiourea host structure is achiral. Consequently, enantioselective synthesis within the thiourea host structure is not possible. However, suitable guest molecules have also been found to encompass substituted cyclohexanes and small organometallic molecules, such as ferrocene. The inclusion of these larger (and possibly more interesting) guest molecules suggests that there may be more potential uses and applications for thiourea inclusion compounds than for urea inclusion compounds.

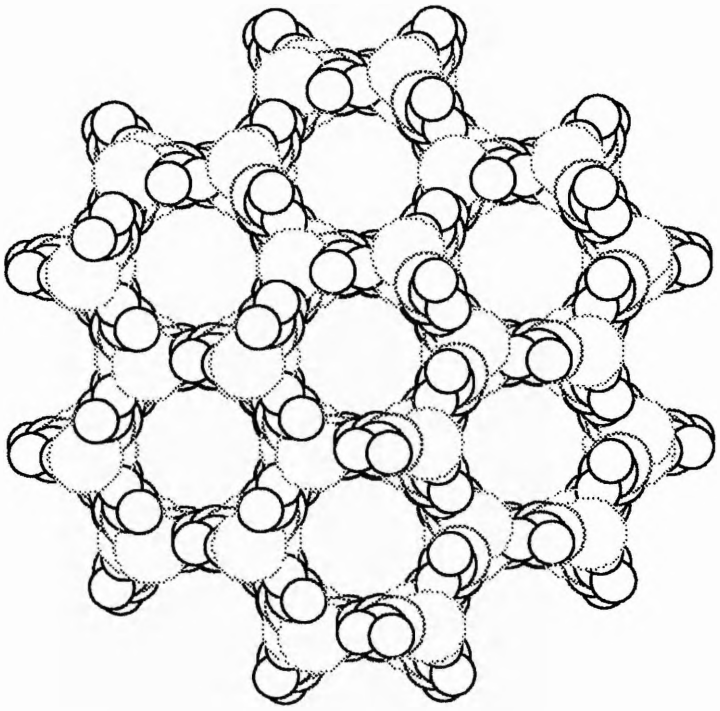

Fig. 1.3: Diagram showing nine tunnels of the thiourea host structure in thiourea inclusion compounds (guest molecules not shown), viewed along the tunnel axis. The distance between the centres of adjacent tunnels is *ca.* 9.2 Å.

Due to the greater fluctuation in the internal tunnel diameter, the thiourea host structure exhibits properties more commonly associated with hosts structure containing interlinked cages. For example, in both the chlorocyclohexane/thiourea inclusion compound and the ferrocene/thiourea inclusion compound, the guest molecules are found to reside preferentially at the widest points of the tunnel. Almost all thiourea inclusion compounds are commensurate; for the chlorocyclohexane/thiourea inclusion compound and the ferrocene/thiourea inclusion compound the molar ratio of host to guest is 3:1 [56,58].

The host structure can impose interesting properties on the guest molecules. It has been established, through Raman spectroscopy [59], infrared spectroscopy [60,61] and solid state NMR [62–64] that the chlorocyclohexane guest molecules in their

thiourea inclusion compound are constrained to adopt the axial conformation. This is in contrast to the way the chlorocyclohexane molecule behaves in its "pure" solid phase or in dispersed phases, in which it is known that there is an excess of the equatorial conformation [65–67]. Subsequent studies on the thiourea inclusion compounds containing bromocyclohexane, iodocyclohexane, *trans*-1,2- and *trans*-1,4-dihalogenocyclohexanes have established that the axial (or diaxial) conformation is predominant in all cases [63,68,69].

In contrast, methylcyclohexane, cyclohexanol and cyclohexylamine preferentially adopt the equatorial conformation in their thiourea inclusion compounds [63].

Studies of the guest dynamics in thiourea inclusion compounds have mainly been carried out by ^{2}H NMR. For substituted cyclohexane guest molecules it has been found that the guests reorientate rapidly about the 3-fold axis of the cyclohexane ring. ^{13}C NMR has shown that rapid ring inversion can also occur [64]. For the ferrocene/thiourea inclusion compound, the ferrocene molecules jump between three sites with the molecular axis perpendicular to the tunnel axis and one site with the molecular axis parallel to the tunnel axis, with activation energies of 10.1 kJ mol^{-1} for perpendicular to perpendicular and 6.4 kJ mol^{-1} for perpendicular to parallel jumps respectively [58]. For the chlorocyclohexane/thiourea inclusion compound, it is known [56] that, although the guest molecules occupy specific sites within the thiourea tunnel structure, there is substantial disorder of the guest molecules, and at ambient temperature, this disorder has been shown [70] to be dynamic in character.

1.5 Research Objectives

In order to glean structural information about the solid state in general, and urea inclusion compounds in particular, it is advantageous to use as wide a range of experimental techniques as possible. In this course of the research here, extensive use has been made of single crystal X-ray diffraction, powder X-ray diffraction, computational modelling and EXAFS spectroscopy to examine the properties of urea

and thiourea inclusion compounds. Particular attention has been paid to studies with the potential to probe information on the properties of the guest molecules and to improve the understanding of the forces controlling the modes of ordering of the guest molecules within the host structure.

This fundamental understanding of the structural properties of these systems is required before the objectives of research in this field can be achieved. The knowledge gained will ultimately enable the "design" of specific crystals for specialist applications – for instance, the second harmonic generation properties of the benzenechromiumtricarbonyl/thiourea inclusion compound [2], potential ferroelectric properties of the diacyl peroxide/urea inclusion compound, and the regular electronic properties of conjugated polyene guest molecules constrained within urea [71].

While the majority of the research has concentrated on urea and thiourea inclusion compounds, two other studies have been carried out. The first of these has examined the potential for polymerisation of monomeric guest molecules within the tunnels of the organic host structure of perhydrotriphenylene [Chapter 6]. The second study has probed the solid state NMR properties of metallocenes, particularly with respect to the effect of magic angle spinning on the observed spectrum [Chapter 7].

References

[1] K. Takemoto and N. Sonoda: *Inclusion Compounds, Vol.2*, eds J.L. Atwood, J.E.D. Davies and D.D. MacNicol, Academic Press, London, 1984, p.47.

[2] W. Tam, D.F. Eaton, J.C. Calabrese, I.D. Williams, Y. Wang and A.G. Anderson, *Chem. Mater.*, **1** (1989) 128.

[3] L.C. Fetterly: *Non-stoichiometric Compounds,* ed L. Mandelcorn, Academic Press, New York, 1964, p.491.

[4] A.E. Smith, *Acta Cryst.*, **5** (1952) 224.

[5] K.D.M. Harris and J.M. Thomas, *J. Chem. Soc. Faraday Trans.*, **86** (1990) 2985.

[6] H.B. Knight, L.P. Witnauer, J.E. Coleman, W.R. Noble and D. Swern, *Anal. Chem.*, **24** (1952) 1331.

[7] H.G. McAdie, *Can. J. Chem.*, **40** (1962) 2195.

[8] S. Swaminathan, B.M. Craven and R.K. McMullan, *Acta Cryst.*, **B40** (1984) 300.

[9] K.D.M. Harris, *J. Phys. Chem. Solids*, **53** (1992) 529.

[10] H.L. Casal, *J. Phys. Chem.*, **94** (1990) 2232.

[11] W. Schlenk, *Experientia*, **8** (1952) 337.

[12] H.L. Casal, P. de Mayo, J.F. Miranda and J.C.Scaiano, *J. Am. Chem. Soc.*, **105** (1983) 5155.

[13] C.A. Nwadinigwe and I.O. Nwobodo, *Fuel*, **73** (1994) 779.

[14] A. Mahdyarfar and K.D.M. Harris, *Chem. Comm.*, (1993) 51.

[15] A.J.O. Rennie and K.D.M. Harris, *Proc. R. Soc. Lond. A*, **430** (1990) 615.

[16] A.J.O. Rennie and K.D.M. Harris, *J. Chem. Phys.*, **96** (1992) 7117.

[17] A.J.O. Rennie and K.D.M. Harris, *Chem. Phys. Lett.*, **188** (1992) 1.

[18] D. Schmicker, S. van Smaalen, J.L. de Boer, C. Haas and K.D.M. Harris, *Phys. Rev. Lett.*, submitted.

[19] D. Schmicker, S. van Smaalen, C. Haas and K.D.M. Harris, *Phys. Rev. B*, **49** (1994) 11572.

[20] M.D. Hollingsworth and C.R. Goss, *Mol. Cryst. Liq. Cryst.*, **219** (1992) 43.

[21] M.D. Hollingsworth, B.D. Santarsiero, H. Oumar-Mahamat and C.J. Nichols, *Chem. Mater.*, **3** (1991) 23.

[22] M.D. Hollingsworth, B.D. Santarsiero and K.D.M. Harris, *Angew. Chem. Int. Ed. Engl.*, **33** (1994) 649.

[23] S.P. Smart, Ph.D. Thesis, University of St. Andrews, 1993.

[24] A. Chenite and F. Brisse, *Macromolecules*, **24** (1991) 2221.

[25] E. Gelerinter, Z. Luz, R. Poupko and H. Zimmerman, *J. Phys. Chem.*, **94** (1990) 5391.

[26] K. Fukao, H. Miyaji and K. Asai, *J. Chem. Phys.*, **84** (1986) 6360.

[27] K.D.M. Harris, *J. Solid State Chem.*, **106** (1993) 83.

[28] K.D.M. Harris and M.D. Hollingsworth, *Proc. R. Soc. Lond. A*, **431** (1990) 245.

[29] K.D.M. Harris, S.P. Smart and M.D. Hollingsworth, *J. Chem. Soc. Faraday Trans.*, **87** (1991) 3423.

[30] R.C. Pemberton and N.G. Parsonage, *Trans. Faraday Soc.*, **61** (1965) 2112.

[31] R.C. Pemberton and N.G. Parsonage, *Trans. Faraday Soc.*, **62** (1966) 553.

[32] R. Forst, H. Boysen, F. Frey, H. Jagodinski and C. Zeyen, *J. Phys. Chem. Solids*, **47** (1986) 1089.

[33] R. Forst, H. Jagodinski, H. Boysen and F. Frey, *Acta Cryst.*, **B43** (1987) 187.

[34] R. Forst, H. Jagodinski, H. Boysen and F. Frey, *Acta Cryst.*, **B46** (1990) 70.

[35] Y. Chatani, H. Anraku and Y. Taki, *Mol. Cryst. Liq. Cryst.*, **48** (1978) 219.

[36] K.D.M. Harris, I. Gameson and J.M. Thomas, *J. Chem. Soc. Faraday Trans.*, **86** (1990) 3135.

[37] M. Kobayashi, H. Koizumi and Y. Cho, *J. Chem. Phys.*, **93** (1990) 4659.

[38] R.L. Vold, R.R. Vold and N.J. Heaton, *Adv. Magn. Reson.*, **13** (1989) 17.

[39] F. Guillaume, A. El Baghdadi and A.J. Dianoux, *Physica Scripta*, **T49** (1993) 691.

[40] K.-J. Lee, W.L. Mattice and R.G. Snyder, *J. Chem. Phys.*, **96** (1992) 9138.

[41] F. Imashiro, D. Kuwahara, T. Nakai and T. Terao, *J. Chem. Phys.*, **90** (1989) 3356.

[42] S.P. Smart, K.D.M. Harris, F. Guillaume and A. El Baghdadi, *Mol. Cryst. Liq. Cryst.*, **211** (1992) 157.

[43] S.P. Smart, A. El Baghdadi, F. Guillaume and K.D.M. Harris, *J. Chem. Soc. Faraday Trans.*, **90** (1994) 1313.

[44] H.L. Casal, D.G. Cameron, E.C. Kelusky and A.P. Tulloch, *J. Chem. Phys.*, **81** (1984) 4322.

[45] M.S. Greenfield, R.L. Vold and R.R. Vold, *J. Chem. Phys.*, **83** (1985) 1440.

[46] M.S. Greenfield, R.L. Vold and R.R. Vold, *Mol. Phys.*, **66** (1989) 269.

[47] H.L. Casal, D.G. Cameron and E.C. Kelusky, *J. Chem. Phys.*, **80** (1984) 1407.

[48] F. Guillaume, C. Sourisseau and A.J. Dianoux, *J. Chem. Phys.*, **93** (1990) 3536.

[49] S.P. Smart, F. Guillaume, K.D.M. Harris, C. Sourisseau and A.J. Dianoux, *Physica B*, **180 & 181** (1992) 687.

[50] F. Guillaume, S.P. Smart, K.D.M. Harris and A.J. Dianoux, *J. Phys.: Condens. Matter*, **6** (1994) 2169.

[51] N.J. Heaton, R.L. Vold and R.R. Vold, *J. Am. Chem. Soc.*, **111** (1989) 3211.

[52] A.E. Aliev, S.P. Smart and K.D.M. Harris, *J. Mater. Chem.*, **4** (1994) 35.

[53] K.D.M. Harris, F. Guillaume, S.P. Smart, C. Sourisseau and A.J. Dianoux, *J. Chem. Res.*, (1992) 276.

[54] W. Schlenk, *Leibigs Ann. Chem.*, **573** (1951) 142.

[55] H.-U. Lenne, *Acta Cryst.*, **7** (1954) 1.

[56] K.D.M. Harris and J.M. Thomas, *J. Chem. Soc. Faraday Trans.*, **86** (1990) 1095.

[57] A.R. George and K.D.M. Harris, manuscript in preparation.

[58] S.J. Heyes, N.J. Clayden and C.M. Dobson, *J. Phys. Chem.*, **95** (1991) 1547.

[59] A. Allen, V. Fawcett and D.A. Long, *J. Raman Spec.*, **4** (1976) 285.

[60] M. Nishikawa, *Chem. Pharm. Bull.*, **11** (1963) 977.

[61] K. Fukushima, *J. Mol. Struct.*, **34** (1976) 67.

[62] M.S. McKinnon and R.E. Wasylishen, *Chem. Phys. Lett.*, **130** (1986) 565.

[63] A.E. Aliev and K.D.M. Harris, *J. Am. Chem. Soc.*, **115** (1993) 6369.

[64] K. Müller, *Magn. Res. Chem.*, **30** (1992) 228.

[65] M. Larnaudie, *Compt. Rend.*, **235** (1952) 154.

[66] P. Klæboe, J.J. Lothe and K. Lunde, *Acta Chem. Scand.*, **10** (1956) 1465.

[67] K. Kozima and K. Sakashita, *Bull. Chem. Soc. Jpn.*, **31** (1958) 796.

[68] K. Fukushima and K. Sugiura, *J. Mol. Struct.*, **41** (1977) 41.

[69] J.E. Gustavsen, P. Klæboe and H. Kvila, *Acta Chem. Scand.*, **A32** (1978) 25.

[70] A.E. Aliev, E.J. MacLean and K.D.M. Harris, manuscript in preparation.

[71] S.K. Lee, Q.-Y. Shang and B.S. Hudson, *Mol. Cryst. Liq. Cryst.*, **211** (1992) 147.

Chapter 2

Structural Properties of Urea Inclusion Compounds via Single Crystal X-Ray Diffraction Methods

2.1 Single Crystal X-Ray Diffraction

X-rays are electromagnetic radiation of wavelength ~ 1 Å. They are produced when high energy charged particles (such as accelerated electrons) collide with matter. The lost energy due to this collision is converted into electromagnetic radiation resulting in a continuum of radiation known as "white radiation", as there are a wide range of X-ray wavelengths radiated [1]. In addition to white radiation, emission lines characteristic of the metal target being bombarded, are also generated by the collision process. The electrons have sufficient energy to ionise some of the K shell electrons from the metal, resulting in an electron from an outer orbital dropping into the K shell with an accompanying release of energy in the X-ray region. The X-ray radiation released is of fixed wavelength, according to the transition occurring. For instance, a transition of 2p $\rightarrow$ 1s is said to produce K_α radiation, while a 3p $\rightarrow$ 1s transition is said to produce K_β radiation. The K_β transition is typically lower in intensity than the K_α transition and is normally filtered out. In many cases, the metal target is made of copper, and the K_α radiation of wavelength 1.5418 Å is used.

Other metals commonly used as the targets in laboratory sources are chromium K_α (λ = 2.2909 Å), iron K_α (λ = 1.9373 Å) and molybdenum K_α (λ = 0.71069 Å). The selection of radiation depends upon both the sample present and the diffraction method being used. For samples with large unit cells it is better to use longer wavelength X-rays in order to improve the accuracy of the readings. Using short wavelength radiation allows the measurement of a larger amount of diffraction data, but this may lead to problems with increased overlap of the diffraction maxima. Mo-K_α radiation is more

penetrating than the others and is often used in diffractometers, whereas Cu-K_α radiation is both penetrating and has low absorption, and is the most appropriate for photographic methods [2].

All diffraction methods are fundamentally based on Bragg's Law:

$$n\lambda = 2d\sin\theta \qquad \text{Eq. 2.1}$$

which is derived from consideration of crystals as being built up in layers such that each acts as a semitransparent mirror [Fig. 2.1]. While reflection is not the true physical process occurring when a crystal is subjected to X-rays, it does predict the correct geometry of diffraction, and the same results may be derived. When Bragg's Law is satisfied, the diffracted beams interfere constructively; otherwise destructive interference occurs [3].

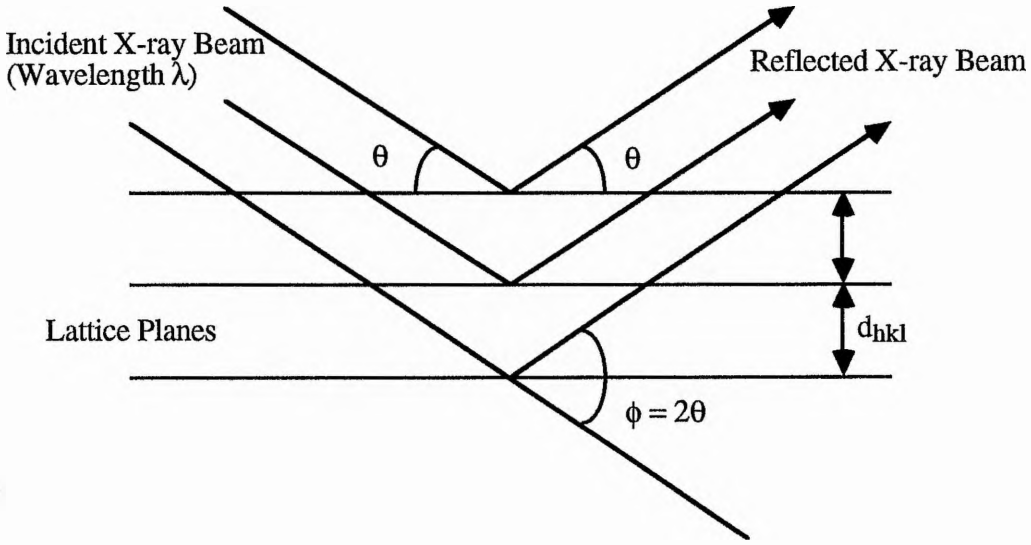

Fig. 2.1: Diagram illustrating Bragg's Law for n = 2.

In a crystalline solid, the atoms and molecules are arranged in a regular repeating array, known as the unit cell. The unit cell is defined as the smallest repeating unit which

shows the full symmetry of the crystal structure. The unit cell can be fully described by the three lattice vectors $\boldsymbol{a}$, $\boldsymbol{b}$ and $\boldsymbol{c}$, in direct space, or alternatively by the magnitudes of these three vectors $|\boldsymbol{a}|$, $|\boldsymbol{b}|$ and $|\boldsymbol{c}|$ along with the angles α, β and γ between these vectors.

Within a crystal there are a large number of d-spacings present, which arise due to different orientations of atomic arrays in three-dimensions. On subjecting a crystal to X-ray radiation the crystal acts as a diffraction grating, and the X-rays are scattered by the electron density around the atoms. Constructive interference of these scattered X-rays generates regions of intense diffraction maxima in specific positions in space.

In a conventional X-ray diffraction experiment the crystal is rotated, in the X-ray beam, through various orientations, and the pattern produced (by the constructive interference) is recorded. From the pattern produced, the intensities and position of the reflexions can be measured. Each reflexion in the photograph, in reciprocal space, can be assigned three Miller Indices (hkl), which uniquely define that reflexion. It is possible to derive the unit cell of the compound from the position of these reflexions, and from systematic absences in the indexings, we can derive the space group symmetry and ultimately solve the crystal structure.

There are two main methods used to solve the exact crystal structure; Patterson Methods may be employed when there are heavy atoms present in the compound, whereas Direct Methods are used more for equal atom structures. These processes allow construction of a three-dimensional electron density map of the crystal [4].

The crystals examined in this work belong to a class of incommensurate compounds which incorporate more than one three-dimensional lattice. As a consequence of this feature, difficulties arise when attempting to use conventional diffractometers to analyse the diffraction patterns from these systems. A conventional diffractometer search will only detect reflexions corresponding to one lattice. In order to measure the reflexions for the other lattices it is necessary to know both their lattice parameters, and the orientational relationship of these other lattices with respect to the known lattice. In this work, therefore, we have made extensive use of photographic X-ray diffraction methods, as it is possible with these to observe information simultaneously on both substructures.

More recently, we have looked at developing the viability for routinely using single crystal diffractometers to look at these compounds (this work is described in Section 2.10).

Two different types of photographic single crystal X-ray diffraction method have been utilised to provide qualitative information about the structural ordering within the inclusion compounds investigated:

i) Oscillation Photography

Oscillation photographs have been recorded on an Enraf-Nonius camera, using Ni-filtered Cu-K_α radiation.

This technique involves a single crystal, mounted on a goniometer head along one of its principal crystallographic axes, being oscillated back and forwards through a small angle [Fig. 2.2]. The diffraction pattern is recorded on photographic film, held in a cylindrical holder around the crystal.

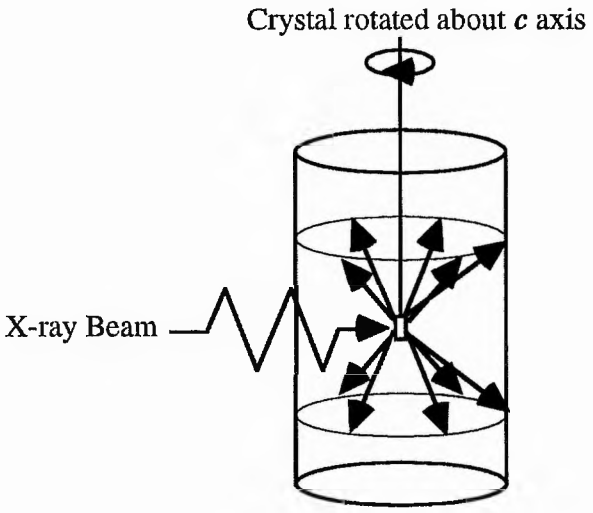

Fig. 2.2: Diagram showing the generation of layer lines in an oscillation photograph. The diffraction pattern is recorded on photographic film held in a cylinder around the crystal.

For urea inclusion compounds, alignment of the crystals is relatively easy on

account of their hexagonal prism shape. The crystal is aligned along the *c* axis, giving a two-dimensional picture which contains parallel rows of reflexions (see Section 2.4). From the distance between the layer lines it is possible to determine |*c*|.

ii) De Jong-Bouman Photography

De Jong-Bouman photographs were recorded on a Stoe "reciprocal lattice explorer", again using Ni-filtered Cu-K_α radiation.

In de Jong-Bouman photography, each reciprocal lattice plane observed in the oscillation photograph may be recorded individually, enabling the determination of |*a**|, |*b**| and γ^*, in reciprocal lattice space. While Weissenberg photography is a more widely used technique for determining this information, de Jong-Bouman photographs provide an undistorted view of the diffraction pattern from which it is easier to visualise the crystal symmetry, and to measure off angles and distances.

From the simple relationship between reciprocal and direct space (and also using the information from the oscillation photography) the dimensions of the unit cell can then be deduced $\{a, b, c, \alpha, \beta, \gamma\}$.

Single crystal X-ray diffraction is limited, clearly, to cases in which sufficiently large single crystals of good quality can be grown. When large enough crystals cannot be obtained, powder diffraction may be used to characterise the compounds – the technique and the limitations of powder diffraction (in comparison to single crystal X-ray diffraction) are discussed in Chapter 3.

While each individual X-ray diffraction event has a short timescale, the collection of X-ray diffraction data usually involves the sum of total of all diffraction events over a longer period of time. Hence, the timescale of an X-ray diffraction experiment is several hours, and so only a time averaged structure is obtained. For structural features that can only be observed on a faster timescale, other techniques such as NMR spectroscopy or X-ray absorption spectroscopy must be employed. A further limitation of X-ray diffraction is that it is normally only possible to detect non-H atoms in the structure. In order to locate the H atoms, neutron diffraction is most often used.

2.2 Families of Urea Inclusion Compounds Examined by Single Crystal X-ray Diffraction

The work carried out on the urea inclusion compounds can be subdivided into studies of compounds containing guest molecules belonging to different homologous series. As described in Chapter 1, suitable guest molecules for inclusion in the tunnels of the urea host are mainly n-alkanes and their linear derivatives.

Five different families of guest molecules have been considered:

i) n-alkane $CH_3(CH_2)_rCH_3$ guests with r = 7–15,18.

ii) α,ω-dibromoalkane $Br(CH_2)_rBr$ guests with r = 7–12.

iii) diacyl peroxide $CH_3(CH_2)_rC(O)OO(O)C(CH_2)_rCH_3$ guests with r = 6,9,10.

iv) carboxylic acid anhydride $CH_3(CH_2)_rC(O)O(O)C(CH_2)_rCH_3$ guests with r = 3–8,10.

v) carboxylic acid $CH_3(CH_2)_rCOOH$ guests with r = 6,8,10.

While several of these systems have been analysed previously at room temperature [5–9], low temperature single crystal X-ray diffraction studies have been limited to the n-alkane/urea inclusion compounds [10–13]. Here, a more thorough systematic study of the series of n-alkane/urea inclusion compounds at room temperature (particularly in relation to the question of incommensurate versus commensurate behaviour) has been carried out, in conjunction with new low temperature studies to examine more closely the phase transition in the host substructure, and if there is any indication of a change in the structural ordering of the guest molecules at low temperature. Previous work on urea inclusion compounds containing α,ω-dibromoalkane, diacyl peroxide and carboxylic acid guest molecules has also been extended to low temperature single crystal X-ray diffraction down to 90 K.

The experiments on carboxylic acid anhydride/urea inclusion compounds represent the study of a new family of guest molecules, both at room temperature and at low temperature.

For urea inclusion compounds containing n-alkanes, α,ω-dibromoalkanes and diacyl peroxides, powder X-ray diffraction has also been used. This work is described in

Chapter 3.

It is important to recognise that a fundamental understanding of the constraints imposed upon guest molecules within solid inclusion environments is crucial for the design and development of applications of these materials. In this regard, there is considerable potential for the development of applications based upon the optical and electronic properties of guest molecules constrained within tunnel structures in organic host materials [14–16]. The development of a fundamental understanding of the factors controlling the packing of guest molecules within solid host structures is of paramount importance in this regard, and substantial future progress in the design and development of applications will clearly result from an understanding of how the degree of ordering, the orientations, and the relative packing of guest molecules within host materials can be predicted, controlled, and altered in premeditated ways.

The aim of these studies was to develop our understanding of how different modes of ordering arise between the guest molecules in different tunnels, by varying the functionality of the guest, and how this ordering is governed by interactions between the host and guest substructures. The studies of structural phase transitions at low temperature will also provide insight into the host-guest interaction.

2.3 Synthesis of Urea Inclusion Compounds

In synthesising urea inclusion compounds containing all the above guest molecules, the common requirement is to obtain a solution in which the host and guest are mixed homogeneously in solution. While the general features of the syntheses are the same for most of these, in some cases small changes are required to the method in order to obtain the best quality inclusion compounds.

Carboxylic acid anhydrides were either obtained commercially or were prepared, following conventional methods [17], by addition of thionyl chloride to an ethereal solution of the carboxylic acid in the presence of pyridine. Other guests were obtained commercially.

For the inclusion compounds containing n-alkane or diacyl peroxide guests, an

excess of the appropriate guest was added to a saturated solution of urea in methanol in a conical flask at *ca.* 40 °C. 2-methylbutan-2-ol (*tertiary*-amyl alcohol) was then added dropwise until the solution was homogeneous. Any precipitate formed was dissolved by addition of more methanol. The flask was stoppered and immersed in a Dewar flask containing water at 40 °C, which was then placed in an incubator and cooled slowly to 0 °C. The crystals formed were collected by filtration and washed with 2,2,4-trimethylpentane to remove any guest molecules adhering to their external surfaces.

When preparing compounds including α,ω-dibromoalkane and carboxylic acid guests, pure methanol could be used as solvent; it was not necessary to add *t*-amyl alcohol in order to dissolve both host and guest components.

Urea inclusion compounds containing carboxylic acid anhydride guest molecules, however, required to be prepared by a different method. Excess carboxylic acid anhydride was added to a saturated solution of urea in pure dry *t*-amyl alcohol in a conical flask at 65 °C. Any precipitate formed was dissolved by addition of more *t*-amyl alcohol. Cooling to 0 °C was carried out as above in an incubator, and the crystals formed were collected, washed with 2,2,4-trimethylpentane, and dried. Dried solvents were used in crystal growth particularly to minimise the possibility of hydrolysis of the carboxylic acid anhydrides. Methanol (the solvent usually used in the preparation of urea inclusion compounds) was not satisfactory for preparation of the carboxylic acid anhydride/urea inclusion compounds since methyl esters produced in small amounts during the crystallisation procedure were included inside the urea tunnel structure together with the carboxylic acid anhydride guest molecules [thus disrupting structural ordering of the carboxylic acid anhydride guests]. On the other hand, the *t*-amyl ester impurities produced during urea inclusion compound formation in *t*-amyl alcohol are too bulky to be included within the urea tunnel structure. The inclusion of methyl esters within the urea tunnel structure, when methanol was used as crystallisation solvent, was confirmed by solution state ^{1}H NMR spectroscopy of crystals dissolved in DMSO-d_6.

Optical examination, under a polarising microscope, showed that the crystals were needle shaped for all samples. While the quality and size of the crystals obtained varied

according to the rate of cooling and the guest species present, in many cases the needles could in fact be seen to be long hexagonal prisms, consistent with the known morphological properties of conventional urea inclusion compounds.

2.4 General Discussion of the Structure of Urea Inclusion Compounds and Interpretation of X-ray Diffraction Photographs

Before the results of this study are presented, it is necessary to describe, in general, the essential structural features of urea inclusion compounds and the corresponding features of their X-ray diffraction patterns [18]. From X-ray oscillation photographs, recorded for a single crystal oscillating about its prism axis, the resulting diffraction pattern can be interpreted as being composed of two components.

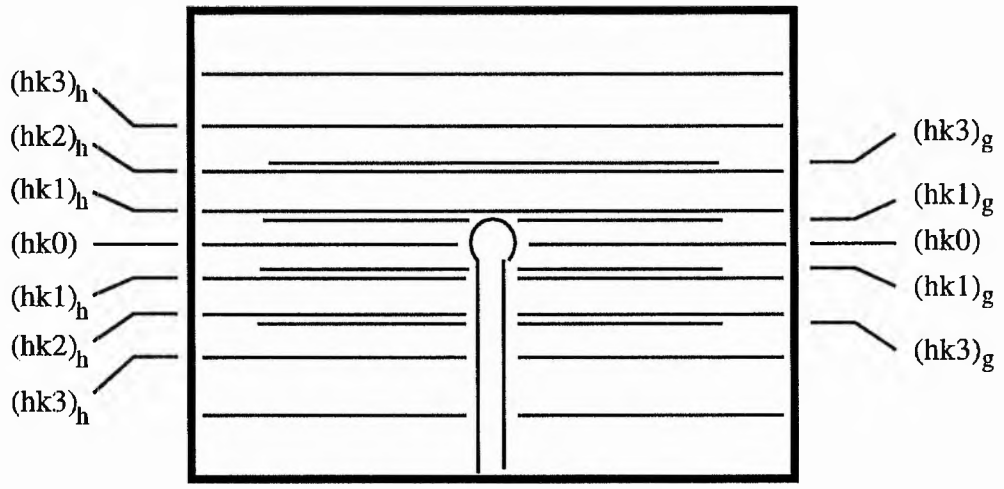

Fig. 2.3: Schematic representation of an oscillation photograph for a single crystal of a urea inclusion compound rotated about its prism axis. The pattern is divided into two components, denoted the "h" and "g" diffraction patterns. Where the layer lines are represented by horizontal lines in the diagram, in practice we see discrete spots for the "h" diffraction pattern, and a combination of discrete spots and diffuse bands for the "g" diffraction pattern.

The first component comprises sets of layer lines resolved into sharp, discrete

diffraction maxima, corresponding to diffraction mainly due to the urea host substructure [Fig. 2.3] – denoted as the "h" diffraction pattern. From measurements of the spacing between these layer lines (indexed with subscript h), a direct space periodicity of $c_h \approx$ 11.0 Å may be determined for the repeat length along the prism axis.

The second component in the diffraction pattern generally comprises layers containing both diffuse and discrete scattering. This component is denoted as the "g" diffraction pattern (indexed by subscript g) as it contains information mainly on the guest substructure. The exact proportions of diffuse and discrete scattering, and the observed pattern of the discrete spots, is dependent on the guest species present. The spacing between the layer lines (much smaller than for the "h" diffraction pattern above) is also guest dependent, and corresponds in most cases to a direct space repeat length (c_g) close to the predicted van der Waals length of the guest molecule in its most extended conformation.

The periodicities of the two components of the diffraction pattern along the prism axis (c_h and c_g in direct space) are usually incommensurate – for the purposes here, this means that it is not possible to find sufficiently small integers p and q for which $pc_g \approx qc_h$ (a more detailed discussion of commensurate and incommensurate behaviour in one-dimensional inclusion compounds, typified by the urea inclusion compounds, is given in Chapter 4). The consequence of this incommensurate relationship is that each component of the diffraction pattern contains information on the other in the form of an incommensurate modulation.

The "h" diffraction pattern arises from diffraction by the basic host structure (and by the incommensurate modulation within the guest substructure). The "g" diffraction pattern arises from diffraction by the basic guest structure (and by the incommensurate modulation within the host substructure).

Transforming this description to direct space, the host substructure can be considered in terms of a "basic structure" which is subjected to an incommensurate modulation mediated by the guest substructure; the basic structure can be described *via* conventional crystallographic principles (e.g. three-dimensional space group symmetry).

Similarly, the guest substructure can be considered in terms of an incommensurately modulated "basic structure". The incommensurate modulations describe perturbations to the basic structures which arise as a result of host-guest interaction. A full discussion of these structural issues for the urea inclusion compounds is given in ref. 18.

As an example of how the host-guest interactions have an effect on the diffraction pattern we can consider the (hk0) reflexions. In the absence of any contribution of the guest substructure to these reflexions, the predicted intensity of these maxima is much greater than that actually observed [particularly for the $(100)_h$ reflexion]. The presence of electron density in the tunnels (due to the guest) greatly modulates the intensities. It has also been observed that, in particular, the intensity of the $(100)_h$ reflexion is critically dependent on the guest species present – for the urea inclusion compounds containing α,ω-dibromoalkane guests this reflexion is much weaker than in the pattern observed for n-alkane guest molecules [see Section 3.4.2].

As indicated above, the "h" diffraction patterns from urea inclusion compounds can be rationalised on the basis of a unique three-dimensionally periodic reciprocal lattice. Previous studies [18] have shown that the basic host structure may be described by hexagonal lattice symmetry [$|\boldsymbol{a}_h| = |\boldsymbol{b}_h| \approx 8.2$ Å, $|\boldsymbol{c}_h| \approx 11.0$ Å, $\alpha_h = \beta_h = 90°$, $\gamma_h = 120°$]. From the similarities in the intensities of the reflexions for urea inclusion compounds with different guests, it can be seen that most urea inclusion compounds possess essentially the same host structure. Extinction conditions for the "h" reflexions are $(00l)_h$: $l = 6n$, from which the space group is assigned as $P6_1$, $P6_122$, or their chiral equivalents $P6_5$ and $P6_522$ for the basic host structure. The structure has been found to solve best in $P6_122$ (or $P6_522$). Note, however, that due to the presence of the guest substructure and the incommensurate modulation, this extinction condition is not strictly adhered to. The host, as described in Chapter 1, comprises an extensively hydrogen bonded arrangement of urea molecules, within which there are essentially infinite, uni-directional tunnels.

From the information in the "g" diffraction pattern it is not usually possible to fully determine the guest substructure on account of substantial dynamic disorder of the guest molecules at room temperature [8,19–22]. However, the "g" diffraction pattern

does contain sufficient information to allow general features of the guest molecule ordering to be determined.

The diffuse scattering is usually in the form of two-dimensional sheets perpendicular to the tunnel axis (in direct space), indicating that there are regions of the crystal in which the guest molecules are ordered only in one-dimension (along the tunnel axis) – i.e. there is no structural recognition between guest molecules in adjacent tunnels. The presence of the discrete diffraction maxima within the "g" diffraction pattern indicates that there are other regions of the crystal in which the guest molecules are ordered in three-dimensions.

It is convenient to discuss the modes of three-dimensional ordering of the guest molecules in urea inclusion compounds in terms of two parameters [7,8] – the periodic repeat distance (c_g) of the guest molecules along the tunnel axis (corresponding to the distance between the centres of mass of adjacent guest molecules in the tunnel), and the offset (Δ_g), along the tunnel axis, between the centres of mass of guest molecules in adjacent tunnels [Fig. 2.4]. Δ_g is calculated from consideration of the de Jong-Bouman photographs.

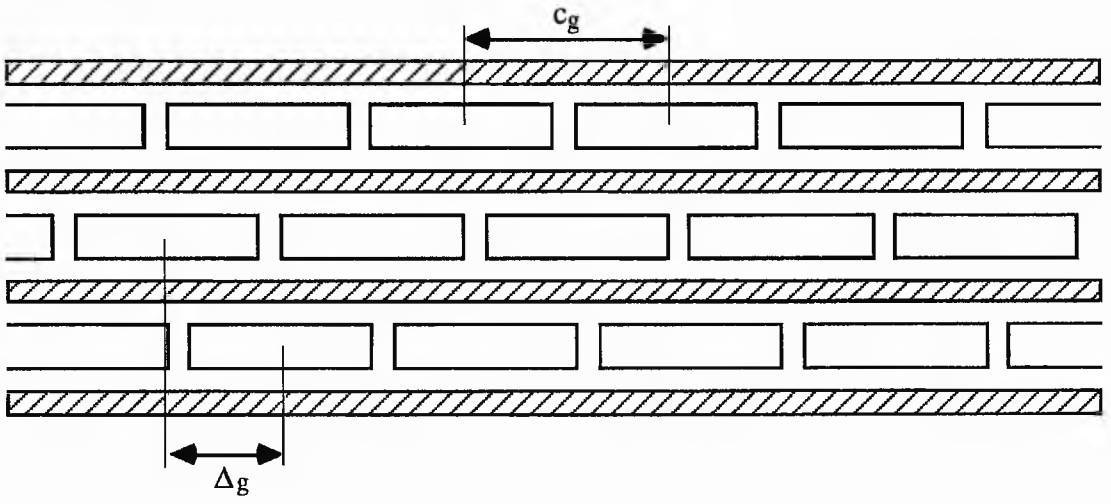

Fig. 2.4: Two-dimensional representation of a urea inclusion compound, viewed perpendicular to the tunnel axis, indicating the definitions of c_g and Δ_g.

From previous studies of urea inclusion compounds containing different families of guest molecules, three different modes of three-dimensional ordering of the guest molecules have been found:

(1) For n-alkane/urea inclusion compounds, $\Delta_g = 0$ (independent of the value of c_g); c_g increases linearly with the number of CH_2 groups in the n-alkane molecule [9,23].

(2) For the diacyl peroxide/urea inclusion compounds with r = 6,9,10, $\Delta_g = 4.6$ Å (independent of the value of c_g) [8].

(3) For the α,ω-dibromoalkane/urea inclusion compounds with r = 7–11, Δ_g depends on the value of c_g, with Δ_g and c_g related by the exact relationship $\Delta_g = \frac{c_g}{3}$ [7].

2.5 n-Alkane/Urea Inclusion Compounds

2.5.1 Room Temperature X-ray Diffraction

Urea inclusion compounds containing $CH_3(CH_2)_rCH_3$; r = 7–15, 18 guests were synthesised and examined by X-ray oscillation and de Jong-Bouman photography initially at room temperature [Plate 2.1].

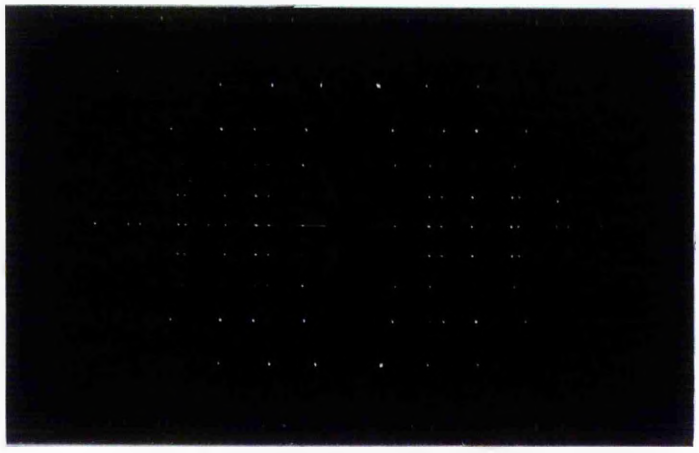

Plate 2.1: X-ray diffraction oscillation photographs, recorded at room temperature, for heptadecane/urea. The crystal was oscillated about its prism axis (parallel to the tunnel axis of the urea host structure).

The interpretation of these photographs for all the n-alkane/urea inclusion compounds was similar. In all cases, interpretation of the "h" diffraction pattern was consistent with the host structure being the same as that previously reported [Space group $P6_122$; $|a_h| = |b_h| \approx 8.2$ Å, $|c_h| \approx 11.0$ Å].

For the shortest n-alkane guests considered, nonane (r = 7) and decane (r = 8), only diffuse scattering was observed in the "g" diffraction pattern, indicating that only one-dimensional ordering of the guest molecules is found in these systems. For all the other guests considered, both diffuse and discrete scattering is observed in the layer lines of the "g" diffraction pattern, showing the presence of regions of both one-dimensional and three-dimensional ordering of the guest substructure. In general, the relative intensity of diffuse scattering decreases with increasing chain length of the guest. The guest periodicities along the tunnel axis (c_g) for all the guests considered were calculated, and the results are given in Table 2.1.

Guest Molecule	c_g / Å
nonane (C_9H_{20})	13.90 ± 0.11
decane ($C_{10}H_{22}$)	15.05 ± 0.12
undecane ($C_{11}H_{24}$)	16.33 ± 0.14
dodecane ($C_{12}H_{26}$)	17.60 ± 0.17
tridecane ($C_{13}H_{28}$)	18.86 ± 0.20
tetradecane ($C_{14}H_{30}$)	20.13 ± 0.23
pentadecane ($C_{15}H_{32}$)	21.60 ± 0.26
hexadecane ($C_{16}H_{34}$)	22.71 ± 0.29
heptadecane($C_{17}H_{36}$)	23.87 ± 0.32
eicosane ($C_{20}H_{42}$)	27.71 ± 0.42

Table 2.1: Guest periodicities (c_g) of n-alkane/urea inclusion compounds determined from single crystal X-ray diffraction experiments at room temperature.

For all compounds showing three-dimensional ordering of the guest substructure, the pattern of discrete scattering in the "g" layers of the tunnel axis oscillation photographs is the same. De Jong-Bouman photographs recorded for these compounds show that the (hk0), $(hk1)_g$ and $(hk1)_h$ layers are directly superimposable upon each other [Plates 2.2(a)&(b)]. From this it can be deduced that the reciprocal lattice vectors $\boldsymbol{c}_h^*$ and $\boldsymbol{c}_g^*$ for the host and guest substructures are both oriented parallel to the tunnel axis $\boldsymbol{c}_h$, which corresponds to the offset between the centres of mass of guest molecules in adjacent tunnels (Δ_g) being zero for all of the n-alkane/urea inclusion compounds, in agreement with previous studies [13,18].

(a)

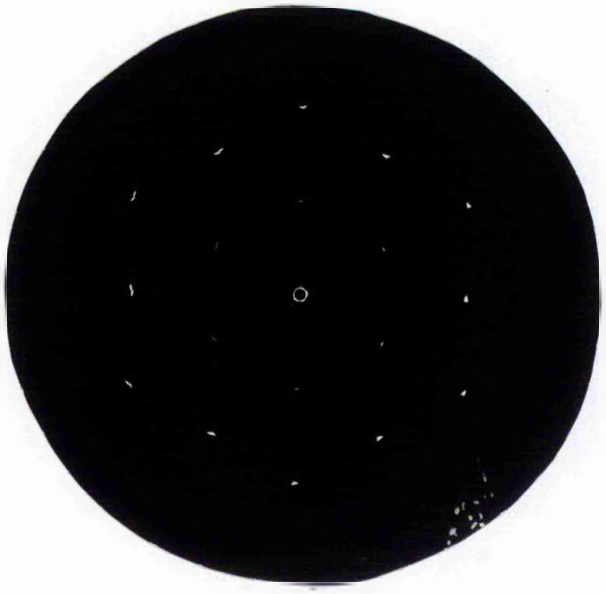

(b)

Plate 2.2: De Jong-Bouman X-ray diffraction photographs, recorded at room temperature, for a single crystal of hexadecane/urea rotating about the tunnel axis of the urea host structure. The reciprocal lattice planes shown are: (a) (hk0); (b) $(hk1)_g$.

Examination of the values determined for c_g [Table 2.1] shows that the periodicity of the guest substructure along the tunnel axis increases linearly with increasing hydrocarbon chain length for the range of guests studied.

2.5.2 Low Temperature X-ray Diffraction

Low temperature X-ray oscillation photographs were recorded for the urea inclusion compounds containing tetradecane, hexadecane and heptadecane as guests. The diffraction patterns were all recorded at 120 K, as this was known to be below the phase transition temperature assessed from heat capacity measurements for all the systems under consideration [24,25].

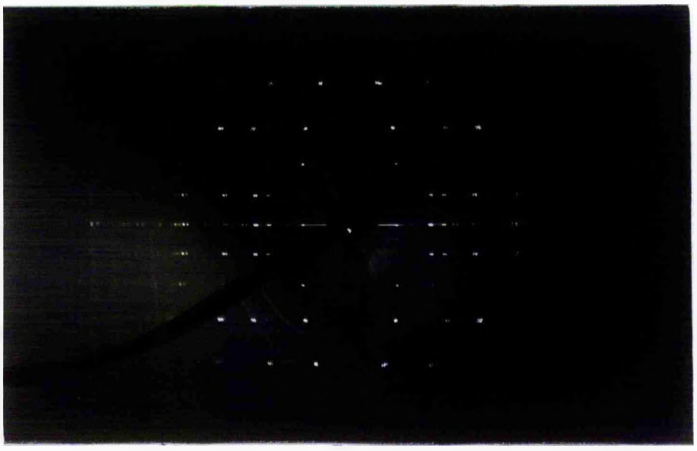

Plate 2.3: X-ray diffraction oscillation photographs, recorded at 120 K, for heptadecane/urea.

In all low temperature X-ray photographs a change was observed in the "h" diffraction pattern, while there were no obvious changes in the "g" diffraction pattern [Plate 2.3]. For all samples the low temperature "h" diffraction pattern was essentially the same – the observation of the new reflexions in all layers lines was consistent with a reduction in the symmetry of the host substructure from hexagonal to orthorhombic. This was confirmed by low temperature powder diffraction, from which it was also possible to determine that the space group was orthorhombic: $P2_12_12_1$, in agreement with previous

assignments [10,12,26] [For more details on the space group assignment, see Chapter 3].

The fact that there was no change in the "g" diffraction patterns for these compounds indicate that Δ_g remains zero down to 120 K. Closer inspection of Plate 2.3 (compared to Plate 2.1), shows a slight increase in the intensity of discrete scattering in the outer "g" layers (notably $l = 3$) as the crystal is cooled. This is consistent with a higher degree of three-dimensional ordering of the guest molecules at lower temperature, as may be expected. While Forst *et al* [6,10,11] observed a great increase in scattering from the guest at low temperature, which they assigned to the formation of a superstructure, we do not observe these features. However, in Plate 2.3 there is evidence for very faint reflexions extremely close to the (hk0) layer, which (when assigned as $l = 1$) correspond to a periodicity of *ca.* 140 Å. Within the measurement errors, this value is six times c_g for the heptadecane/urea inclusion compound at room temperature, and thirteen times c_h. Thus, these reflexions may correspond to the formation of a superstructure in the low temperature phase of periodicity 140 Å along the tunnel axis, and containing six guest molecules. This commensurate relationship for heptadecane/urea was predicted prior to experiment by computational modelling (the results of which are discussed in Chapter 4).

2.6 α,ω-Dibromoalkane/Urea Inclusion Compounds

2.6.1 Room Temperature X-ray Diffraction

Urea inclusion compounds containing α,ω-dibromoalkane guests, at room temperature have previously been investigated [7,27]. The "h" diffraction pattern is qualitatively the same as that observed for the n-alkane/urea inclusion compounds above [i.e. space group $P6_122$; $|\boldsymbol{a}_h| = |\boldsymbol{b}_h| \approx 8.2$ Å, $|\boldsymbol{c}_h| \approx 11.0$ Å].

For the compounds with guests $Br(CH_2)_rBr$; r = 7–11, both discrete and diffuse scattering are observed in the "g" diffraction pattern, again showing that there are regions of one and three-dimensional ordering [Plate 2.4]. For the compound with 1,12-dibromododecane (r = 12) as guest it was only possible to obtain a sample with one-

dimensional ordering of the guest. The spacings between the layer lines are consistent with the trend of increasing c_g with increasing length of the guest molecule present [Table 2.2].

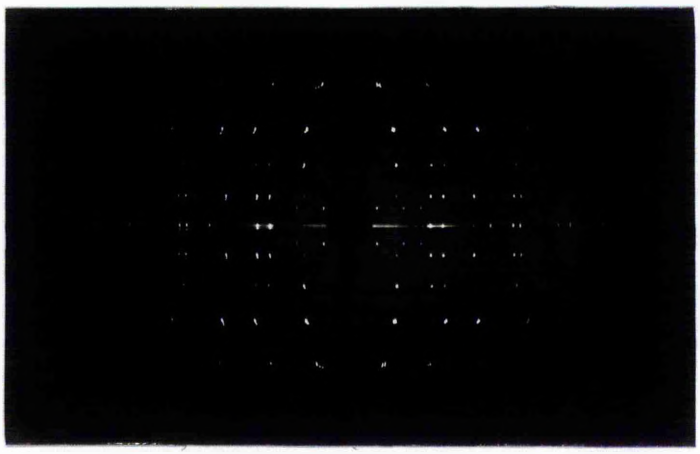

Plate 2.4: X-ray diffraction oscillation photographs, recorded at room temperature, for 1,10-dibromodecane/urea.

The pattern of discrete scattering within each layer line is, however, different from that observed for the n-alkane/urea inclusion compounds. De Jong-Bouman photographs of the (hk0) and $(hk1)_g$ layers for the α,ω-dibromoalkane/urea inclusion compounds were not superimposable. The pattern in the $(hk1)_g$ layer may be rationalised as a convolution of a pair of spots with a portion of the (hk0) lattice net [Fig. 2.5], from which it can be determined that two domains of guest ordering exist (rotated by 180° with respect to each other).

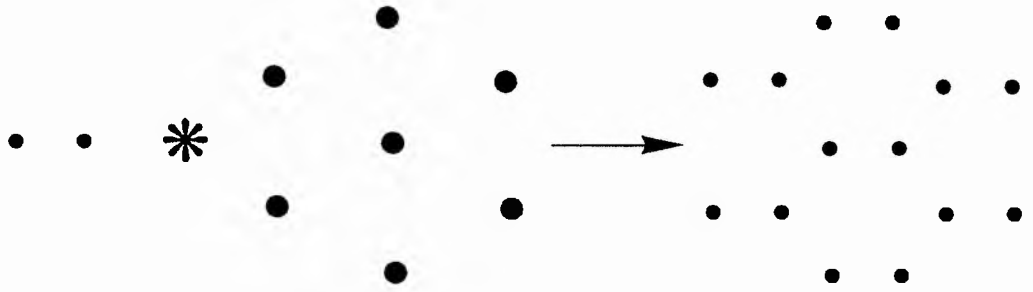

Fig. 2.5: Rationalisation of the $(hk1)_g$ reciprocal lattice plane for the α,ω-dibromoalkane/urea inclusion compounds as the convolution between an array identical to the (hk0) reciprocal lattice net and a pair of points.

For all the guests which show three-dimensional ordering, $\Delta_g = \frac{c_g}{3}$, where c_g is the periodicity of the guest present (within experimental error) [Table 2.2].

Guest Molecule	c_g / Å	Δ_g / Å
1,7-dibromoheptane	14.1 ± 0.11	4.65
1,8-dibromooctane	15.5 ± 0.13	5.13
1,9-dibromononane	17.4 ± 0.17	5.79
1,10-dibromodecane	18.1 ± 0.18	6.03
1,11-dibromoundecane	19.3 ± 0.21	6.41
1,12-dibromododecane	20.2 ± 0.23	1-dimensional

Table 2.2: Single crystal X-ray diffraction data for the inclusion compounds formed between urea and α,ω-dibromoalkanes at room temperature.

2.6.2 Low Temperature X-ray Diffraction

So far in this study, we have looked at urea inclusion compounds containing $Br(CH_2)_rBr$; r = 10–12.

For 1,10-dibromodecane/urea at T =120 K [Plate 2.5], the tunnel axis oscillation photograph shows that the same lowering of symmetry of the host from hexagonal to

orthorhombic occurs as for the n-alkane/urea inclusion compounds above. At this temperature, the discrete component of the "g" diffraction pattern is the same as in the high temperature phase, indicating that there is no change in the type of guest ordering observed. There is, however, a great increase in the intensity of the diffuse scattering for the "g" diffraction pattern, with layers being observed out to $l = 6$, which is consistent with an increase in the long range ordering of the guest molecules.

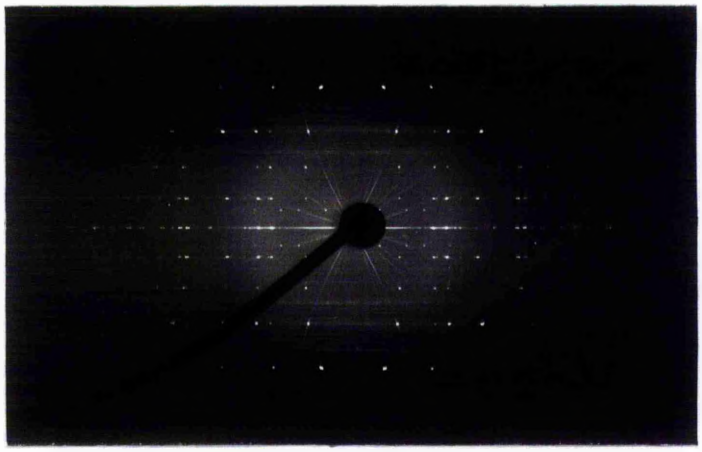

Plate 2.5: X-ray diffraction oscillation photographs, recorded at 120 K, for 1,10-dibromodecane/urea.

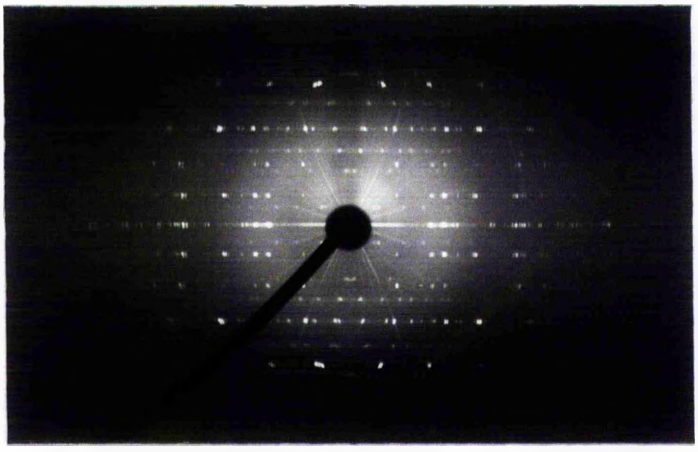

Plate 2.6: X-ray diffraction oscillation photographs, recorded at 100 K, for 1,10-dibromodecane/urea.

Further lowering of the temperature to 100 K, reveals a further change in the observed diffraction pattern [Plate 2.6]. At this temperature, the diffuse scattering in the higher layers for the "g" diffraction pattern (observed up to $l = 7$) has become resolved into discrete reflexions, from which it is clear that the guest substructure becomes substantially more three-dimensionally ordered at this temperature. All the reflexions that were present in the "g" diffraction pattern in the high temperature phase are still seen, though extra reflexions are also observed in the $l = 1$ layer.

There are two possible explanations for this guest transition: the first is that a substantial change is occurring in the dynamical properties of the guest molecules without being influenced by the host substructure, resulting in the appearance of these reflexions. Secondly, we must consider the possibility of an incommensurate → commensurate phase transition. The $(hk5)_g$ layer and $(hk3)_h$ layer appear to be coincident in the oscillation photograph, and it may be that at 100 K the guest molecules become locked into specific positions within the host structure.

This second explanation is supported by the changes observed for the 1,11-dibromoundecane/urea inclusion compound, for which the same transition in the "g" diffraction pattern occurs, but at higher temperature (at 120 K the guest is already in the low temperature phase). For the 1,11-dibromoundecane/urea inclusion compound, layer lines up to $l = 7$ for the guest are observed in the oscillation photograph, and in this case the $(hk7)_g$ and $(hk4)_h$ layer lines appear to be coincident.

For 1,12-dibromododecane/urea the guest molecules were only one-dimensionally ordered (i.e. guest molecules in adjacent tunnels are not ordered uniformly with respect to each other within the crystal) at high temperature. On cooling this sample to 120 K, the hexagonal → orthorhombic host transition is observed as before, but there is no change in the ordering of the guest molecules.

Extension of these studies to the other shorter guest i.e. 1,9-dibromononane and 1,8-dibromooctane is required to see if this apparent incommensurate → commensurate phase transition is common to the whole series of α,ω-dibromoalkane guests. By examination of the periodicities for these compounds at room temperature, the most likely

commensurate structure for 1,9-dibromononane/urea would have $5c_g = 8c_h$, i.e. $(hk8)_g$ coincident with $(hk5)_h$. For the 1,8-dibromooctane/urea inclusion compound $7c_g = 10c_h$ provides the most likely ratio, though these layers are not observable by the diffraction methods employed here.

De Jong-Bouman photographs were also recorded for the 1,10-dibromodecane/urea system at 120 K and 100 K. For the (hk0) layer in the photographs recorded at 120 K and 100 K, each reflexion from the original hexagonal pattern now appears as three spots; this is due to the triple twinning of the low temperature host structure, and the distortion from hexagonal symmetry being small. For the $(hk1)_g$ layer, problems with icing on the capillary and the long exposure times required have meant it was not possibly to distinguish the reflexions from the background, and so it has not been possible to obtain any further information on the guest structure below the transition *via* this method.

2.7 Diacyl Peroxide/Urea Inclusion Compounds

2.7.1 Room Temperature X-ray Diffraction

For $CH_3(CH_2)_rC(O)OO(O)C(CH_2)_rCH_3$ guests with r = 6,9,10 in their urea inclusion compounds the "h" diffraction pattern is again the same as that above at room temperature. The "g" diffraction pattern, however, shows a different pattern of reflexions characteristic of the third type of three-dimensional ordering [Plate 2.7].

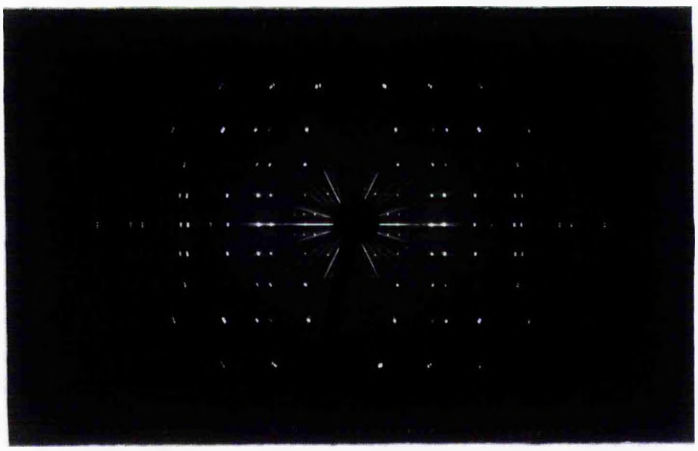

Plate 2.7: X-ray diffraction oscillation photographs, recorded at room temperature, for undecanoyl peroxide/urea.

Guest Molecule	c_g / Å	Δ_g / Å
octanoyl peroxide	23.9	4.63
undecanoyl peroxide	31.5	4.59
dodecanoyl peroxide	34.2	4.57

Table 2.3: Single crystal X-ray diffraction data for the inclusion compounds formed between urea and α,ω-dibromoalkanes at room temperature (from ref. 8).

From the measurement of the spacings between the "g" layer lines, the expected trend of increasing c_g with increasing chain length is observed. De Jong-Bouman photographs of the (hk0) and $(hk1)_g$ layers are non-superimposable [8]. As shown in Fig. 2.6, the $(hk1)_g$ reciprocal lattice plane for diacyl peroxide/urea inclusion compounds can be rationalised as a convolution between the pattern of spots in the (hk0) reciprocal lattice plane and a group of six spots, arranged at the corners of a small hexagon with each of these spots representing a different position of the $(001)_g$ reciprocal lattice point.

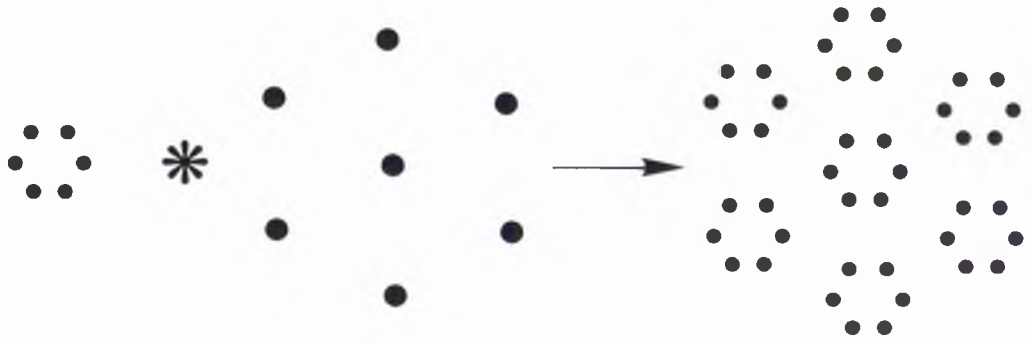

Fig. 2.6: Rationalisation of the $(hk1)_g$ reciprocal lattice plane for diacyl peroxide/urea inclusion compounds and heptanoic anhydride/urea as the convolution between an array identical to the (hk0) reciprocal lattice net and a set of six points arranged at the corners of a hexagon.

Following from this rationalisation of the "g" diffraction pattern, there are six distinct domains of the basic guest structure, each containing an identical packing of guest molecules, and related to each other by $\frac{n\pi}{3}$ rotation (n = integer) about the tunnel axis [Fig. 2.7]. Thus, for the diacyl peroxide/urea inclusion compounds, seven distinct three-dimensionally periodic reciprocal lattices are required to rationalise the positions of all diffraction maxima in the X-ray diffraction pattern (six for the "g" diffraction pattern and one for the "h" diffraction pattern). The intertunnel guest-guest offset has been determined (*via* measurements from the oscillation photograph and the $(hk1)_g$ de Jong-Bouman photograph) and found to be a constant $\Delta_g = 4.6$ Å, irrespective of the length of the guest molecule, at room temperature [8].

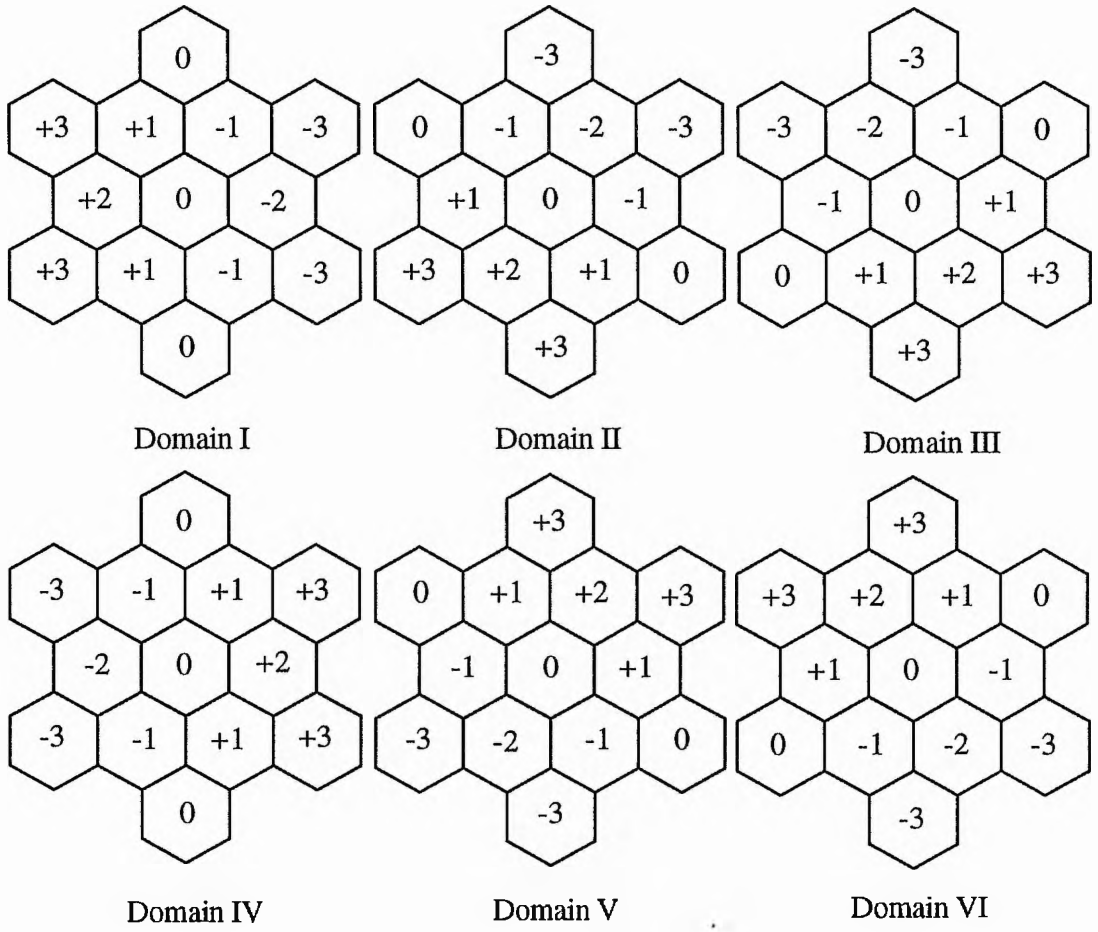

Fig. 2.7: Definition of the six possible domains of the basic guest structure (I to VI), related to each other by $\frac{n\pi}{3}$ rotation (n = integer) about the tunnel axis. Each tunnel is labelled s, indicating that the relative z-coordinates of the guest molecules in that tunnel are $s\Delta_g + tc_g$ (where s and t are integers and, in principle, $t = -\infty, ..., -1, 0, 1, ..., \infty$).

It is interesting to note that the offset of 4.6 Å is close to the "length" of a diacyl peroxide functional group [-C(O)OO(O)C-], and therein lies a possible explanation for observation of this offset. It is believed that the steric size of the diacyl peroxide group may cause local distortions in the urea tunnel structure which render it impossible for guest molecule to sit in adjacent tunnels with a zero offset.

2.7.2 Low Temperature X-ray Diffraction

On cooling the diacyl peroxide/urea inclusion compounds to low temperature, no

change is observed in the diffraction pattern (aside from slight thermal contraction of the lattices). Previous powder diffraction experiments on dodecanoyl peroxide/urea have shown that there is no phase transition down to 46 K [28]. The host substructure retains the hexagonal symmetry, and there is no significant increase in the degree of ordering of the diacyl peroxide guest molecules as the temperature is lowered.

2.8 Carboxylic Acid Anhydride/Urea Inclusion Compounds

2.8.1 Room Temperature X-Ray Diffraction

The X-ray diffraction patterns for all the carboxylic acid anhydride/urea inclusion compounds studied can be interpreted in a similar manner. From the "h" diffraction pattern, it is concluded that the basic host structure in all the urea inclusion compounds studied is the hexagonal structure of the conventional urea inclusion compounds [18] (space group $P6_122$; $|\boldsymbol{a}_h| = |\boldsymbol{b}_h| = 8.2$ Å, $|\boldsymbol{c}_h| = 11.0$ Å). The "g" diffraction patterns contain both diffuse and discrete scattering, indicating the presence of both one-dimensionally and three-dimensionally ordered regions of the guest substructure.

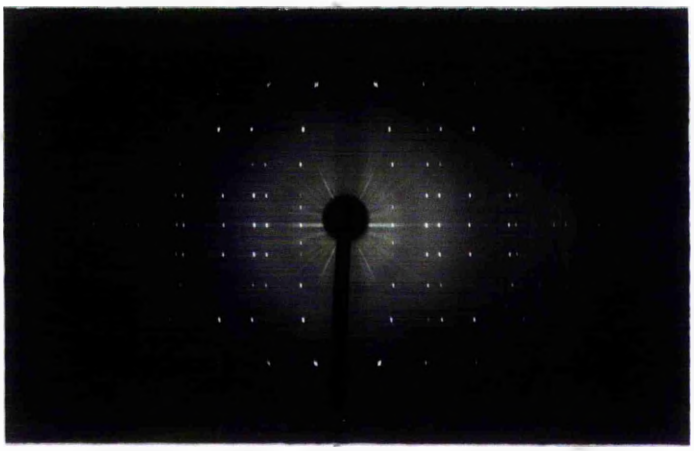

Plate 2.8: X-ray diffraction oscillation photographs, recorded at room temperature, for hexanoic anhydride/urea.

The periodicity of the basic guest structure along the tunnel axis (c_g) was

determined from the "g" diffraction pattern in the tunnel-axis oscillation photographs [Plates 2.8&2.9], and the results are summarised in Table 2.4. Close inspection of the tunnel-axis oscillation photographs reveals that the arrangement of discrete diffraction maxima in the "g" diffraction pattern for heptanoic anhydride/urea [Plate 2.9] is different from that for the other carboxylic acid anhydride/urea inclusion compounds investigated [Plate 2.8].

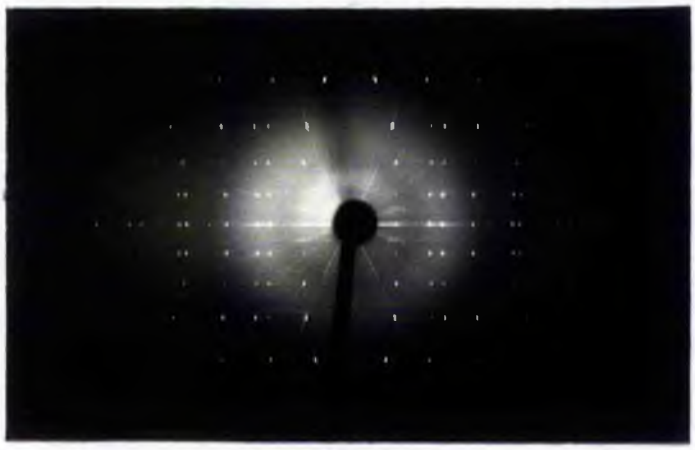

Plate 2.9: X-ray diffraction oscillation photographs, recorded at room temperature, for heptanoic anhydride/urea.

To determine the three-dimensional ordering of the guest molecules, de Jong-Bouman photographs were recorded for single crystals oscillated about their tunnel axes. For all the carboxylic acid anhydride/urea inclusion compounds, with the exception of heptanoic anhydride/urea, the positions of diffraction maxima in the (hk0) and $(hk1)_g$ de Jong-Bouman photographs are directly superimposable upon each other, indicating that the value of Δ_g is zero. The (hk0) and $(hk1)_g$ de Jong-Bouman photographs for heptanoic anhydride/urea are shown in Plate 2.10. The $(hk1)_g$ reciprocal lattice plane for heptanoic anhydride/urea can be rationalised as a convolution of the (hk0) reciprocal lattice plane and a group of six spots, arranged at the corners of a small hexagon, as for the diacyl peroxide/urea inclusion compounds discussed above [Fig 2.6], i.e. there are six distinct domains of the basic guest structure related to each other by $\frac{n\pi}{3}$ rotation (n =

integer) about the tunnel axis [Fig. 2.7]. Using the same methodology developed for the diacyl peroxide/urea systems [8], the value of Δ_g for heptanoic anhydride/urea was determined to be 2.27 Å.

(a)

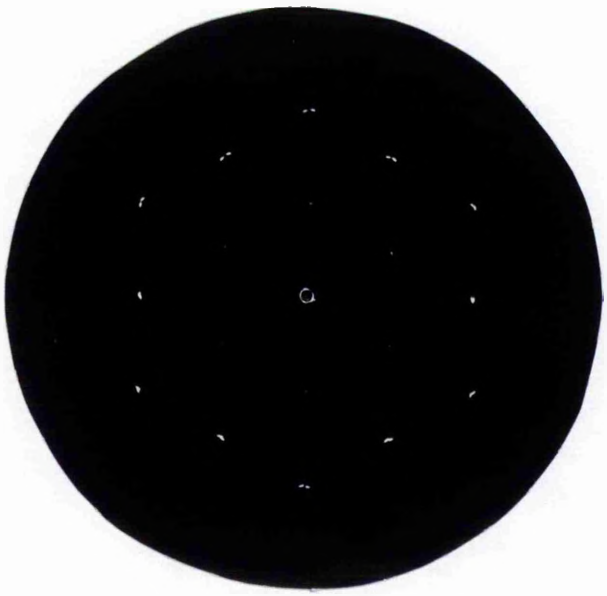

(b)

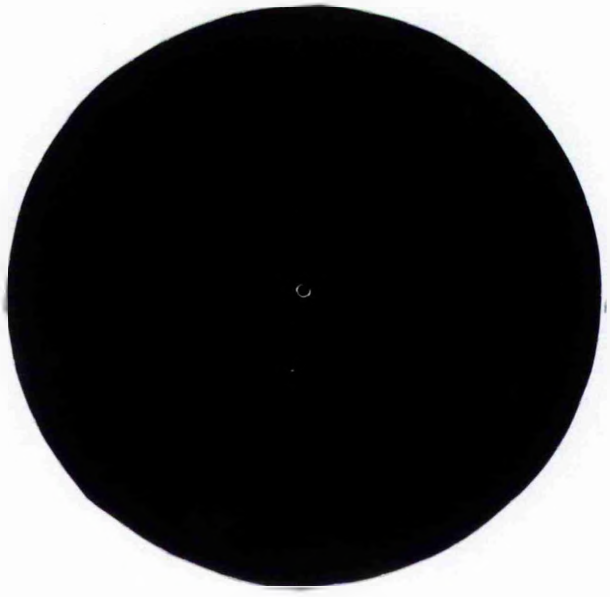

Plate 2.10: De Jong-Bouman X-ray diffraction photographs, recorded at room temperature, for a single crystal of heptanoic anhydride/urea rotating about the tunnel axis of the urea host structure. The reciprocal lattice planes shown are: (a) (hk0); (b) $(hk1)_g$.

The guest periodicities (c_g) measured from the oscillation photographs demonstrate the expected trend of increasing c_g with increasing length of the guest molecule [Table 2.4]. The relatively large errors in these values of c_g, particularly for the longer carboxylic acid anhydrides, arise from the large errors associated with measuring the small distance between layer lines of the "g" diffraction pattern on the oscillation photographs.

Guest Molecule	Guest Periodicity c_g / Å	Δ_g / Å
pentanoic anhydride	16.14 ± 0.14	0
hexanoic anhydride	18.10 ± 0.18	0
heptanoic anhydride	21.09 ± 0.25	2.27 ± 0.10
octanoic anhydride	23.30 ± 0.31	0
nonanoic anhydride	26.03 ± 0.38	0
decanoic anhydride	28.54 ± 0.46	0
dodecanoic anhydride	33.37 ± 0.61	0

Table 2.4: Values of c_g and Δ_g for urea inclusion compounds containing carboxylic acid anhydride ($CH_3(CH_2)_rC(O)O(O)C(CH_2)_rCH_3$) guest molecules at room temperature.

The above results represent the first example of a structural anomaly (specifically with regard to the mode of three-dimensional guest molecule ordering) for a family of urea inclusion compounds containing a homologous series of guest molecules within the conventional urea tunnel structure. We now suggest an explanation for the anomalous behaviour of the heptanoic anhydride/urea inclusion compound with regard to its mode of intertunnel guest molecule ordering.

First, we note that the periodicity of the basic guest structure (c_g = 21.09 Å) along the tunnel direction in heptanoic anhydride/urea is very close to being commensurate with the periodicity of the basic host structure [$\frac{c_g}{c_h} = 1.92 \approx \frac{19}{10}$ (within the experimental errors

in the determination of c_g and c_h)]. If the host and guest substructures are commensurate along the tunnel axis, it is a necessary condition that the intertunnel offset Δ_g should also be commensurate with c_h. For heptanoic anhydride/urea the intertunnel offset (Δ_g = 2.27 Å) does indeed obey this requirement, with $\frac{\Delta_g}{c_h} = 0.21 \approx \frac{1}{5}$ (within the experimental errors in the determination of Δ_g and c_h).

While the existence of a commensurate relationship between the host and guest substructures may distinguish the heptanoic anhydride/urea from the other carboxylic acid anhydride/urea inclusion compounds investigated, this fact alone cannot explain the different mode of intertunnel ordering of the guest molecules in heptanoic anhydride/urea, and we now consider this issue in more detail. For the incommensurate inclusion compounds, the guest molecules do not reside in any specific (preferred) position relative to the basic host structure, but they do (for well-defined Δ_g) reside in specific positions with respect to the guest molecules in neighbouring tunnels. Thus, for the incommensurate carboxylic acid anhydride/urea inclusion compounds the guest molecules choose to occupy positions relative to the guest molecules in neighbouring tunnel which correspond to $\Delta_g = 0$. This mode of intertunnel ordering must therefore be the most favourable arrangement for the guest molecules in the absence of any ordering effects arising from host-guest interaction. Extrapolating this argument from the incommensurate carboxylic acid anhydride/urea inclusion compounds, we may predict that a commensurate carboxylic acid anhydride/urea inclusion compound should also have $\Delta_g = 0$ as the most favourable configuration (it being noted that $\Delta_g = 0$ satisfies the requirement that Δ_g is commensurate with c_h). However, extrapolating from the incommensurate systems to the commensurate systems in the way embodied within the above argument is valid only under the assumption that the commensurate and incommensurate systems differ only in the guest periodicity c_g; in particular, the above argument has assumed implicitly that the conformation of the guest molecules is the same for the commensurate and incommensurate systems. Furthermore, this argument has not considered the influence of the incommensurate modulations within the host and guest substructures in controlling intertunnel ordering of the guest molecules [29].

We now consider the possibility that the above assumption (that the commensurate and incommensurate systems differ only in the guest periodicity c_g) does not hold. Suppose that a given guest molecule in the "default" conformation exhibited by the incommensurate inclusion compounds has a value of c_g close to a value of c_g that would correspond to a commensurate structure, and suppose that this molecule could alter its conformation in such a way that the exact "commensurate" value of c_g could be attained (and thus, by becoming commensurate with the basic host structure, the guest molecules would avail themselves of a more favourable average host-guest interaction energy than would be possible for the corresponding incommensurate system). It is probable that the preferred mode of intertunnel ordering of the guest molecules is influenced crucially by the conformation adopted by the guest molecules, and may therefore be altered significantly by the type of conformational distortion discussed above for bringing the guest molecules into commensurate structural registry with the basic host structure.

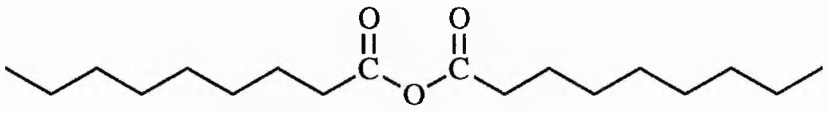

Fig. 2.8: Schematic representation of nonanoic anhydride in the "all-trans" conformation. Note the parallel alignment of the two C=O groups.

We predict that, for the incommensurate carboxylic acid anhydride/urea inclusion compounds, the guest molecules will adopt a conformation close to the linear "all-trans" conformation observed for n-alkane [30] and α,ω-dibromoalkane [31] guest molecules in their urea inclusion compounds. In this conformation, the C=O groups on the guest molecule are parallel to each other and project from the same side of the guest molecule [Fig. 2.8]. This conformation could clearly lead to long range dipole-dipole interactions between guest molecules in adjacent tunnels, and promote intertunnel ordering of the guest molecules with $\Delta_g = 0$; similar arguments have been invoked previously to

rationalise the mode of intertunnel ordering of the guest molecules in ketone/urea inclusion compounds [32]. Conversely, as discussed above, the heptanoic anhydride molecules may adopt a conformation which is distorted from this linear "all-trans" conformation in order to attain a commensurate structural relationship with the basic host structure. [Presumably the carboxylic acid anhydrides other than heptanoic anhydride are too far from a "commensurate" value of c_g, for a conformational distortion to bring them into commensurate structural registry with the basic host structure]. This conformational alteration may involve disruption of the "parallel" alignment of C=O groups, which could thus promote a different preferred mode of intertunnel ordering. In view of the confined environment within the urea tunnel structure, any conformational distortion of the type proposed here is probably a comparatively small distortion.

2.8.2 Low Temperature X-ray Diffraction

For all the carboxylic acid anhydride/urea inclusion compounds examined above, oscillation photographs were also recorded at temperatures in the range 100–120 K.

It was found that the behaviour, in terms of transitions occurring within these systems, was different according to the guest species present. The results of these studies are tabulated in Table 2.5. From the table, there appears to be no uniformity of behaviour between systems.

The inclusion compounds of urea with pentanoic anhydride, heptanoic anhydride and decanoic anhydride (r = 3,5,8) all show the same hexagonal → orthorhombic phase transition for the host substructure as observed for the n-alkane/urea and α,ω-dibromoalkane/urea inclusion compounds. However, all the other compounds behave in a manner similar to the diacyl peroxide/urea inclusion compounds, with no transition occurring in the host substructure.

Guest Molecule	T = 120 K		T = 100 K	
	Δ_g / Å	Host	Δ_g / Å	Host
pentanoic anhydride	–	–	New	O
hexanoic anhydride	–	–	New	H
heptanoic anhydride	New	O	–	–
octanoic anhydride	New	H	New	H
nonanoic anhydride	0	H	0	H
decanoic anhydride	0	O	–	–
dodecanoic anhydride	0	H	–	–

Table 2.5: Single crystal X-ray diffraction data for the inclusion compounds formed between urea and carboxylic acid anhydrides.

For those guests with r = 3,4,6 (pentanoic, hexanoic and octanoic anhydrides), there are substantial changes in the "g" diffraction pattern at low temperature [Plate 2.11]. There is an increase in the intensity and distribution of scattering in the guest layer lines, with discrete scattering being clearly observable up to the $l = 3$ layer (compared to only being observable in the $l = 1$ layer at room temperature). Within the $l = 1$ layer, many extra reflexions are seen compared to the room temperature oscillation photographs. The same pattern of reflexions is seen in the oscillation photographs for all the guests with r = 3,4,6. These changes suggest that there is an increase in the degree of three-dimensional ordering of the guest molecules at low temperature, though it is not yet clear if this transition is accompanied by a change in the mode of guest ordering. In all the low temperature oscillation photographs, the reflexions which correspond to the ordering mode of $\Delta_g = 0$ in the room temperature photos remains the strongest feature of the "g" diffraction pattern. The changes are similar to those observed for the α,ω-dibromoalkanes/urea inclusion compounds, where more discrete scattering was observed in the "g" diffraction pattern at the lowest temperature.

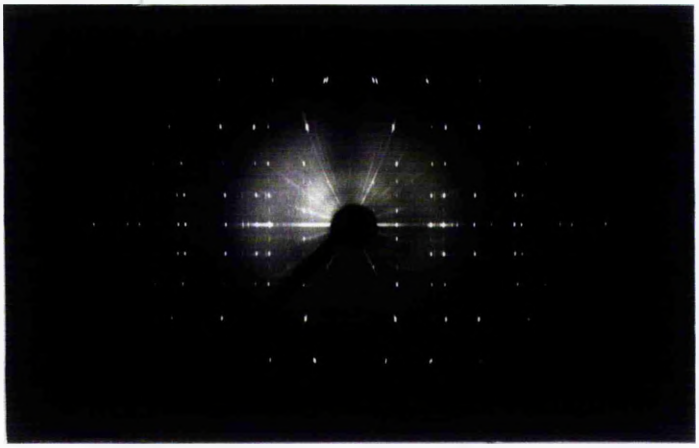

Plate 2.11: X-ray diffraction oscillation photographs, recorded at 120 K, for octanoic anhydride/urea.

From $(hk1)_g$ layer de Jong-Bouman photographs, it should be possible to determine if the new reflexions observed represent a new mode of ordering for the guests at room temperature, or alternatively an increase in the degree of ordering with $\Delta_g = 0$. In the $(hk1)_g$ layer de Jong-Bouman photograph for octanoic anhydride/urea at 120 K, however, only the reflexions which corresponded to $\Delta_g = 0$ in the room temperature photograph were observed above the background radiation level, and it has not been possible to make such assignments. Other methods to derive information about the guest substructure have since been developed, making use of a diffractometer fitted with an area detector to record the full diffraction pattern for octanoic anhydride/urea at 110 K, and this work is discussed in Section 2.10.

For the heptanoic anhydride/urea inclusion compound, a change in the mode of ordering of the guest substructure is observed at low temperature [Plate 2.12]. While at room temperature this compound was anomalous to the series of carboxylic acid anhydride/urea inclusion compounds, having $\Delta_g = 2.27$ Å at 120 K, the ordering is the same as that observed for the pentanoic, hexanoic and octanoic anhydride/urea inclusion compounds above.

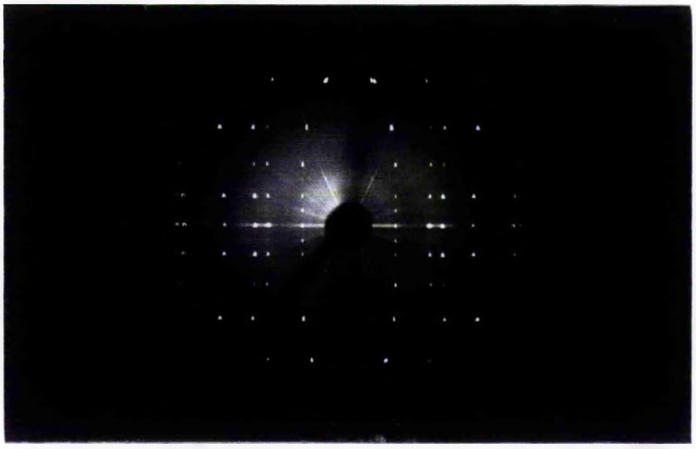

Plate 2.12: X-ray diffraction oscillation photographs, recorded at 120 K, for heptanoic anhydride/urea.

There are several explanations as to why heptanoic anhydride/urea is no longer anomalous. Remember from above that the room temperature structure was believed to be commensurate, but the guest was required to adopt a conformation distorted from the expected all-trans form, in order to attain this commensurate periodicity with the host substructure. On cooling this system down, it is clear that it is now more favourable for the heptanoic anhydride guest molecules to reside in the same conformation as the other anhydrides with r = 3–6, and take up the same mode of guest ordering. Whether there is a change from commensurate to incommensurate behaviour is not yet known (note that it was not possible to observe such changes in the c_g to c_h ratio within the errors of measurement of the oscillation photographs); differing coefficients of thermal expansion for the host and the guest substructures (i.e. the two substructures expand and contract at different rates) may mean that the room temperature guest conformation is no longer required to attain a commensurate relationship, or else it may be destabilised by the transition in the host to the low temperature orthorhombic phase. In order to examine this hypothesis, other techniques which can give an insight to the conformational properties of molecules are required to be used (such as Raman and infrared spectroscopy).

Preliminary differential scanning calorimetry experiments, and precession photography on the heptanoic anhydride/urea inclusion compound [33], has in fact

shown that two transitions occur for this system at around 170 K and 140 K. Below the first transition Δ_g changes to a smaller constant value with no change in the host symmetry; the second transition shows the change in the host combined with a further change in the guest ordering to a situation with $\Delta_g = 0$.

Plate 2.13: X-ray diffraction oscillation photographs, recorded at 120 K, for nonanoic anhydride/urea.

For the guests with r = 7,8,10 (nonanoic, decanoic and dodecanoic anhydrides), there are no changes in the "g" diffraction pattern at low temperature [Plate 2.13]. The observed patterns indicate that Δ_g remains zero for these compounds over the range of temperatures analysed.

2.9 Carboxylic Acid/Urea Inclusion Compounds

2.9.1 Room Temperature X-ray Diffraction

For $CH_3(CH_2)_rCOOH$ guests with r = 6,8,10 in their urea inclusion compounds at room temperature, the host is again found to be in the hexagonal form [Space group $P6_122$; $|\boldsymbol{a}_h| = |\boldsymbol{b}_h| \approx 8.2$ Å, $|\boldsymbol{c}_h| \approx 11.0$ Å]. The "g" diffraction pattern shows only diffuse scattering in the layer lines, indicating that the guest molecules are only one-dimensionally ordered along the tunnel axis [Plate 2.14].

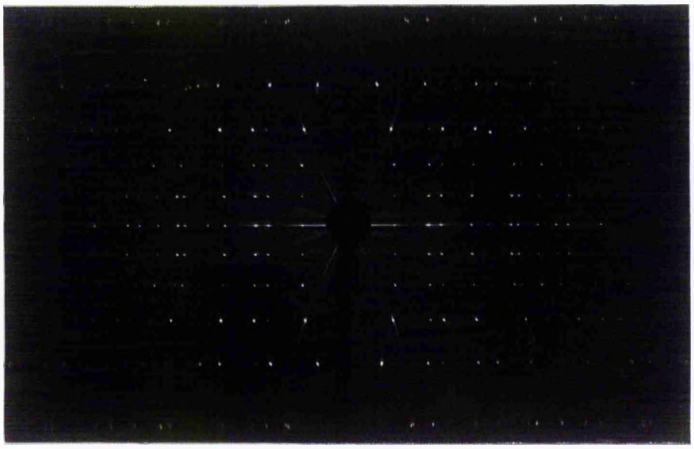

Plate 2.14: X-ray diffraction oscillation photographs, recorded at room temperature, for dodecanoic acid/urea.

Guest Molecule	c_g / Å	Δ_g / Å
octanoic acid	25.1 ± 0.36	1-dimensional
decanoic acid	29.6 ± 0.50	1-dimensional
dodecanoic acid	35.0 ± 0.68	1-dimensional

Table 2.6: Single crystal X-ray diffraction data for the inclusion compounds formed between urea and carboxylic acids at room temperature.

The periodicity c_g is approximately twice the length of a single carboxylic acid molecule ($2L_g$) in the extended linear conformation that it must adopt to fit inside the urea tunnel [Table 2.6]. These periodicities are in agreement with those found previously by Laves *et al* [9], and are rationalised as being due to dimerisation of the carboxylic acid guest molecules, as shown in Fig. 2.9 below.

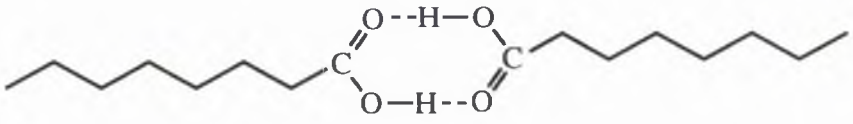

Fig. 2.9: Diagram showing an octanoic acid dimer, as formed in the tunnels of the urea host structure, which accounts for the observed "double period" ($c_g \approx 2L_g$).

2.9.2 Low Temperature X-ray Diffraction

X-ray oscillation photographs recorded at 120 K for all carboxylic acid/urea inclusion compounds show the same features [Plate 2.15]. The "h" diffraction pattern has undergone a transition to the pattern observed for the orthorhombic lattice. The layer lines corresponding to those in the "g" diffraction pattern at room temperature remain as diffuse bands in the low temperature photographs, which suggests that the guest molecules are still only one-dimensionally ordered; however, new reflexions are also observed which do not coincide with the host layer or the guest layer lines seen in the room temperature oscillation photographs. These new reflexions are in the form of discrete spots, with high intensity, very close to the (hk0) layer line, and thus correspond to a large repeat length.

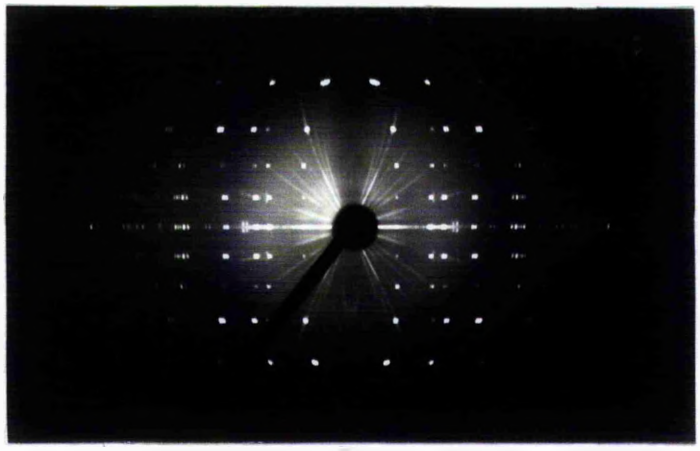

Plate 2.15: X-ray diffraction oscillation photographs, recorded at 120 K, for dodecanoic acid/urea.

For the octanoic acid/urea inclusion compound, indexing this layer as $l = 1$ corresponds to $c_g \approx 50$ Å, which is close to four times the length of a single octanoic acid molecule ($4L_g$). For dodecanoic acid/urea, indexing the equivalent layer as $l = 1$ gives a periodicity of $c_g \approx 95$ Å, which is nearly three times the room temperature guest periodicity [Note that the errors in these long periodicities are large due to the difficulties in measuring accurately very small distances on the oscillation photographs].

The proximity of the new layer of spots to the (hk0) layer also renders it difficult for de Jong-Bouman photographs to be recorded. However, from measurements made from the oscillation photographs along the layer lines, it can been shown that these spots correspond to a periodicity of *ca.* 16.4 Å in the $\boldsymbol{a}_h$ (or $\boldsymbol{b}_h$) direction, which is twice the periodicity in these directions in the high temperature phase.

Further discrete reflexions are observed on either side of the higher host layer lines, which suggests that these reflexions may be "satellite" peaks corresponding to the host diffraction pattern, and due to a long periodicity distortion in the host structure i.e. the generation of a new superstructure. This second possibility is perhaps favoured, as the new reflexions are discrete spots – if they corresponded solely to the "g" diffraction pattern, we would expect to see resolution of the formerly diffuse bands of the guest layer corresponding to $c_g \approx 2L_g$ into discrete spots. However, the position of the new reflexions is clearly guest dependent as the distance from the host layer lines varies with the length of the guest molecules present.

2.10 Diffractometer Measurements

The development of diffractometric techniques to allow the routine examination of the complex structural properties of incommensurate urea inclusion compounds, particularly in relation to the ordering of the guest molecules, represents a step forward.

The sample chosen for initial experiments to develop the necessary techniques was octanoic anhydride/urea. For this system, a substantial increase in the intensity of discrete scattering in the "g" diffraction pattern is observed in the oscillation photographs at low temperature (though it has not yet been possible to rationalise the changes

occurring by the photographic methods employed above). The absence of a transition in the host substructure for this sample means that no complications could arise due to twinning of the host in the low temperature phase, and the orientation of the guest substructure with respect to the host substructure would be well defined.

X-ray diffraction data were recorded on an Enraf-Nonius FAST-TV area detector system, at the EPSRC Crystallography Service, University of Wales in Cardiff, using Mo-K_α radiation (λ = 0.71069 Å) for a single crystal of octanoic anhydride/urea at 110 K. The reflexion intensities from one hemisphere in the range $0 \leq \theta \leq 30°$ were collated to form a unique data set, which consisted of the "h" diffraction pattern. A systematic sweep of the same region of reciprocal space was then carried out.

From these data it was possible to extract the positions in reciprocal space of all diffraction maxima, corresponding to both "h" and "g" diffraction patterns, and to determine further information on the structural ordering.

At 110 K, the "h" diffraction pattern indexed on a hexagonal cell $|\boldsymbol{a}_h| = |\boldsymbol{b}_h|$ = 8.1540(6) Å, $|\boldsymbol{c}_h|$ = 11.0174(16) Å.

On eliminating the reflexions due to the "h" diffraction pattern from the full diffraction pattern for octanoic anhydride/urea, the remaining reflexion (the "g" diffraction pattern) indexed on the hexagonal cell: $|\boldsymbol{a}_g| = |\boldsymbol{b}_g|$ = 16.286(27) Å, $|\boldsymbol{c}_g|$ = 22.11(25) Å. The orientation of the lattice is the same as that for the host substructure. From these observations, several conclusions may be drawn:

i) For the guest substructure, $\Delta_g = 0$ in the low temperature phase. The similarities in the pattern of reflexions in the $(hk1)_g$ layers of the oscillation photographs for pentanoic anhydride/urea, hexanoic anhydride/urea and heptanoic anhydride/urea at low temperature, as well as the precession photographs for heptanoic anhydride/urea, suggest that this mode of ordering exists for all these compounds.

ii) There is a doubling of the lattice in both the $\boldsymbol{a}$ and $\boldsymbol{b}$ directions for the guest substructure in the low temperature phase – this suggests that each guest molecule is fixed in a specific orientation within the tunnel, and is in the same orientation as guest molecules two tunnels away along $\boldsymbol{a}$ and $\boldsymbol{b}$, with different orientations for guest

molecules in adjacent tunnels along a and b. An example of such ordering is shown in Fig. 2.10.

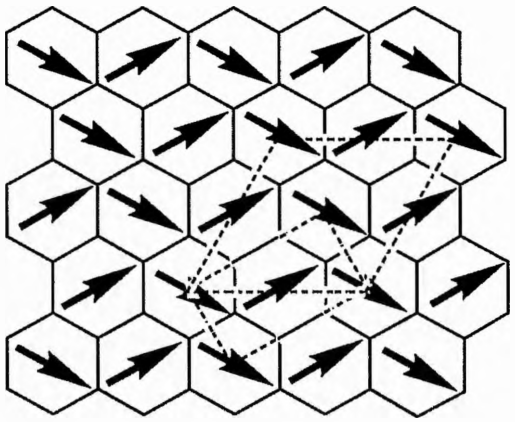

Fig. 2.10: Diagram showing a possible configuration of the guest molecules in the urea tunnel structure such that $a_g = 2a_h$ and $b_g = 2b_h$. The arrows (→) indicate the orientation of the C=O bonds in the anhydride guest molecules. Note, however, that this guest structure is not hexagonal even though the lattice has hexagonal metric symmetry; a smaller orthorhombic cell exists for the guest substructure.

iii) At 110 K the octanoic anhydride/urea inclusion compound is close to being commensurate along the c-axis with $\frac{c_g}{c_h} = 2$, although from the oscillation photograph [Plate 2.11] the $(hk1)_h$ layer and the $(hk2)_g$ layer appear quite distinct.

Processing of this data to solve the guest substructure from this data has not yet proved to be successful. The problems of solving separately the two components, in two different cells, for the incommensurate structure are heightened by the fact that each reflexion contains contributions from both the basic structure of one component and the incommensurate modulation within the other. Work on tackling this problem is ongoing.

2.11 Concluding Remarks and Experiments for the Future

The results presented above show a wide range of differing structural properties dependent on the guest species present within the urea inclusion compound. For the n-

alkane, α,ω-dibromoalkane, diacyl peroxide and carboxylic acid guest molecules, all of the guests studied within each homologous family show the same behaviour as each other at both room temperature and at low temperature. For all cases in which a host transition occurs, the data are consistent with the hexagonal → orthorhombic transition characterised previously for n-alkane/urea inclusion compounds [26]:

i) For the n-alkanes (r = 7–15,18), $\Delta_g = 0$ for all systems at both room temperature and at low temperature. At low temperature, the host undergoes the phase transition.

ii) For α,ω-dibromoalkanes with r = 7–12, $\Delta_g = \frac{c_g}{3}$. As the temperature is lowered, the host transition occurs with no change in the guest ordering, followed at lower temperature by a guest transition (as yet undefined).

iii) The diacyl peroxides (r = 6,8,10) show no phase transition in either host or guest substructures: $\Delta_g = 4.6$ Å at all temperatures.

iv) The carboxylic acid guests (r = 6,8,10) are one-dimensionally ordered at room temperature, but changes occur in conjunction with the transition in the host structure at low temperature.

The results for the carboxylic acid anhydride/urea inclusion compounds, however, have demonstrated the first example of structural anomalies within a homologous family of guest molecules within the conventional (hexagonal) urea tunnel structure. At room temperature, the different mode of guest molecule ordering exhibited by heptanoic anhydride/urea ($\Delta_g = 2.27$ Å), in comparison with that exhibited by the other carboxylic acid anhydride/urea inclusion compounds ($\Delta_g = 0$), is believed to arise from a difference in conformation of the guest molecules in heptanoic anhydride/urea. It is proposed that this conformational distortion occurs in order for the guest substructure to attain a commensurate structural relationship with the host substructure. It is relevant to note that other commensurate urea inclusion compounds are known (e.g. sebaconitrile/urea [34] and 1,6-dibromohexane/urea [35]), but in these cases the host structure is distorted significantly from the conventional urea tunnel structure; there is no evidence from the X-ray diffraction data recorded in this work for any significant structural differences between the urea tunnel structure in heptanoic anhydride/urea in

comparison with the urea tunnel structures in the other carboxylic acid anhydride/urea inclusion compounds.

Direct investigations of the conformational properties of carboxylic acid anhydride guest molecules within their urea inclusion compounds are clearly required before the structural anomaly discussed in this paper can be rationalised fully; with this aim, Raman and infrared spectroscopic investigations of these inclusion compounds are currently in progress.

The low temperature X-ray diffraction data for the carboxylic acid anhydride/urea inclusion compounds show no clear pattern of behaviour across the series of guest molecules studied. Nonanoic and dodecanoic anhydride/urea show no transition in either host or guest, while changes in both the host and guest occur for pentanoic and heptanoic anhydride/urea. Hexanoic and octanoic anhydride/urea exhibit only a guest transition, whereas for decanoic anhydride/urea only the host transition is observed. At the guest transition, the offset $\Delta_g = 0$ is retained (or changed to this value for heptanoic anhydride/urea) and the $\boldsymbol{a}_g$ and $\boldsymbol{b}_g$ axes are doubled.

Although not yet fully understood, it is clear from the changes occurring for the carboxylic acid anhydride/urea inclusion compounds that it is no longer possible to classify, in terms of structural ordering, urea inclusion compounds simply by the homologous family that the guest molecule belongs to. Each urea inclusion compound must be treated as a separate system on its own merits.

The initial experiments developing diffractometric techniques for analysing incommensurate urea inclusion compounds (and, indeed, for application to other incommensurate and twinned systems) point the way forward to more routine and accurate rationalisation of their structural properties. In particular, this technique will be useful for systems such as the low temperature phases of the carboxylic acid anhydride/urea and the α,ω-dibromoalkane/urea inclusion compounds, for which there is substantial discrete scattering from the guest substructure.

References

[1] A.R. West: *Solid State Chemistry and its Applications*, Wiley, Chichester, 1990, p.115.

[2] G.H. Stout and L.H. Jensen: *X-ray Structure Determination*, Wiley, New York, 1989, p.1.

[3] J.P. Glusker and K.N. Trueblood: *Crystal Structure Analysis*, OUP, New York, 1972, p.3.

[4] C. Giacovazzo, H.L. Monaco, D. Viterbo, F. Scordari, G. Gilli, G. Zanotti and M. Catti: *Fundamentals of Crystallography*, OUP, New York, 1992, p.319.

[5] K.D.M. Harris, *J. Solid State Chem.*, **106** (1993) 83.

[6] R. Forst, H. Jagodinski, H. Boysen and F. Frey, *Acta Cryst.*, **B46** (1990) 70.

[7] K.D.M. Harris, S.P. Smart and M.D. Hollingsworth, *J. Chem. Soc. Faraday Trans.*, **87** (1991) 3423.

[8] K.D.M. Harris and M.D. Hollingsworth, *Proc. R. Soc. Lond. A*, **431** (1991) 245.

[9] F. Laves, N. Nicolaides and K.C. Peng, *Z. Krist.*, **121** (1965) 258.

[10] R. Forst, H. Boysen, F. Frey, H. Jagodinski and C. Zeyen, *J. Phys. Chem. Solids*, **47** (1986) 1089.

[11] R. Forst, H. Jagodinski, H. Boysen and F. Frey, *Acta Cryst.*, **B43** (1987) 187.

[12] Y. Chatani, H. Anraku and Y. Taki, *Mol. Cryst. Liq. Cryst.*, **48** (1978) 219.

[13] K. Fukao, H. Miyaji and K. Asai, *J. Chem. Phys.*, **84** (1986) 6360.

[14] W. Tam, D.F. Eaton, J.C. Calabrese, I.D. Williams, Y. Wang and A.G. Anderson, *Chem. Mater.*, **1** (1989) 128.

[15] Q.-Y. Shang, X. Dou and B.S. Hudson, *Nature*, **352** (1991) 703.

[16] S.K. Lee, Q.-Y. Shang and B.S. Hudson, *Mol. Cryst. Liq. Cryst.*, **211** (1992) 147.

[17] W. Gerrard and A.M. Thrush, *J. Chem. Soc.*, (1952) 741.

[18] K.D.M. Harris and J.M. Thomas, *J. Chem. Soc. Faraday Trans.*, **86** (1990) 2985.

[19] F. Guillaume, C. Sourisseau and A.J. Dianoux, *J. Chim. Phys. (Paris),* **88** (1991) 1721.

[20] S.P. Smart, F. Guillaume, K.D.M. Harris, C. Sourisseau and A.J. Dianoux, *Physica B,* **180&181** (1992) 687.

[21] J.D. Bell and R.E. Richards, *Trans. Faraday Soc.*, **65** (1969) 2529.

[22] K.D.M. Harris and P. Jonsen, *Chem. Phys. Lett.*, **154** (1989) 593.

[23] A.J.O. Rennie and K.D.M. Harris, *Chem. Phys. Lett.*, **188** (1992) 1.

[24] R.C. Pemberton and N.G. Parsonage, *Trans. Faraday Soc.*, **61** (1965) 2112.

[25] R.C. Pemberton and N.G. Parsonage, *Trans. Faraday Soc.*, **62** (1966) 553.

[26] K.D.M. Harris, I. Gameson and J.M. Thomas, *J. Chem. Soc. Faraday Trans.*, **86** (1990) 3135.

[27] S.P. Smart, PhD Thesis, University of St. Andrews, 1993.

[28] K.D.M. Harris, PhD Thesis, University of Cambridge, 1988.

[29] S. van Smaalen and K.D.M. Harris, *Proc. R. Soc.*, submitted.

[30] H.L. Casal, *J. Phys. Chem.*, **94** (1990) 2232.

[31] S.P. Smart, A. El Baghdadi, K.D.M. Harris and F. Guillaume, *J. Chem. Soc. Faraday Trans.*, **90** (1994) 1313.

[32] M.D. Hollingsworth and C.R. Goss, *Mol. Cryst. Liq. Cryst.,* **219** (1992) 43.

[33] K.D.M. Harris, unpublished work.

[34] M.D. Hollingsworth, B.D. Santarsiero and K.D.M. Harris, *Angew. Chem. Int. Ed. Engl.*, **33** (1994) 649.

[35] M.D. Hollingsworth, K.D.M. Harris, S.P. Smart, J.C. Huffman and B.D. Santarsiero, manuscript in preparation.

Chapter 3

X-Ray Powder Diffraction of Urea Inclusion Compounds

3.1 X-ray Powder Diffraction

X-ray powder diffraction embodies the same underlying theories as single crystal X-ray diffraction. There are differences, however, between the two techniques in terms of both the geometry of the experiment and the form of the diffraction information obtained.

Powder diffraction is used extensively to study materials for which crystals of sufficient size or quality for single crystal X-ray diffraction cannot be grown. In single crystal X-ray diffraction a single crystallite is exposed to the X-rays, and the diffraction pattern is recorded as a function of three-dimensions in reciprocal space. In powder diffraction the sample under investigation is composed of a large number of (ideally) randomly oriented crystallites (each clearly of unknown orientation), and the diffraction pattern is recorded as a function of one-dimension in reciprocal space. Thus, experimental results of a powder X-ray diffraction experiment represent compression of the three-dimensional diffraction data into one-dimension. This information is normally expressed in the form of a plot of diffraction intensity versus the diffraction angle 2θ (or the interplanar d-spacing) [1].

The loss of orientational information and the compression of the diffraction data into one-dimension results in a severe overlapping of reflexions, which makes it difficult to extract individual intensities of the diffraction maxima. The techniques for routine structure solution by powder X-ray diffraction are consequently less well developed than the corresponding techniques for single crystal diffraction, though great advances in this field have been made in recent years [2–4]. In particular, the use of synchrotron radiation for recording the diffraction pattern results in much narrower peaks than those from

laboratory diffractometers, reducing the problem of overlapping reflexions [5]. For samples for which a good starting structural model exists, structure refinement from this model *via* the Rietveld method [6] can generally be carried out fairly routinely.

3.2 Powder Diffraction of Urea Inclusion Compounds

For urea inclusion compounds [7–9], there is no difficulty in growing sufficiently large and good enough quality single crystals (as evident from the results discussed in Chapter 2). However, for several reasons it is also beneficial to study these materials by powder diffraction, particularly at low temperature.

The short time required to record a powder diffractogram, especially in comparison to the time required for an X-ray oscillation photograph, allows us to easily follow changes in the diffraction pattern with temperature and to accurately pinpoint phase transition temperatures in these systems. These results may be compared with those from other techniques such as differential scanning calorimetry.

At present, routine methods for analysis of single crystal diffraction data are not readily applicable to twinned systems (though the methodology developed in Section 2.10 is applicable to twinned crystals as well as incommensurate crystals). At low temperature, it is known that the host substructure in many urea inclusion compounds undergoes a transition to a triply twinned orthorhombic structure [10]. The temperature of this transition depends on the length of the guest molecule [11,12].

Several attempts have been made previously to solve the low temperature host structure but a satisfactory solution has not yet been reported. From single crystal diffraction data, Chatani *et al* [13,14] reported a structure solution for the hexadecane/urea inclusion compound, based on a triply twinned orthorhombic structure with symmetry $P2_12_12_1$. The guest molecules become highly ordered in the low temperature phase, and it was also shown that $|a|$ increased sharply on crossing the transition, and continued to increase with decreasing temperature below the phase transition temperature. The quality of the reported structure, however, is poor (R-factor

= 10 %) – this is due in part to the difficulty in extracting intensities from the closely overlapping reflexions from the triply twinned domains.

Forst *et al* [15–17] have carried out a similar single crystal X-ray diffraction investigation on the hexadecane/urea inclusion compound, but also failed to obtain a structure of satisfactory quality. They suggest that the formation of a superstructure violates the extinction conditions on the space group $P2_12_12_1$, and through consideration of diffuse scattering propose a different ordering of the guest. Some of the features observed in the diffraction patterns of Forst *et al* have not been observed in other studies (including our own studies described in Chapter 2). The differences arise presumably due to different methods of preparation of the samples, and solvent inclusion may account for some of the extra features observed by Forst *et al*.

Harris *et al* [10] attempted to solve the host structure in the low temperature phase by using powder X-ray diffraction, which eliminates the problems due to twinning. This study recognised that the structure of the low temperature phase represents only a small distortion of the hexagonal high temperature structure, and utilised the high temperature host structure as a starting model for refinement of the low temperature structure. The failure to obtain a satisfactory structure refinement was attributed to a combination of factors. Preferred orientation of the crystallites in the sample, the fact that the guest substructure contributes to the "h" diffraction pattern *via* incommensurate modulations and the coincidence of the (hk0) reflexions for the "h" and "g" diffraction patterns, are discussed as possible reasons for the difficulties in the refinement.

The urea inclusion compounds containing n-alkane and α,ω-dibromoalkane guests, studied by single crystal X-ray diffraction described in the previous chapter, have been investigated by powder diffraction in order to gain information about the phase transitions occurring in both the host and guest substructures.

Synchrotron X-ray powder diffraction data were recorded for the heptadecane/urea inclusion compound, and structure solution of the low temperature host structure has been initiated.

3.3 Experimental

Urea inclusion compounds were prepared by the method described previously [Section 2.3].

A crystalline sample of inclusion compound was ground to a powder and loaded into a glass capillary. Powder X-ray diffraction data were collected on a Stoe Stadi-P high-resolution powder X-ray diffractometer in transmission mode, using Cu-K_α radiation (λ = 1.5418 Å). Temperatures below room temperature were obtained using a cryostream cooler (Oxford Cryosystems Ltd), with liquid nitrogen as coolant. The cryostream cooler was calibrated by studying materials with known phase transitions occurring at sharply defined phase transition temperatures, and giving rise to significant changes in the powder X-ray diffractogram.

Synchrotron X-ray powder diffraction data (λ = 0.80 Å) were measured on station 9.1 at the SRS facility at Daresbury Laboratory. The X-ray powder diffraction pattern for the heptadecane/urea inclusion compound was recorded twice, at 70 K, and the two diffractograms were combined to improve the signal/noise ratio.

The diffraction patterns were indexed using the program TREOR [18]. Rietveld refinement calculations were carried out within the program GSAS [19].

3.4 Results

3.4.1 Low Temperature Powder Diffraction of the 1,10-Dibromodecane/Urea Inclusion Compound

Powder X-ray diffractograms for 1,10-dibromodecane/urea were recorded at several temperatures between 122 K and 295 K [Fig. 3.1]; the temperature-dependence of the diffractogram was investigated in particular detail around the known phase transition temperature at *ca.* 140 K.

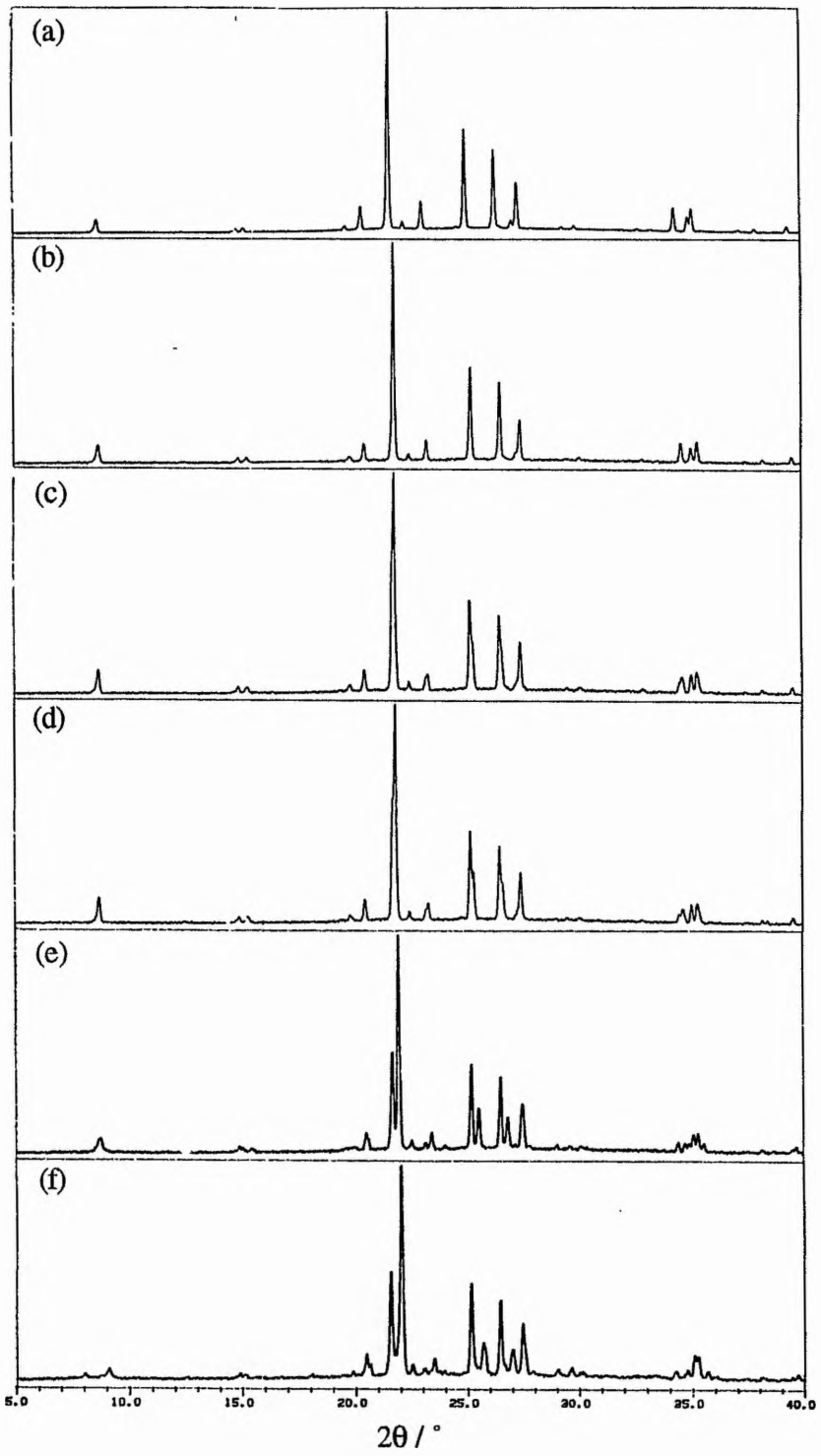

Fig. 3.1: Powder X-ray diffraction data recorded for the 1,10-dibromodecane/urea inclusion compound at: (a) T = 295 K, (b) T = 142 K, (c) T = 140 K, (d) T = 138 K, (e) T = 122 K and (f) T = 102 K.

At 295 K, the majority of the peaks in the diffractogram are from the "h" diffraction pattern, and can be indexed on the basis of a hexagonal lattice [$|a_h| = |b_h| =$ 8.206 Å, $|c_h| = 11.002$ Å; $\alpha = \beta = 90°$, $\gamma = 120°$]; this is completely consistent with the known symmetry ($P6_122$) of the basic host structure determined previously from single crystal X-ray diffraction data [9]. The peaks which are not indexed on the basis of this lattice are at $2\theta = 8.70°$, 15.20°, 19.68°, and these peaks represent reflexions in the "g" diffraction pattern [20].

It is clear from the diffractogram recorded at 122 K that the structural properties of the 1,10-dibromodecane/urea inclusion compound at this temperature are substantially different from those at 295 K. At 122 K, the peaks due to the "h" diffraction pattern can be indexed on the basis of an orthorhombic lattice [$|a_O| = 8.198$ Å, $|b_O| = 13.954$ Å, $|c_O| = 10.963$ Å; $\alpha = \beta = \gamma = 90°$], and the conditions for systematic absences are consistent with space group $P2_12_12_1$. The details of the transition are discussed further in Section 3.4.3.

From the set of diffractograms [Fig. 3.1] recorded between 122 K and 295 K, the phase transition temperature is assigned as 140 ± 1 K.

From the diffractogram recorded at 102 K for the 1,10-dibromodecane/urea inclusion compound [Fig. 3.1(f)], changes in the reflexions due to the "g" diffraction pattern are evident . Notably, the peak at $2\theta \approx 8.6°$ is split into a pair of peaks. While it has not been possible to deduce directly any structural information on the basis of these changes in the "g" diffraction pattern, it is clear that they represent the same transition in the guest substructure observed in the single crystal X-ray diffraction studies [Section 2.6.2].

3.4.2 Low Temperature Powder Diffraction of the Hexadecane/Urea Inclusion Compound

The diffraction pattern of the hexadecane/urea inclusion compound was recorded over a range of temperatures in the region of the known phase transition at *ca.* 150 K [Fig. 3.2].

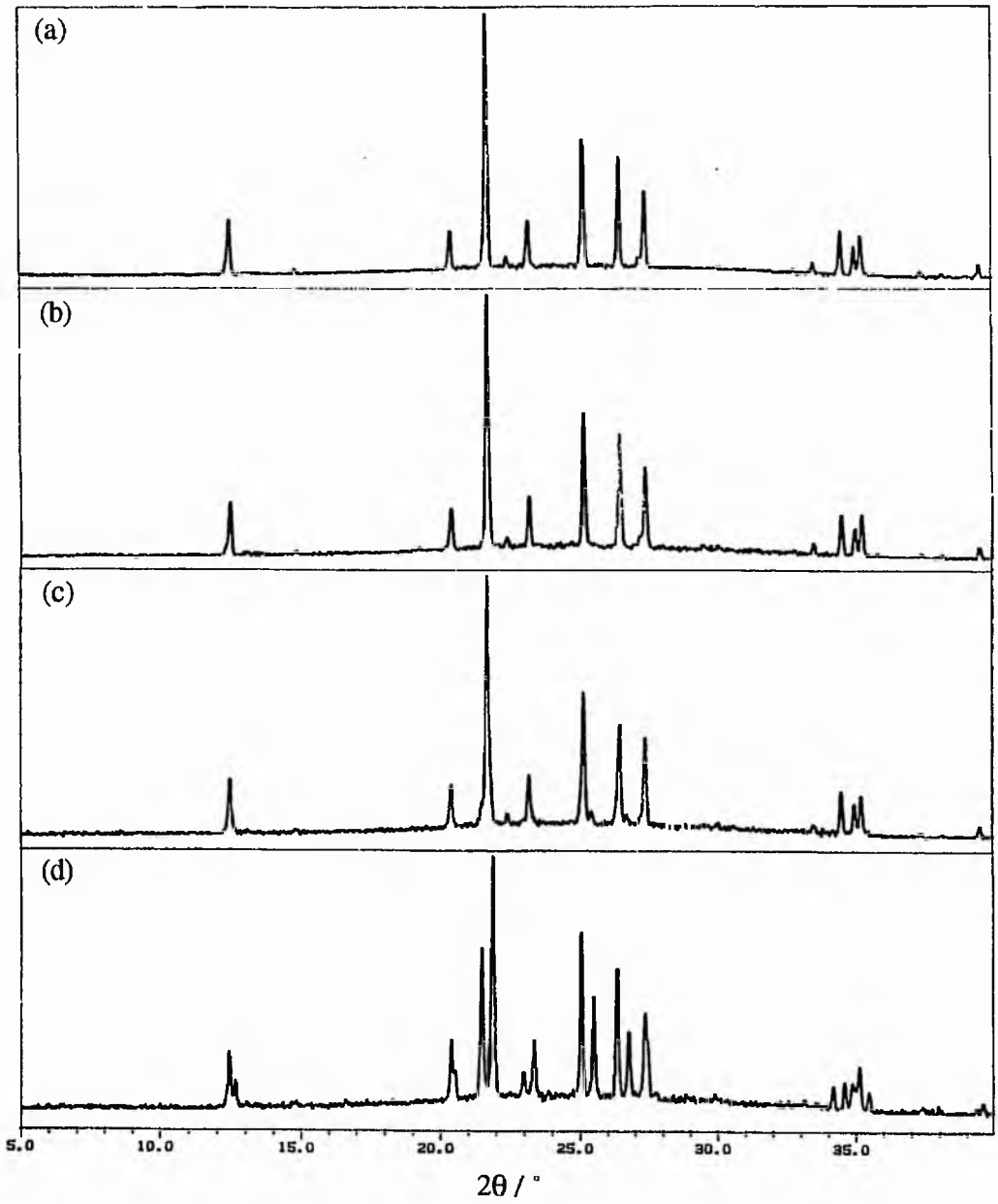

Fig. 3.2: Powder X-ray diffraction data recorded for the hexadecane/urea inclusion compound at: (a) T = 152 K, (b) T = 150 K, (c) T = 149 K and (d) T = 142 K.

At 152 K [Fig. 3.2(a)], the majority of the peaks in the diffractogram can be indexed on the basis of a hexagonal lattice [$|a_h| = |b_h| = 8.162$ Å, $|c_h| = 11.001$ Å; $\alpha = \beta = 90°$, $\gamma = 120°$], which is again consistent with the known symmetry of the high temperature phase ($P6_122$) from previous studies [9]. The small peak at $2\theta = 22.27°$ represents a small impurity amount of the pure crystalline phase of urea.

In qualitative terms, the "h" diffraction pattern is the same as that reported above for the 1,10-dibromodecane/urea inclusion compound, with the exception that the intensity of the (100) peak (at $2\theta = 12.44°$) is significantly greater for the hexadecane/urea inclusion compound. This striking difference is a consequence of the fact that scattering from both the basic host structure and the basic guest structure contribute to the reflexions of type (h,k,0) for the urea inclusion compounds (the z-axis, in direct space, is parallel to the tunnel axis).

From the lowest temperature diffractogram, at 142 K [Fig. 3.2(d)], the hexadecane/urea inclusion compound can be seen to have passed through a phase transition. This pattern can be indexed on an orthorhombic lattice [$|a_O| = 8.248$ Å, $|b_O| = 13.958$ Å, $|c_O| = 10.992$ Å; $\alpha = \beta = \gamma = 90°$], with the space group $P2_12_12_1$. Note that this cell suggests an expansion of the host along the a-axis on passing through the transition, as also shown in ref. 13. The low intensity peak at $2\theta = 16.80°$ is from the "g" diffraction pattern.

The diffractograms recorded at intermediate temperatures [Fig. 3.2(b)&(c)] follow the changes occurring close to the transition temperature. From these results, the phase transition temperature is 150 ± 1 K.

3.4.3 Rationalisation of the Changes in the Diffraction Pattern

The structural transformation associated with the phase transitions for the hexadecane/urea inclusion compound and the 1,10-dibromodecane/urea inclusion compound can be rationalised on the basis of the general approach developed previously [10] for a hexagonal to orthorhombic phase transition involving a minor structural distortion. Briefly, a hexagonal lattice {a_H, b_H, c_H} (e.g. the basic host structure in the

high-temperature phase) can be described alternatively as a C-centred orthorhombic lattice $\{\boldsymbol{a}_O^h, \boldsymbol{b}_O^h, \boldsymbol{c}_O^h\}$ (referred to as "orthohexagonal") for which the condition $|\boldsymbol{b}_O^h| = 2|\boldsymbol{a}_O^h|\cos 30^\circ$ necessarily holds [Fig. 3.3].

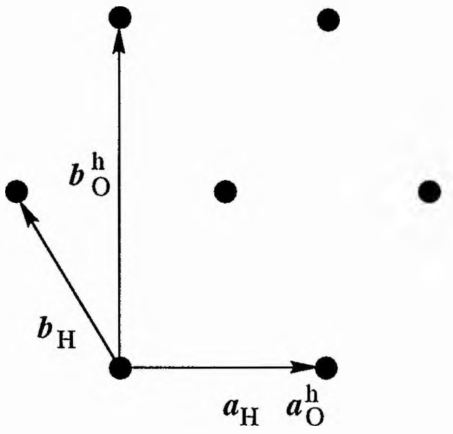

Fig. 3.3: Diagram showing both the hexagonal and C-centred orthohexagonal descriptions of a lattice with hexagonal symmetry.

A transformation from a hexagonal lattice to an orthorhombic lattice may be considered in terms of this strict equality being relaxed, with the possibility that the C-centring is also lost. Here, the subscripts H and O describe reflexions in the hexagonal and orthorhombic systems respectively, and the use of the superscript h together with the subscript O denotes the orthohexagonal setting of a hexagonal system.

In general, each peak in a diffractogram consists of a superposition of many reflexions with nominally different Miller indices. Reflexions at the same 2θ correspond to a form of lattice planes (denoted $\{h,k,l\}$) in the holosymmetric point group of the relevant crystal system, and we refer here to the number of individual reflexions within a given form as its "multiplicity". All individual reflexions contributing to a given powder diffraction peak will have the same intensity only if the Laue group of the diffraction pattern is the same as the holosymmetric point group of the crystal. This is true for both

the low-temperature and high-temperature phases of the host structure in 1,10-dibromodecane/urea.

If we consider only general forms $\{h,k,l\}$ (for which there is no special relationship between h, k and l and none of h, k and l is equal to zero), a general form of the holosymmetric hexagonal point group ($6/mmm$) has multiplicity 24, whereas a general form of the holosymmetric orthorhombic point group (mmm) has multiplicity 8. Each general peak in the diffractogram for the high-temperature phase therefore consists of contributions from 24 reflexions (each with different Miller indices $\{h,k,l\}_H$). On transforming to the orthohexagonal system, these 24 reflexions comprise three separate forms, each with multiplicity 8. These forms can be generalised as $\{H,K,L\}_O^h$, $\{(K-H)/2, -(3H+K)/2, L\}_O^h$ and $\{-(H+K)/2, (3H-K)/2, L\}_O^h$, where $H = h$, $K = h + 2k$, $L = l$. In the orthohexagonal system, these three forms correspond to the same 2θ value. When the hexagonal (orthohexagonal) to orthorhombic phase transition occurs, these three forms become inequivalent and give rise to three separate peaks (barring accidental equivalence).

The changes in the powder X-ray diffractogram occurring at the phase transition for the hexadecane/urea and 1,10-dibromodecane/urea inclusion compounds can be understood on this basis. As an illustration, the $(201)_H$ peak in the high-temperature phase represents the overlap of 12 individual reflexions (rather than 24, as $k = 0$). In the orthohexagonal setting, this peak corresponds to two forms of reflexions: $(221)_O^h$ with multiplicity 8, and $(041)_O^h$ with multiplicity 4. On transforming to the orthorhombic system, the condition $|\boldsymbol{b}_O| = 2|\boldsymbol{a}_O|\cos 30^\circ$ no longer holds, and these two forms of reflexions do not occur at the same value of 2θ. Under the assumption (valid for a hexagonal to orthorhombic phase transition involving only a minor structural distortion) that all reflexions within the $(221)_O$ and $(041)_O$ forms have approximately equal intensity, the pair of peaks resulting from the hexagonal to orthorhombic phase transition results in an intensity ratio of approximately 8:4 (i.e. 2:1) for the intensities of the $(221)_O$ and $(041)_O$ peaks in the diffractogram of the orthorhombic phase. From the formula:

$$\frac{4\sin^2\theta}{\lambda^2} = \frac{H^2}{|a_O|^2} + \frac{K^2}{|b_O|^2} + \frac{L^2}{|c_O|^2} \qquad \text{Eq. 3.1}$$

which applies to orthorhombic systems, and since $|b_O| < 2|a_O|\cos 30^\circ$ for the low-temperature phase of 1,10-dibromodecane/urea, $(221)_O$ should occur at lower 2θ than $(041)_O$. This is seen clearly in the diffractogram recorded at 122 K. The behaviour of all other reflexions upon passing from the high-temperature phase to the low-temperature phase can be rationalised in the same manner as for the $(201)_H$ peak.

3.4.4 Structure Refinement of the Low Temperature Host Structure in the Heptadecane/Urea Inclusion Compound

Synchrotron X-ray powder diffraction data have been recorded with $\lambda = 0.80$ Å for the heptadecane/urea inclusion compound at 70 K [Fig 3.4]. The "h" diffraction pattern was indexed using the unit cell $|a_O| = 8.277$ Å, $|b_O| = 13.820$ Å, $|c_O| = 10.980$ Å. From the systematic absences, the space group cannot be uniquely assigned, but in agreement with all previous studies, the space group $P2_12_12_1$ is consistent with the observed absences. In fact, it can be shown that if the 6_1-axis is lost and replaced by a 2_1-axis, and the origin shifted by $(\frac{1}{4},0,\frac{1}{12})$, the room temperature host structure can be described by this space group. The asymmetric unit contains three urea molecules (rather than half a urea molecule) and the unit cell is doubled in size.

As a starting model for structure refinement, the room temperature host structure for the hexadecane/urea inclusion compound was used, with space group transformed from $P6_122$ to $P2_12_12_1$ and the fractional atomic coordinates transformed into the orthohexagonal description [9]. Unit cell parameters were set to the values given above.

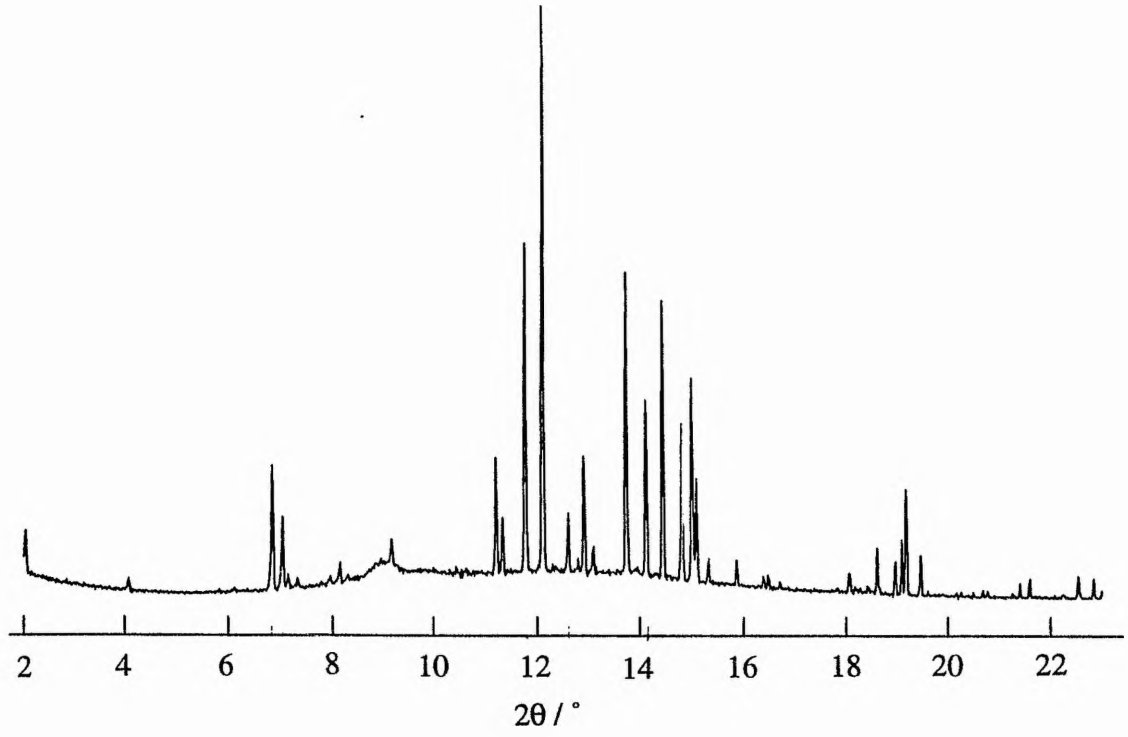

Fig. 3.4: Synchrotron powder X-ray diffraction pattern recorded for the heptadecane/urea inclusion compound at 70 K ($\lambda = 0.8$ Å).

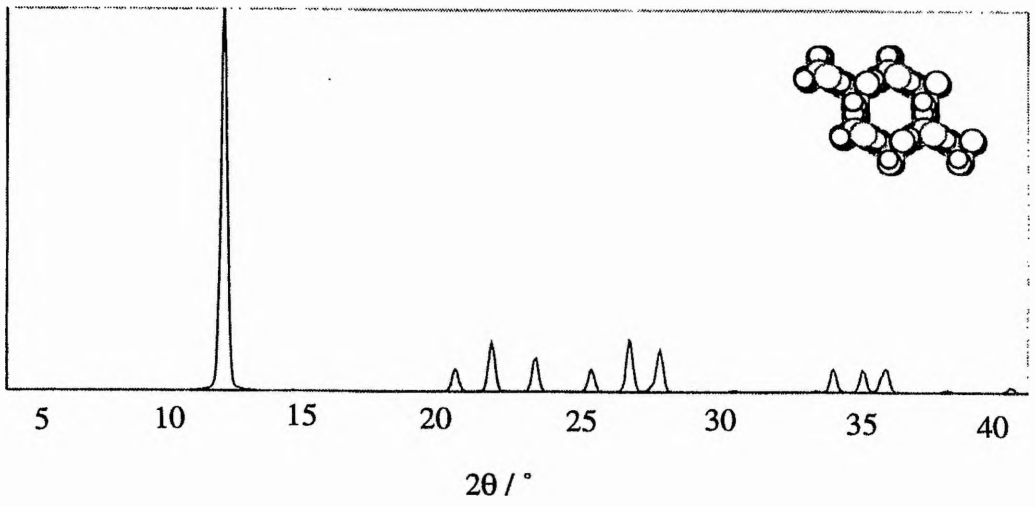

Fig. 3.5: Simulated powder X-ray diffraction pattern for the "host only" structure of the hexadecane/urea inclusion compound at 295 K ($\lambda = 1.5418$ Å).

As discussed in Section 3.4.2, the guest substructure contributes to the observed intensities of the (*hk*0) reflexions, but also (to a lesser extent) affects the rest of the "h" diffraction pattern, due to the incommensurate modulation imposed on the guest substructure by the host substructure. In Fig. 3.5, the simulated diffraction pattern for the host structure in the absence of any electron density representing guest molecules is shown. The discrepancies between this simulated diffractogram and the experimental data shows the marked effect that the presence of the guest in the tunnels has on the "h" diffraction pattern. Thus, clearly structure refinement using the "h" diffraction pattern requires a good model representing the contribution of the guest substructure to the "h" diffraction pattern.

Initial refinement was carried out with "dummy" carbon atoms placed inside the tunnels of the host structure to model the contribution of the guest substructure to the "h" diffraction pattern; these "guest" atoms were taken as those refined from the room temperature single crystal "h" diffraction pattern of hexadecane/urea. However, stable refinement from this starting point was not achieved. As there is less disorder in the guest substructure at low temperature [21], it is possible that the use of the representation of the guest substructure determined at room temperature is not a good enough initial structural model for the representation of the guest substructure at 70 K. For this reason, a variety of other starting models for the guest substructure were also tried. In no case was a satisfactory refinement obtained. A major problem proved to be the inability to model the peak shape (modelled using a pseudo-voigt function). It is believed that error in the scale factor is compensating for inaccuracies in the modelling of the guest substructure, and that this prevents the profile parameters from refining correctly.

Further attempts at refinement were made with the (*hk*0) reflexions initially excluded from the diffraction pattern. This minimised the possible effects of a poor model for the averaged guest substructure, but still did not lead to a satisfactory refinement.

If a room temperature synchrotron X-ray diffraction pattern had been recorded for the heptadecane/urea inclusion compound, then accurate peak profile parameters could

have been derived (as the room temperature urea host structure is known from single crystal X-ray diffraction). These parameters could then have been used in fitting the pattern recorded for the low temperature phase.

3.5 Conclusion

While attempts to solve the structure of the urea host structure at low temperature have not yet proved to be successful, powder diffraction nevertheless still represents the most viable technique for this purpose on account of the twinning of the crystals in the low temperature phase. The diffractometric techniques being developed for single crystal diffraction of twinned and incommensurate structures [Section 2.10] will also provide an alternative approach to this problem.

The better resolution of the synchrotron data (in terms of less peak overlap) and the better signal to noise ratio have not proved to be decisive in the determination of the host structure, and clearly there are many other factors which may contribute to the lack of success in this work. As discussed above, the use of an inadequate model for the guest substructure (to represent the effects of the incommensurate modulation imposed on the guest substructure by the host substructure and the contribution of the guest substructure to the (*hk*0) reflexions) may contribute significantly to the inability to refine the structure. This has an effect on the ability to fit the peak profile parameters. Preferred orientation within the sample may also be a cause of the unstable refinement, though the Rietveld refinement program used does embody parameters to account for the preferred orientation.

Qualitatively, the changes in the host structure on crossing the phase transition have been shown to be the same for both n-alkane and α,ω-dibromoalkane guests, and have been rationalised in terms of a small distortion of the hexagonal structure to an orthorhombic structure.

In the case of the 1,10-dibromodecane/urea inclusion compound a transition in the guest substructure has also been observed. However, on account of the low intensity and small number of peaks observed for the "g" diffraction pattern, it has not been

possible to derive significant structural information from these reflexions – the single crystal X-ray diffraction studies described in Chapter 2 provide greater information on the changes in the ordering of the guest substructure with temperature.

References

[1] C. Giacovazzo, H.L. Monaco, D. Viterbo, F. Scordari, G. Gilli, G. Zanotti and M. Catti: *Fundamentals of Crystallography*, OUP, New York, 1992, p.287.

[2] G. Cascarano, L. Favia and C. Giacovazzo, *J. Appl. Cryst.*, **25** (1992) 310.

[3] G. Bricogne and C.J. Gilmore, *Acta Cryst.*, **A46** (1990) 284.

[4] K.D.M. Harris, M. Tremayne, P. Lightfoot and P.G. Bruce, *J. Am. Chem. Soc.*, **116** (1994) 3543.

[5] A.K. Cheetham and A.P. Wilkinson, *J. Phys. Chem. Solids*, **52** (1991) 1199.

[6] H.M. Rietveld, *J. Appl. Cryst.*, **2** (1969) 65.

[7] L.C. Fetterly: *Non-stoichiometric Compounds,* ed L. Mandelcorn, Academic Press, New York, 1964, p.491.

[8] K. Takemoto and N. Sonoda: *Inclusion Compounds, Vol.2*, eds J.L. Atwood, J.E.D. Davies and D.D. MacNicol, Academic Press, London, 1984, p.47.

[9] K.D.M. Harris and J.M. Thomas, *J. Chem. Soc. Faraday Trans.*, **86** (1990) 2985.

[10] K.D.M. Harris, I. Gameson and J.M. Thomas, *J. Chem. Soc. Faraday Trans.*, **86** (1990) 3135.

[11] R.C. Pemberton and N.G. Parsonage, *Trans. Faraday Soc.*, **61** (1965) 2112.

[12] R.C. Pemberton and N.G. Parsonage, *Trans. Faraday Soc.*, **62** (1966) 553.

[13] Y. Chatani, Y. Taki and H. Tadokoro, *Acta Cryst.*, **B33** (1977) 309.

[14] Y. Chatani, H. Anraku and Y. Taki, *Mol. Cryst. Liq. Cryst.*, **48** (1978) 219.

[15] R. Forst, H. Boysen, F. Frey, H. Jagodzinski and C. Zeyen, *J. Phys. Chem. Solids*, **47** (1986) 1089.

[16] R. Forst, H. Jagodinski, H. Boysen and F. Frey, *Acta Cryst.*, **B43** (1987) 187.

[17] R. Forst, H. Jagodinski, H. Boysen and F. Frey, *Acta Cryst.*, **B46** (1990) 70.

[18] P.-E. Werner, L. Eriksson and M. Westdahl, *J. Appl. Cryst.*, **18** (1985) 367.

[19] A.C. Larson and R.B. Von Dreele: Los Alamos Laboratory Report No. LA-UR-86-748, 1987.

[20] K.D.M. Harris, S.P. Smart and M.D. Hollingsworth, *J. Chem. Soc. Faraday Trans.*, **87** (1991) 3423.

[21] K. Fukao, H. Miyaji and K. Asai, *J. Chem. Phys.*, **84** (1986) 6360.

Chapter 4

Predicting Structural Properties of Urea and Thiourea Inclusion Compounds: Application of the Mathematical Model of One-Dimensional Inclusion Compounds

4.1 Introduction

Computational modelling has become an increasingly important tool to the chemist due to its ability to predict, often ahead of experiment, the behaviour of chemical systems at the molecular level. It can also provide explanations for experimental observations.

For urea and thiourea inclusion compounds, an important question is whether a given inclusion compound is commensurate or incommensurate. Previously, these tunnel inclusion compounds have been defined as being commensurate if it is possible to find sufficiently "small" positive integers, p and q, such that:

$$pc_h \approx qc_g \qquad \text{Eq. 4.1}$$

where c_h is the periodicity of the host along the tunnel axis, and c_g is the periodicity of the guest along.

If it is not possible to find suitable "small" integers p and q, the compound is said to be incommensurate.

This definition is unsatisfactory, for the following reasons:

i) It is difficult to measure c_h and c_g to a high enough degree of accuracy. While diffractometric measurements can be taken for the host structure on a conventional diffractometer (see Section 2.10) and the host periodicity c_h can be accurately determined, in many cases c_g can only be determined *via* photographic diffraction methods, which are

intrinsically less accurate. Within the errors of the measurement of c_g and c_h, it is usually possible to find comparatively small values of p and q which satisfy the above condition.

ii) There is no indication how large p and q have to be for them not to be considered as "small" integers? Are we talking about tens, hundreds or thousands?

The consequence of an incommensurate relationship between the host and guest substructures is that, in theory, no two guest molecules, within the same tunnel, are in the same environment with respect to the host structure. This means the interaction between the host and guest substructures is insensitive to the position of the guest substructure along the tunnel – alternatively, it may be said that the guest molecules do not preferentially bind to specific sites of the host structure.

With questions such as these in mind, a more rigorous definition of the terms commensurate and incommensurate is required, and has now been developed [1]. The chosen method was to derive a model which would find the most energetically stable guest structure within the inclusion compound. By considering the ratio c_g:c_h for this inclusion compound, it would be possible to assign the system as commensurate or incommensurate, based upon consideration of the energetics of host-guest interaction.

4.2 Mathematical Model for One-Dimensional Inclusion Compounds

To a good approximation, it can be assumed that, in urea and thiourea inclusion compounds, the interaction between guest molecules in different tunnels is weak – as a consequence, these inclusion compounds can be modelled as strictly one-dimensional systems, with each tunnel of the "real" inclusion compound considered to behave essentially independently. For a crystalline one-dimensional inclusion compound, the structural periodicity of the guest molecules is defined by the single parameter – c_g – the periodic repeat distance of the guest molecules along the tunnel, which corresponds to the distance between the centres of mass of adjacent guest molecules in the tunnel. The periodic repeat distance of the host substructure along the tunnel axis is denoted c_h.

Here, we apply a mathematical model developed previously [1] to understand and rationalise structural properties of one-dimensional inclusion compounds. In particular,

this model provides a theoretical framework that allows potential energy functions (for host-guest interaction, guest-guest interaction and intramolecular potential energies) computed for any one-dimensional inclusion compound of interest to be used to predict and rationalise structural properties of the inclusion compound.

A rigorous development of the mathematics underlying the model has been published previously [1,2], and only the most important features are summarised here. Within the model, the one-dimensional inclusion compound is considered to comprise an infinite, rigid, periodic, linear host tunnel containing a finite number n of equally spaced, rigid identical guest molecules [Fig. 4.1]. The unit of length is taken to be the periodic repeat distance of the host substructure, c_h (note: $c_h \approx 11.0$ Å for most urea inclusion compounds), and the periodicity of the guest substructure is then denoted α (where $\alpha = \frac{c_g}{c_h}$). The conformation of each guest molecule within the host tunnel is assumed to be the same. An arbitrary zero point is assigned to the host substructure, and the position of the first guest molecule relative to this zero point is denoted λ. The structure of the host tunnel and the conformation of the guest molecules are assumed to be independent of λ, α and n.

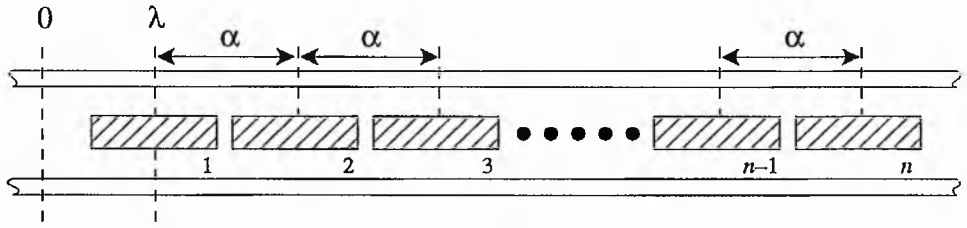

Fig. 4.1: Schematic representation of the one-dimensional inclusion compound corresponding to the triplet (λ,α,n). The inclusion compound comprises n guest molecules arranged periodically (with repeat distance α) along an infinite, one-dimensional host tunnel. The position of the first guest molecule is denoted λ.

In ref. 1, a characteristic energy function $\hat{E}(\alpha,n)$ was defined for the inclusion compound, with the entailment that, if $\hat{E}(\alpha_1,n) < \hat{E}(\alpha_2,n)$, then α_1 represents a more

favourable guest periodicity than α_2, provided n is the same in both cases. The characteristic energy is defined [1] as:

$$\hat{E}(\alpha,n) = \frac{1}{\alpha}\left(\hat{E}_{host}(\alpha,n) + \hat{E}_{guest}(\alpha) + \hat{E}_{intra}\right) \qquad \text{Eq. 4.2}$$

where $\hat{E}_{host}(\alpha,n)$ is the minimum average host-guest interaction energy, per guest molecule, when the periodicity of the guest substructure is α, $\hat{E}_{guest}(\alpha)$ is the guest-guest interaction energy, per guest molecule, when the periodicity of the guest substructure is α, and $\hat{E}_{intra}$ is the intramolecular potential energy of the guest molecule (assumed to be the same for all guest molecules in the structure). $\hat{E}_{host}(\alpha,n)$ is given by:

$$\hat{E}_{host}(\alpha,n) = \inf_{\lambda}\left(\frac{1}{n}\sum_{k=0}^{n-1} E_h(k\alpha+\lambda)\right) \qquad \text{Eq. 4.3}$$

where $E_h(t)$ represents the energy of an individual guest molecule, due to host-guest interaction, when the guest molecule is located at position t along the host tunnel.

The objective of this model is to enable the calculation of the optimum value(s) of α for each inclusion compound under study. In order to determine these values, it is necessary to eliminate the dependence of the energy on both λ and n. The method developed involves construction of a graph to represent the energy profile of the inclusion compound, from which the optimum region of α can be easily calculated. This graph is called the "characteristic energy diagram", and its construction and interpretation are defined below.

In using the characteristic energy to assess the optimum guest periodicity, it is important to give careful consideration to the dependence of the characteristic energy on n. Consideration of only a fixed number of guest molecules, n, would limit us to a small subset of all the possible inclusion compounds. The characteristic energy diagram constructed represents a superposition of all graphs of $\hat{E}(\alpha,n)$ versus α for all values of n. It has been shown that, as $n \rightarrow \infty$, these graphs converge pointwise to a graph which is continuous at all irrational α, but discontinuous at all rational α [1]; however, it was

also shown that, for all n greater than a critical lower limit N, the graphs of $\hat{E}(\alpha,n)$ versus α are confined within a definable subarea of the characteristic energy diagram. It is then possible to determine a range guaranteed to contain the points $(\alpha,\hat{E}(\alpha,n))$ for which $\hat{E}(\alpha,n)$ is minimal for each $n \geq N$, and projection of this region onto the α axis gives a range containing the optimal value(s) of α for all $n \geq N$.

A graphical method has been developed which allows the range containing optimal α to be determined from a knowledge of the potential energy functions $E_h(t)$, $\hat{E}_{guest}(\alpha)$, and $\hat{E}_{intra}$ for the inclusion compound of interest.

4.3 Construction of the Characteristic Energy Diagram in Practice

It is clear from the definition of $\hat{E}(\alpha,n)$ that, in order to apply the theoretical approach to determine the optimum guest periodicity for any particular one-dimensional inclusion compound, we require potential energy functions for host-guest interaction ($E_h(t)$), for guest-guest interaction ($\hat{E}_{guest}(\alpha)$), and for the intramolecular potential energy of the guest molecules ($\hat{E}_{intra}$). At this stage, it is not important to discuss the actual procedures that can be used to determine these potential energy functions in practice – details of the specific computational approaches used for the three different classes of inclusion compound studied in this work are given in later Sections (4.5.1, 4.6.1 and 4.7.1).

Before construction of the characteristic energy diagram, it is necessary to choose energy parameters ε and ε' such that $0 < \varepsilon' < \frac{\varepsilon}{2}$. The factors governing the choice of these parameters have been discussed elsewhere [2], and a detailed consideration of the physical significance of these parameters is given in Section 4.8. A Fourier series p(t), which is periodic in t with period 1, is constructed to represent the host-guest interaction energy function $E_h(t)$ [in practice, it is convenient to compute $E_h(t)$ at K evenly spaced points ranging from $t = 0$ to $t = 1 - \kappa$, where $\kappa = \frac{1}{K}$]:

$$p(t) = \int_0^1 E_h(x)dx + \sum_{m=1}^{M} a_m\cos(2\pi mt) + \sum_{m=1}^{M} b_m\sin(2\pi mt) \qquad \text{Eq. 4.4}$$

The quality of fit of this Fourier series (dictated largely by the number (2M) of coefficients) must be such that the maximum residue $[p(t) - E_h(t)]$ is less than $\frac{\varepsilon'}{3}$. Thus,

$$\sup_t |p(t) - E_h(t)| < \frac{\varepsilon'}{3} \qquad \text{Eq. 4.5}$$

From the parameters M, $\{a_m\}$ and $\{b_m\}$ in the expression for p(t), the value of N (introduced in Section 4.2) can be determined from:

$$N = \frac{4M^2}{\varepsilon'} \sum_{m=1}^{M} \sqrt{a_m{}^2 + b_m{}^2} \qquad \text{Eq. 4.6}$$

The importance of these parameters will be discussed further later in relation to the results for the specific compounds studied.

In order to construct the characteristic energy diagram, it is necessary to determine the following parameters:

(a) $$\delta = \frac{1}{2M^2} \qquad \text{Eq. 4.7}$$

(b) $$\mu(d) = \left| \inf_t \left(\sum_{d|m} a_m \cos(2\pi m t) + \sum_{d|m} b_m \sin(2\pi m t) \right) \right| \qquad \text{Eq. 4.8}$$

for each integer d from d = 1 to d = M, and $\sum_{d|m}$ represents the summation over m, where m takes all the values $\{m : m = nd, n \in \mathbb{Z} \text{ and } nd < M\}$. The calculation of $\mu(d)$ is particularly important in the application of the mathematical model; $\mu(d)$ is related to the energy of stabilisation of the inclusion compound with commensurate periodicity $\alpha_0 = \frac{p}{d}$, where $p \in \mathbb{Z}$, compared to the energy of the inclusion compounds with irrational α close to α_0. The exact role of $\mu(d)$ in the construction of the characteristic energy diagram is further discussed below.

(c) The set $\Gamma = \{d : \mu(d) > \varepsilon - \varepsilon'\}$, and the mesh $\mathbb{M}$ of rational numbers (α_0) with denominator in Γ. Thus, $\mathbb{M} = \{\alpha_0 = \frac{p}{q} : p \in \mathbb{Z}, q \in \Gamma\}$. The mesh $\mathbb{M}$ represents rational values of α at which a commensurate inclusion compound may be formed. [The definition of a commensurate inclusion compound, in relation to the model, is given at the end of this section.]

(d) The punctured line, defined by $\mathbb{L} = \{\alpha \in \mathbb{R} : \alpha \notin (\alpha_0 - \delta, \alpha_0 + \delta) \text{ for } \alpha_0 \in \mathbb{M}\}$. This punctured line represents the real line minus a δ-neighbourhood [where δ is as defined in (a)] around each of the rational numbers ($\alpha_0 \in \mathbb{M}$) with denominator in Γ.

The characteristic energy diagram (energy versus α) is constructed as a series of bounding curves, which define a region within which the actual energies (for $n \geq N$) are guaranteed to lie. The construction is carried out in the following stages:

(a) First, the following curve is drawn on the characteristic energy diagram over a suitable range of α (i.e. a range typically a few Å wide in the region of the minimum of the $\hat{E}_{guest}(\alpha)$ curve) which will contain the optimal α:

$$\frac{1}{\alpha}\left(\int_0^1 E_h(t)\, dt + \hat{E}_{guest}(\alpha) + \hat{E}_{intra}\right) \qquad \text{Eq. 4.9}$$

This curve represents the upper energy bound on the characteristic energy diagram; for all $n \geq N$, all the points $(\alpha,\hat{E}(\alpha,n))$ are guaranteed to lie below this line.

(b) For $\alpha \in \mathbb{L}$, the following curve is drawn on the characteristic energy diagram:

$$\frac{1}{\alpha}\left(\int_0^1 E_h(t)\, dt - \varepsilon + \hat{E}_{guest}(\alpha) + \hat{E}_{intra}\right) \qquad \text{Eq. 4.10}$$

This represents the part of the lower energy bound on the characteristic energy

diagram for the region $\alpha \in \mathbb{L}$. For $n \geq N$, it can be shown that for all $\alpha \in \mathbb{L}$, all the points $(\alpha,\hat{E}(\alpha,n))$ lie above this line. The lower energy bound is completed (for the region $\alpha \notin \mathbb{L}$) in (iv) below.

(c) For each $\alpha_0 \in \mathbb{M}$, the minimum d_0 such that $\alpha_0 d_0 \in \mathbb{Z}$ is found, and a vertical line (called a "downspike") is drawn on the characteristic energy diagram between:

$$\frac{1}{\alpha_0}\left(\int_0^1 E_h(t)\,dt + \hat{E}_{guest}(\alpha_0) + \hat{E}_{intra}\right) \qquad \text{Eq. 4.11}$$

and

$$\frac{1}{\alpha_0}\left(\int_0^1 E_h(t)\,dt - \mu(d_0) + \varepsilon' + \hat{E}_{guest}(\alpha_0) + \hat{E}_{intra}\right) \qquad \text{Eq. 4.12}$$

The downspikes at these values α_0 correspond to a potential "lock in" of host and guest substructures. For $n \geq N$, the point $(\alpha_0,\hat{E}(\alpha_0,n))$ lies below the bottom of this downspike.

(d) Finally, for each $\alpha_0 \in \mathbb{M}$ and with d_0 defined as above, the following curve is drawn on the characteristic energy diagram over the range $\alpha \in (\alpha_0 - \delta, \alpha_0 + \delta)$ (i.e. α in the δ-neighbourhood of each mesh point α_0):

$$\frac{1}{\alpha}\left(\int_0^1 E_h(t)\,dt - \mu(d_0) - \varepsilon' + \hat{E}_{guest}(\alpha) + \hat{E}_{intra}\right) \qquad \text{Eq. 4.13}$$

For $n \geq N$, it can be shown that, for all $\alpha \in (\alpha_0 - \delta, \alpha_0 + \delta)$, the points $(\alpha, \hat{E}(\alpha,n))$ lie above this line. This completes the lower energy bound on the characteristic energy diagram.

These stages in the construction of the characteristic energy diagram are illustrated in Fig. 4.2.

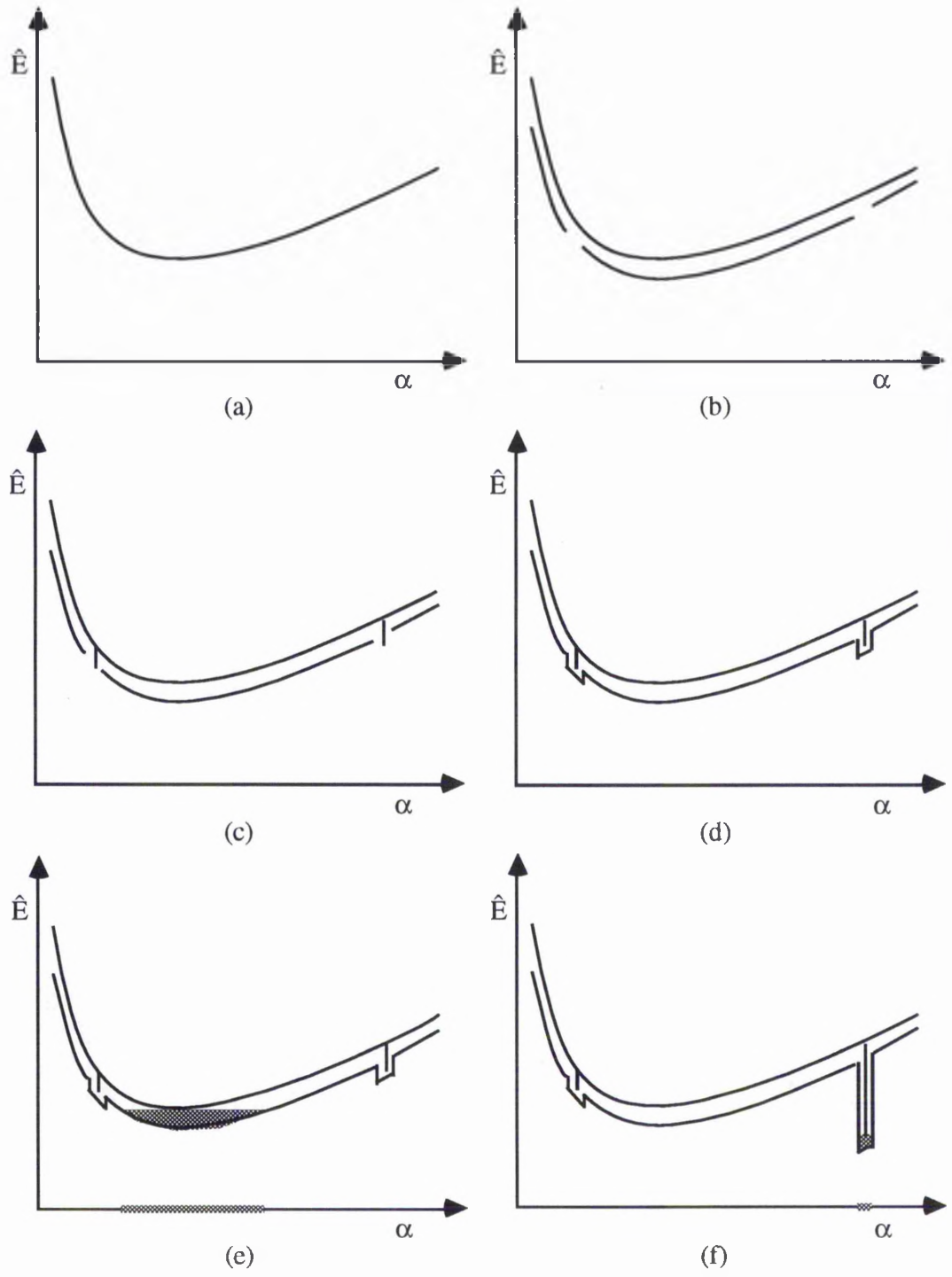

Fig. 4.2: Diagram showing the construction of the characteristic energy diagram. (a) to (d) represent the stages in the drawing of the upper and lower bounds described above. (e) and (f) show two completed characteristic energy diagrams, which have different ranges of optimal α (indicated by the shaded regions along the α-axis).

For all numbers of guest molecules $n \geq N$ and all α, the points $(\alpha,\hat{E}(\alpha,n))$ all lie between the upper energy bound and the lower energy bound on the characteristic energy diagram. To locate a region containing optimal α, a horizontal line is drawn through the lowest point reached by either the upper energy bound or one of the downspikes. The region between this horizontal line and the lower energy bound on the characteristic energy diagram must contain at least one point $(\alpha,\hat{E}(\alpha,n))$ for every $n \geq N$. Thus, the projection of this region onto the α axis must contain the optimal value of α for all guest substructures with $n \geq N$ [Fig. 4.2(e)&(f)].

Assignment of the inclusion compound as either commensurate or incommensurate may then be made from the graph. It is only possible for an inclusion compound to be assigned as commensurate if the minimum of the upper energy bound and the downspikes corresponds to the bottom of a downspike. The assignment, however, is dependent on the choices of ε and ε' – selection of smaller values of ε and ε' will lead to a corresponding smaller region of optimal α, but will give rise to a larger value of N (and will hence correspond to a longer length of tunnel – in this regard, it is important that the value of N corresponds to a tunnel length shorter than those found in practice). If the region containing optimal α corresponds to the δ-neighbourhood of one of the downspikes, then $\alpha \in (\alpha_0 - \delta, \alpha_0 + \delta)$ for $\alpha_0 \in \mathbb{M}$ and the compound may be said to be commensurate; if $\alpha \notin (\alpha_0 - \delta, \alpha_0 + \delta)$ for $\alpha_0 \in \mathbb{M}$ then the compound is assigned as incommensurate. It follows that these conditions may be more rigorously defined [2] in terms of the following inequalities:

$$l(\alpha,n) = \left| \hat{E}_{host}(\alpha,n) - \int_0^1 E_h(t)dt \right| > \varepsilon - 2\varepsilon' \qquad \text{Eq. 4.14}$$

$$l(\alpha,n) = \left| \hat{E}_{host}(\alpha,n) - \int_0^1 E_h(t)dt \right| < \varepsilon \qquad \text{Eq. 4.15}$$

If $l(\alpha,n)$ is greater than $\varepsilon - 2\varepsilon'$, then the lock in of the guest substructure and the host substructure can be significant; if $l(\alpha,n)$ is less than ε then lock in is not significant. Providing suitable values of ε and ε' are chosen (such as to minimise the region of

overlap between the two inequalities), this method can provide physically significant information from the characteristic energy diagram.

The implementation of this definition and the whole procedure described here for construction and interpretation of the characteristic energy diagram are illustrated in more detail in Sections 4.5.2, 4.6.2 and 4.7.2 for the inclusion compounds studied.

4.4 Applications of the Mathematical Model

So far, the model has been applied to three different types of system:

i) n-Alkane/Urea Inclusion Compounds

The inclusion compound formed between hexadecane and urea was one of the first urea inclusion compounds to be examined after their discovery [3]. Initially, it was believed that this compound was commensurate with one hexadecane guest molecule to two periods of the host along the tunnel axis (i.e. $c_g = 2c_h$). More recent experimental work has shown that the guest periodicity ($c_g = 22.6$ Å) is, in fact, significantly longer than two host repeat lengths ($2c_h \approx 22.0$ Å). Experimentally, it has also been found that for the n-alkane/urea inclusion compounds the guest periodicity c_g is *ca.* $\frac{1}{2}$ Å shorter than the expected length of an n-alkane molecule in its extended all-trans conformation. While this shortening has previously been attributed to coiling or tilting of the guest molecules within the urea tunnel structure [4], it has also been suggested that this may be due to the guest molecules residing in a repulsive environment with respect to each other [2,5,6].

Applying the model to the hexadecane/urea system, along with urea inclusion compounds containing other n-alkane guest molecules, enables us to obtain theoretical proof of these observations, and also to determine if any of the other compounds in this series are predicted to show commensurate or incommensurate behaviour.

ii) The Chlorocyclohexane/Thiourea Inclusion Compound

The chlorocyclohexane/thiourea inclusion compound represents a classic example of a molecule (chlorocyclohexane) being constrained to behave differently within a solid host structure from the way it behaves in its "pure" solid phase or in dispersed phases.

In the liquid and vapour phases there is an excess of the equatorial conformation [7–9]; in the solid state at sufficiently low temperature or high pressure it exists only in the equatorial conformation [10]. However, when included within the thiourea host tunnel structure, chlorocyclohexane exists predominantly as the axial conformation – these results (and similar findings for bromocyclohexane/thiourea and iodocyclohexane/thiourea) have been established from infrared [11,12], Raman [13] and high-resolution solid state ^{13}C NMR [14–16] techniques.

Application of the model enables us to rationalise this unusual conformational behaviour of chlorocyclohexane within the thiourea tunnel structure.

iii) Dimethylketone/Urea Inclusion Compounds

X-ray diffraction studies carried out on the series of urea inclusion compounds containing the symmetric dimethylketone guests molecules [$CH_3CO(CH_2)_rCOCH_3$; r = 4–9] has suggested that, in many cases, a commensurate relationship exists between the host and guest substructures along the tunnel axis [17].

Application of the mathematical model to this series of compounds was carried out to serve as a further test of the model, to see if this property was predicted theoretically.

4.5 n-Alkane/Urea Inclusion Compounds

4.5.1 Computation of Potential Energy Functions for n-Alkane/Urea Inclusion Compounds

We now consider the actual approach that we have used to compute the potential energy functions for host-guest interaction ($E_h(t)$), for guest-guest interaction ($\hat{E}_{guest}(\alpha)$) and for the intramolecular potential energy of the guest molecules ($\hat{E}_{intra}$), that are required in order to construct characteristic energy diagrams for the n-alkane/urea inclusion compounds.

The host (urea) structure used in our calculation of $E_h(t)$ was constructed from the

crystallographic data for hexadecane/urea given in ref. 18 [note that it was not possible to refine the positions of the urea H atoms in a satisfactory manner from these X-ray diffraction data, and, for our calculations, H atoms were added to the refined positions of the urea O, C and N atoms in positions which generate a standard geometry for the $-NH_2$ group.] For the n-alkane guests with $r \leq 18$, the host structure used in the calculation comprised 288 crystallographic unit cells ($6a_h \times 6b_h \times 8c_h$). An n-alkane molecule, constructed using standard bond lengths and angles [19–22] and assuming a planar, all-trans conformation, was positioned in the central tunnel of the host structure with the long axis of this guest molecule parallel to the tunnel axis, c_h. The potential energy for host-guest interaction with the guest molecule at position tc_h (t denoting the scaled coordinate of the centre of mass) along the tunnel axis, and at rotation angle ϕ (defined in Fig. 4.3), was calculated using the following summation:

$$E_{hg}(tc_h,\phi) = \sum_{i=1}^{H} \sum_{j=1}^{G} \delta_{ij}(r_c)\left[-A_{ij}(r_{ij})^{-6} + B_{ij}(r_{ij})^{-12} + Cq_iq_j(r_{ij})^{-1}\right] \quad \text{Eq. 4.16}$$

where: (i) there are G atomic "interaction sites" in the guest molecule and H atomic "interaction sites" within the host structure; (ii) $\delta_{ij}(r_c) = 0$ if the distance between the centres of mass of the molecules containing atoms i and j is greater than the cut-off distance r_c, and $\delta_{ij}(r_c) = 1$ if the distance between the centres of mass of the molecules containing atoms i and j is less than or equal to r_c; (iii) r_{ij} is the distance between atoms i and j; (iv) A_{ij} and B_{ij} are Lennard-Jones parameters, the values of which depend on the "type" (i.e. O, C, N or H) of atom i and the "type" (i.e. C (CH_3), C (CH_2) or H) of atom j; (v) q_i and q_j are the charges associated with atoms i and j respectively; and (vi) C is the constant which establishes the correct units for the final term in the summation.

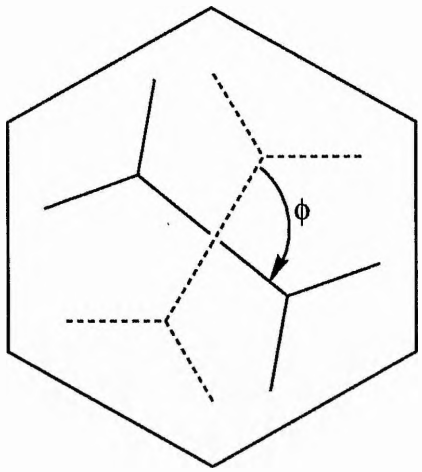

Fig. 4.3: View down the urea tunnel axis, defining the rotation angle ϕ of the n-alkane guest molecule relative to the urea tunnel structure.

The Lennard-Jones potential parameters for homoatomic atom-atom interactions and the atomic charges were taken from Table IV of ref. 23; the Lennard-Jones parameters for heteroatomic interactions were derived using $A_{ij} = \sqrt{A_{ii}A_{jj}}$ and $B_{ij} = \sqrt{B_{ii}B_{jj}}$. For the n-alkane guests $CH_3(CH_2)_rCH_3$ with $r \leq 18$, r_c was taken as 23 Å (justified by demonstrating that $E_{hg}(tc_h,\phi,r_c)$ converges satisfactorily for this value of r_c). $E_{hg}(tc_h,\phi)$ was computed for values of t in a net of 500 equally-spaced points in the range $[0,1-\frac{1}{500}]$, and for ϕ taking values in the net $\{0,\frac{\pi}{3},\frac{2\pi}{3},\pi,\frac{4\pi}{3},\frac{5\pi}{3}\}$ [situations in which ϕ is a multiple of $\frac{\pi}{3}$ represent energetically favourable orientations of the n-alkane molecule]. The strictly one-dimensional potential energy function $E_h(t)$ was then derived from $E_{hg}(tc_h,\phi)$ by:

$$E_h(t) = \inf_{\phi} \{E_{hg}(tc_h,\phi)\} \qquad \text{Eq. 4.17}$$

for the sampled points (tc_h,ϕ). Graphs of $E_h(t)$ versus t for the heptadecane/urea inclusion compound and the hexadecane/urea inclusion compound are shown in Figs. 4.4(a) and 4.5(a) respectively. Note that, as a consequence of our method for calculating $E_h(t)$, and the presence of a 6_1 screw axis along the host tunnel structure, the graphs of

$E_h(t)$ versus t are periodic with period $\Delta t = \frac{1}{6}$.

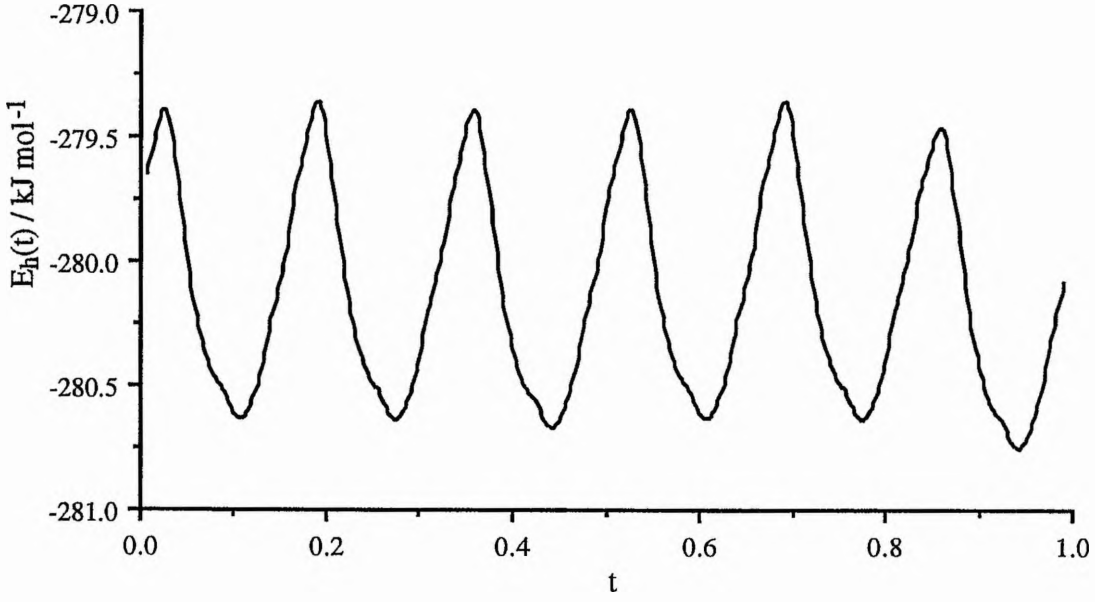

Fig. 4.4(a): Computed host-guest potential energy function $E_h(t)$ for heptadecane/urea.

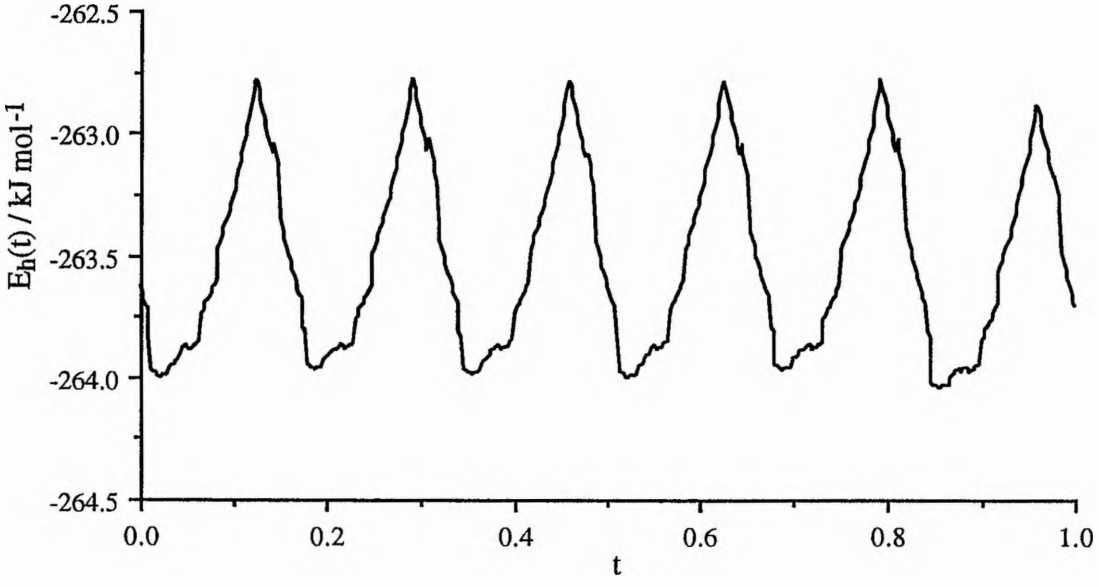

Fig. 4.5(a): Computed host-guest potential energy function $E_h(t)$ for hexadecane/urea.

For computation of $\hat{E}_{guest}(\alpha)$, a pair of n-alkane molecules in the planar, all-trans

conformation were constructed using standard molecular geometry [22] and positioned with their centres of mass separated by αc_h and their molecular axes aligned coincident with each other. Denoting the angle between the planes of the guest molecules as θ, the potential energy of guest-guest interaction was calculated, as a function of αc_h and θ, using the following summation:

$$E_{gg}(\alpha c_h,\theta) = \sum_{i=1}^{G}\sum_{j=1}^{G}\left[-A_{ij}(r_{ij})^{-6} + B_{ij}(r_{ij})^{-12}\right] \qquad \text{Eq. 4.18}$$

where: (i) there are G interaction sites (of type CH_2 or CH_3, centred on the position of the C atom) in the n-alkane molecule – these interaction sites are labelled i and j on the two molecules respectively; (ii) r_{ij} is the distance between sites i and j; (iii) A_{ij} and B_{ij} are Lennard-Jones parameters.

The Lennard-Jones parameters for interactions between sites of the same type were taken from the parameterisation for n-butane in Table III of ref. 22. The parameters for interaction between sites of different types were calculated using: $A_{ij} = \sqrt{A_{ii}A_{jj}}$; $B_{ij} = \sqrt{B_{ii}B_{jj}}$. $E_{gg}(\alpha c_h,\theta)$ was computed for a net of 150 equally-spaced values of αc_h in a range of 3 Å containing, and roughly centred on, the minimum of the curve, and for θ in the net $\{0,\frac{\pi}{3},\frac{2\pi}{3},\pi,\frac{4\pi}{3},\frac{5\pi}{3}\}$. The strictly one-dimensional potential energy function $\hat{E}_{guest}(\alpha)$ was computed from $E_{gg}(\alpha c_h,\theta)$ by:

$$\hat{E}_{guest}(\alpha) = \inf_{\theta}\{E_{gg}(\alpha c_h,\theta)\} \qquad \text{Eq. 4.19}$$

for the sampled points $(\alpha c_h,\theta)$. Graphs of $\hat{E}_{guest}(\alpha)$ versus α for heptadecane and for hexadecane are shown in Figs. 4.4(b) and 4.5(b) respectively.

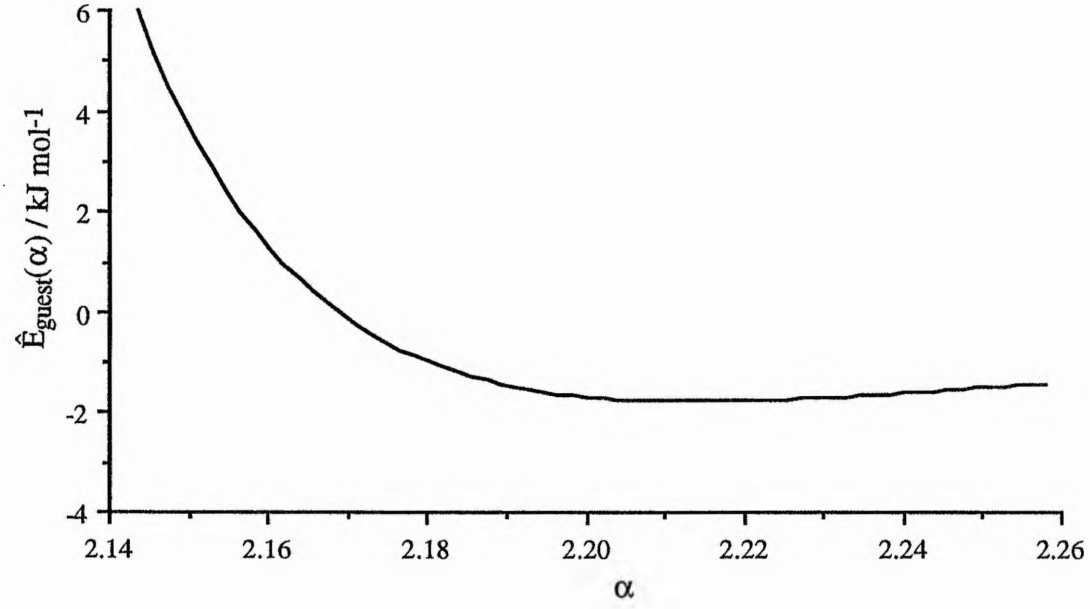

Fig. 4.4(b): Computed guest-guest potential energy function $\hat{E}_{guest}(\alpha)$ for a pair of heptadecane molecules approaching each other in the relative orientation that they are constrained to adopt inside the urea tunnel structure (see text).

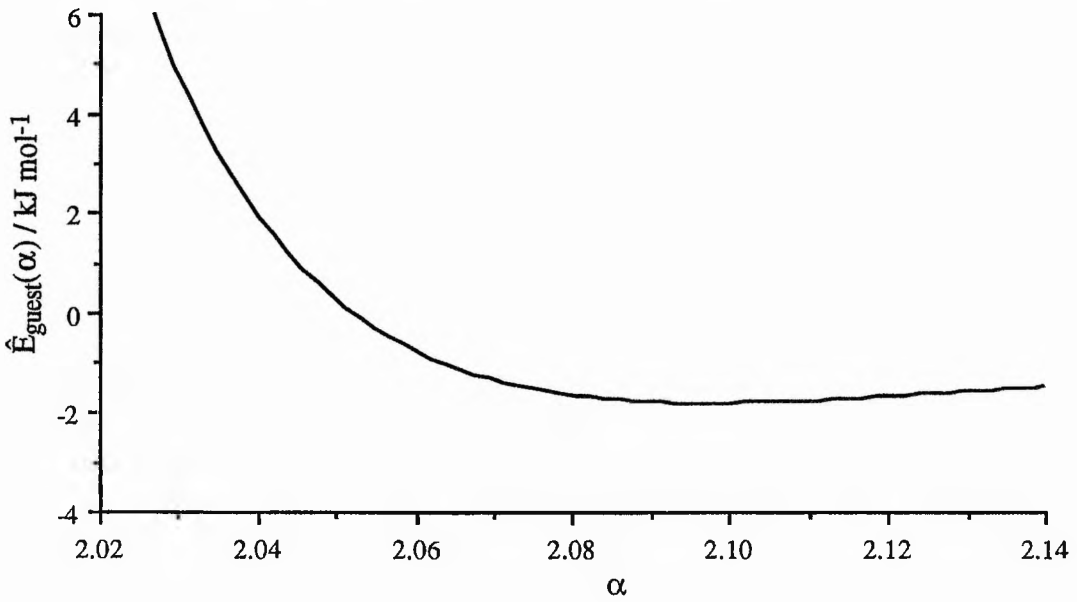

Fig. 4.5(b): Computed guest-guest potential energy function $\hat{E}_{guest}(\alpha)$ for a pair of hexadecane molecules approaching each other in the relative orientation that they are constrained to adopt inside the urea tunnel structure.

The value of $\hat{E}_{intra}$ was taken to be zero for the n-alkane molecules in the all-trans conformation.

4.5.2 Results from Application of the Mathematical Model to the n-Alkane/Urea Inclusion Compounds

The characteristic energy diagram has been constructed for each of the $CH_3(CH_2)_rCH_3$/urea inclusion compounds from r = 2 to r = 18. To assess whether these inclusion compounds exhibit commensurate behaviour, the mesh point with the lowest energy downspike has been determined in each case. Due to the generally small size of the downspikes (resulting from the small values of $\mu(d_0)$) for the n-alkane/urea inclusion compounds, only those compounds with a mesh point close to the minimum of the upper energy bound on the characteristic energy diagram need to be considered as potential commensurate systems; the guest molecules in this category were found to be those with r = 2, 12, 15 and 18. The procedure for assessing these inclusion compounds for commensurate behaviour is now discussed in detail for the case with r = 15 (heptadecane).

The function $E_h(t)$ for heptadecane/urea was represented by a Fourier series with M = 96, corresponding to a maximum residue $\sup_t |p(t) - E_h(t)| = 0.040$ kJ mol^{-1}. The energies $\mu(d)$ were calculated, and the largest values are shown in Table 4.1.

d	$\mu(d)$ / kJ mol^{-1}
1	0.63
3	0.59
2	0.59
6	0.58
4	0.14

Table 4.1: The five largest values of $\mu(d)$ for heptadecane/urea

Taking $\varepsilon' = 0.13$ kJ mol^{-1} satisfies the requirement that the maximum residue is less than $\frac{\varepsilon'}{3}$, and setting $\varepsilon = 0.27$ kJ mol^{-1} satisfies the requirement $0 < \varepsilon' < \frac{\varepsilon}{2}$. The values of $\{a_m\}$, $\{b_m\}$, ε' and M give the critical number of guest molecules N = 344 000. From the values of $\alpha_0 = \frac{p}{q}$ where $q \in \{d : \mu(d) > \varepsilon - \varepsilon'\}$ and $p \in \mathbb{Z}$, only the point $\alpha_0 = \frac{13}{6}$ [note: $\mu(6) = 0.58$ kJ mol^{-1}] requires consideration as a potential commensurate inclusion compound (i.e. having a downspike extending to sufficiently low energy). From the characteristic energy diagram [Fig. 4.4(c)], the region containing optimal α corresponds to the δ-neighbourhood of the mesh point $\alpha_0 = \frac{13}{6}$ – thus, the heptadecane/urea inclusion compound may be assigned from the characteristic energy diagram as commensurate, with optimal α in the range $\frac{13}{6} \pm \delta$. However, $\delta = \frac{1}{2M^2} \approx 0.00005$ is so small that the δ-neighbourhood is insignificant, and we assign the optimum value as $\alpha = \frac{13}{6}$. Thus, the optimum c_g is 23.87 Å (note: $c_g = \alpha c_h$). This result is conditional on the length of the tunnel in the inclusion compound being longer than $N\alpha c_h = 0.8$ mm. As required, the lengths (typically several mm) of heptadecane/urea crystals found in practice are generally longer than this, thus validating our ability to compare the results predicted from the theoretical analysis with experimental results. The energy "stabilisation" for the commensurate structure at $\alpha_0 = \frac{13}{6}$ can be assessed from the "length" $(\mu(d_0) - \varepsilon')/\alpha_0$ of the downspike at $\alpha_0 = \frac{13}{6}$ on the characteristic energy diagram, and this energy is equal to 0.21 kJ mol^{-1}. The ways in which such stabilisation energies for one-dimensional inclusion compounds should be interpreted (particularly in relation to "thermal" energies) is discussed in Section 4.8.

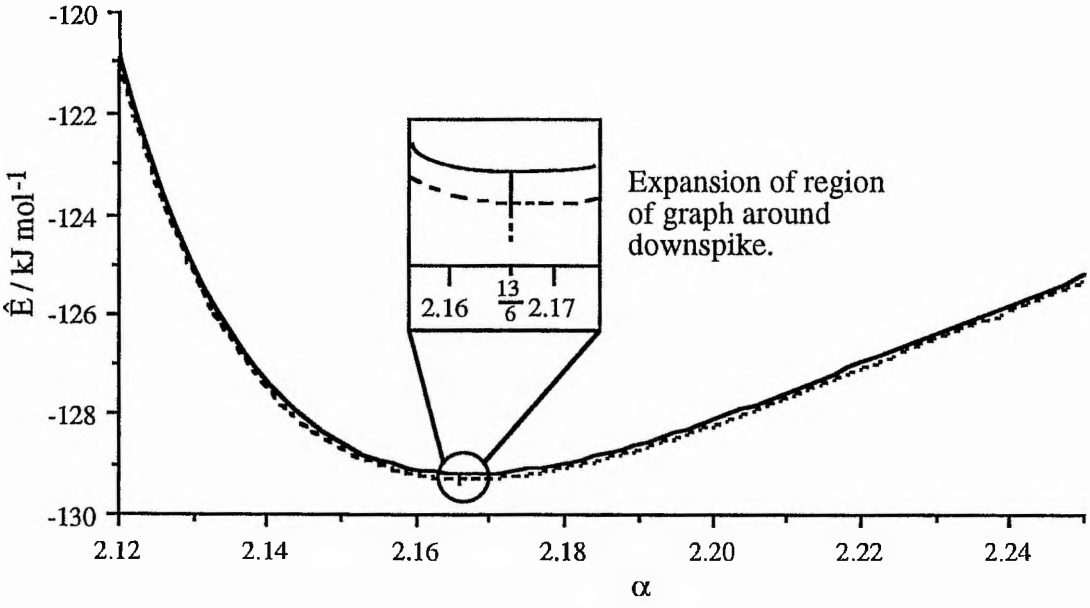

Fig. 4.4(c): The characteristic energy diagram for the heptadecane/urea inclusion compound. As shown, the optimal α is $\alpha_0 = \frac{13}{6}$ and corresponds to commensurate behaviour of the inclusion compound. As discussed in the text, the δ-neighbourhood of this mesh point α_0 is negligibly small.

The choices of M, ε' and ε are critical in the construction and interpretation of the characteristic energy diagram. For example, if M = 48 is used for heptadecane/urea, then the maximum residue $\sup_t |p(t) - E_h(t)|$ is larger (than for M = 96) and values of $\varepsilon' = 0.20$ kJ mol^{-1} and $\varepsilon = 0.42$ kJ mol^{-1} are required to satisfy the conditions on the values of ε' and ε. However, in the characteristic energy diagram constructed with these values, the downspike at $\alpha_0 = \frac{13}{6}$ does not break through the lower energy bound on the diagram, and, under these circumstances, the inclusion compound at $\alpha_0 = \frac{13}{6}$ cannot be assigned as exhibiting commensurate behaviour. Indeed, for these choices of ε' and ε, we cannot assign the optimal α as $\frac{13}{6}$, but we can only deduce that optimal α will lie in the range $\alpha = 2.167 \pm 0.005$; for this range of α and for these choices of ε' and ε, the inclusion compound will exhibit incommensurate behaviour. This illustrates how selection of suitable values for ε' and ε can influence the interpretation of the results from the characteristic energy diagram. A discussion on the factors governing the choice of ε' and

ε and, in particular, an assessment of their physical significance is given in Section 4.8.

We now consider the other cases (r = 2, 12, 18) that were considered as potential candidates for commensurate behaviour. For r = 2 (butane), the mesh point $\alpha_0 = \frac{2}{3}$ corresponds to commensurate behaviour (for N = 35300), with $\varepsilon = 0.42$ kJ mol^{-1} and ε' = 0.2 kJ mol^{-1}. The energy "stabilisation" for this commensurate structure at $\alpha_0 = \frac{2}{3}$, assessed from the "length" $(\mu(d_0) - \varepsilon')/\alpha_0$ of the downspike at $\alpha_0 = \frac{2}{3}$ on the characteristic energy diagram, is equal to 0.99 kJ mol^{-1}. It should be noted, however, that the butane/urea inclusion compound is not known experimentally – the butane molecule is shorter than the critical minimum molecular length, established empirically, for the formation of n-alkane/urea inclusion compounds [24] (at ambient temperature).

For r = 12 and r = 18, on the other hand, the mesh points (at $\alpha_0 = \frac{11}{6}$ for r = 12 and $\alpha_0 = \frac{5}{2}$ for r = 18) corresponding to potential commensurate behaviour are on the edge of the region around the minimum of the upper energy bound, and it has not been possible to find values of ε' and ε such that the inclusion compound can be assigned unambiguously as commensurate.

Longer guest molecules (r = 28, 31, 44, 57 and 60) were also considered as potential commensurate systems, assessed on the basis of the linear c_g versus r graph (see later) determined for the guests with $r \leq 18$. Of these guest molecules, it is only for r = 28 that values of ε' and ε can be found that allow the inclusion compound to be assigned from the characteristic energy diagram as commensurate ($\alpha_0 = \frac{11}{3}$). [In computing $E_h(t)$ and $\hat{E}_{guest}(\alpha)$ for these inclusion compounds, the host structure and the value of r_c were larger than those discussed in Section 4.5.1 for the compounds with $r \leq 18$.]

For all other n-alkane/urea inclusion compounds investigated, the downspikes at the mesh points were insufficient even to penetrate beneath the minimum point of the upper energy bound on the characteristic energy diagram; thus, the energy "stabilisation" at these mesh points is too small to represent commensurate behaviour, and the range containing optimal α corresponds to incommensurate behaviour. An example of this type of behaviour may be observed in Fig. 4.5(c) for hexadecane/urea. This result provides

theoretical justification that the hexadecane/urea inclusion compound is not commensurate, hence refuting suggestions based on early experimental work [3] (see above).

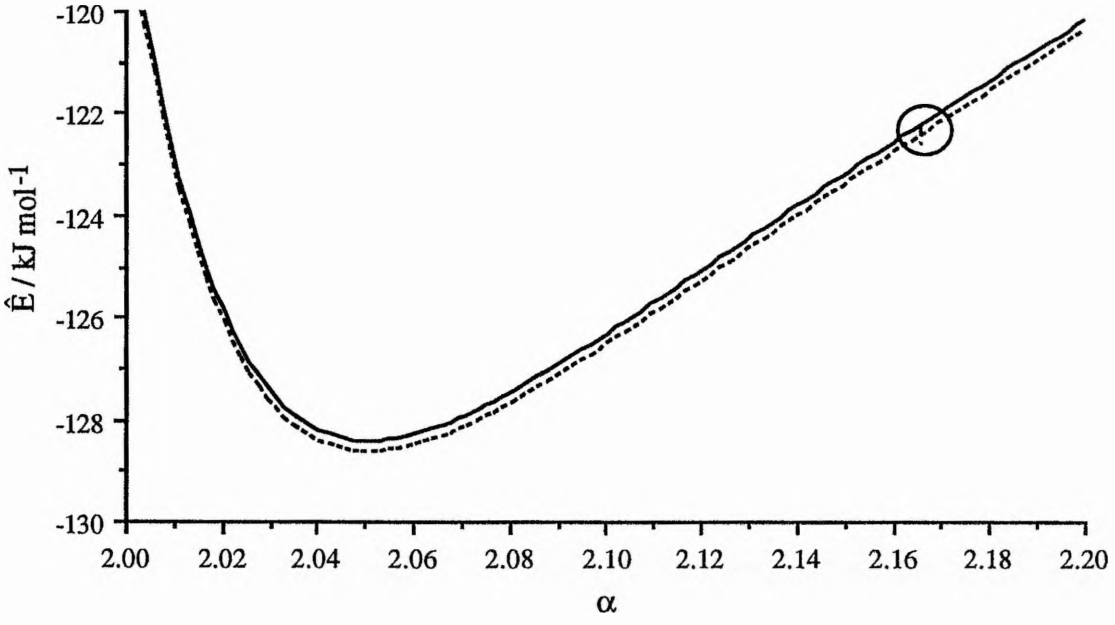

Fig. 4.5(c): The characteristic energy diagram for the hexadecane/urea inclusion compound. As shown, optimal α lie in the range α = 2.04–2.06, and correspond to incommensurate behaviour of the inclusion compound. The only significant downspike, at $\alpha_0 = \frac{13}{6}$ (circled), is shown on the characteristic energy diagram, but clearly does not correspond to optimal α.

In the characteristic energy diagrams for n-alkane/urea inclusion compounds, the lengths of the downspikes at potential commensurate values of α_0 are generally very small, and is a direct consequence of the fact that the host-guest interaction energy ($E_h(t)$) is rather insensitive to the actual position (t) of the n-alkane molecule along the tunnel [see Figs. 4.4(a) and 4.5(a) – in each case, the fluctuation in $E_h(t)$ as t is varied is less than *ca.* 1 % of the mean value of $E_h(t)$]. As discussed in Section 4.8, the behaviour of other families of one-dimensional inclusion compound is expected be significantly different in

this regard.

The optimal guest periodicities derived from the characteristic energy diagrams for the n-alkane/urea inclusion compounds with r = 2–18 are tabulated in Table 4.2, and these results are compared with the experimental data in Section 4.5.3.

Guest Molecule	Optimal α	c_g / Å	$N\alpha c_h$ / mm
butane (C_4H_{10})	0.6667 ($\frac{2}{3}$)	7.34	0.03
pentane (C_5H_{12})	0.78 – 0.80	8.73 ± 0.1	0.03
hexane (C_6H_{14})	0.89 – 0.91	9.93 ± 0.1	0.02
heptane (C_7H_{16})	1.01 – 1.03	11.23 ± 0.1	0.02
octane (C_8H_{18})	1.12 – 1.14	12.46 ± 0.1	0.02
nonane (C_9H_{20})	1.24 – 1.26	13.77 ± 0.1	0.03
decane ($C_{10}H_{22}$)	1.35 – 1.37	14.98 ± 0.1	0.06
undecane ($C_{11}H_{24}$)	1.47 – 1.49	16.31 ± 0.1	0.04
dodecane ($C_{12}H_{26}$)	1.58 – 1.60	17.52 ± 0.1	0.03
tridecane ($C_{13}H_{28}$)	1.70 – 1.72	18.84 ± 0.1	0.03
tetradecane ($C_{14}H_{30}$)	1.81 – 1.83	20.05 ± 0.1	0.61
pentadecane ($C_{15}H_{32}$)	1.93 – 1.95	21.37 ± 0.1	0.08
hexadecane ($C_{16}H_{34}$)	2.04 – 2.06	22.59 ± 0.1	0.05
heptadecane ($C_{17}H_{36}$)	2.1667 ($\frac{13}{6}$)	23.87	0.82
octadecane ($C_{18}H_{38}$)	2.27 – 2.29	25.12 ± 0.1	0.30
nonadecane ($C_{19}H_{40}$)	2.39 – 2.41	26.44 ± 0.1	0.36
eicosane ($C_{20}H_{42}$)	2.50 – 2.52	27.65 ± 0.1	0.45

Table 4.2: Guest periodicities (c_g) for n-alkane/urea inclusion compounds predicted from their characteristic energy diagrams. The reported results from the theoretical analysis are conditional on the length of the host tunnel being longer than $N\alpha c_h$.

The theoretically predicted guest periodicities (c_g) for the incommensurate n-alkane/urea inclusion compounds lie on a straight line when graphed against the number (r) of CH_2 groups in the n-alkane [see Fig. 4.6]. This provides direct confirmation of the theoretical result, derived from the mathematical model and proved formally elsewhere [5], that for the incommensurate n-alkane/urea inclusion compounds, the relationship between c_g and r becomes linear in the limit of sufficiently large r. [Here, "sufficiently large r" is such that $r \geq 2$].

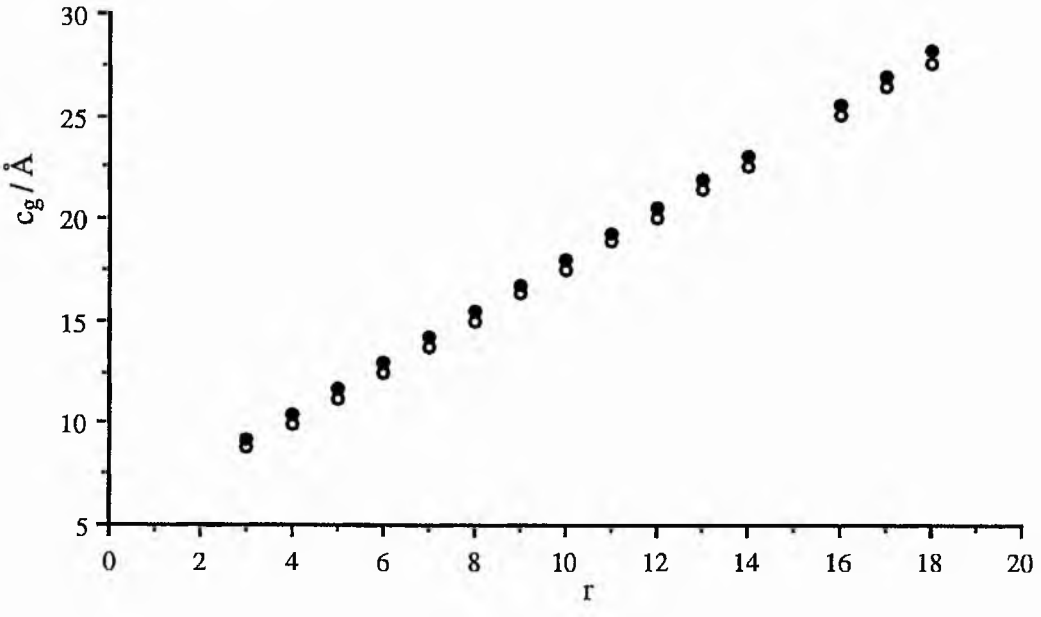

Fig. 4.6: Graphs of optimal c_g (○) versus r and the value of c_g which minimises $\hat{E}_{guest}$ (●) versus r, for incommensurate n-alkane/urea inclusion compounds. In each case, the optimal c_g has been determined from the centre of the range of optimal α (see Table 4.2) on the characteristic energy diagram. The best-fit straight line for optimal c_g versus r is: $c_g/Å = 1.26\ r + 4.90$. The best-fit straight line for the value of c_g which minimises $\hat{E}_{guest}$ versus r is: $c_g/Å = 1.27\ r + 5.38$. Note that the intercept of the line for optimal c_g is *ca.* 0.5 Å lower than the intercept of the line for the value of c_g which minimises $\hat{E}_{guest}$.

From the data shown in Fig. 4.6, the relationship between c_g and r is essentially linear over the range of r investigated, with: $c_g/\text{Å} = 1.26\ r + 4.90$. This linear relationship between c_g and r is not, in fact, "disrupted" by the occurrence of the potentially commensurate inclusion compound (heptadecane/urea) at r = 15, because c_g for this system lies very close to the value (c_g = 23.87 Å) predicted from the above linear relationship (for incommensurate systems). Indeed, for the n-alkane/urea inclusion compounds, it appears that the residues $\mu(d)$ are sufficiently small that no structure will be commensurate unless the mesh point α_0 is very close to the minimum of the upper energy bound on the characteristic energy diagram (and hence very close to the range that would contain optimal α if the inclusion compound were to exhibit incommensurate behaviour).

4.5.3 Comparison of Theoretically Predicted and Experimentally Determined Guest Periodicities

The theoretically predicted values of c_g (Table 4.2) agree well with the experimental values (Table 2.1 in Chapter 2), vindicating the applicability of our theoretical approach and supporting the choice of potential energy parameterisation used in this work. In all cases (both theoretical and experimental), the optimum c_g is *ca.* 0.5 Å shorter than the value of c_g corresponding to the minimum of the guest-guest potential energy curve ($\hat{E}_{guest}(\alpha)$ versus α) – thus, the optimum c_g corresponds to a repulsive interaction between adjacent guest molecules in the tunnel. This agrees with previous suggestions [2,5,6], and arises directly from the requirement to determine the guest periodicity which minimises the characteristic energy of the inclusion compound (rather than to determine the guest periodicity which minimises the total energy per guest molecule). The existence, for the n-alkane/urea inclusion compounds, of this approximate 0.5 Å discrepancy between the optimal c_g determined from the characteristic energy diagram and the value of c_g corresponding to the minimum of the function $\hat{E}_{guest}(\alpha)$ is readily apparent from Fig. 4.6.

The graph of optimum c_g versus r [Fig. 4.6] for the incommensurate n-

alkane/urea inclusion compounds is essentially linear over the range of r investigated, with $c_g/Å = 1.26\ r + 4.90$. This is very similar to the equation ($c_g/Å = 1.26\ (r+2) + 2.48 = 1.26\ r + 5.00$) derived from X-ray diffraction data by Laves *et al* [4].

4.6 Chlorocyclohexane/Thiourea Inclusion Compound

In this study, the intention was to rationalise the unusual conformational behaviour of chlorocyclohexane within the thiourea tunnel structure by applying the mathematical model developed to predict and rationalise structural properties of real one-dimensional inclusion compounds.

While it is clear that $\hat{E}_{intra}$ will depend critically on the conformation of the guest molecules, it is important to stress that $\hat{E}_{guest}(\alpha)$ and $E_h(t)$ will also depend on the conformation of the guest molecules. Hence, in order to assess the relative energetic favourability of two different conformations of a given guest molecule within the inclusion compound (such as comparing the axial and equatorial conformations of chlorocyclohexane discussed here) it is necessary to compare the characteristic energy at optimal α for one conformation of the guest with the characteristic energy at optimal α for the other conformation of the guest.

4.6.1 Computation of Potential Energy Functions for the Chlorocyclohexane/Thiourea Inclusion Compound

The potential energy functions $E_h(t)$, $\hat{E}_{guest}(\alpha)$ and $\hat{E}_{intra}$ for *axial*-chlorocyclohexane/thiourea and *equatorial*-chlorocyclohexane/thiourea were calculated using the CHEM-X program package [25]. The host structure used in the calculation of $E_h(t)$ was the known crystal structure of the thiourea host in the chlorocyclohexane/thiourea inclusion compound [26]. Again, hydrogen atoms were not located, and were added in positions to give a standard geometry for the $-NH_2$ groups. Chlorocyclohexane guest molecules were constructed in the axial and equatorial conformations using standard bond lengths and angles, and assuming the chair conformation for the cyclohexane ring.

The potential energy parameterisation used to compute $E_h(t)$, $\hat{E}_{guest}(\alpha)$ and $\hat{E}_{intra}$ was that of Del Re *et al* [27], and this parameterisation was not specifically adapted or optimised for the particular system under investigation. However, the excellent agreement between the theoretical predictions reported here and the known experimental information provides some justification for the suitability of this potential energy parameterisation for chlorocyclohexane/thiourea.

The orientation of the guest molecule in the calculation of $E_h(t)$ and $\hat{E}_{guest}(\alpha)$ was selected such that the 3-fold axis of the cyclohexane ring was parallel to the tunnel axis for the axial conformation [Fig. 4.7(a)]; for the equatorial conformation of the guest, the 3-fold axis of the cyclohexane ring was oriented perpendicular to the tunnel axis [Fig. 4.7(b)]. For both conformations, the 3-fold axis of the cyclohexane ring of the chlorocyclohexane molecule was placed on the tunnel axis.

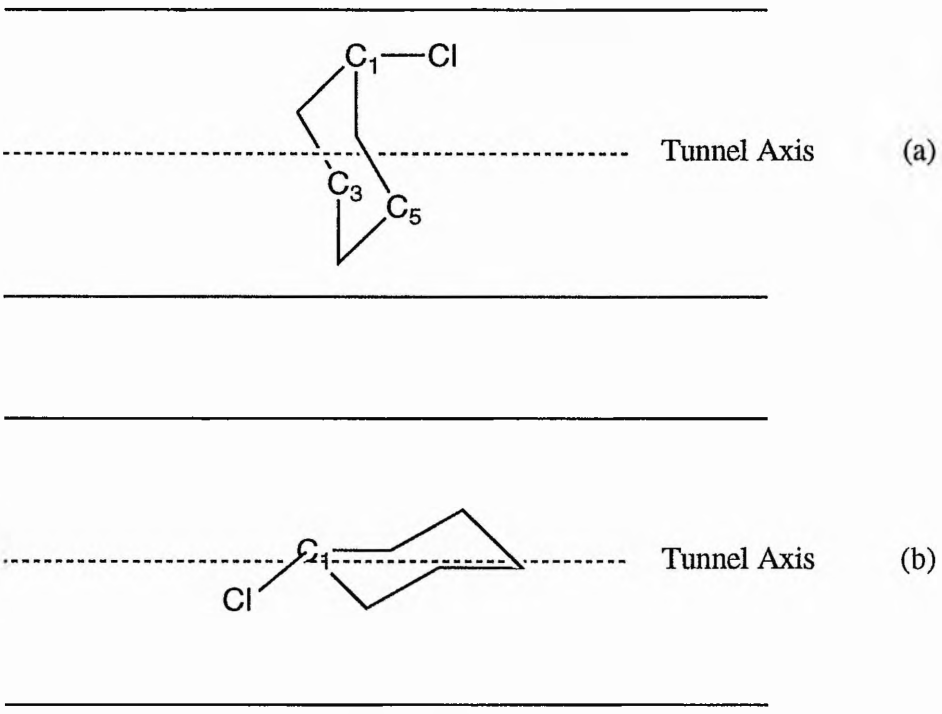

Fig. 4.7: Diagram showing the orientation of the chlorocyclohexane guest molecule in the thiourea tunnel structure, used in the calculation of $E_h(t)$, for (a) *axial*-chlorocyclohexane/thiourea, and (b) *equatorial*-chlorocyclohexane/thiourea.

$E_{hg}(tc_h,\phi)$, for each guest conformation, was computed for 180 equally spaced values of t in the range $[0, 1-\frac{1}{180}]$, and for ϕ taking values $\{0,\frac{\pi}{3},\frac{2\pi}{3},\pi,\frac{4\pi}{3},\frac{5\pi}{3}\}$. The one dimensional function, $E_h(t)$, was obtained from $E_{hg}(tc_h,\phi)$ by considering, for each value of t, the value of ϕ giving rise to the lowest E_{hg}. Similarly, $E_{gg}(\alpha c_h,\theta)$ was obtained for 150 equally spaced values of αc_h and θ taking values $\{0,\frac{\pi}{3},\frac{2\pi}{3},\pi,\frac{4\pi}{3},\frac{5\pi}{3}\}$, and reduced to the one-dimensional form $\hat{E}_{guest}(\alpha)$ for both the axial and equatorial conformations of the guest.

While the experimental studies have shown that the chlorocyclohexane molecules are predominantly in the axial conformation, there is a proportion of the equatorial conformation present [15]. The application of the model assumes that all chlorocyclohexane guest molecules are in the same conformation within the thiourea tunnel. Futhermore, in the calculation of $E_{gg}(\alpha c_h,\theta)$ only rotation about the 3-fold axis of the cyclohexane ring was allowed for the orientation of one guest relative to the next. In practice, reorientation of the chlorocyclohexane molecule can also occur about an axis perpendicular to the tunnel axis.

$\hat{E}_{intra}$ was calculated for an isolated guest molecule of each conformation. For use in the mathematical model, $\hat{E}_{intra}$ for the lower energy equatorial conformation was taken to be zero, and the value of $\hat{E}_{intra}$ for the axial conformation was taken relative to this.

4.6.2 Results from Application of the Mathematical Model to the Chlorocyclohexane/Thiourea Inclusion Compound

Characteristic energy diagrams [Fig. 4.8] for *axial*-chlorocyclohexane/thiourea and *equatorial*-chlorocyclohexane/thiourea inclusion compounds were constructed using the computed potential energy functions $E_h(t)$, $\hat{E}_{guest}(\alpha)$, and $\hat{E}_{intra}$ by following the methods developed previously (Section 4.3). In construction of the characteristic energy diagrams, selection of ε = 10.5 kJ mol^{-1} and ε' = 4.2 kJ mol^{-1} satisfied the required conditions on ε and ε' (Note: it is important to select the same values of ε and ε' for the characteristic energy diagrams for both the conformations of the chlorocyclohexane

guest, so that the results can be compared directly). These values give the critical number of guest molecules as $N \approx 831000$, for it to be valid to relate the results from the characteristic energy diagram with the properties of the real inclusion compounds. In constructing the characteristic energy diagram, values of $\hat{E}_{intra}$ were taken relative to the intramolecular potential energy of the isolated *equatorial*-chlorocyclohexane molecule. This gave $\hat{E}_{intra} = +5.76$ kJ mol^{-1} for the *axial*-chlorocyclohexane molecule.

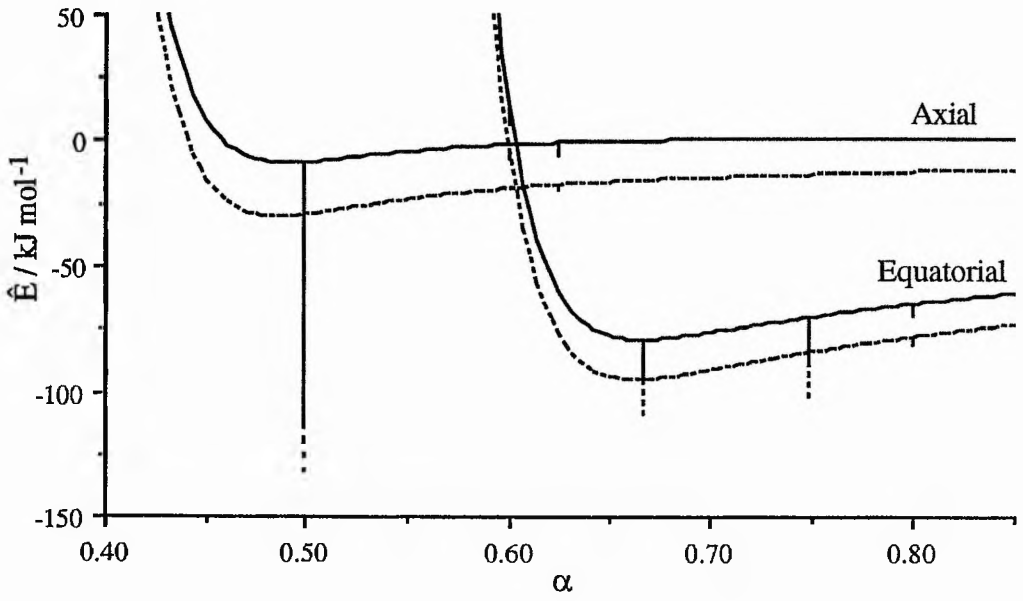

Fig. 4.8: Characteristic energy diagrams for *axial*-chlorocyclohexane/thiourea and *equatorial*-chlorocyclohexane/thiourea. The lowest point on the two characteristic energy diagrams corresponds to the "downspike" at $\alpha = \frac{1}{2}$ for *axial*-chlorocyclohexane/thiourea. At this value of α, the *axial*-chlorocyclohexane/thiourea inclusion compound exhibits commensurate behaviour.

In the characteristic energy diagram for *axial*-chlorocyclohexane/thiourea, downspikes were significant at $\alpha = \frac{1}{2}$ and $\frac{5}{8}$. Optimal α for the axial conformation corresponds to the large "downspike" at $\alpha = \frac{1}{2}$, and represents commensurate behaviour of the inclusion compound. The δ-neighbourhood associated with this point is $\delta \approx 10^{-4}$, which is negligibly small. The results of the theoretical analysis are conditional on the

tunnel length being greater than $N\alpha c_h$ = 0.52 mm – as required, this is shorter than the tunnel lengths found in practice (typically *ca.* 2 mm for a single crystal of the inclusion compound). The energy stabilisation (giving rise to "lock in" of host and guest structures) for *axial*-chlorocyclohexane/thiourea at $\alpha = \frac{1}{2}$ is 107.5 kJ mol^{-1}, determined from the magnitude of the downspike at $\alpha = \frac{1}{2}$.

For the *equatorial*-chlorocyclohexane/thiourea inclusion compound, downspikes at $\alpha = \frac{3}{5}, \frac{2}{3}, \frac{3}{4}$ and $\frac{4}{5}$ require to be considered. For the chosen values of ε and ε', there are two regions of optimal α at $\alpha = \frac{2}{3}$ and $\frac{3}{4}$, corresponding to commensurate behaviour of the inclusion compound.

Considering both characteristic energy diagrams together, the optimum α for *axial*-chlorocyclohexane/thiourea corresponds to a lower characteristic energy than any value of α for *equatorial*-chlorocyclohexane/thiourea. Thus, our theoretical analysis predicts correctly the preference for the axial conformation within the thiourea tunnel structure. The optimal guest periodicity ($c_g = \alpha c_h = \frac{c_h}{2}$ = 6.24 Å) predicted for *axial*-chlorocyclohexane/thiourea is in good agreement with information inferred (but not proved) from X-ray diffraction data [26]. It is interesting to note that the minimum of the function $\hat{E}_{guest}(\alpha)$ for a pair of chlorocyclohexane molecules in the axial conformation and approaching each other in the manner that they are constrained to approach within the thiourea tunnel structure corresponds to c_g = 5.95 Å [Fig. 4.9]. This is in contrast to the situation for the n-alkane/urea inclusion compounds discussed above (Section 4.5.3) for which the value of c_g for the inclusion compound is *ca.* 0.5 Å shorter than that corresponding to the minimum of $\hat{E}_{guest}(\alpha)$.

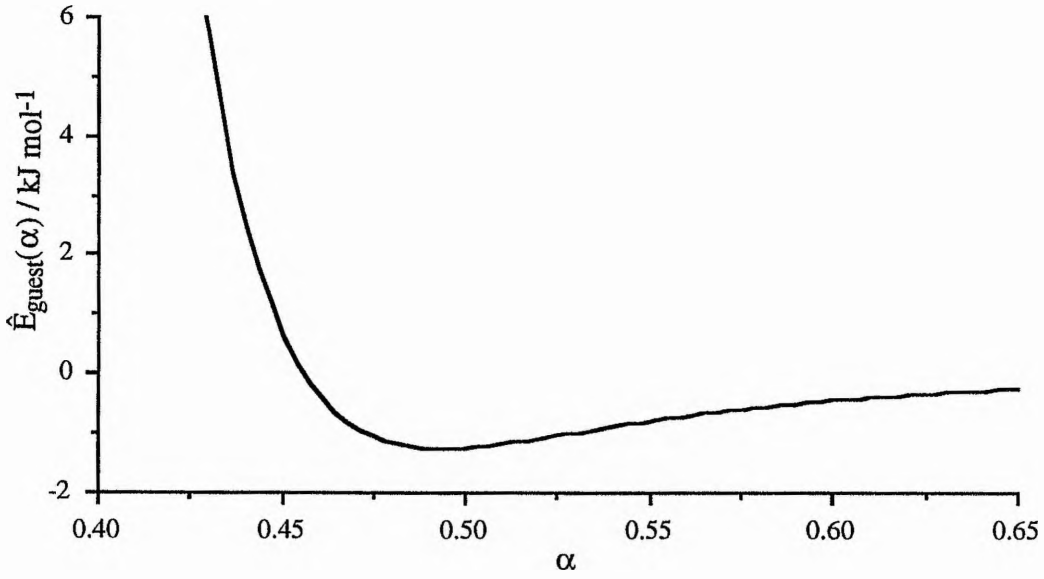

Fig. 4.9: Computed guest-guest potential energy function $\hat{E}_{guest}(\alpha)$ for a pair of *axial*-chlorocyclohexane molecules approaching each other in the relative orientation that they are constrained to approach inside the thiourea tunnel structure.

From consideration of these results we can understand more fully the energetic reasons underlying the preference for the axial conformation of chlorocyclohexane in the thiourea tunnel structure.

Equatorial-chlorocyclohexane has a more negative $\hat{E}_{intra}$ than *axial*-chlorocyclohexane, and the observed preference for the axial conformation in the thiourea tunnel structure requires that other factors are sufficient to outweigh the influence of $\hat{E}_{intra}$. From the results of the present study, the major factors to consider are $E_h(t)$ and the $\frac{1}{\alpha}$ term in the expression for $\hat{E}(\alpha,n)$.

For *equatorial*-chlorocyclohexane/thiourea the computed function $E_h(t)$ is relatively insensitive to the position of the guest molecule along the tunnel, whereas for *axial*-chlorocyclohexane/thiourea $E_h(t)$ contains significant fluctuations [Figs. 4.10(a) & 4.10(b)]. Furthermore, although the average $E_h(t)$ is higher for *axial*-chlorocyclohexane/thiourea, there are specific sites for *axial*-chlorocyclohexane in the thiourea tunnel at which $E_h(t)$ is very favourable, and more negative than for any position

of *equatorial*-chlorocyclohexane in the thiourea tunnel. Thus, a commensurate guest structure for *axial*-chlorocyclohexane/thiourea in which only these sites corresponding to minimum $E_h(t)$ are occupied should be particularly favourable.

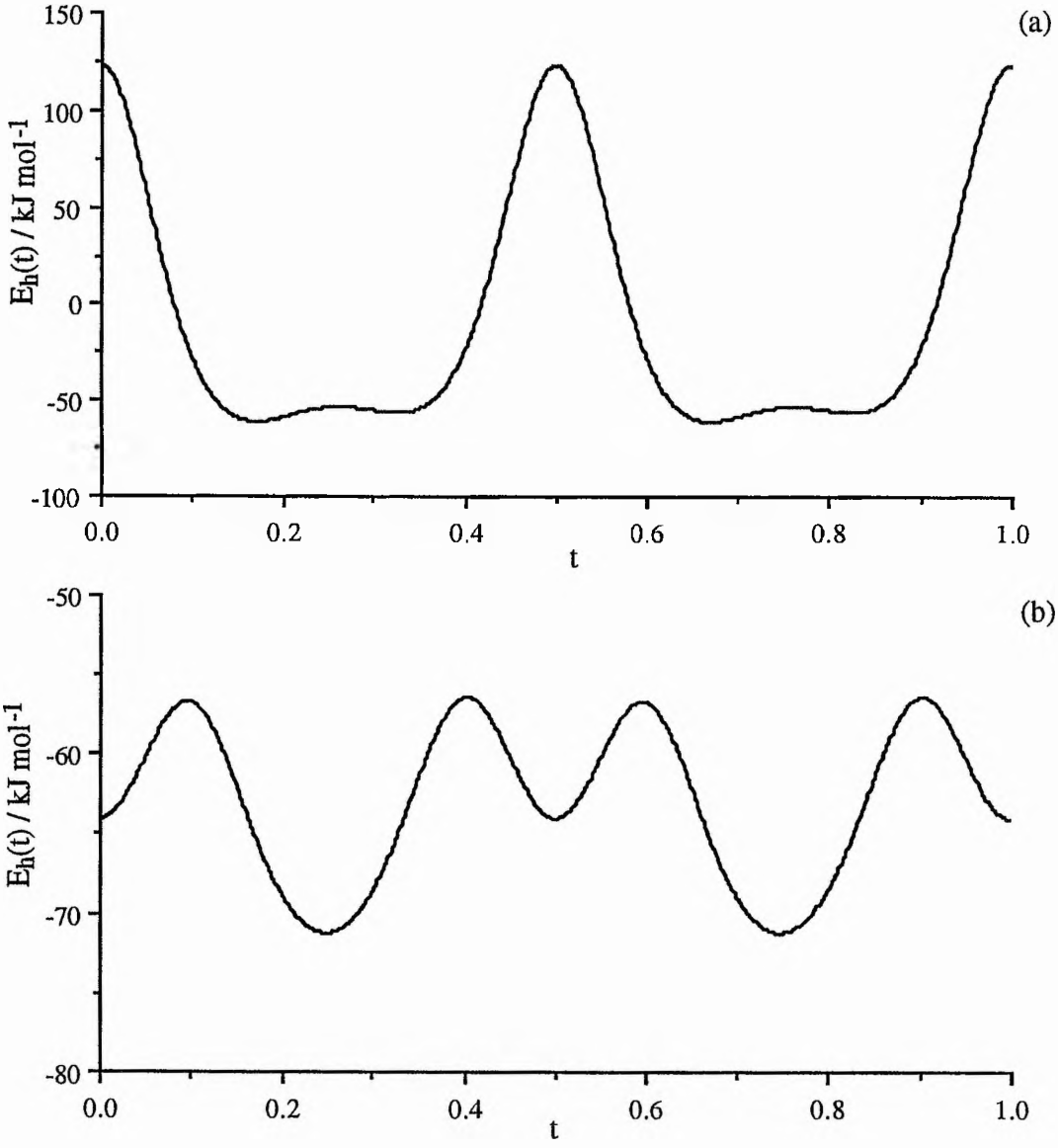

Fig. 4.10: Computed host-guest potential energy function $E_h(t)$ for (a) *axial*-chlorocyclohexane/thiourea, and (b) *equatorial*-chlorocyclohexane/thiourea.

Furthermore, *axial*-chlorocyclohexane can be packed much more efficiently (smaller α) within the constrained environment of the thiourea tunnel than can *equatorial*-

chlorocyclohexane; this fact contributes to the more favourable characteristic energy (energy per unit length of tunnel) for the axial conformation, as a consequence of the factor $\frac{1}{\alpha}$ in the expression for the characteristic energy [this factor ensures that the characteristic energy refers to an energy per unit length of host tunnel rather than an energy per guest molecule].

Within the level of approximation in the theoretical approach employed here, the results provide a clear and rigorous rationalisation of the unusual conformational properties of chlorocyclohexane guest molecules within the thiourea tunnel structure. The analysis provides theoretical justification for the observation that the preferred conformation of chlorocyclohexane within the thiourea tunnel structure is the axial conformation, and confirms that the optimum periodicity of the guest molecules along the tunnel is commensurate with the thiourea host structure.

This study is currently being expanded to examine other monosubstituted cyclohexane guest molecules in their urea inclusion compounds [28]. For larger substituents on the cyclohexane ring, fixing the guest molecule in the same orientation as used for the chlorocyclohexane molecule above was found to result in a repulsive interaction between the substituent and the host structure. Hence, in addition to translation of the guest molecules along the tunnel axis, the 3-fold axis of the cyclohexane ring has been allowed to move perpendicular to the tunnel axis, and the guest allowed to rotate about an axis perpendicular to the tunnel axis. Monte Carlo methods are being used to find the minimum energy at each interval along the tunnel axis.

4.7 Dimethylketone/Urea Inclusion Compounds

4.7.1 Computation of Potential Energy Functions for Dimethylketone/Urea Inclusion Compounds

The potential energy functions $E_h(t)$, $\hat{E}_{guest}(\alpha)$ and $\hat{E}_{intra}$ for urea inclusion compounds with symmetric dimethylketone guests [$CH_3CO(CH_2)_rCOCH_3$; r = 4–9], were calculated using the INSIGHT program package [29]. The potential energy

parameterisation used in the generation of these functions was the Consistent Valence Forcefield (CVFF). The host structure was the same as that used for the n-alkane/urea inclusion compounds, namely the room temperature host structure of hexadecane/urea (see Section 4.5.1). The dimethylketone guest molecules were constructed using standard bond lengths and angles, in the all-trans conformation, with the carbonyl groups oriented such that the C=O bond was in the same plane as the all-trans alkyl backbone. No energy minimisation of the isolated guest molecules was carried out.

For calculation of $E_{hg}(tc_h,\phi)$, a single guest molecule was placed with its centre of mass at the centre of the urea host tunnel and aligned such that its long axis was parallel to the tunnel axis. The energy was computed for 30 points in the region $t = [0, \frac{1}{6}]$ for translation of the guest molecule along the host tunnel, and through 2π in steps of $\frac{\pi}{12}$ for rotation about the tunnel axis (rotation angle denoted ϕ). $E_{hg}(tc_h,\phi)$ was reduced to the one-dimensional function $E_h(t)$ by:

$$E_h(t) = \inf_{\phi} \{E_{hg}(tc_h,\phi)\} \qquad \text{Eq. 4.20}$$

Note that it was only necessary to consider translation through $\frac{c_h}{6}$, because in reducing $E_{hg}(tc_h,\phi)$ to the one-dimensional energy term $E_h(t)$, the 6_1-screw symmetry of the host structure requires that $E_h(t)$ has period $\frac{c_h}{6}$ rather than c_h.

For computation of $\hat{E}_{guest}(\alpha)$, a pair of dimethylketone molecules in the planar, all-trans conformation were constructed and positioned with their centres of mass separated by αc_h and their molecular axes aligned coincident with each other. Keeping one molecule fixed, the other molecule was translated (variable α) along the molecular axes, rotated about the tunnel axis through the range $\theta = 0$ to 2π in steps of $\frac{\pi}{12}$, and the energy $E_{gg}(\alpha c_h,\theta)$ computed. The energy was reduced to a one-dimensional form to give the function $\hat{E}_{guest}(\alpha)$ using:

$$\hat{E}_{guest}(\alpha) = \inf_{\theta} \{E_{gg}(\alpha c_h,\theta)\} \qquad \text{Eq. 4.21}$$

For use in the mathematical model, the value of $\hat{E}_{intra}$ was taken as zero for the dimethylketone molecules in the all-trans conformation, as we are not considering changes in the conformation of the guest molecules when included within the urea host structure.

4.7.2 Results from Application of the Mathematical Model to the Dimethylketone/Urea Inclusion Compounds

The characteristic energy diagram was constructed for each of the $CH_3CO(CH_2)_rCOCH_3$/urea inclusion compounds from r = 4 to r = 9. To assess whether these inclusion compounds exhibit commensurate behaviour, the mesh points with the lowest energy downspikes were determined in each case. For all the guest molecules considered, mesh points were found for which potential commensurate lock in could occur in the region of the minimum of the upper energy bound on the characteristic energy diagram.

The function $E_h(t)$ for each inclusion compound was represented by a Fourier series with M = 36. For all compounds, the values $\varepsilon' = 0.20$ kJ mol^{-1} and $\varepsilon = 0.50$ kJ mol^{-1} satisfied the requirements that $0 < \varepsilon' < \frac{\varepsilon}{2}$ and that the maximum residue $\sup_t |p(t) - E_h(t)| < \frac{\varepsilon'}{3}$.

The largest values of $\mu(d)$ were calculated are shown in Table 4.3.

d	$\mu(d)$ / kJ mol^{-1}
1	0.86
3	0.86
2	0.86
6	0.86
4	0.14

Table 4.3: The five largest values of $\mu(d)$ for 2,9-decanedione/urea.

The values of $\{a_m\}$, $\{b_m\}$, ε' and M give N = 35400. From the values of $\alpha_0 = \frac{p}{q}$ where $q \in \{d : \mu(d) > \varepsilon - \varepsilon'\}$ and $p \in \mathbb{Z}$, only the point $\alpha_0 = \frac{3}{2}$ requires consideration as a potential commensurate inclusion compound, as this value of α_0 is closest to the minimum in the upper bound energy. From the characteristic energy diagram [Fig. 4.11], the region containing optimal α corresponds to the region bounded by the minimum point in the upper energy bound and the lower energy bound, projected onto the α axis (as shown). The energy lock in of the mesh point at $\alpha_0 = \frac{3}{2}$ is too small (0.44 kJ mol^{-1}) for this periodicity to correspond to the most stable inclusion compound. Thus, the model predicts that the 2,9-decanedione/urea inclusion compound is incommensurate, with optimal α in the range 1.39 ± 0.02. Thus, the optimum c_g is 15.31 ± 0.22 Å. This result is conditional on the length of the tunnel in the inclusion compound being longer than $N\alpha c_h = 0.06$ mm, and again this is much smaller than the actual tunnel lengths found in practice.

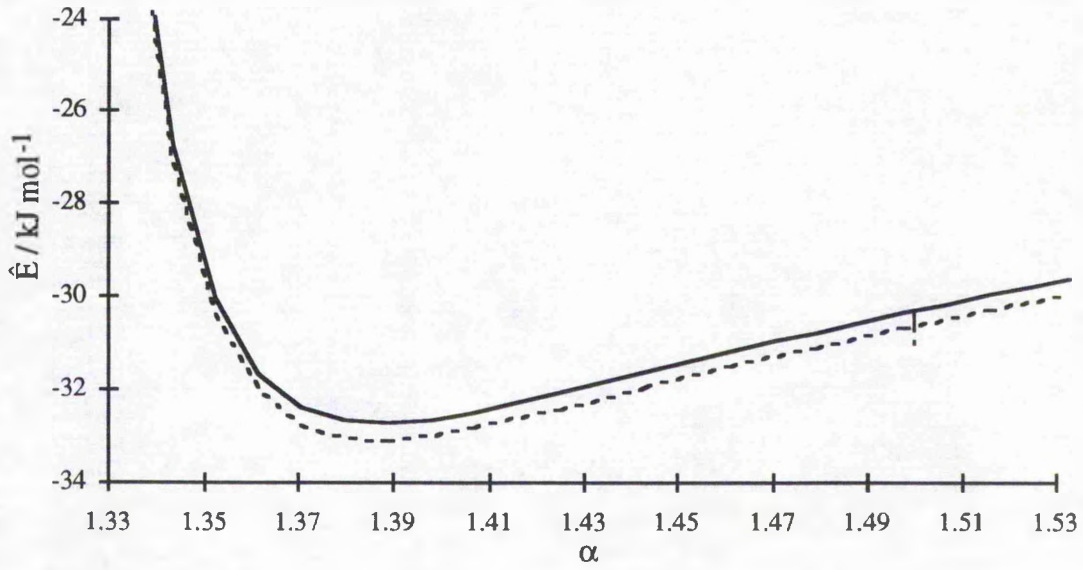

Fig. 4.11: The characteristic energy diagram for the 2,9-decanedione/urea inclusion compound. Optimal α lie in the range α = 1.37–1.41, and correspond to incommensurate behaviour of the inclusion compound.

For all the dimethylketone guests considered, only 2,10-undecanedione/urea (r = 7) was predicted to be commensurate. The characteristic energy diagram for this inclusion compound [Fig. 4.12] demonstrates that lock in of the guest substructure occurs at $\alpha_0 = \frac{3}{2}$, with an energy stabilisation of 0.56 kJ mol^{-1}. For 2,11-dodecanedione/urea (r = 8), the characteristic energy diagram [Fig. 4.13] shows two regions of optimal α. The downspike at $\alpha_0 = \frac{5}{3}$ extends below the minimum of the upper energy bound on the characteristic energy diagram, but does not extend below the minimum of the lower energy bound for $\alpha \notin (\alpha_0 - \delta, \alpha_0 + \delta)$. Thus, either the inclusion compound will exhibit commensurate behaviour with $\alpha_0 = \frac{5}{3}$ or will exhibit incommensurate behaviour with α in the range α = 1.60–1.63.

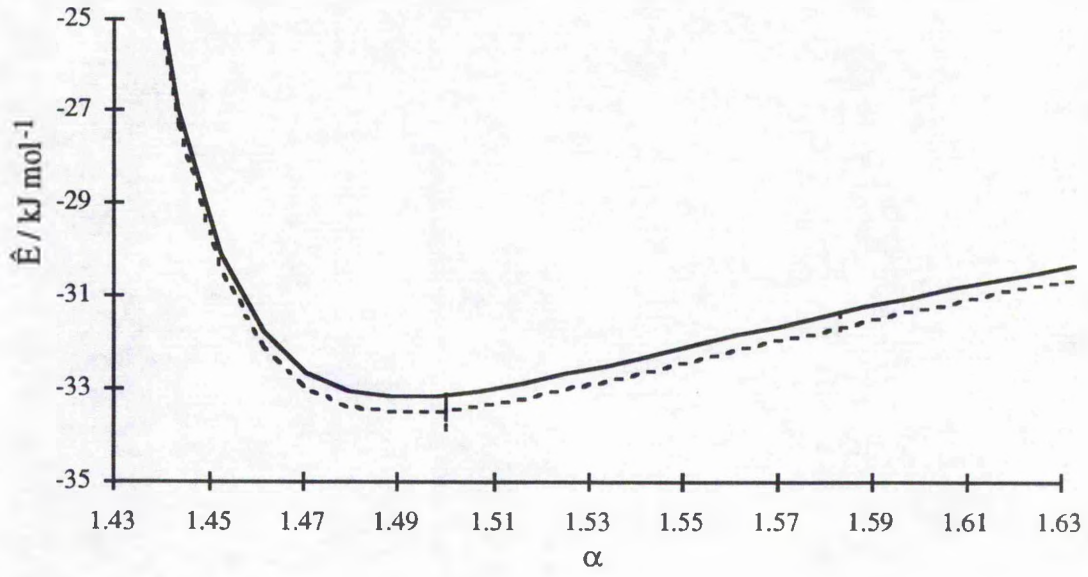

Fig. 4.12: The characteristic energy diagram for the 2,10-undecanedione/urea inclusion compound. The diagram predicts commensurate behaviour for the inclusion compound with α = 1.5 ($\frac{3}{2}$).

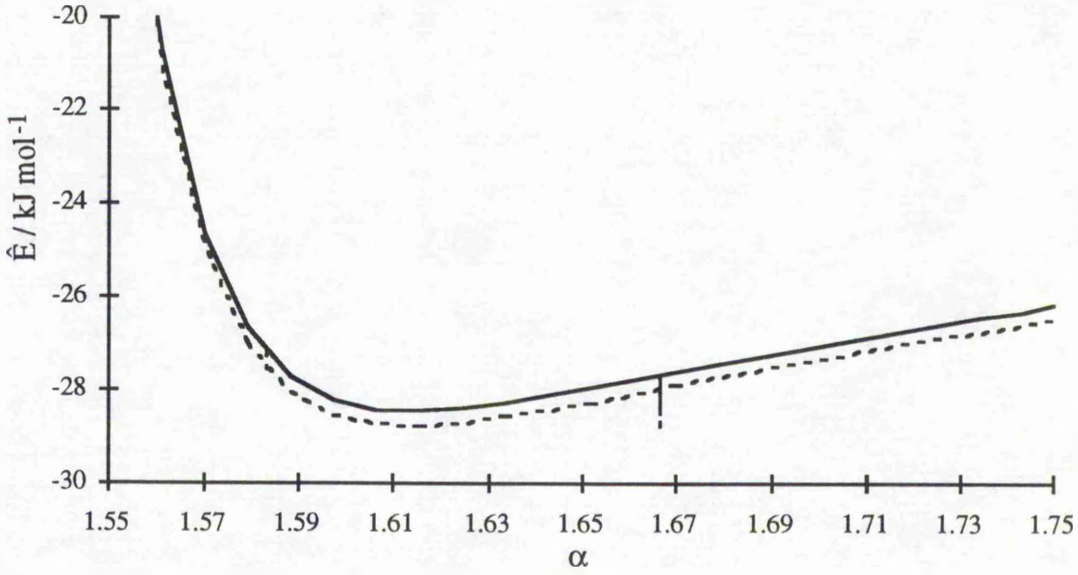

Fig. 4.13: The characteristic energy diagram for the 2,11-dodecanedione/urea inclusion compound. Optimal α lies either in the region α = 1.60–1.63 or at α = 1.667 ($\frac{5}{3}$).

For 2,7-octanedione/urea (r = 4), the characteristic energy diagram [Fig. 4.14] shows that the region of optimal α contains the downspike at $\alpha_0 = \frac{7}{6}$. However the downspike is not long enough for the δ-neighbourhood of $\alpha_0 = \frac{7}{6}$ to be assigned uniquely as the optimal A, and hence it can only be deduced that optimal α lies in the range α = 1.14–1.17. Hence, this compound is assigned as being incommensurate.

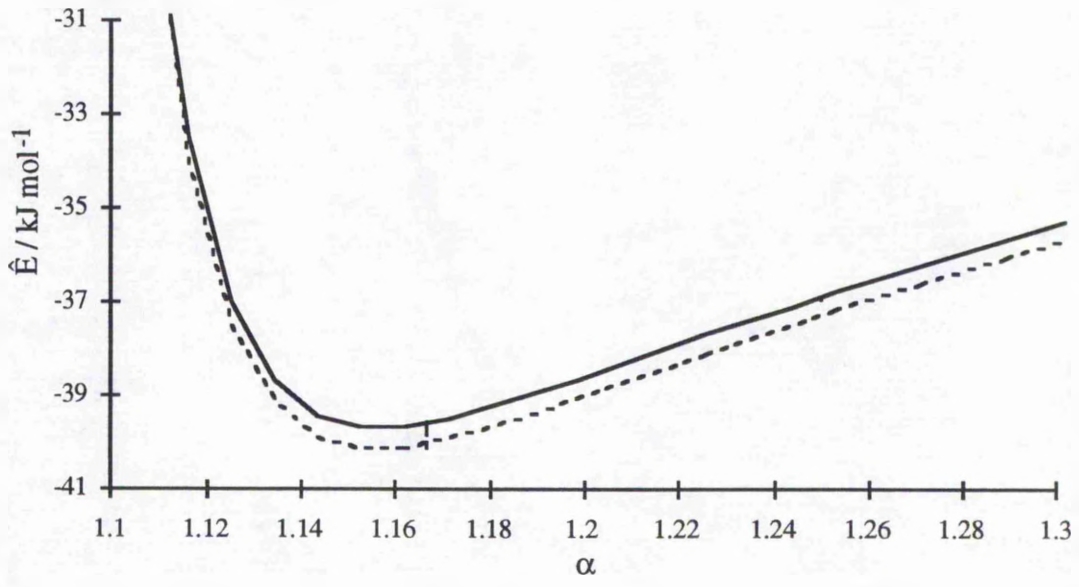

Fig. 4.14: The characteristic energy diagram for the 2,7-octanedione/urea inclusion compound. Optimal α lie in the range α = 1.14–1.17, and correspond to incommensurate behaviour of the inclusion compound. The downspike at $\alpha = \frac{7}{6}$ does not penetrate through the lower bound, and so does not represent enough stabilisation to represent an optimal α exhibiting commensurate behaviour.

The results for all the dimethylketone guests are tabulated below (Table 4.4)

Guest Molecule	Optimal α	c_g / Å	$N\alpha c_h$ / mm
2,7-octanedione	1.14 – 1.17	12.72 ± 0.17	0.02
2,8-nonanedione	1.26 – 1.30	14.10 ± 0.22	0.03
2,9-decanedione	1.37 – 1.41	15.31 ± 0.22	0.06
2,10-undecanedione	1.50 ($\frac{3}{2}$)	16.53	0.04
2,11-dodecanedione	1.60 – 1.63, 1.667 ($\frac{5}{3}$)	17.52 ± 0.17, 18.36	0.03
2,12-tridecanedione	1.70 – 1.75	27.65 ± 0.28	0.45

Table 4.4: Guest periodicities (c_g) for the dimethylketone/urea inclusion compounds, from application of the mathematical model for one-dimensional inclusion compounds.

4.7.3 Discussion of Results for the Dimethylketone/Urea Inclusion Compounds

The periodicities predicted for the dimethylketone/urea inclusion compounds do not agree with the values obtained experimentally, except in the case of 2,10-undecanedione/urea for which the structure is predicted to be commensurate with $2c_g = 3c_h$. In all the other cases, the structure could not unambiguously be assigned as commensurate. It is important to remember, however, that several assumptions were made regarding the structure of the host and the conformation of the guest molecules prior to application of the mathematical model.

First, we recall that guest molecules in an all-trans conformation were considered. While this conformation had been shown to be preferred for n-alkanes [30] and α,ω-dibromoalkanes in their urea inclusion compounds [31], before this work there had been no similar studies to determine the conformation of dimethylketone guest molecules in their urea inclusion compounds.

Second, the host structure used in the simulation was a fixed, rigid structure corresponding to the refined, average host structure for hexadecane/urea. Local relaxation of the host structure around the included guest molecule was not considered (in any of the studies). Any significant local distortion of the host structure would be expected to alter the host-guest energy profile, and the resulting characteristic energy diagram.

In fact, since this study was undertaken the crystal structure of 2,10-undecanedione/urea has been solved, and it has been found that the structure is indeed commensurate [32]. In the structure, the host is distorted from the conventional urea tunnel structure, with the urea molecules adjacent to the C=O groups of the guest flipping round about their two-fold axis to hydrogen bond to these C=O groups . This results in a lengthening of the ***a*** axis to 8.34 Å, and the structure possesses a 33 Å repeat along the ***c*** axis. This repeat length contains two 2,10-undecanedione guest molecules, as expected. Similarly, 2,7-octanedione/urea has been shown to be commensurate with a periodicity of 77 Å along the tunnel axis and containing six guest molecules. In both these compounds,

the guest molecules are in fact found to be in the all-trans conformation, as was used in our calculations [32].

The disagreements between the results obtained from the model and the results from the experimental studies, therefore, may be occurring, not because of limitations of the mathematical model for one-dimensional inclusion compounds, but due to limitations in our chemical knowledge of the systems under investigation (in this case the structure of the host). Reapplication of the model to the 2,10-undecanedione/urea inclusion compound and the 2,7-octanedione/urea inclusion compound using the real host structures in these systems is necessary to see if the model correctly predicts commensurate behaviour.

4.8 Concluding Remarks

The good agreement between the experimental values of c_g and those predicted theoretically for the n-alkane/urea and the chlorocyclohexane/thiourea inclusion compounds augurs well for the future application of this theoretical approach for the prediction and rationalisation of structural properties of other one-dimensional inclusion compounds (provided, of course, that reliable potential energy parameterisations are available for computing $E_h(t)$, $\hat{E}_{guest}(\alpha)$ and $\hat{E}_{intra}$ for the inclusion compounds of interest). The case of the dimethylketone/urea inclusion compounds, however, serves as a warning as to the limitations of applying the mathematical model when structural information is not known. Assumptions concerning the conformation of the guest molecules and the absence of distortion of the host structure, due to the interaction of the guest molecules with the host, must clearly be considered carefully.

Avenues for future expansion of this work include the investigation of urea inclusion compounds containing other functionalised alkane guests (such as α,ω-dihalogenoalkanes [33] and diacyl peroxides [34]). These functionalised guests (as in the case of the dimethylketones compared to the n-alkanes) will give rise to larger residues $\mu(d)$ than those found for the n-alkane guests, leading to the possibility of commensurate values of α far from the minimum of the upper energy bound on the characteristic energy

diagram. In the case of the α,ω-dibromoalkanes, the conformation of the guest is known to be predominantly all-trans. A wide range of other families of inclusion compound, containing one-dimensional tunnel host structures, also present themselves for consideration. Amongst organic solid hosts in this category are the inclusion compounds of cholic acid, deoxycholic acid, tri-*ortho*-thymotide and perhydrotriphenylene. Although all based on one-dimensional tunnel structures, the exact structural nature of these different host materials differs markedly (as does the chemical identity of the functional groups which form the walls of the tunnel), and the characteristics of the function $E_h(t)$ will reflect these structural differences. Detailed investigation of the way in which this manifests itself in terms of the features of the characteristic energy diagram will be an interesting and important facet of the application of the theoretical approach to these families of inclusion compound.

Another important area of application of the theoretical approach concerns comparison of the energetics of inclusion compounds containing different conformations of a particular guest molecule in the same host structure, such as the case of the chlorocyclohexane/thiourea inclusion compound – (while this may seem to overlap with the question of guest conformation discussed above in the case of the dimethylketones, the number of guest conformations that would require to be considered for an alkyl chain would prove computationally prohibitive). In such studies, careful consideration of $\hat{E}_{intra}$ for the different conformations is crucial, and the way in which the functions $E_h(t)$ and $\hat{E}_{guest}(\alpha)$ are affected by the different conformations of the guest molecule is also important. Application of the model to a series of substituted cyclohexane guest molecules in their thiourea inclusion compounds is presently underway [28].

The significance of the choice of ε and ε' is also critical. In Section 4.3, an inclusion compound is assigned as commensurate or incommensurate on the grounds of the choice of ε and ε'. Lock in of the guest substructure is said to be significant if it is greater than $\varepsilon - 2\varepsilon'$, but not significant if it is less than ε. There is, however, a region of overlap between these two assignments, in which it is not definite whether lock in is significant or not.

For example, in the case of heptadecane/urea, while the model predicts the inclusion compound to be commensurate on the basis of the values of ε and ε' used, the energy of stabilisation at lock in is only 0.21 kJ mol^{-1}, which is greater than ε – 2ε' but less than ε.

It is clear, however, that ε (and ε') should have physical significance. The stabilisation of 0.21 kJ mol^{-1} for heptadecane/urea is substantially less than the thermal energy, kT (≈ 2.5 kJ mol^{-1} at 298 K), and so in reality this compound would not be expected to exhibit "true" commensurate behaviour. Recent Brillouin scattering experiments carried out at room temperature have demonstrated that the heptadecane/urea inclusion compound is incommensurate at room temperature (as a result of the observation of a sliding mode in addition to the three normal acoustic modes [35]), although there is evidence from the X-ray diffraction studies on this compound (see Chapter 2) that the structure does indeed become commensurate at low temperature, with the ratio $6c_g = 13c_h$. [In association with this change, there is also a phase transition in the host structure, believed to occur at *ca.* 160–170 K.]

In order for the model to provide physically significant results, ε and ε' should be selected prior to commencement of application of the model to assume significant values greater than kT. [Note that for chlorocyclohexane/thiourea, ε = 10.5 kJ mol^{-1} and ε' = 4.2 kJ mol^{-1} satisfy this requirement.] Subsequent calculations carried out, with these fixed values of ε and ε', will then provide a greater insight into the true properties of the commensurate or incommensurate nature of one-dimensional inclusion compounds.

References

[1] A.J.O. Rennie and K.D.M. Harris, *Proc. R. Soc. Lond. A*, **430** (1990) 615.

[2] A.J.O. Rennie and K.D.M. Harris, *J. Chem. Phys.*, **96** (1992) 7117.

[3] A.E. Smith, *Acta Cryst.*, **5** (1952) 224.

[4] F. Laves, N. Nicolaides and K.C. Peng, *Z. Krist.*, **121** (1965) 258.

[5] A.J.O. Rennie and K.D.M. Harris, *Chem. Phys. Lett.*, **188** (1992) 1.

[6] N.G. Parsonage and R.C. Pemberton, *Trans. Faraday Soc.*, **63** (1967) 311.

[7] M. Larnaudie, *Compt. Rend.*, **235** (1952) 154.

[8] P. Klæboe, J.J. Lothe, K. Lunde, *Acta Chem. Scand.*, **10** (1956) 1465.

[9] K. Kozima, K. Sakashita, *Bull. Chem. Soc. Jpn.*, **31** (1958) 796.

[10] P. Klæboe, *Acta Chem. Scand.*, **23** (1969) 2641.

[11] M. Nishikawa, *Chem. Pharm. Bull.*, **11** (1963) 977.

[12] K. Fukushima, *J. Mol. Struct.*, **34** (1976) 67.

[13] A. Allen, V. Fawcett, D.A. Long, *J. Raman Spectrosc.*, **4** (1976) 285.

[14] M.S. McKinnon, R.E. Wasylishen, *Chem. Phys. Lett.*, **130** (1986) 565.

[15] A.E. Aliev, K.D.M. Harris, *J. Am. Chem. Soc.*, **115** (1993) 6369.

[16] K. Müller, *Magn. Reson. Chem.*, **30** (1992) 228.

[17] M.D. Hollingsworth, personal communication.

[18] K.D.M. Harris and J.M. Thomas, *J. Chem. Soc. Faraday Trans.*, **86** (1990) 2985.

[19] *Tables of Interatomic Distances and Configuration in Molecules and Ions*, Specialist Publication No. 11, The Chemical Society, London 1958.

[20] *Tables of Interatomic Distances and Configuration in Molecules and Ions*, Supplement, Specialist Publication No. 18, The Chemical Society, London 1965.

[21] F.H. Allen, O. Kennard, D.G. Watson, L. Brammer, A.G. Orpen and R. Taylor, *J. Chem. Soc., Perkin Trans II*, (1987) 51.

[22] W.L. Jorgensen, J.D. Madura and C.J. Swenson, *J. Am. Chem. Soc.*, **106** (1984) 6638.

[23] A.T. Hagler, E. Huler and S. Lifson, *J. Am. Chem. Soc.*, **96** (1974) 5319.

[24] K. Takemoto and N. Sonoda: *Inclusion Compounds, Vol. 2*, eds J.L. Atwood, J.E.D. Davies and D.D. MacNicol, Academic Press, London, 1984, p.47.

[25] 'Chem-X', developed and distributed by Chemical Design Ltd., Oxford, England.

[26] K.D.M. Harris, J.M. Thomas, *J. Chem. Soc. Faraday Trans.*, **86** (1990) 1095.

[27] G. Del Re, E. Gavuzzo, E. Giglio, F. Lelj, F. Mazza and V. Zappia, *Acta Cryst.*, **B33** (1977) 3289.

[28] S. Camus, I.J. Shannon and K.D.M. Harris, work in progress.

[29] BIOSYM Techologies Inc., 8625 ScrantonRoad, San Diego, 92151 CA, U.S.A.

[30] H.L. Casal, *J. Phys. Chem.*, **94** (1990) 2232.

[31] S.P. Smart, K.D.M. Harris, F. Guillaume and A. El Baghdadi, *Mol. Cryst. Liq. Cryst.*, **211** (1992) 157.

[32] M.D. Hollingsworth and M.E. Brown, unpublished results.

[33] K.D.M. Harris, S.P. Smart and M.D. Hollingsworth, *J. Chem. Soc. Faraday Trans.*, **87** (1991) 3423.

[34] K.D.M. Harris and M.D. Hollingsworth, *Proc. R. Soc. Lond. A*, **431** (1990) 245.

[35] D. Schmicker, S. van Smaalen, J.L. de Boer, C. Haas and K.D.M. Harris, *Phys. Rev. Lett.*, submitted.

Chapter 5

Bromine EXAFS Spectroscopic Studies of the Inclusion Compounds of Urea, Thiourea and Zeolites Containing Brominated Guest Molecules.

5.1 EXAFS Spectroscopy

Extended X-ray absorption fine structure (EXAFS) is a relatively new spectroscopic technique, which can be used to examine all types of compound at an atomic level, giving valuable information about interatomic distances. The phenomenon of EXAFS was discovered in the 1930's, when it was observed that there was a sinusoidal variation in the X-ray absorption as a function of energy, above an absorption edge. However, it was not until the early 1970's that the structural content of these oscillations was understood, and it is only since the advent of synchrotron radiation sources, which have greatly cut the experimental time required and increased the sensitivity and accuracy of results [1], that the technique has really come into significant use.

The fact that it is possible to analyse not only crystalline and amorphous solids, but also liquids and even gases, renders EXAFS a more versatile structural tool, in some respects, than conventional X-ray diffraction. In EXAFS, it is the local environment around an atom that is probed (up to a radius of ~ 6 Å from the X-ray absorbing atom); hence, EXAFS is suited to examining materials even when there is no long range order present. EXAFS has had particular importance in the field of catalysis [3], where it has been used to discover the binding geometry of substrates to the actual catalyst surface, and, *via* in situ studies, the mechanisms of reactions.

EXAFS is a particularly powerful technique, as absorption edges of all elements higher than Argon in the periodic table (Z = 18) are readily accessible to be probed individually, as each element has its own unique core electron energy.

5.1.1 Fundamentals of EXAFS Spectroscopy

The process of extended X-ray absorption fine structure involves an X-ray photon ejecting a core electron; this photoelectron is modelled in the form of a spherical wave radiating out from the absorber [Fig. 5.1]. When this wave reaches a neighbouring atom it is backscattered by this atom. Depending on the nature of this backscattering atom and its distance from the absorber, there is a characteristic change in both the amplitude, phase and period of the backscattered wave. The resultant of all outgoing and incoming waves is detected as sinusoidal variations in the X-ray absorption coefficient, as a function of energy above the absorption edge. It is these oscillations that give rise to EXAFS spectroscopy [4].

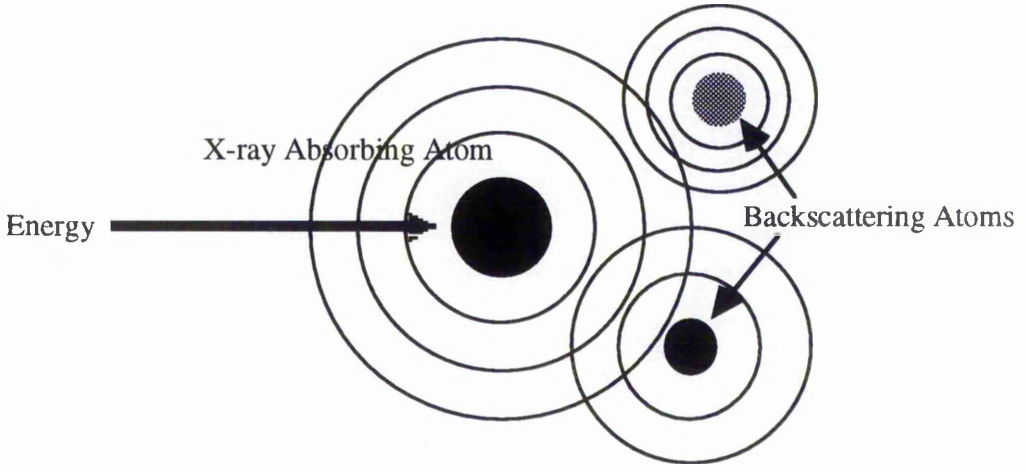

Fig. 5.1: Diagram showing the photoelectron wave emanating from an X-ray absorbing atom. This wave is backscattered by the surrounding atoms; the resulting interference gives rise to oscillations in the X-ray absorption coefficient, from which structural information can be determined.

Experimentally, the X-ray absorption coefficient, μ, is recorded as a function of photon energy, E, above the absorption edge under study [Fig. 5.2(a)]. μx, where x is the sample thickness, is given by:

$$\mu(E)x = \ln \frac{I_0(E)}{I(E)}$$

where I_0 is the intensity of the incident beam, and I is the intensity of the transmitted beam.

The EXAFS function $\chi(\mathbf{k})$ is defined as:

$$\chi(\mathbf{k}) = \frac{(\mu(\mathbf{k}) - \mu_0(\mathbf{k}))}{\mu_0(\mathbf{k})}$$

where μ is the measured X-ray absorption coefficient and μ_0 is the absorption coefficient of the isolated atom. The quantity $\mu - \mu_0$ represents the background subtracted EXAFS oscillations [Fig. 5.2(b)]. The photoelectron wavevector **k** is related to the energy ($h\nu - E_0$) of the electron by the equation:

$$h\nu - E_0 = \frac{h^2\mathbf{k}^2}{2m}$$

where $h\nu$ is the photon energy and E_0 is the electron binding energy. The transformation from measuring in energy to the wavevector, **k**, enables the EXAFS oscillations to be related to structural parameters.

The general equation governing EXAFS, which relates the important structural parameters to the observed EXAFS oscillations, is [5]:

$$\chi(\mathbf{k}) = \sum \frac{N_j F_j(\mathbf{k}) \exp(-2\sigma_j^2\mathbf{k}^2) \exp(-2r_j/\lambda) \sin(2\mathbf{k}r_j + \phi_j(\mathbf{k}))}{\mathbf{k}r_j^2}$$

where the summation is over j shells of backscattering atoms, N_j is the number of scattering atoms (assumed to be of the same type) in the jth shell, $F_j(\mathbf{k})$ is the structure

factor for the backscatterer, σ_j is the Debye-Waller factor, r_j is the distance of shell j from the X-ray absorbing atom, λ is the electron mean free path and $\phi_j(\mathbf{k})$ the total phase shift experienced by the photoelectron.

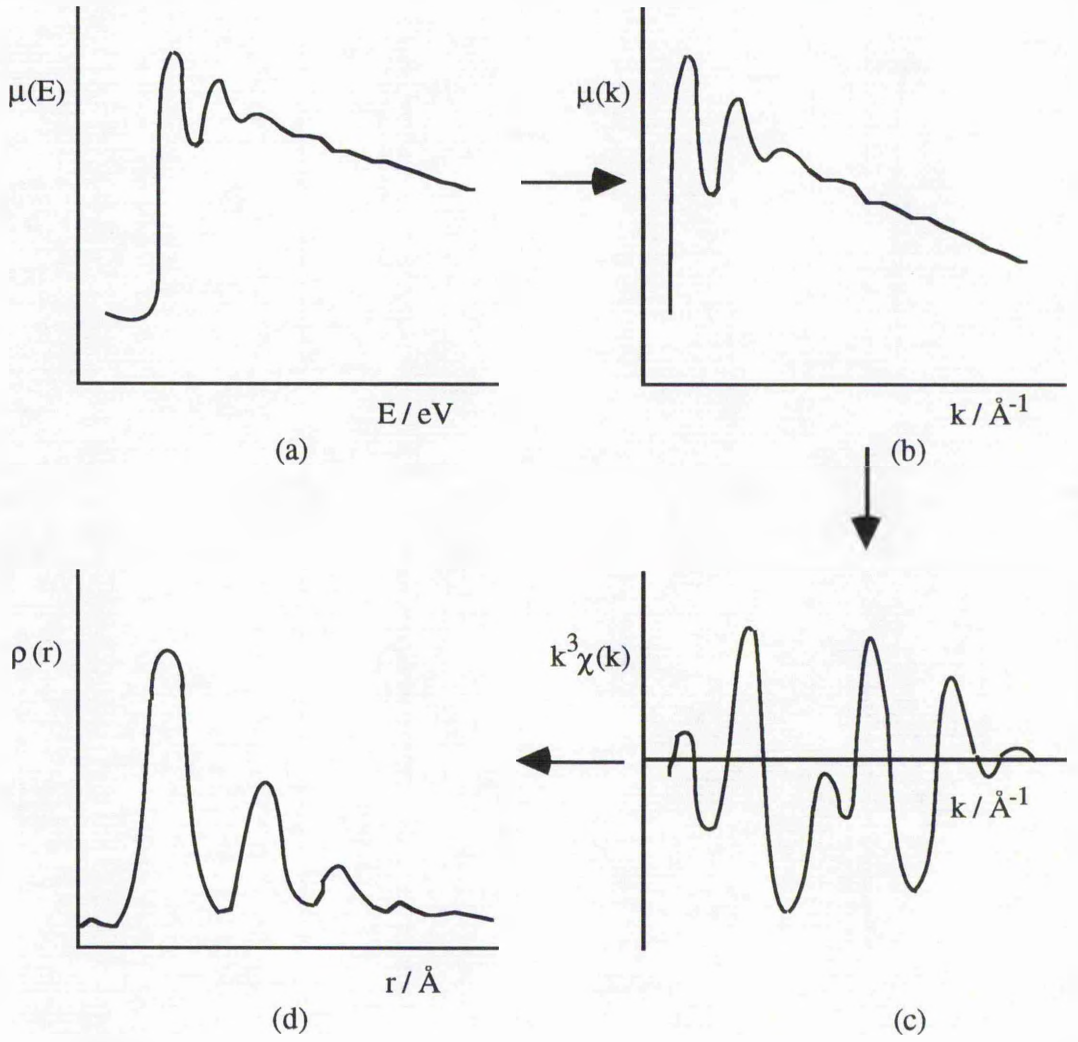

Fig. 5.2: Diagram showing the stages in the processing of EXAFS data. The raw spectrum (a) is background subtracted and normalised (b), to give the EXAFS function $\chi(k)$, which is weighted by a factor k^3 (c). Fourier transformation of this function results in a one-dimensional radial distribution function of electron density $\rho(r)$ around the absorbing atom (d).

In practice, the function $\chi(\mathbf{k})$ is generally weighted by a factor of k^2 or k^3 in order to equalise the amplitude of the EXAFS envelope over the **k**-range considered [Fig. 5.2(c)]. Fourier transformation of the function $k^n\chi(\mathbf{k})$ converts the EXAFS spectrum to a one-dimensional radial distribution function of the local atomic environment around the absorbing atom [Fig. 5.2(d)]. The contribution to the EXAFS oscillations from individual peaks in the radial distribution function may be selectively isolated by using Fourier filtering followed by inverse transformation back into **k**-space. This technique can simplify the fitting process and provide better resolution in the spectrum, but has the disadvantage that it invalidates the use of statistical testing on whether the addition of new shells of neighbouring atoms are significant.

To assess the phase shifts experimentally, standard compounds, of known structure, are considered. For greatest accuracy, it is important to use standards as close as possible in structure to the unknown compounds under investigation. More recently, improvements in the accuracy of theoretically derived phase shifts have led to a reduction in the necessity to use standards.

The main limitation of EXAFS spectroscopy is that no information can be derived about the three-dimensional structure around the X-ray absorbing atom (the data is of the form of a one-dimensional radial distribution function), except when multiple scattering, which gives information on collinearity of atoms, requires to be considered. Also, the short range of the technique limits the obtainable information to the first three or four shells of neighbours. However, for many types of material, EXAFS remains the most powerful method for obtaining information on short range order.

5.2 Data Analysis

In the work reported here, data analysis used programs from the Daresbury SRS program library. The program EXCALIB was used to process and calibrate the raw experimental data. Background subtraction was performed using the program EXBROOK, with the relevant parameters modified until the EXAFS oscillations were just visible in the derivative of the background. Subsequent fitting of the spectrum used

the interactive program EXCURV90 for the series of experiments on α,ω-dibromoalkane/urea inclusion compounds, and the upgraded program EXCURV92 [6] for the experiments on the halocyclohexane/thiourea inclusion compounds. In both EXCURV90 and EXCURV92 the photoelectron is treated as a curved wave [7].

When using EXCURV90, theoretically-derived phase shifts were modified by fitting the measured Br EXAFS spectra (as shown in Fig. 5.4) of the standard compounds 1,12-dibromododecane and sodium bromide, the crystal structures of which are known [8,9]. 1,12-dibromododecane was used to optimise parameters relevant to backscattering from carbon, whereas sodium bromide was used to optimise parameters relevant to backscattering from bromine. In fitting spectra of these standard compounds, the following were treated as refinable parameters in EXCURV90: the Debye-Waller factor (σ_j) for each shell j (values quoted are $2\sigma_j^2$), the energy zero parameter E_0, the photoelectron inelastic scattering parameter VPI, and the shake up correction parameter AFAC. The coordination number (N_j) and interatomic distance (r_j) for each shell were constrained to the values known from the crystal structures of these materials. Fourier filtering was applied to the spectra of the standard compounds.

The major upgrade between the programs EXCURV90 and EXCURV92 is in the introduction of a more reliable set of phase shifts. For the experiments on the halocyclohexane/thiourea inclusion compounds and the zeolites, theoretically-derived phase shifts were generated within EXCURV92, using von-Barth ground states and X_α exchange potentials. [Phase shifts generated using Hedin-Lundqvist exchange potentials were also tried, but these did not prove satisfactory for fitting beyond the first shell.] The photoelectron inelastic scattering parameter VPI, and the shake-up correction parameter AFAC were refined for the standard compound, 1,12-dibromododecane, at 77 K. In the final refinement calculations, these values of AFAC and VPI were used [as fixed parameters (AFAC = 0.89, VPI = –3.71 eV)] in fitting the spectra recorded for a given material at all temperatures. The following parameters were treated as refinable in EXCURV92: the interatomic distance (r_j) for each shell j, the Debye-Waller factor (σ_j) for each shell j, and the energy zero parameter E_0. The coordination number (N_j) for each

shell was set to the value expected from chemical knowledge. Multiple scattering was not considered for any of the samples examined.

The EXAFS data were processed without Fourier filtering in order that statistical significance testing [10] could be applied. The addition of each new shell to the structural model was considered to be statistically significant if the improvement in fit index was greater than *ca.* 4 % in comparison with the minimised fit index for the corresponding model without the new shell added.

5.3 Br EXAFS Studies of α,ω-Dibromoalkane/Urea Inclusion Compounds

5.3.1 Introduction to EXAFS Spectroscopy on Urea Inclusion Compounds

As discussed previously (Chapter 2), the features of the host substructure in urea inclusion compounds are relatively well understood, but little is known about the guest substructure, due to the guest molecules undergoing rapid reorientation about the tunnel axis and translation along the this axis [11]. Nevertheless, there is sufficient ordering to allow an average periodicity to be defined, and measured, for the guest substructure, even at ambient temperature [12].

In the conventional urea inclusion compounds, the periodicity of the guest molecules along the tunnel axis is about 0.5 Å shorter than the "van der Waals length" of the guest molecule in the linear, extended conformation that it must adopt to fit within the host tunnel structure. Different interpretations of the source of this "shortening" have been proposed. An early paper [13] suggested that it is due to coiling or tilting of the guest molecule within the tunnel, whereas more recent opinion (and the results for the n-alkane/urea inclusion compounds described in Chapter 4) [14–17] supports the view that the interaction between adjacent guest molecules in the same tunnel is repulsive, leading to adjacent guest molecules being closer together than van der Waals contact.

Because EXAFS spectroscopy can determine the local structure around an X-ray absorbing atom, this technique offered itself as ideal for revealing local structural information on the guest substructure in urea (and other organic) inclusion compounds, provided the guest molecules contain an appropriate X-ray absorbing atom. Hence, we have carried out Br K-edge EXAFS investigations of the urea inclusion compounds containing α,ω-dibromoalkane $Br(CH_2)_nBr$ guest molecules with n = 6–11.

It is important to recall that for the urea inclusion compounds containing $Br(CH_2)_nBr$ guests with n = 7–11, the host and guest substructures are incommensurate with respect to each other [12]. Conversely, the 1,6-dibromohexane/urea inclusion compound (n = 6) differs structurally from the "conventional" α,ω-dibromoalkane/urea inclusion compounds discussed above. In the 1,6-dibromohexane/urea inclusion compound, the relationship between the host and guest substructures is commensurate and the crystal symmetry is described by a single 3-dimensional space group ($P2_1/n$). The crystal structure of this inclusion compound has been determined from single crystal X-ray diffraction data [18,19] at both 113K and room temperature, revealing that the $Br(CH_2)_6Br$ guest molecules are fixed in a well-defined position relative to the host structure (consistent with the commensurate structural relationship between the host and guest components in this inclusion compound) and contain a gauche bond (CC-CBr) at each end of the molecule.

Due to the incommensurate structural relationship between the host and guest components for those guests with n = 7–11, each guest molecule in a given tunnel is, in principle, in a different environment with respect to the host. As a consequence, there will be a broad distribution of distances between the bromine atoms of the guest and the atoms of the host, and therefore atoms of the host should not give well-defined features in the bromine radial distribution function. In contrast, the commensurate relationship between the host and guest components in the 1,6-dibromohexane/urea inclusion compound means that there are well-defined distances between the bromine atoms of the guest and the atoms of the host substructure.

The primary aim of our Br K-edge EXAFS investigations of these inclusion compounds was to determine the intratunnel, interatomic Br....Br distance, for the series of α,ω-dibromoalkane/urea inclusion compounds discussed above. The observation of an unusually short Br....Br distance would be consistent with the view that the interaction between adjacent guest molecules in the same tunnel is repulsive.

5.3.2 Experimental

The crystalline materials 1,12-dibromododecane and sodium bromide were used as standards in the EXAFS experiments. Before use, the sodium bromide sample was dried in an oven at *ca.* 60 °C; powder X-ray diffraction confirmed that the sample of sodium bromide used in the EXAFS studies was the anhydrous form.

Urea inclusion compounds containing α,ω-dibromoalkane guest molecules [$Br(CH_2)_nBr$; n = 6–11] were prepared by the method described previously [Section 2.3], and the identity of these crystals was confirmed by powder X-ray diffraction.

Br K-edge X-ray absorption spectra of the α,ω-dibromoalkane/urea inclusion compounds were measured on stations 7.1 and 9.2 at the SRS facility at Daresbury Laboratory; all the data analysed below was recorded on station 9.2. For each sample, the spectrum was recorded at room temperature and at *ca.* 77 K. For each sample at each temperature, the spectrum was recorded over a period of about 30 minutes, and three spectra were recorded and combined in order to improve the signal/noise ratio. In addition, spectra were recorded for 1,10-dibromodecane/urea and 1,6-dibromohexane/urea at several temperatures between room temperature and 80 K, in order to monitor progressively any structural changes with temperature. The spectrum for 1,10-dibromodecane/urea was also recorded at 9 K. These variable-temperature Br EXAFS studies were of particular interest for the 1,10-dibromodecane/urea inclusion compound [Fig 5.3], which is known to undergo a phase transition [20] at *ca.* 140 K (see Chapter 3). The other α,ω-dibromoalkane/urea inclusion compounds with n = 7–11 are also known to undergo a phase transition between 80 K and room temperature [19].

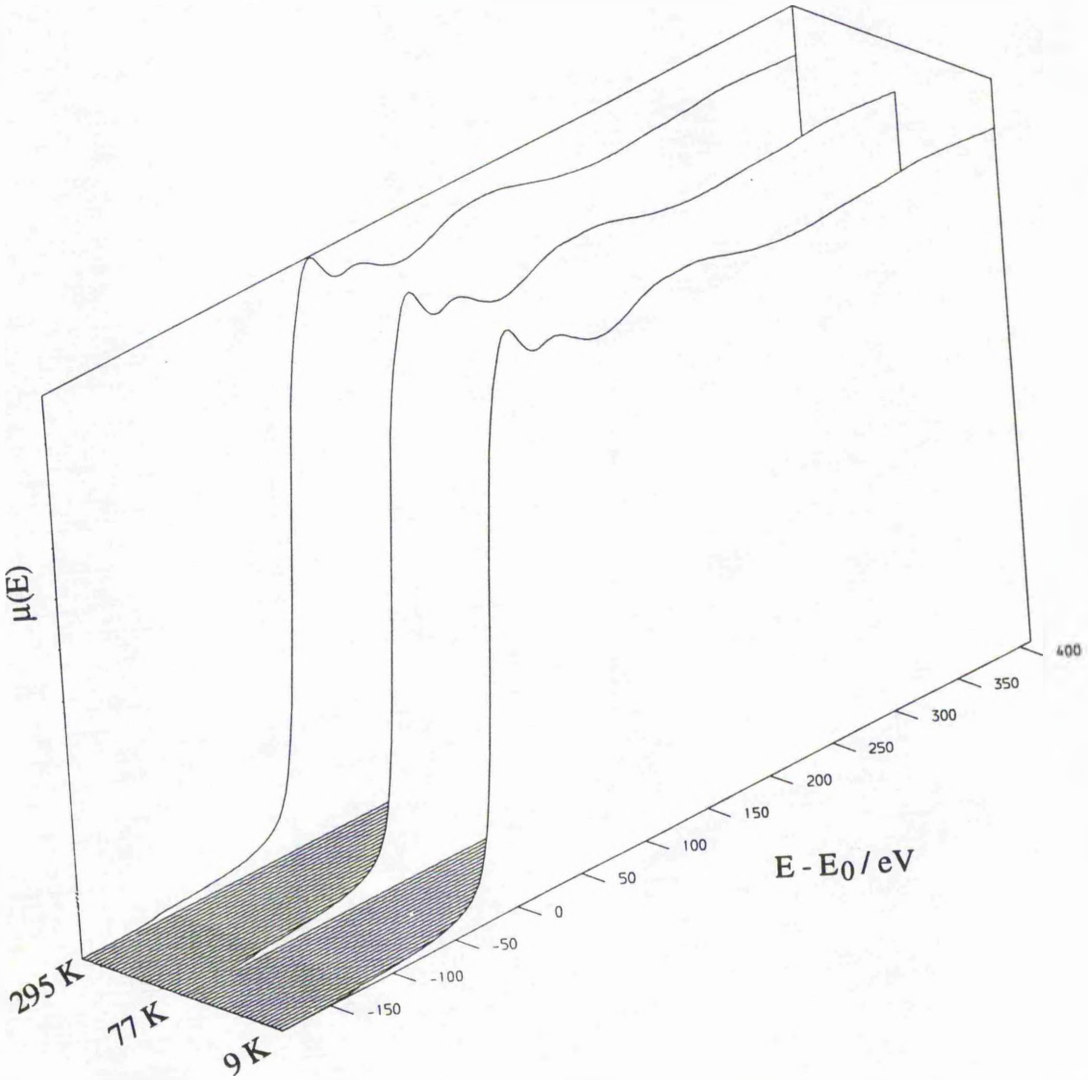

Fig. 5.3: Stack plot of EXAFS Spectra for the 1,10-dibromodecane/urea inclusion compound as a function of temperature.

5.3.3 Results

For crystalline 1,12-dibromododecane and for all of the α,ω-dibromoalkane/urea inclusion compounds studied, the Br K-edge was the same (13477 eV), within experimental error. The measured Br K-edge energy for sodium bromide was 13481 eV.

5.3.3.1 Standard Compounds

Fitted EXAFS spectra for the standard materials 1,12-dibromododecane and sodium bromide are shown in Figs. 5.4(a) and 5.4(b) respectively. For 1,12-dibromododecane, an R factor of 11 % was obtained for the first two shells (each comprising a single carbon atom) for filtered data modelled over the range k = 2.5–12.2 $Å^{-1}$; for sodium bromide the R factor was 8 % for two shells (sodium and bromine respectively) for filtered data modelled over the range k = 2.8–12.5 $Å^{-1}$. In each case, k^2 weighting was used and only the first two shells of backscatterers were considered.

5.3.3.2 1,10-Dibromodecane/Urea Inclusion Compound

Data analysis for 1,10-dibromodecane/urea was carried out for the spectra recorded at room temperature, 77 K and 9 K (Figs. 5.5(a)–(c)). This analysis was carried out on unfiltered data, in order that statistical testing could be used to assess whether the addition of each new shell to the structural model was statistically significant. The analysis has shown that, at each temperature, the first two shells, at 1.95 Å and 2.84 Å, each contain a single carbon atom. A third shell containing a single carbon atom at 4.35 Å also appears to be present, although the introduction of this additional shell satisfied the significance test rigorously only for the data recorded at 9 K. On introducing this additional shell, a 5 % improvement in the FI was observed for the 9 K data compared with 3 % improvements in the FI for the 77 K data and for the room temperature data. These interatomic distances correlate closely with the corresponding distances in 1,12-dibromododecane [8], as expected for intramolecular interatomic distances in these similar molecules (note: the average Br–C bond distance for sp^3 carbon in reported crystal structures is 1.97 Å [21]).

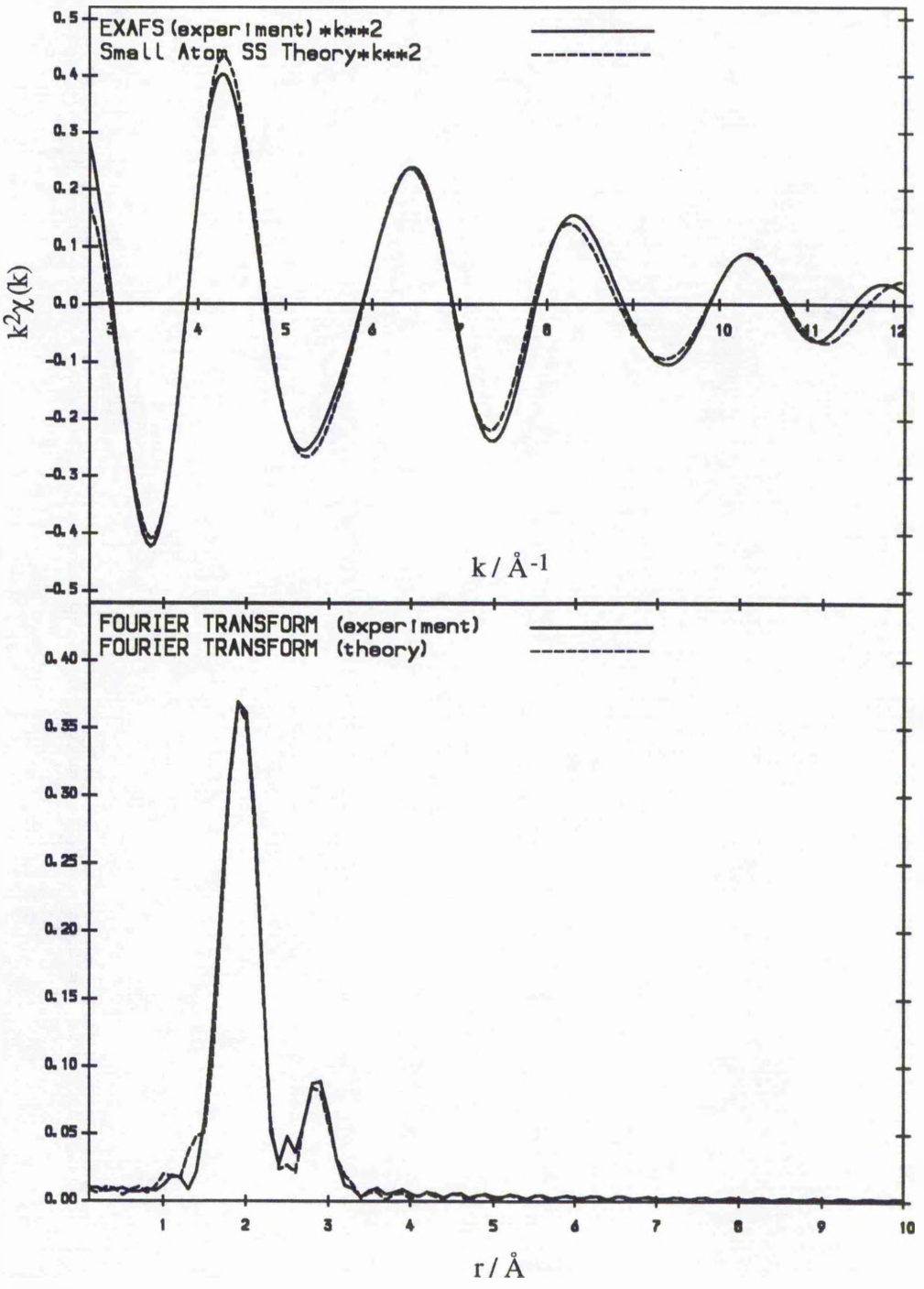

Fig. 5.4(a): Br K-edge EXAFS spectrum of pure crystalline 1,12-dibromododecane at 77 K and its Fourier transform (only the first two peaks in the RDF are shown). The theoretical fit is for a model consisting of two shells, each comprising a single carbon atom at 1.95 Å and 2.89 Å respectively, and with $2\sigma^2 = 0.008$ Å^2 for each shell. (Parameters relevant to data analysis: R = 11.34 %; VPI = –3.75 eV; AFAC = 0.87).

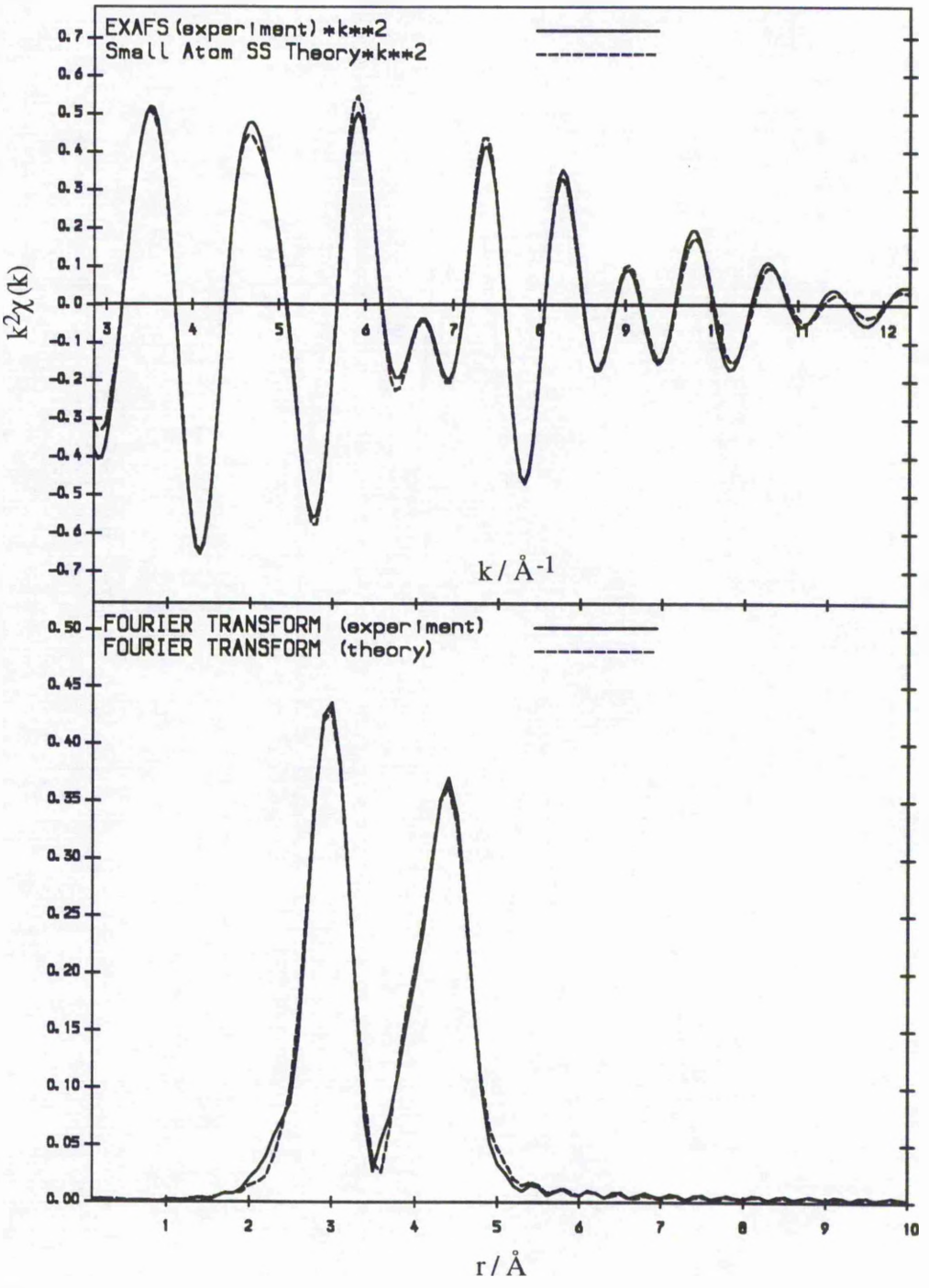

Fig. 5.4(b): Br K-edge EXAFS spectrum of sodium bromide at 77 K and its Fourier transform (only the first two peaks in the RDF are shown). The theoretical fit is for a model comprising a shell of 6 sodium atoms at 2.98 Å ($2\sigma^2 = 0.018$ Å^2), and a shell of 12 bromine atoms at 4.22 Å ($2\sigma^2 = 0.027$ Å^2). (Parameters relevant to data analysis: R = 8.16 %; VPI = –4.53 eV; AFAC = 0.64).

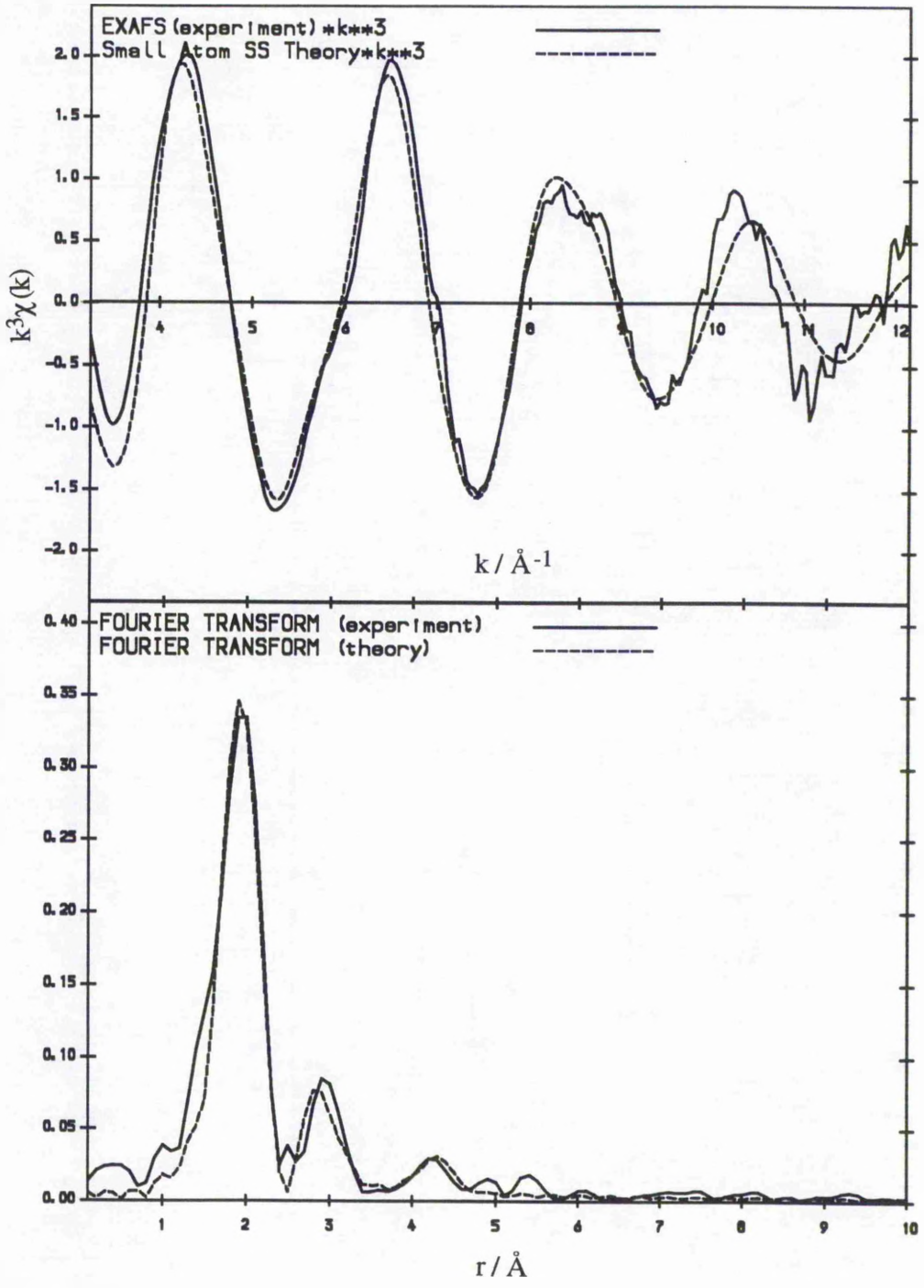

Fig. 5.5(a): Br K-edge EXAFS spectrum of the 1,10-dibromodecane/urea inclusion compound at room temperature and its Fourier transform. The theoretical fit is for three shells, corresponding to single carbon atoms at 1.95 Å ($2\sigma^2 = 0.014$ Å^2), 2.82 Å ($2\sigma^2 = 0.031$ Å^2) and 4.37 Å ($2\sigma^2 = 0.026$ Å^2). (Parameters relevant to data analysis: R = 25.90 %; VPI = –3.40 eV; AFAC = 0.92).

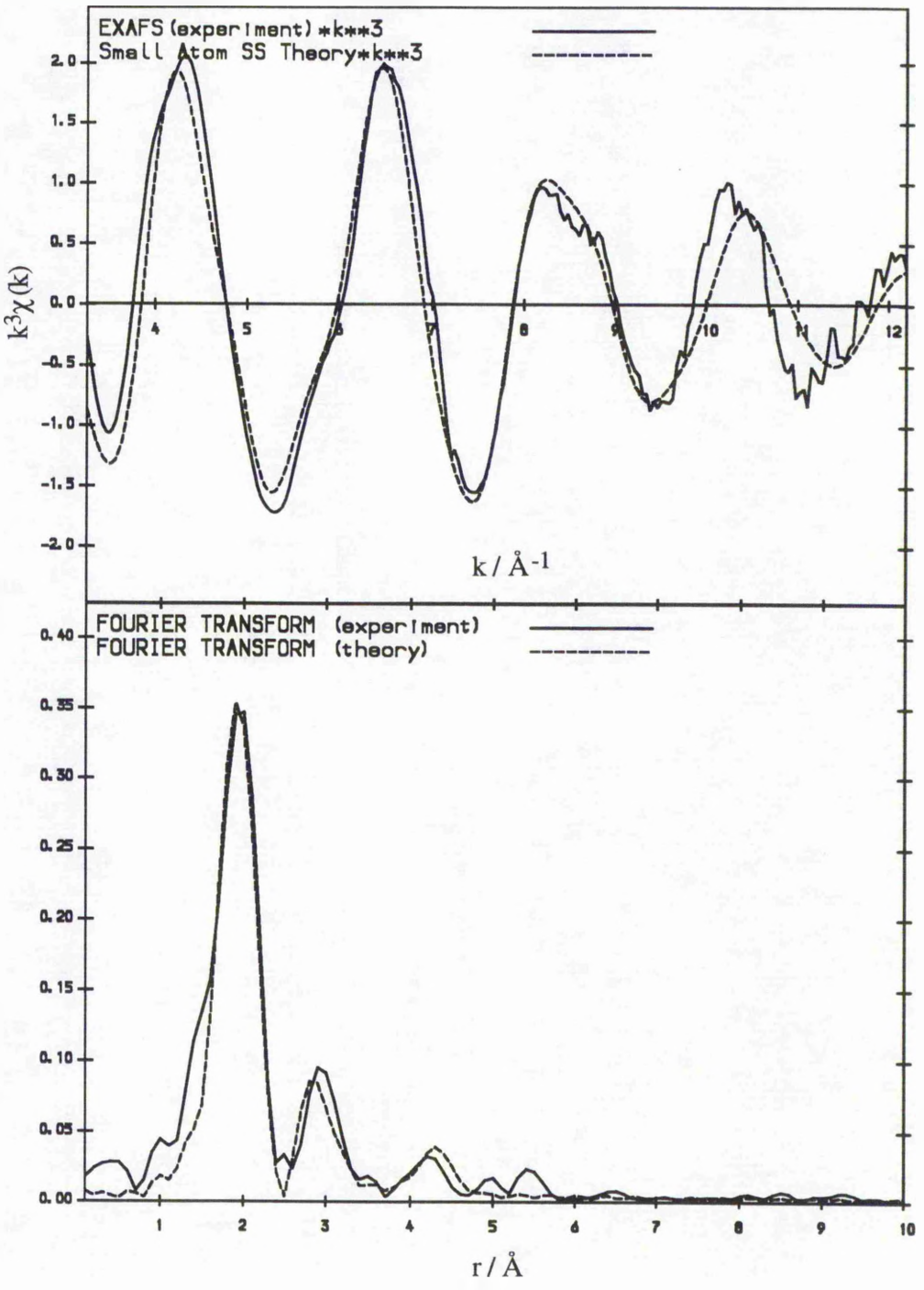

Fig. 5.5(b): Br K-edge EXAFS spectrum of the 1,10-dibromodecane/urea inclusion compound at 77 K and its Fourier transform. The theoretical fit is for three shells, corresponding to single carbon atoms at 1.95 Å ($2\sigma^2$ = 0.013 Å), 2.82 Å ($2\sigma^2$ = 0.027 Å) and 4.37 Å ($2\sigma^2$ = 0.020 Å). (Parameters relevant to data analysis: R = 26.69 %; VPI = –3.34 eV; AFAC = 0.90).

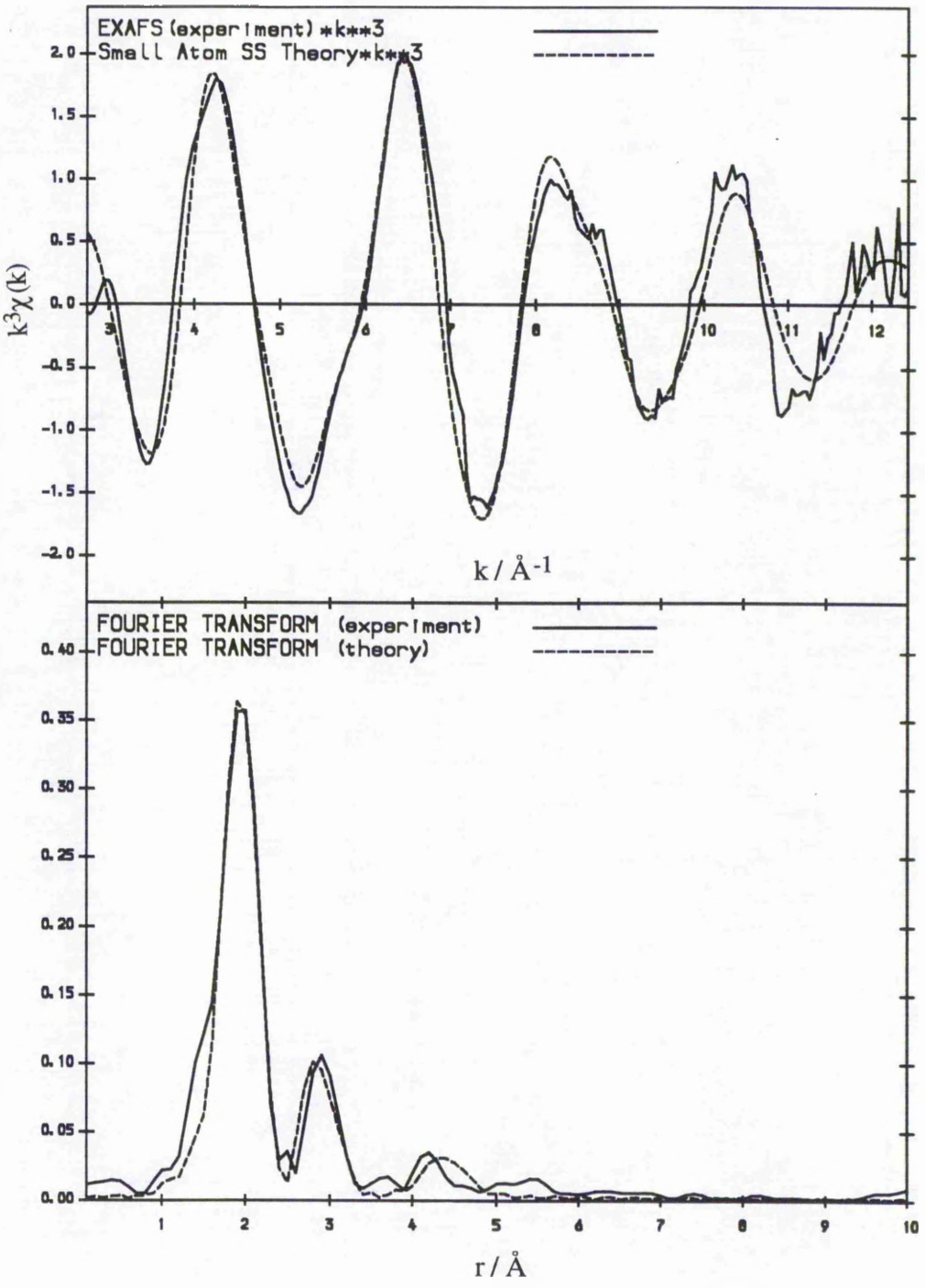

Fig. 5.5(c): Br K-edge EXAFS spectrum of the 1,10-dibromodecane/urea inclusion compound at 9 K and its Fourier transform. The theoretical fit is for three shells, corresponding to single carbon atoms at 1.95 Å ($2\sigma^2$ = 0.012 Å^2), 2.84 Å ($2\sigma^2$ = 0.021 Å^2) and 4.37 Å ($2\sigma^2$ = 0.019 Å^2). (Parameters relevant to data analysis: R = 25.09 %; VPI = –3.89 eV; AFAC = 0.88).

The values of $2\sigma^2$ for the first three carbon shells are shown as a function of temperature in Table 5.1; as expected, the values of $2\sigma^2$ decrease with decrease of temperature. It should be noted that static disorder, as described below, is probably not a significant factor in these intramolecular distances.

Atom	Room temperature	T = 77 K	T = 9 K
Br-$\underline{C}H_2$-CH_2-	0.014	0.013	0.012
Br-CH_2-$\underline{C}H_2$-	0.031	0.027	0.021
Br-CH_2-CH_2-$\underline{C}H_2$-	0.026	0.020	0.019

Table 5.1: Values of $2\sigma^2/Å^2$ for the C1, C2 and C3 intramolecular carbon neighbours of the bromine atoms in the 1,10-dibromodecane/urea inclusion compound as a function of temperature.

There is no major difference between the spectra recorded above (room temperature) and below (77 K) the phase transition at *ca.* 140 K in 1,10-dibromodecane/urea. Importantly, there is no evidence for the introduction of well-defined interatomic distances between the Br atom of the guest molecule and the atoms of the host substructure in the low-temperature phase. This is consistent with the suggestion that there is no "locking in" of the guest molecules to specific sites within the host framework (as would occur, for example, in an incommensurate → commensurate phase transition), despite the fact that this phase transition is associated with a major change in symmetry of the host structure [20] (see also Chapter 3).

The remaining features in the bromine radial distribution function (RDF) are very weak at all temperatures, and there is no clear evidence for well-defined Br....Br distances. We have nevertheless explored the possibility that there is a weak Br....Br contribution to the RDF, by introducing a new shell with a single bromine neighbour into the structural model at a distance of 3.7 Å. This extra shell made the quality of the

agreement between theory and experiment markedly worse, unless the value of $2\sigma^2$ for this shell was large. This suggests that there must be considerable disorder associated with the Br....Br distance. The minimum extent of this disorder can be estimated by increasing $2\sigma^2$ until the Br....Br contribution becomes comparable to the noise in the spectrum. When $2\sigma^2$ was increased to 0.06 $Å^2$, the FI fell to a value only 4 % larger than the FI found with the bromine neighbour removed from the structural model. At this value, statistical arguments show that the contribution of the neighbouring bromine shell to the spectrum is similar to the contribution from the noise in the data [10]. This value of $2\sigma^2$ corresponds to a root mean square displacement $\sigma \approx 0.2$ Å about the mean Br....Br distance of 3.7 Å; this large root mean square displacement for the Br....Br distance is attributed to dynamic disorder at higher temperatures and to static positional disorder at lower temperatures. At room temperature, the guest molecules are known to undergo rapid translational and reorientational motions within the host tunnels [11], and it is clear from the EXAFS results reported here that each Br....Br distance covers a distribution of distances over time (resulting in the large value of $2\sigma^2$). At 9 K, on the other hand, there will be no appreciable motion of the guest molecules, and there is presumably a distribution of "static" Br....Br distances throughout the structure. Both of these sources of disorder lead to "smearing out" of the peak due to the bromine neighbour in the bromine RDF. It is possible that the introduction of static positional disorder at low temperature could have been minimised by cooling the sample extremely slowly, such that the system remained in "equilibrium" at all times during cooling.

It is important to note that there are no features in the bromine RDF corresponding to neighbouring atoms in the host substructure, at any temperature studied. As discussed above, this is a consequence of the fact that the periodicities of the host and guest substructures are incommensurate along the tunnel axis, and so there is a broad range of Br....host atom distances over the whole sample. In addition, it is not necessary to consider backscattering from guest molecules in adjacent tunnels; the shortest possible intertunnel Br....Br distance is greater than 8 Å.

5.3.3.3 $Br(CH_2)_nBr$/Urea Inclusion Compounds with n = 7,8,9,11

The urea inclusion compounds containing 1,7-dibromoheptane, 1,8-dibromooctane, 1,9-dibromononane and 1,11-dibromoundecane guest molecules all gave essentially the same bromine RDF as 1,10-dibromodecane/urea. Again, it was possible to fit only the first three shells, representing three intramolecular carbon neighbours, at the same radii found for 1,10-dibromodecane/urea. This suggests, as perhaps expected, that the local environment around the bromine atom is the same for all of the conventional α,ω-dibromoalkane/urea inclusion compounds.

5.3.3.4 1,6-Dibromohexane/Urea Inclusion Compound

It is clear from inspection of the EXAFS spectrum of 1,6-dibromohexane/urea at 80 K [Fig. 5.6] that the local environment around the bromine is substantially different from that in the α,ω-dibromoalkane/urea inclusion compounds with n = 7–11. This difference reflects the presence of well-defined interatomic distances between the bromine atom of the guest molecule and the backscattering atoms in the host structure. Thus, for 1,6-dibromohexane/urea, the contributions from the host atoms are not "smeared out" by an incommensurate relationship between the host and guest structures. The EXAFS spectrum recorded at 80 K has been fitted, and the final refined structural parameters are listed in Table 5.2; the known crystallographic information for the 1,6-dibromohexane/urea inclusion compound at 113 K [18,19] was used to establish the initial structural parameters used in this refinement.

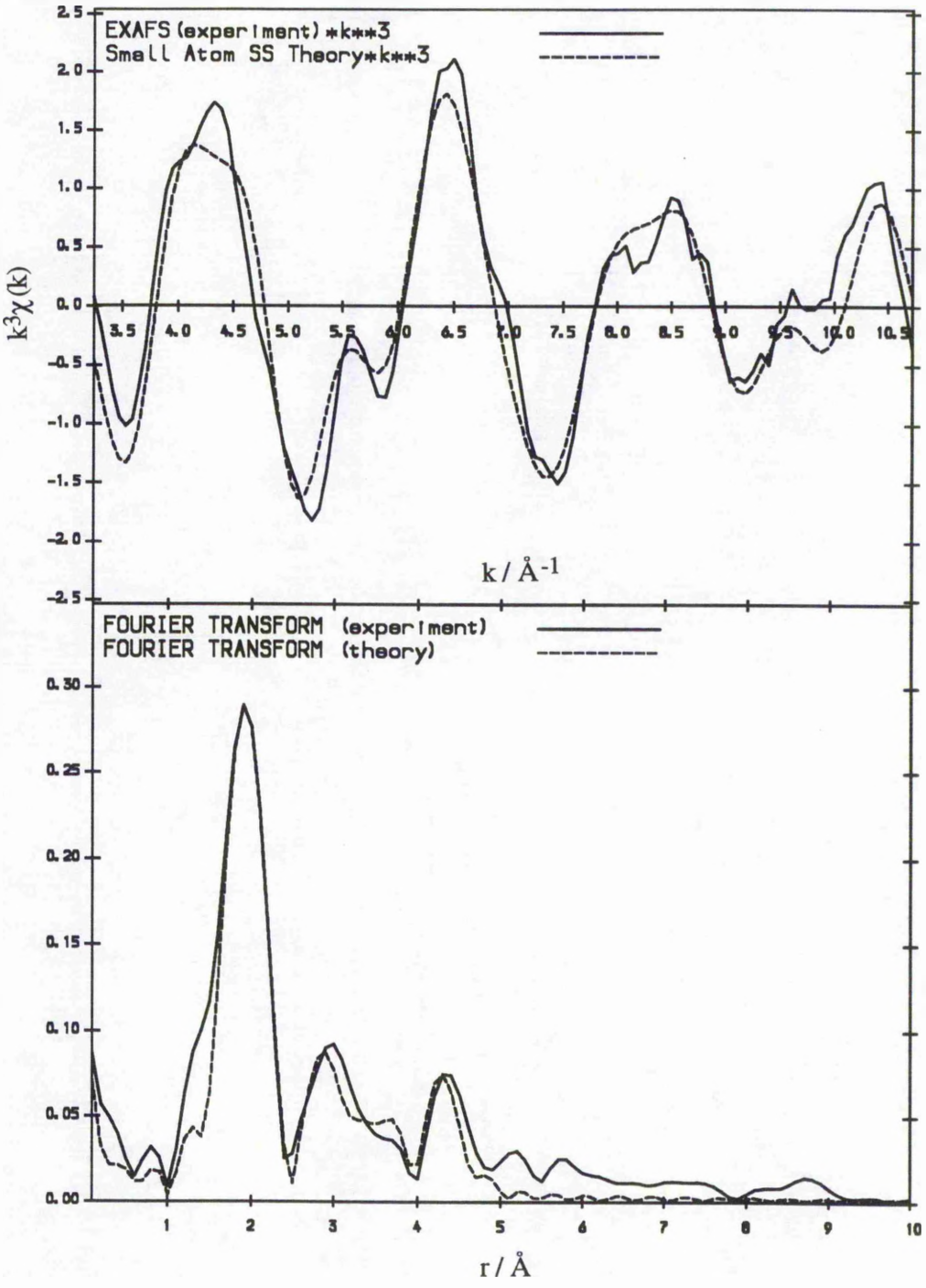

Fig. 5.6: Br K-edge EXAFS spectrum of the 1,6-dibromohexane/urea inclusion compound at 80 K and its Fourier transform. The theoretical fit has been obtained using the parameters listed in Table 5.2. (Parameters relevant to data analysis: R = 29.77 %; VPI = –4.62 eV; AFAC = 0.92).

Atom Type	N_j	r_{ij} / Å	$2\sigma_j^2$ / Å^2
C	1	1.96	0.016
C	1	2.83	0.025
N	2	3.53	0.029
N	2	3.81	0.007
C	2	3.91	0.018
Br	1	4.06	0.026

Table 5.2: Number of atoms in shell (N_j), shell radius (r_{ij}) and value of $2\sigma_j^2$ for the six shells used in modelling the Br EXAFS spectrum of 1,6-dibromohexane/urea inclusion compound at 80 K [See Fig. 5.6].

Six shells of neighbours were found to be statistically significant: two shells of carbon atoms (in the guest molecule) occur at similar distances to those in 1,10-dibromodecane/urea, two further shells reflect Br....N distances due to nitrogen atoms of the host at 3.53 Å and 3.81 Å, and a shell due to two carbon neighbours of the host occurs at 3.91 Å. There is also a definite contribution from the bromine atom in the neighbouring guest molecule at a distance of 4.06 Å. The similarity between the refined interatomic distances determined from the Br EXAFS spectrum at 80 K and the corresponding interatomic distances determined from single crystal X-ray diffraction data at 113 K [18,19] is noteworthy. Furthermore, the observation of well-defined interatomic distances between the bromine atom of the guest molecule and atoms of the host at 80 K is consistent with the known commensurate structural relationship between the host and guest components in this inclusion compound.

The EXAFS spectrum of 1,6-dibromohexane/urea recorded at room temperature has also been fitted, but in this case only the first two neighbours (representing intramolecular Br....C distances, as discussed above) contribute significantly to the Br EXAFS spectrum.

5.4 Br EXAFS Studies of Halogenocyclohexane/Thiourea Inclusion Compounds

5.4.1 Introduction to EXAFS Spectroscopy on Thiourea Inclusion Compounds

As described in Chapter 1 (and justified theoretically in Chapter 4 for the case of the chlorocyclohexane/thiourea inclusion compound), monohalogenocyclohexane molecules are constrained to behave differently within the thiourea host structure from the way they behave in their "pure" solid phase and in dispersed phases. When included within the thiourea tunnel structure, monohalogenocyclohexane molecules exists predominantly in the axial conformation.

Of the thiourea inclusion compounds containing halogenocyclohexanes that have so far been investigated, only the chlorocyclohexane/thiourea inclusion compound has been studied extensively *via* a wide range of techniques. For this inclusion compound, it is known [22] that, although the guest molecules occupy specific sites within the thiourea tunnel structure, there is substantial disorder of the guest molecules, and at ambient temperature, this disorder has been shown [23] to be dynamic in character. Similar behaviour may be expected for other halogenocyclohexane guest molecules in their thiourea inclusion compounds. In view of this disorder, difficulties similar to those for the α,ω-dibromoalkane/urea inclusion compounds arise, in determining information about the guest substructure. Thus, as discussed above, information on the conformational properties of the guest molecules (for chlorocyclohexane/thiourea and for thiourea inclusion compounds containing other halogenocyclohexane guest molecules) has been established primarily from a combination of spectroscopic approaches [24–29].

Again, the ability of EXAFS spectroscopy to determine the local structure around an X-ray absorbing atom renders EXAFS the ideal technique to elucidate local structural information concerning the guest substructures in halogenocyclohexane/thiourea inclusion compounds, particularly when the guest molecules contain a bromine substituent.

In this section, we describe Br K-edge EXAFS investigations of the *trans*-1-bromo-2-chlorocyclohexane/thiourea inclusion compound and the bromocyclohexane/thiourea inclusion compound. The primary aims of these investigations were: (a) for the *trans*-1-bromo-2-chlorocyclohexane/thiourea inclusion compound, to determine the intramolecular Br....Cl distance in order to assess the preferred conformation (diaxial or diequatorial) of the guest molecules within the thiourea tunnel structure, and (b) for both of the thiourea inclusion compounds studied, to assess the possible existence of well-defined intermolecular (Br....Br) interactions between adjacent guest molecules. It should be noted that, as a consequence of orientational disorder of the guest molecules in the thiourea inclusion compounds, backscattering from the atoms of the host substructure is not expected to be significant, and it is therefore expected that no well-defined distances to atoms of the host substructure will be observed in the Br radial distribution function.

For *trans*-1-bromo-2-chlorocyclohexane, the diaxial and diequatorial conformations [Fig. 5.7] can be readily distinguished on the basis of the intramolecular Br....Cl distance. It can be shown readily, from molecular modelling, that for an isolated *trans*-1-bromo-2-chlorocyclohexane molecule in the diaxial conformation, the Br....Cl distance is *ca.* 4.43 Å and the Br....C3(5) distance is *ca.* 3.43 Å, whereas for an isolated *trans*-1-bromo-2-chlorocyclohexane molecule in the diequatorial conformation, the Br....Cl distance is *ca.* 3.42 Å and the Br....C3(5) distance is *ca.* 4.25 Å. [These distances have been determined for molecular structures obtained *via* energy minimisation calculations using the parameterisation in the INSIGHT program package [30]. The diequatorial conformation is predicted to be lower in energy by 4.25 kJ mol^{-1}.]

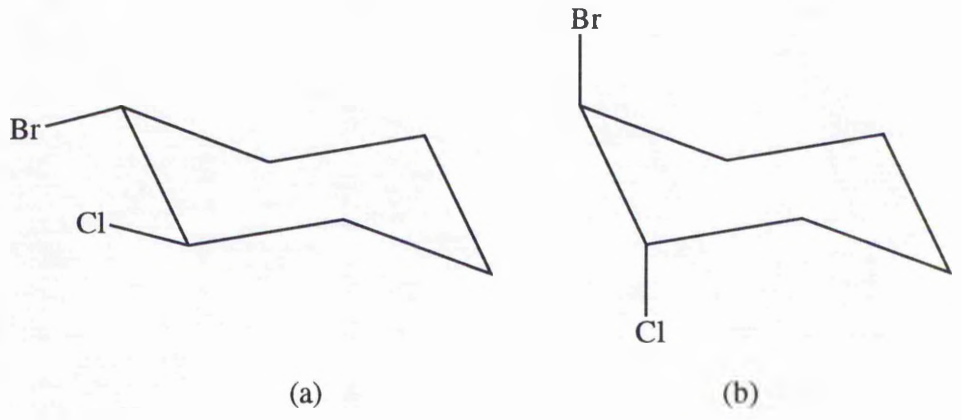

Fig. 5.7: Diagram showing the *trans*-1-bromo-2-chlorocyclohexane molecule in: (a) the diequatorial conformation, and (b) the diaxial conformation. In the diaxial conformation, the Br....Cl distance is *ca.* 4.43 Å and the Br....C3(5) distance is *ca.* 3.43 Å. In the diequatorial conformation, the Br....Cl distance is *ca.* 3.42 Å and the Br....C3(5) distance is *ca.* 4.25 Å.

It is relevant to note that Br EXAFS spectroscopy has been applied previously to investigate the solution state conformational properties of *trans*-1,2-dibromocyclohexane, with particular emphasis on assessing the effect of different solvents on the molecular conformation [31]. However, in these studies, no clear correlations were found between the type of solvent and the conformational properties of the *trans*-1,2-dibromocyclohexane molecules.

5.4.2 Experimental

Bromocyclohexane and thiourea were obtained commercially and were used as received. *Trans*-1-bromo-2-chlorocyclohexane was synthesised by addition of cyclohexene to a solution of antimony pentachloride ($SbCl_5$) and bromine in carbon tetrachloride, and purified by fractional distillation [32].

The bromocyclohexane/thiourea and *trans*-1-bromo-2-chlorocyclohexane/thiourea inclusion compounds were prepared as follows. An excess of the guest component was added to a saturated solution of thiourea in methanol in a conical flask at 50 °C. Any

precipitate (thiourea inclusion compound) formed at this stage was dissolved by addition of further methanol. The flask was then stoppered and immersed in a Dewar flask containing water at 50 °C and allowed to cool to room temperature. The conical flask and Dewar flask were then transferred to an incubator and cooled to 4 °C over a period of 4 days. The crystals that formed were collected and washed with 2,2,4-trimethylpentane to remove any bromocyclohexane or *trans*-1-bromo-2-chlorocyclohexane molecules adhering to their external surfaces. The crystallographic identity of these crystals (i.e. thiourea inclusion compounds possessing the conventional thiourea tunnel structure at room temperature) was confirmed *via* powder X-ray diffraction, carried out at room temperature.

Bromine K-edge X-ray absorption spectra were measured on station 7.1 at the SRS facility at the Daresbury Laboratory. For each sample, spectra were recorded both at room temperature (*ca.* 295 K) and at *ca.* 80 K. For each sample at each temperature, the spectrum was recorded over a period of about 45 minutes, and two spectra were recorded and combined in order to improve the signal/noise ratio. For *trans*-1-bromo-2-chlorocyclohexane/thiourea, spectra were also recorded at several temperatures between 295 K and 80 K, in order to monitor progressively any structural changes with temperature. Data were also recorded for the *trans*-1,2-dibromocyclohexane/thiourea inclusion compound, but these data were found to be of poor quality. This system will be reexamined at a future date.

5.4.3 Results

5.4.3.1 Bromocyclohexane/Thiourea Inclusion Compound

Br K-edge EXAFS spectra were recorded for bromocyclohexane/thiourea at 80 K and at 295 K [Fig. 5.8(a) and 5.8(b)]. Although this material undergoes a phase transition at *ca.* 230 K (known to be associated with a change in symmetry of the thiourea tunnel structure), there is no significant difference between the spectra recorded above and below this temperature.

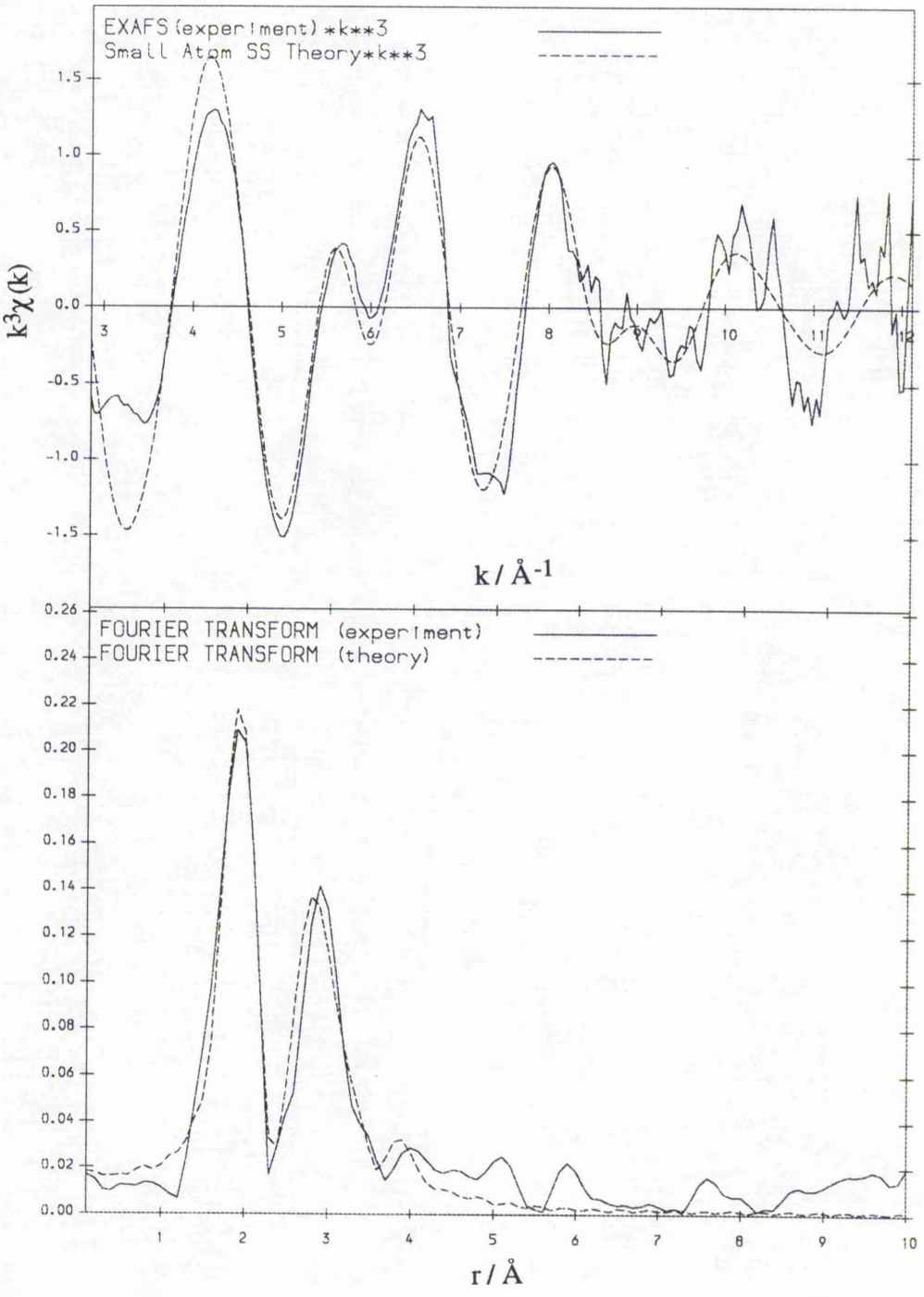

Fig. 5.8(a): Br K-edge EXAFS spectrum, and its Fourier transform, for the bromocyclohexane/thiourea inclusion compound at 295 K. The theoretical fit is for shells corresponding to carbon atoms at 1.96 Å (N = 1; $2\sigma^2 = 0.014$ Å^2), 2.80 Å (N = 2; $2\sigma^2 = 0.022$ Å^2), and 3.24 Å (N = 2; $2\sigma^2 = 0.024$ Å^2), and a bromine atom at 3.80 Å (N = 1; $2\sigma^2 = 0.044$ Å^2). FI = 12.2 %, R = 39.5 %.

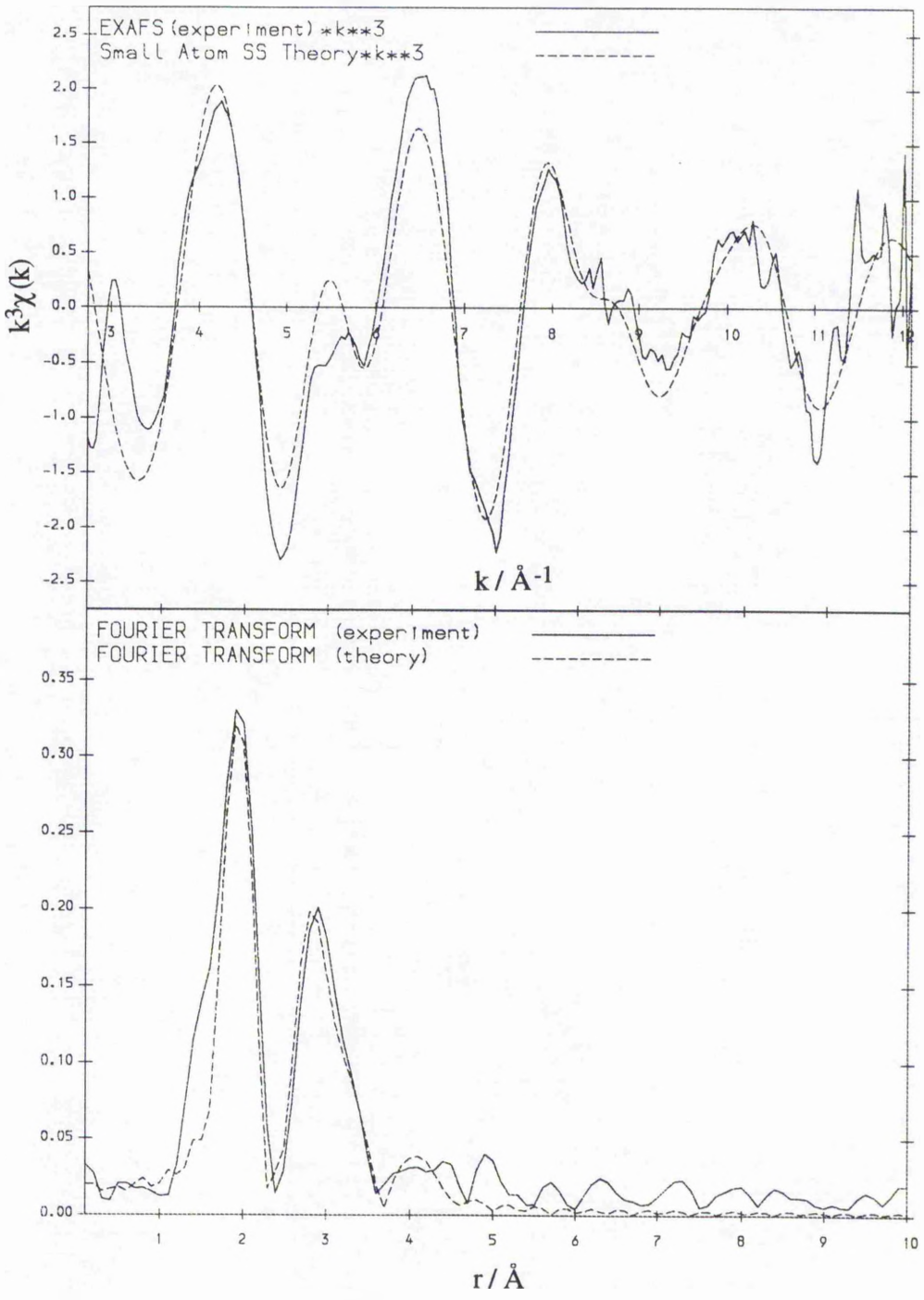

Fig. 5.8(b): Br K-edge EXAFS spectrum, and its Fourier transform, for the bromocyclohexane/thiourea inclusion compound at 80 K. The theoretical fit is for shells corresponding to carbon atoms at 1.95 Å (N = 1; $2\sigma^2 = 0.006$ Å^2), 2.82 Å (N = 2; $2\sigma^2 = 0.014$ Å^2), and 3.30 Å (N = 2; $2\sigma^2 = 0.019$ Å^2), and a bromine atom at 3.90 Å (N = 1; $2\sigma^2 = 0.036$ Å^2). FI = 13.9 %, R = 41.3 %.

For the spectrum recorded at 295 K, Br....C distances can be fitted at 1.95 Å, 2.79 Å (N = 2) and 3.27 Å (N = 2) corresponding to the C1, C2(6) and C3(5) carbons of the cyclohexane ring. This Br....C3(5) distance implies that the bromocyclohexane guest molecules are in the axial conformation. A further shell at 3.82 Å could be fitted only by a Br....Br distance; the comparatively high Debye-Waller factor ($2\sigma^2 = 0.044$ Å^2 at 295 K) for this bromine neighbour indicates a broad distribution of Br....Br distances. The existence of the neighbouring Br shell, which has been fitted with occupancy N = 1, suggests that the bromocyclohexane molecules are arranged in a head-to-head manner within the thiourea tunnel structure. In this regard, it is significant to note that 3.82 Å is close to the interatomic distance for two bromine atoms in van der Waals contact.

From high-resolution solid state ^{13}C NMR spectroscopy [28], it had been shown that, at 208 K, 95 % of the guest molecules in the bromocyclohexane/thiourea inclusion compound are in the axial conformation of bromocyclohexane. In the analysis of our EXAFS data, it was not possible to fit any significant neighbouring shells which would correspond to the 5 % of bromocyclohexane molecules in the equatorial conformation (specifically there was no significant carbon shell at *ca.* 4.25 Å, which would correspond to the Br....C3(5) distance in the equatorial conformation).

The fact that Debye-Waller factors for the intramolecular carbon neighbours and the intermolecular bromine neighbour are lower at 80 K than at 295 K is noteworthy, and is attributed to a reduction in the motional freedom of the guest molecules upon lowering the temperature.

5.4.3.2 *Trans*-1-Bromo-2-Chlorocyclohexane/Thiourea Inclusion Compound

For *trans*-1-bromo-2-chlorocyclohexane/thiourea, Br K-edge EXAFS data were measured over a range of temperatures between 295 K and 80 K [Fig. 5.9 & Figs. 5.10(a)–(c)].

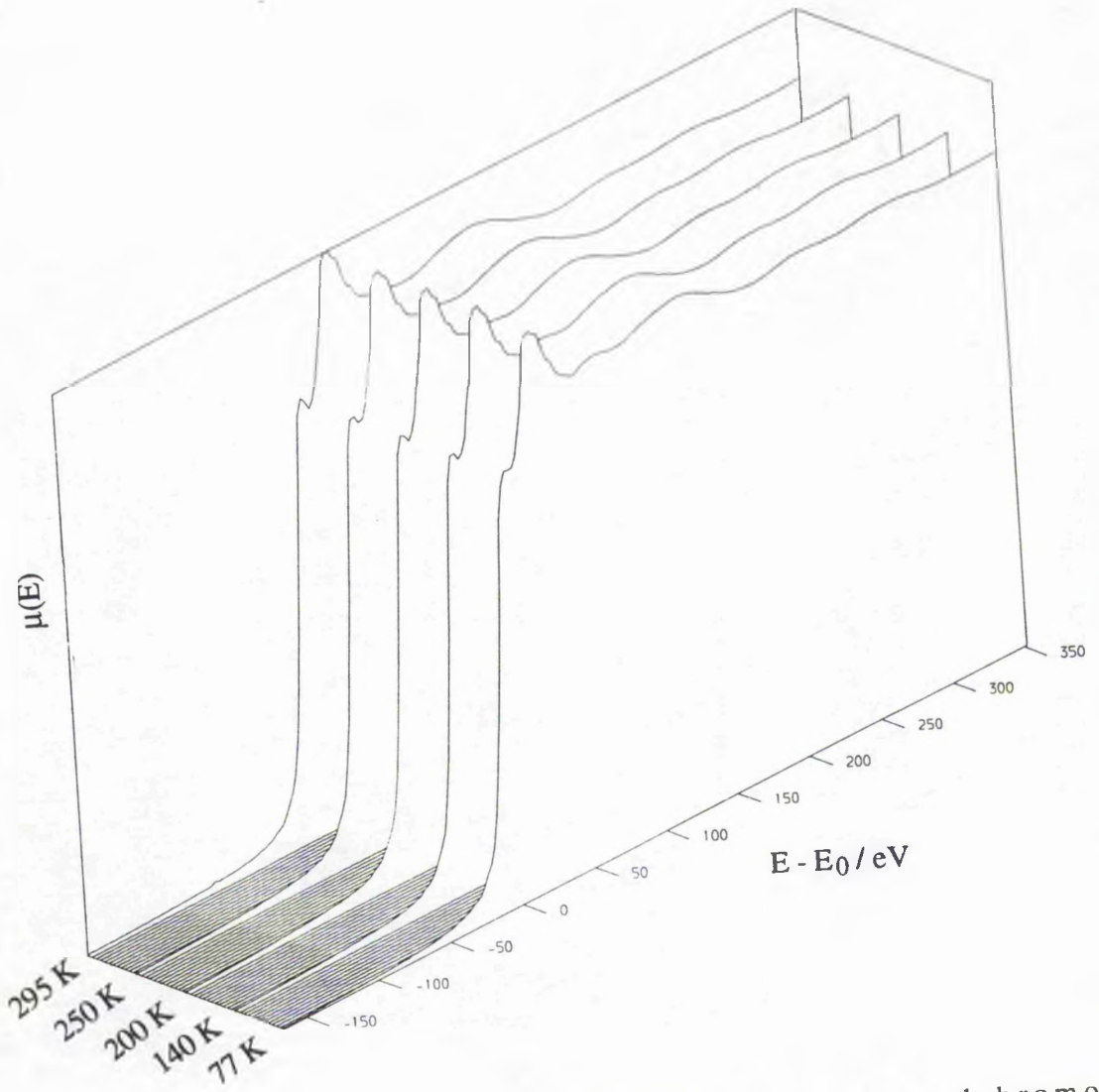

Fig. 5.9: Stack plot of EXAFS Spectra for the *trans*-1-bromo-2-chlorocyclohexane/thiourea inclusion compound as a function of temperature.

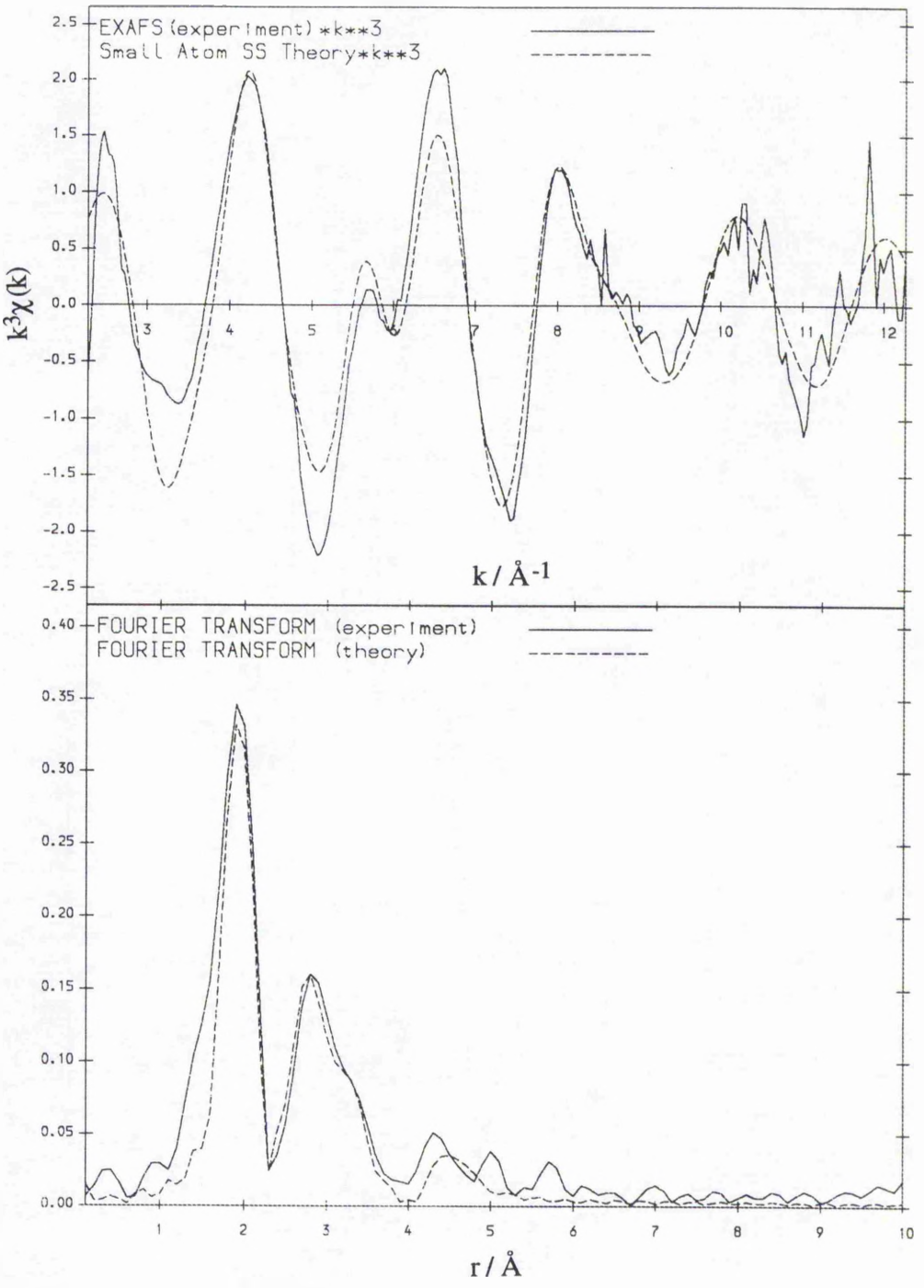

Fig. 5.10(a): Br K-edge EXAFS spectrum, and its Fourier transform, for the *trans*-1-bromo-2-chlorocyclohexane/thiourea inclusion compound at 295 K. The theoretical fit is for shells corresponding to carbon atoms at 1.94 Å (N = 1; $2\sigma^2$ = 0.006 Å^2), 2.79 Å (N = 2; $2\sigma^2$ = 0.020 Å^2), and 3.24 Å (N = 2; $2\sigma^2$ = 0.020 Å^2), and a chlorine atom at 4.52 Å (N = 1; $2\sigma^2$ = 0.033 Å^2). FI = 10.2 %, R = 39.1 %.

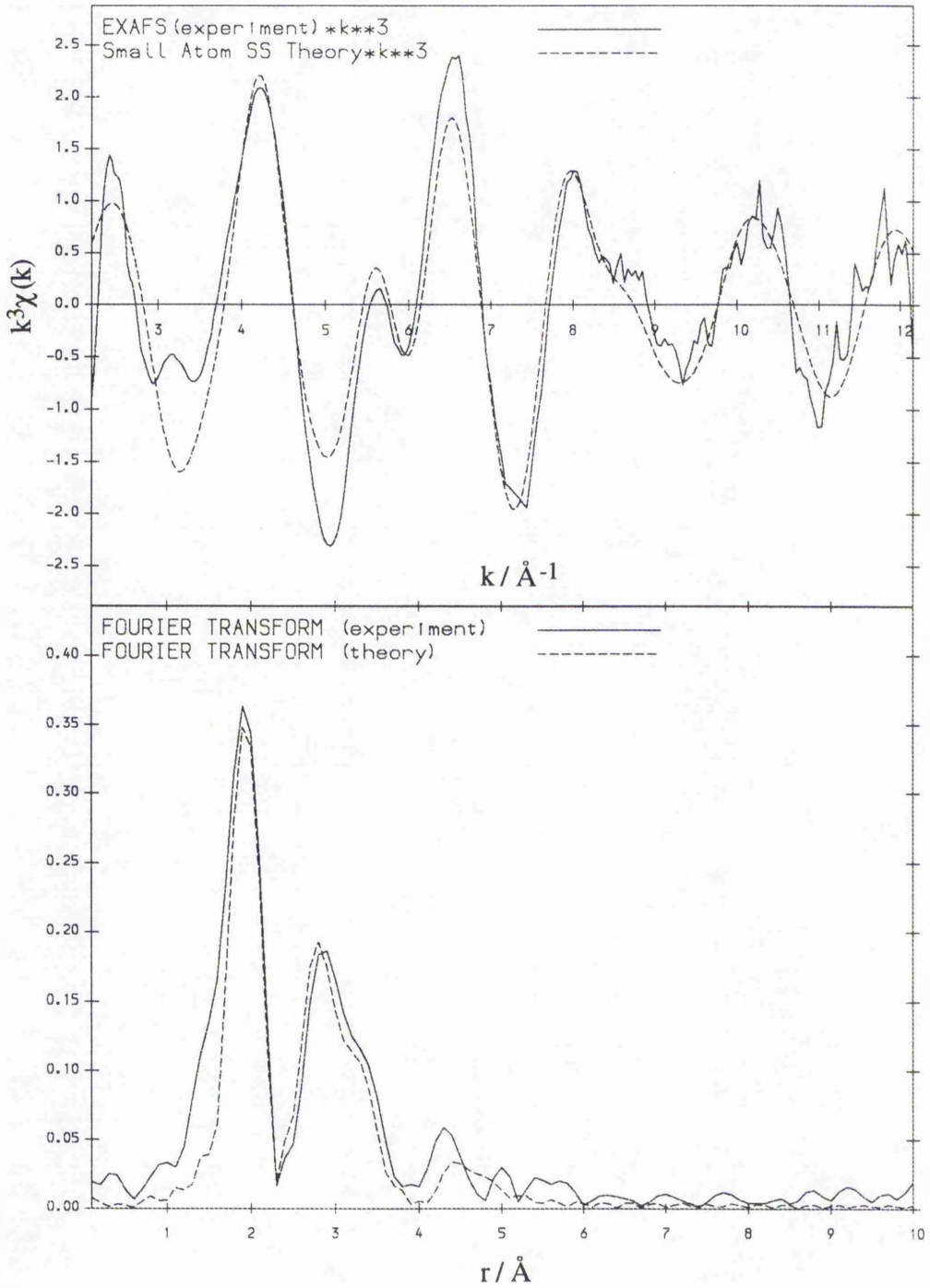

Fig. 5.10(b): Br K-edge EXAFS spectrum, and its Fourier transform, for the *trans*-1-bromo-2-chlorocyclohexane/thiourea inclusion compound at 140 K. The theoretical fit is for shells corresponding to carbon atoms at 1.95 Å (N = 1; $2\sigma^2 = 0.005$ Å^2), 2.80 Å (N = 2; $2\sigma^2 = 0.015$ Å^2), and 3.27 Å (N = 2; $2\sigma^2 = 0.017$ Å^2), and a chlorine atom at 4.53 Å (N = 1; $2\sigma^2 = 0.034$ Å^2). FI = 11.1 %, R = 39.9 %.

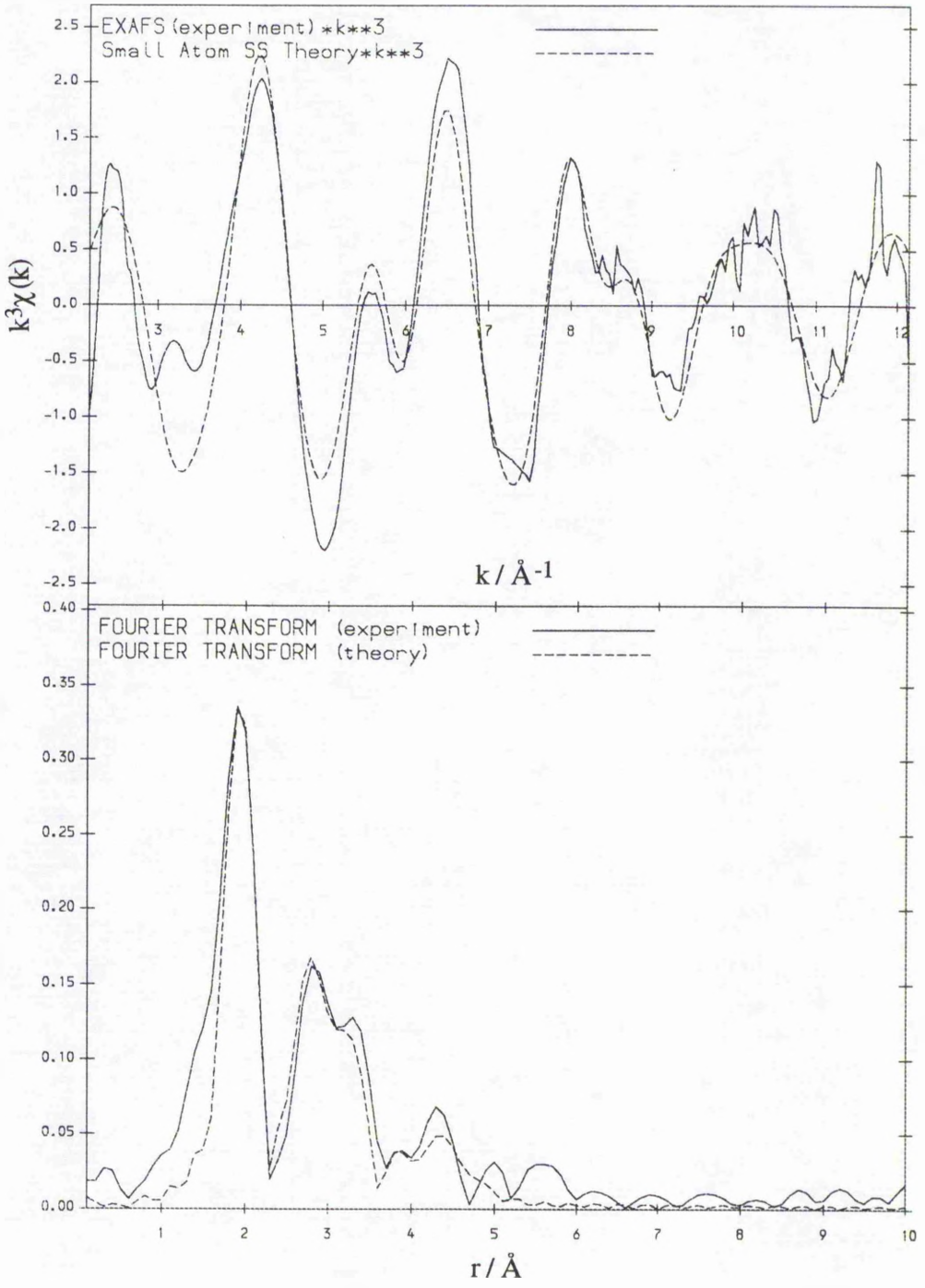

Fig. 5.10(c): Br K-edge EXAFS spectrum, and its Fourier transform, for the *trans*-1-bromo-2-chlorocyclohexane/thiourea inclusion compound at 80 K. The theoretical fit corresponds to carbon atoms at 1.95 Å (N = 1; $2\sigma^2$ = 0.006 Å^2), 2.80 Å (N = 2; $2\sigma^2$ = 0.020 Å^2), and 3.29 Å (N = 2; $2\sigma^2$ = 0.015 Å^2), a bromine atom at 3.87 Å (N = 1; $2\sigma^2$ = 0.033 Å^2), and a chlorine atom at 4.48 Å ($2\sigma^2$ = 0.034 Å^2). FI = 12.0 %, R = 40.9 %.

For the spectra recorded at all temperatures studied, Br....C distances can be fitted at 1.95 Å, 2.80 Å (N = 2) and 3.24–3.29 Å (N = 2), corresponding to the C1, C2(6) and C3(5) carbons of the cyclohexane ring respectively. This Br....C3(5) distance implies that the bromine atom is in an axial position with respect to the cyclohexane ring. There is no significant contribution from C4 (which would represent a Br....C distance at *ca.* 4.0 Å for the bromine atom in an axial position), as assessed from the statistical tests employed. At all temperatures, a Br....Cl distance can be fitted at *ca.* 4.48–4.53 Å, corresponding to *trans*-1-bromo-2-chlorocyclohexane molecules in the diaxial conformation. [Although, in the Fourier transform of the EXAFS spectrum the fit for the Cl neighbour does not appear particularly good, it must be recalled that it is the actual EXAFS oscillations that are being fitted – the Fourier transform merely provides a convenient representation from which the local environment around the absorbing atom can be more easily envisaged.] This shell can be fitted equally well by a carbon neighbour at 4.35 Å, but the low Debye-Waller factor required ($2\sigma^2 = 0.010$ Å^2) is not physically sensible for a neighbouring atom at this distance from the absorber. There is no evidence for any Br....Cl distance in the region of *ca.* 3.4–3.5 Å, which would correspond to *trans*-1-bromo-2-chlorocyclohexane molecules in the diequatorial conformation.

At the lowest temperature studied (T = 80 K), a further significant shell, corresponding to a Br....Br distance at 3.87 Å, can be fitted. This shell did not fit either as a chlorine atom or as a carbon atom. This observation is similar to that for the bromocyclohexane/thiourea inclusion compound, and again suggests that there is head-to-head ordering of the guest molecules within the thiourea tunnel structure. The fact that this well-defined Br....Br distance is identified only at 80 K suggests that there is a substantial increase in the ordering of the guest molecules at low temperature.

5.5 Br EXAFS Studies of Halogenocyclohexane/Zeolite Systems

5.5.1 Introduction to EXAFS Spectroscopy on Zeolites

Zeolitic host materials [33], like urea and thiourea inclusion compounds, contain large cavities in which molecules may be included. In contrast to urea and thiourea inclusion compounds, zeolites may be obtained with a wide range of different sizes of tunnels and cages (and hence are able to include a vast array of sizes and shapes of molecules), and they generally remain stable when there are no guest molecules present.

In the experiments carried out here, a series of zeolite-type host materials have been investigated with *trans*-1,2-dibromocyclohexane included as the guest component. The focus of the experiments was to determine how the conformation of the *trans*-1,2-dibromocyclohexane guest molecules is affected by both the size and the chemical topography of the pores within the zeolites. Because zeolites are generally stable in the absence of guest molecules, it may be expected that the efficiency of packing of guest molecules within these host structures is not as important to the overall stability of the system, as for the thiourea inclusion compounds (for which 100 % packing of the guest in the tunnels is necessary for the stability of the thiourea tunnel structure. In a previous study of monosubstituted cyclohexane molecules within the tunnels of these zeolites the loading of the guest molecules was *ca.* 0.1–1.0 guest molecules per 1000 $Å^3$ [34], and so the probability of observing intermolecular distances between guest molecules is low.

The three different zeolites used in this investigation were H-ZSM-5, zeolite NH_4-Y and NH_4-mordenite. In addition, the aluminophosphate ALPO-5 was also studied. H-ZSM-5 (Si:Al ratio *ca.* 20) contains two sets of intersecting tunnels. Both tunnels have 10-membered ring openings – the straight tunnels have diameter of *ca.* 5.3–5.6 Å, whereas the diameter of the sinusoidal tunnels is *ca.* 5.1–5.5 Å. NH_4-Y (Si:Al ratio *ca.* 3) contains larger tunnels, with cavities of diameter *ca.* 7.4 Å and supercages with diameter *ca.* 13 Å. NH_4-Mordenite (Si:Al ratio *ca.* 10.1) contains unidirectional tunnels of diameter *ca.* 6.5–7.4 Å. ALPO-5 also contains unidirectional tunnels of diameter *ca.* 7.3 Å.

Previously [34], from ^{13}C solid state NMR applied to study monosubstituted cyclohexane molecules in these zeolites, it was found that the equatorial conformation of the guest was preferred in all cases, with the equatorial:axial ratio of in excess of 4:1 at room temperature.

5.5.2 Experimental

Samples comprising *trans*-1,2-dibromocyclohexane included within the H-ZSM-5, NH_4-Y, NH_4-mordenite and ALPO-5 host materials were prepared by the following method.

Before use, all zeolites were calcined in a muffle furnace at 773 K for at least 24 hours. A round bottomed flask containing *ca.* 1.0 g of the appropriate powdered zeolite (or aluminophosphate) and 5 ml of *trans*-1,2-dibromocyclohexane was placed under vacuum for 3 days, to allow the 1,2-dibromocyclohexane to be adsorbed into the host structure. After this period, the excess liquid was removed under vacuum, and the solid allowed to dry before being used for experiments.

Bromine K-edge X-ray absorption spectra were measured on station 7.1 at the SRS facility at the Daresbury Laboratory. For each sample, spectra were recorded both at room temperature (*ca.* 295 K) and at *ca.* 80 K. For each sample at each temperature, the spectrum was recorded over a period of about 45 minutes, and two spectra were recorded and combined to improve the signal/noise ratio.

5.5.3 Results

5.5.3.1 *Trans*-1,2-Dibromocyclohexane/H-ZSM-5

For *trans*-1,2-dibromocyclohexane/H-ZSM-5, Br K-edge EXAFS data were recorded at 295 K and 80 K [Fig. 5.11(a) & (b)].

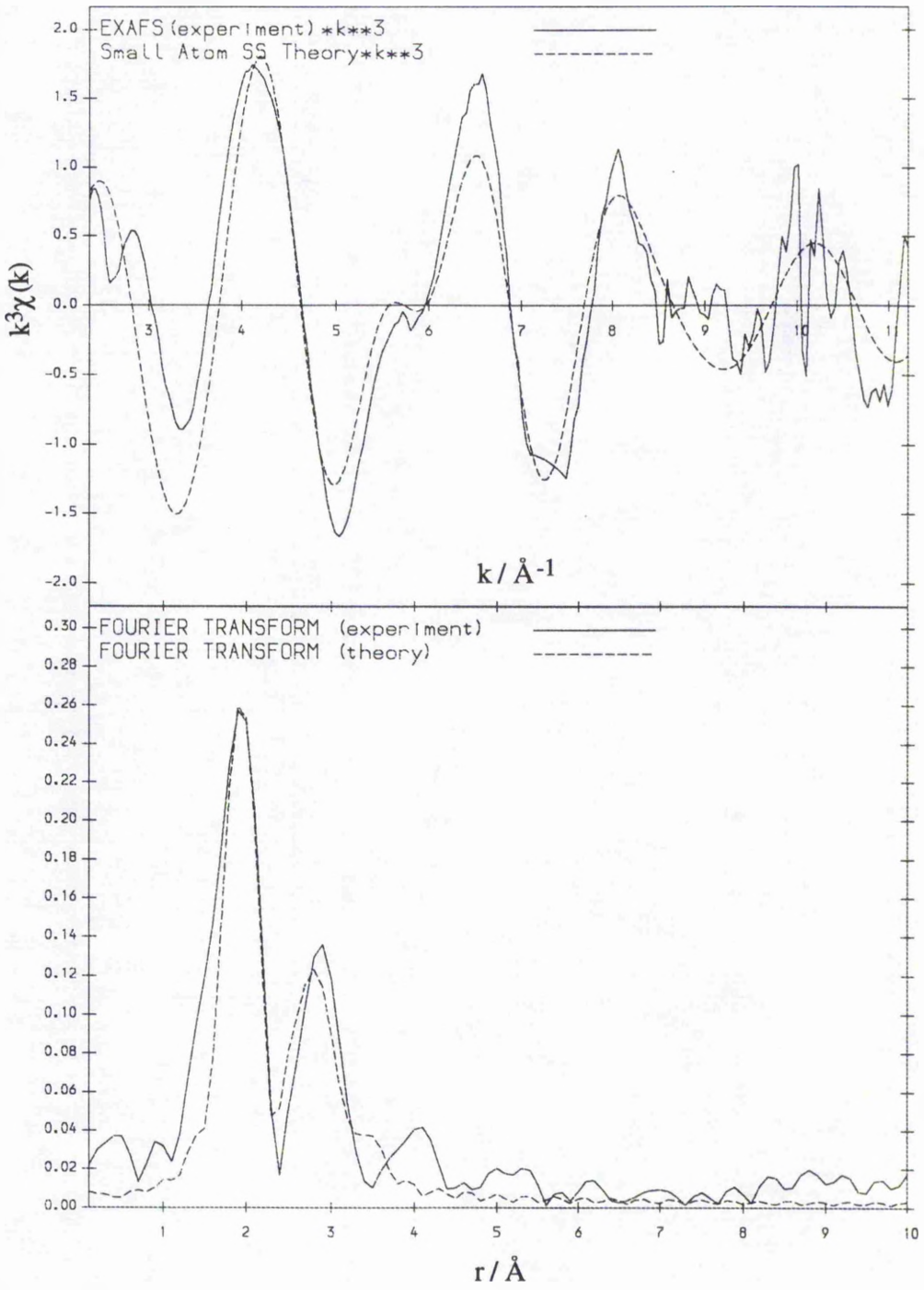

Fig. 5.11(a): Br K-edge EXAFS spectrum, and its Fourier transform, for *trans*-1,2-dibromocyclohexane/H-ZSM-5 at 295 K. The theoretical fit is for shells corresponding to carbon atoms at 1.95 Å (N = 1; $2\sigma^2 = 0.011$ Å^2), 2.80 Å (N = 2; $2\sigma^2 = 0.027$ Å^2), and 3.26 Å (N = 2; $2\sigma^2 = 0.037$ Å^2). FI = 18.3 %. R = 49.6 %.

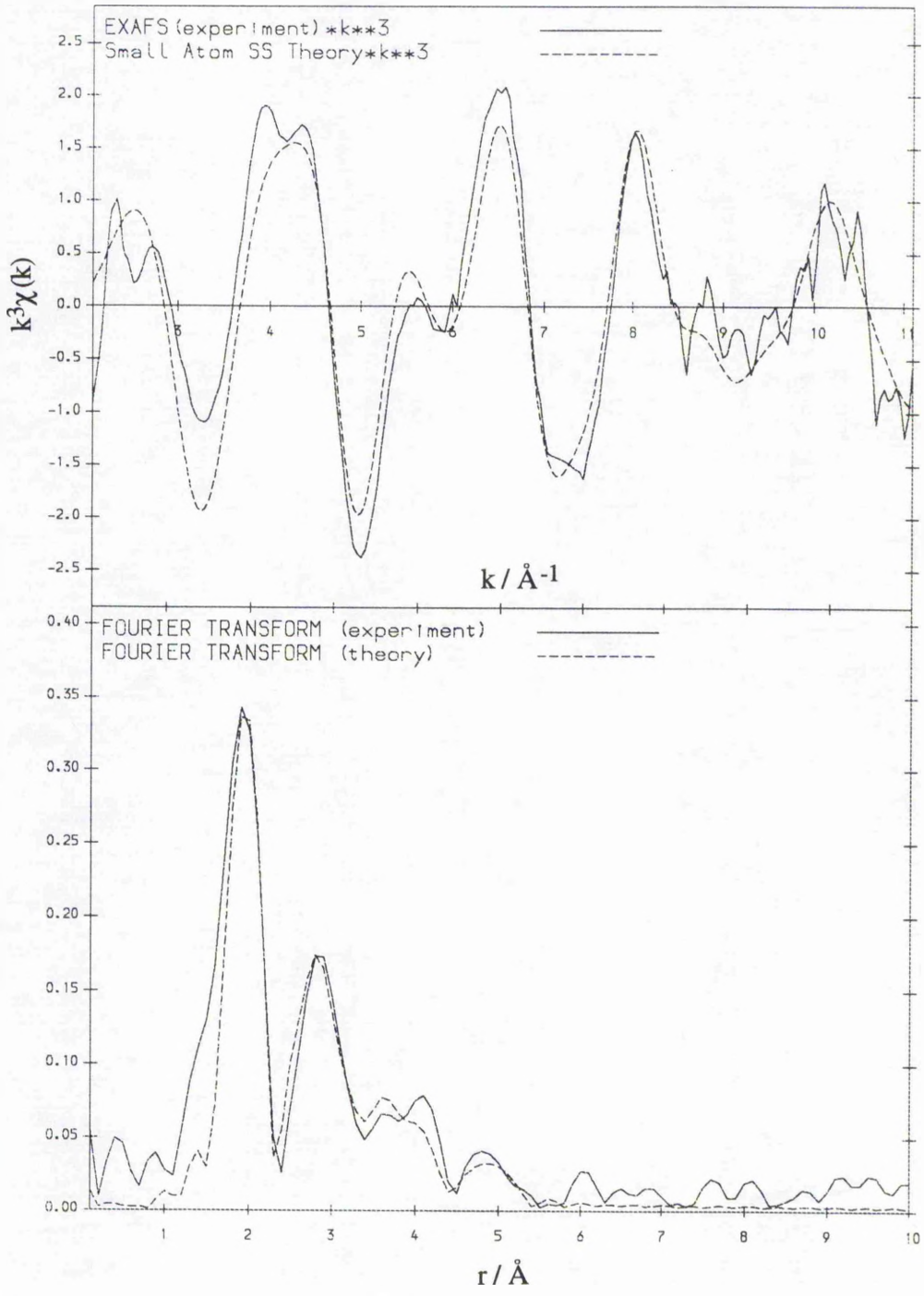

Fig. 5.11(b): Br K-edge EXAFS spectrum, and its Fourier transform, for *trans*-1,2-dibromocyclohexane/H-ZSM-5 at 80 K. The theoretical fit is for shells corresponding to carbon atoms at 1.95 Å (N = 1; $2\sigma^2$ = 0.005 Å^2), 2.81 Å (N = 2; $2\sigma^2$ = 0.015 Å^2), and 3.25 Å (N = 2; $2\sigma^2$ = 0.028 Å^2), a bromine atom at 4.63 Å (N = 1; $2\sigma^2$ = 0.029 Å^2), and a oxygen atoms at 3.84 Å (N = 2, $2\sigma^2$ = 0.027 Å^2). FI = 11.5 %. R = 41.0 %.

For the spectra recorded at both temperatures studied, Br....C distances can be fitted at 1.96 Å, 2.81 Å (N = 2) and 3.25–3.26 Å (N = 2), corresponding to the C1, C2(6) and C3(5) carbons of the cyclohexane ring respectively. This Br....C3(5) distance implies that the bromine atoms are in axial positions with respect to the cyclohexane ring. At T = 80 K, a Br....Br distance can be fitted at *ca.* 4.63 Å, corresponding to the intramolecular Br....Br distance for *trans*-1,2-dibromocyclohexane molecules in the diaxial conformation. It was not possible to fit a significant shell to a Br....Br distance in the region of *ca.* 3.5 Å, which would correspond to *trans*-1,2-dibromocyclohexane molecules in the diequatorial conformation. The inability to fit a significant shell representing a Br....Br distance in the spectra recorded at room temperature may be due to dynamic disorder leading to a distribution of Br....Br distances.

It was possible to fit an additional shell representing oxygen, aluminium, or silicon neighbours. In modelling this feature, occupancies have been constrained to take integer values, though, in practice, non-integer values are possible. The best fit was obtained for a shell of two oxygens (r = 3.84 Å, $2\sigma^2$ = 0.029 Å^2, FI = 11.5 %), though this was not significantly better than the fit with either N = 3 (r = 3.84 Å, $2\sigma^2$ = 0.041 Å^2, FI = 11.6 %), or N = 4 (r = 3.84 Å, $2\sigma^2$ = 0.053 Å^2, FI = 11.7 %). For a single silicon neighbour, the fit index was less good, and the Debye-Waller factor was lower (r = 4.17 Å, $2\sigma^2$ = 0.021 Å^2, FI = 12.1 %). It is also possible that this contribution may arise due to an aluminium neighbour (although the Si:Al ratio is high, the *trans*-1,2-dibromocyclohexane guest molecules may preferentially seek out the aluminium sites in the zeolite framework). When modelling this shell as a single aluminium neighbour, the resulting fit was slightly poorer than for a silicon neighbour (r = 4.21 Å, $2\sigma^2$ = 0.021 Å^2, FI = 12.3 %). Due to the close similarities in the backscattering properties of silicon and aluminium, it is expected that the differences in the fittiing of the EXAFS oscillations will be small.

Although the precise nature of this contribution cannot be determined by EXAFS alone, the presence of this shell suggests that the *trans*-1,2-dibromocyclohexane guest molecules may bind to specific sites in the ZSM-5 host framework. To gain more

information on the interactions between the zeolite framework and the *trans*-1,2-dibromocyclohexane guest, it will be necessary to carry out complementary studies *via* other techniques (e.g. computer modelling).

The EXAFS data did not fit significantly to a model in which the *trans*-1,2-dibromocyclohexane molecules were in the diequatorial conformation, or for a distribution of both diaxial and diequatorial conformations being present.

5.5.3.2 *Trans*-1,2-Dibromocyclohexane/Zeolite-Y

For *trans*-1,2-dibromocyclohexane/NH_4-Y, the Br K-edge EXAFS data recorded at 295 K and 80 K [Fig. 5.12(a) & (b)] show similar features to the spectra of *trans*-1,2-dibromocyclohexane/H-ZSM-5.

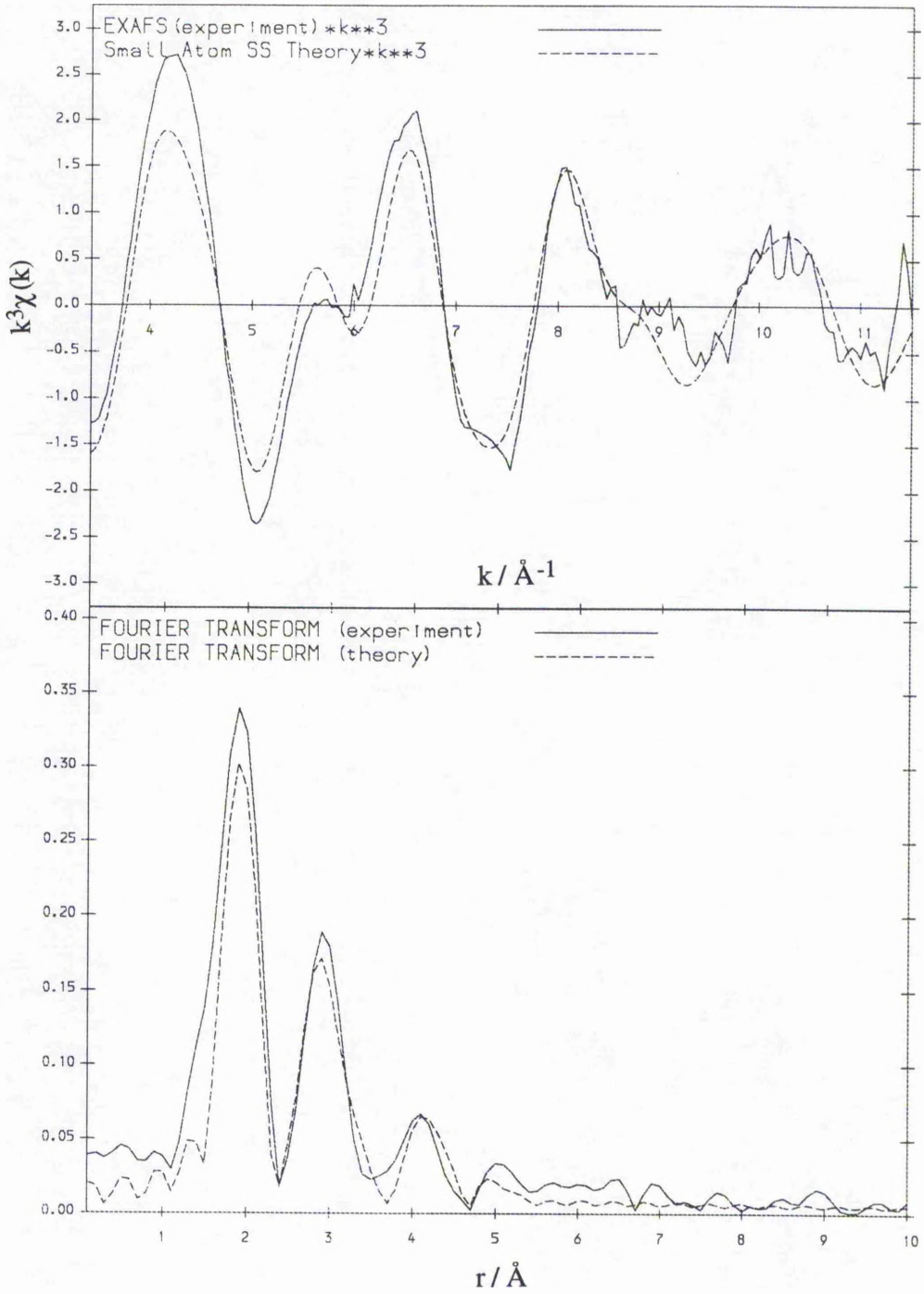

Fig. 5.12(a): Br K-edge EXAFS spectrum, and its Fourier transform, for *trans*-1,2-dibromocyclohexane/NH_4-Y at 295 K. The theoretical fit is for shells corresponding to carbon atoms at 1.95 Å (N = 1; $2\sigma^2$ = 0.005 $Å^2$), 2.79 Å (N = 2; $2\sigma^2$ = 0.017 $Å^2$), and 3.26 Å (N = 2; $2\sigma^2$ = 0.033 $Å^2$), a bromine atom at 4.65 Å (N = 1; $2\sigma^2$ = 0.037 $Å^2$), and a single silicon atom at 4.10 Å ($2\sigma^2$ = 0.023 $Å^2$). FI = 11.1 %. R = 37.6 %.

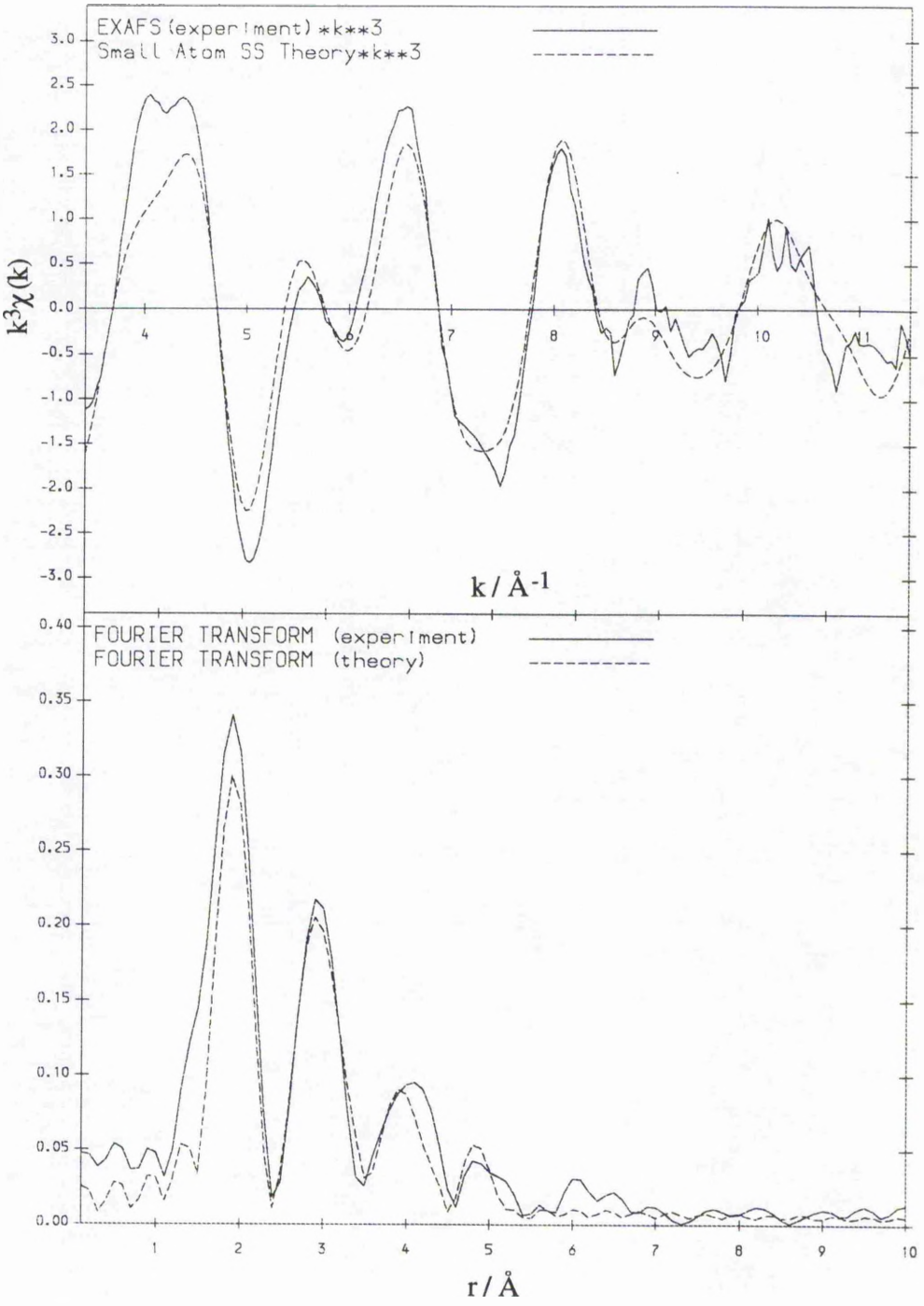

Fig. 5.12(b): Br K-edge EXAFS spectrum, and its Fourier transform, for *trans*-1,2-dibromocyclohexane/NH_4-Y at 80 K. The theoretical fit is for shells corresponding to carbon atoms at 1.94 Å (N = 1; $2\sigma^2$ = 0.005 $Å^2$), 2.79 Å (N = 2; $2\sigma^2$ = 0.014 $Å^2$), and 3.23 Å (N = 2; $2\sigma^2$ = 0.016 $Å^2$), a bromine atom at 4.62 Å (N = 1; $2\sigma^2$ = 0.027 $Å^2$), and oxygen atoms at 3.84 Å (N = 2, $2\sigma^2$ = 0.018 $Å^2$). FI = 11.0 %. R = 35.6 %.

Br....C distances could be fitted at 1.94–1.95 Å, 2.79 Å (N = 2) and 3.23–3.26 Å (N = 2), corresponding to the C1, C2(6) and C3(5) carbons of the cyclohexane ring respectively. At both temperatures, a Br....Br distance can be fitted at *ca.* 4.62–4.65 Å, indicating that the guest molecules are in the diaxial conformation.

An extra shell could be fitted to a contribution from oxygen, aluminium and silicon neighbours at both temperatures. At 295 K, the best fit was obtained for a single silicon neighbour (r = 4.10 Å, $2\sigma^2 = 0.023$ Å^2, R = 11.1 %), while at 80 K two oxygen atoms fitted best (r = 3.84 Å, $2\sigma^2 = 0.018$ Å^2, R = 11.0 %). The same arguments concerning the presence of this shell for the *trans*-1,2-dibromocyclohexane/H-ZSM-5 compound are applicable in the case of *trans*-1,2-dibromocyclohexane/NH_4-Y.

The data did not fit to *trans*-1,2-dibromocyclohexane molecules in the diequatorial conformation.

5.5.3.3 *Trans*-1,2-Dibromocyclohexane/Mordenite

For *trans*-1,2-dibromocyclohexane/mordenite, Br K-edge EXAFS data were obtained at 128 K [Fig. 5.13]. Fitting of the data showed shells of neighbouring C atoms at 1.95 Å, 2.78 Å (N = 2) and 3.24 Å (N = 2), and a Br neighbour at 4.62 Å. Analysis carried out in a similar manner to that on the *trans*-1,2-dibromocyclohexane/H-ZSM-5 and *trans*-1,2-dibromocyclohexane/NH_4-Y compounds of the further feature in the EXAFS spectrum showed that it fitted best to a single Si atom at 4.15 Å, and fitted poorly to oxygen neighbours.

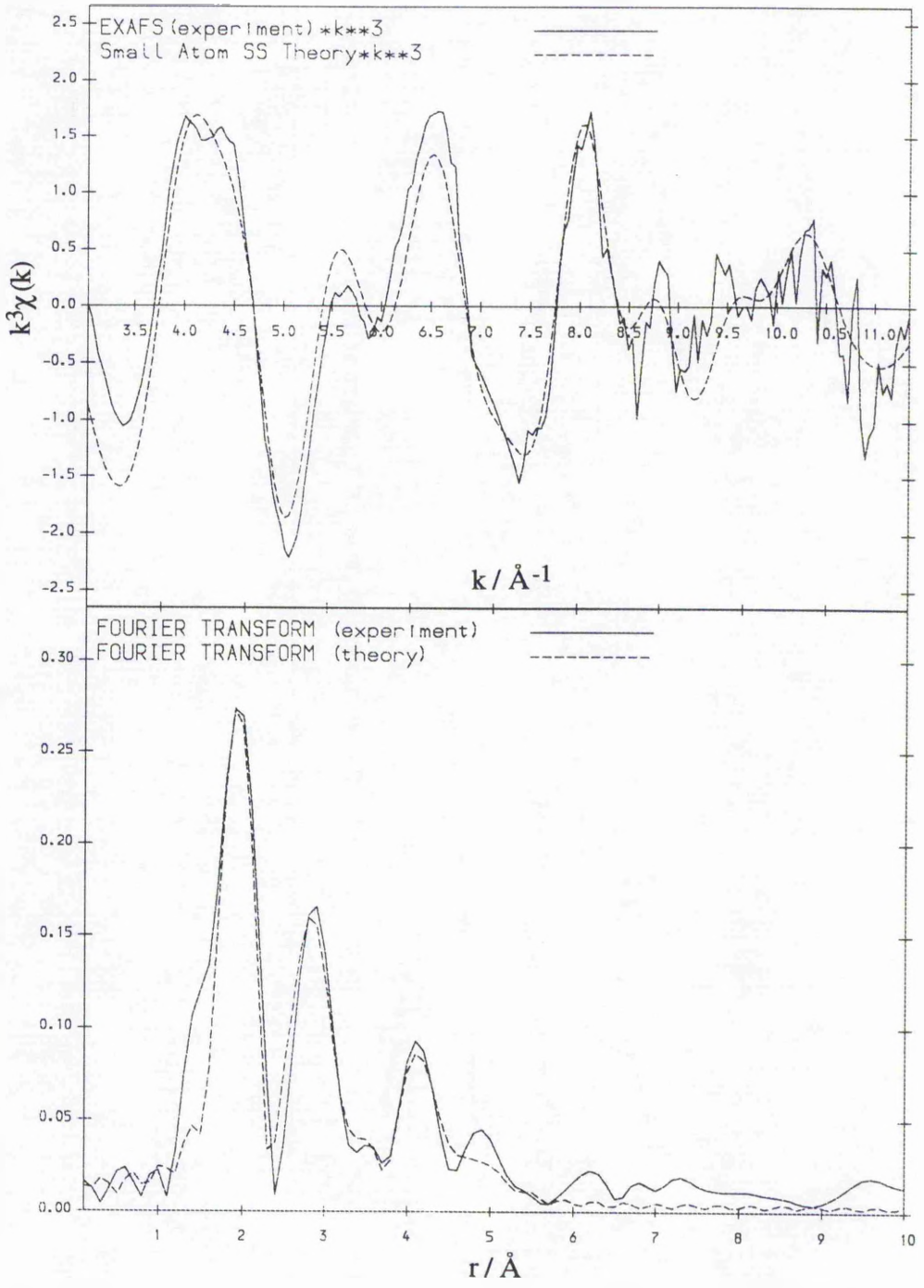

Fig. 5.13: Br K-edge EXAFS spectrum, and its Fourier transform, for *trans*-1,2-dibromocyclohexane/NH_4-mordenite at 128 K. The theoretical fit is for shells corresponding to carbon atoms at 1.95 Å (N = 1; $2\sigma^2$ = 0.009 $Å^2$), 2.78 Å (N = 2; $2\sigma^2$ = 0.019 $Å^2$), and 3.24 Å (N = 2; $2\sigma^2$ = 0.027 $Å^2$), a bromine atom at 4.62 Å (N = 1; $2\sigma^2$ = 0.028 $Å^2$), and a silicon atom at 4.15 Å ($2\sigma^2$ = 0.016 $Å^2$). FI = 12.0 %. R = 39.1 %.

Fitting of the EXAFS data to a model in which the *trans*-1,2-dibromocyclohexane molecules were in the diequatorial conformation was significantly poorer than for the guest in the diaxial conformation. The results indicate that the *trans*-1,2-dibromocyclohexane guest molecules are in the diaxial conformation within the mordenite host structure.

5.5.3.4 *Trans*-1,2-Dibromocyclohexane/ALPO-5

The Br K-edge EXAFS spectrum of *trans*-1,2-dibromocyclohexane/ALPO-5 at 295 K [Fig. 5.14] may be fitted by Br....C distances at 1.95 Å, 2.79 Å (N = 2) and 3.26 Å (N = 2), corresponding to the C1, C2(6) and C3(5) intramolecular neighbours, as before. Although a small peak could be fitted with Br character at *ca.* 4.6 Å, this shell was not significant using statistical significance testing at the 4 % level.

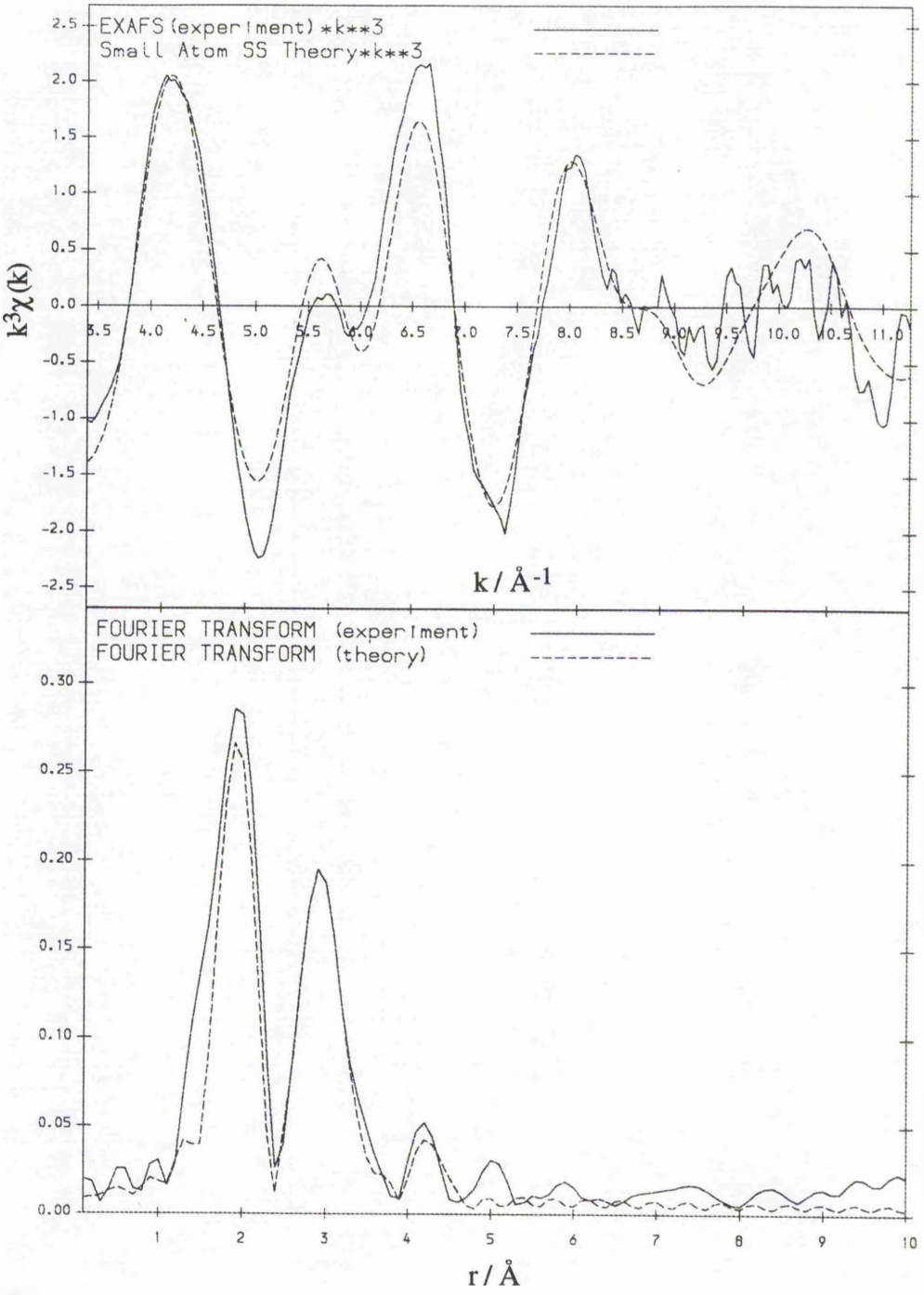

Fig. 5.14: Br K-edge EXAFS spectrum, and its Fourier transform, for *trans*-1,2-dibromocyclohexane/ALPO-5 at 295 K. The theoretical fit is for shells corresponding to carbon atoms at 1.95 Å (N = 1; $2\sigma^2$ = 0.007 Å^2), 2.79 Å (N = 2; $2\sigma^2$ = 0.016 Å^2), 3.26 Å (N = 2; $2\sigma^2$ = 0.017 Å^2), and 4.34 Å (N = 1; $2\sigma^2$ = 0.011 Å^2). FI = 10.2 %. R = 35.4 %.

A further shell could be fitted significantly to a carbon neighbour (N = 1, r = 4.34 Å, $2\sigma^2$ = 0.011 Å^2, R = 10.2 %), though the Debye Waller factor is very low. This shell fitted equally as well to an oxygen neighbour (N = 1, r = 4.28 Å, $2\sigma^2$ = 0.013 Å^2, R = 10.3 %), but was poorer for silicon or aluminium neighbours or for shells with N > 1. The distance modelled for the carbon shell is close to that expected for C(4) of the cyclohexane ring in the axial conformation.

The observation of the C3(5) peak at 3.26 Å, and evidence for a peak with bromine character at 4.6 Å (though not significant), suggests that the guest molecules are in the diaxial conformation. The data did not fit to a model in which the *trans*-1,2-dibromocyclohexane molecules were in the diequatorial conformation.

5.6 Concluding Remarks

From the Br EXAFS data for the conventional $Br(CH_2)_nBr$/urea inclusion compounds (i.e. those with n = 7–11) studied, it has not been possible to determine the Br....Br distance between adjacent guest molecules in the same tunnel. This is due to the presence of substantial dynamic disorder at high temperature and static positional disorder at low temperature. There is no abrupt change in the Br EXAFS spectra on crossing the known phase transition temperatures for these inclusion compounds. These results provide the first indication that the guest substructures in these inclusion compounds do not become substantially more ordered at low temperature than they are at higher temperatures (it is already well-established, from incoherent quasielastic neutron scattering [11] and solid state NMR [19] studies, that there is substantial dynamic disorder within the guest substructure, at least in the high-temperature phase). The exact nature of the static positional disorder, with regard to the interactions between the end-groups of adjacent guest molecules, poses an interesting question. Molecular dynamics simulation of the bromine radial distribution function for α,ω-dibromoalkane/urea inclusion compounds [35] have indeed predicted a broad range of Br....Br distances centred at *ca.* 3.7 Å to be present. The relative width of this peak, when compared to the

widths of the peaks for the intramolecular Br....C distances, is in agreement with the inability to observe a Br....Br distance experimentally.

As discussed in Section 5.3.1, the EXAFS experiments carried out on the α,ω-dibromoalkane/urea inclusion compounds were intended, in part, to serve as an experimental probe of the interaction between adjacent guest molecules within the urea tunnel structure, it having been proposed, on the basis of theoretical predictions, that the interaction between adjacent guest molecules is repulsive. In view of the results reported here, it appears that EXAFS spectroscopy of urea inclusion compounds containing guest molecules terminally functionalised with an X-ray absorbing atom is not a satisfactory approach for investigating this question. Diffraction-based methods have also proved to be unsuitable for probing this issue. Nevertheless, there is still considerable scope for exploiting the power and versatility of solid state NMR spectroscopy to provide experimental insights into this question, and computer simulation techniques also have an important role to play in this regard.

From Br K-edge EXAFS spectroscopy of the *trans*-1-bromo-2-chlorocyclohexane/thiourea inclusion compound, it has been possible to determine the intramolecular Br....Cl distance, from which the preferred conformation of the guest molecule has been determined. It has also been possible to observe intermolecular Br....Br distances for neighbouring guest molecules within the same tunnel for the bromocyclohexane/thiourea inclusion compound at all temperatures studied and for the *trans*-1-bromo-2-chlorocyclohexane/thiourea inclusion compound at 80 K. No well-defined contributions arising from backscattering from atoms of the thiourea host structure could be identified, as expected from the dynamic disorder of the guest molecules in these inclusion compounds.

The successful determination of intermolecular Br....Br distances for the thiourea inclusion compounds contrasts with the inability to determine an intermolecular Br....Br distance for α,ω-dibromoalkane guest molecules in urea inclusion compounds. This observation presumably arises from differing degrees of disorder within the guest substructures in these inclusion compounds.

There are no abrupt changes in the Br K-edge EXAFS spectrum upon crossing the phase transition temperature for the bromocyclohexane/thiourea inclusion compound. From the investigations reported here, there is no evidence that there is any substantial increase in the ordering of the guest molecules relative to the host substructure at low temperature. Thus, dynamic disorder at sufficiently high temperature presumably becomes "frozen in" as static positional disorder at sufficiently low temperature.

The EXAFS studies to probe *trans*-1,2-dibromocyclohexane guest molecules within other microporous solid host materials (zeolites and aluminophosphates) have revealed that, in all cases studied, the guest molecules prefer the diaxial conformation. This contrasts the preference of monohalogenocyclohexane guest molecules for the equatorial conformation in the same host materials, as established by solid state NMR [34]. A possible explanation is that due to the larger size of the *trans*-1,2-dibromocyclohexane guest molecules leads to more stringent steric requirements being imposed on this guest molecule within the tunnels. On the basis of the results of this study, the conformation of the guest is not influenced significantly by the detailed structural characteristics of the pores within the set of host frameworks studied. Evidence for well-defined interaction between the guest and host is observed, but it has not been possible to determine the exact nature of the interactions present. More detailed insights into this issue requires investigation *via* other techniques such as computational modelling.

In the light of the results discussed above, we now assess, in more general terms, the future role of EXAFS spectroscopy in the study of solid organic inclusion compounds. Despite the lack of success in the determination of intermolecular interatomic distances (Br....Br) for the guest molecules in the α,ω-dibromoalkane/urea inclusion compounds, the success in determining, with reasonable accuracy, the intramolecular interatomic distances (Br....C) in the guest molecule is noteworthy. The further success in the determination of intramolecular interatomic distances for substituted cyclohexane molecules within thiourea inclusion compounds and zeolites, leading to elucidation of the conformational properties of the guests, demonstrates that using

EXAFS spectroscopy to probe intramolecular structural features of guest molecules included within solid host materials is certainly a profitable area for future study. In general, such information cannot be determined from diffraction-based investigations in view of positional and/or orientational disorder of the guest molecules, even although, in many cases [12,36], a well-defined diffraction pattern can be obtained from the guest substructure.

The combination of the knowledge gained from EXAFS experiments on systems such as urea and thiourea inclusion compounds for which there are both crystalline and disordered components within the crystal, with the information obtained from diffraction based techniques, will lead to a greater understanding of the structural features of such materials.

References

[1] C.R.A. Catlow and G.N. Greaves: *Chemistry in Britain*, Sept 1986, p.803.

[2] S.M. Heald and J.M. Tranquada: *Physical Methods of Chemistry, Vol.5: Determination of Structural Features of Crystalline and Amorphous Solids*, eds B.W. Rossiter and J.F. Hamilton, Wiley, New York, 1986, p.189.

[3] J.B.A.D. van Zon, D.C. Koningsberger, H.F.J. van't Blik and D.E. Sayers, *J. Chem. Phys.*, **82** (1985) 5742.

[4] J.B. Eberhart: *Structural and Chemical Analysis of Materials*, Wiley, Chichester, 1991, p.350.

[5] B.K. Teo, *Acc. Chem. Res.*, **13** (1980) 412.

[6] N. Binsted, J.W. Campbell, S.J. Gurman and P.C. Stephenson, "SERC Daresbury Laboratory program", 1991.

[7] P.A. Lee and J.B. Pendry, *Phys. Rev. B*, **11** (1975) 1279.

[8] S. Kulpe, I. Seidel, K. Szulzewsky, U. Steger and E. Steger, *Cryst. Res. Technol.*, **16** (1981) 349.

[9] J.E. Nickels, M.A. Fineman and W.E. Wallace, *J. Phys. Chem.*, **53** (1949) 625.

[10] R.W. Joyner, K.J. Martin and P. Meehan, *J. Phys. C*, **20** (1987) 4005.

[11] F. Guillaume, S.P. Smart, K.D.M. Harris and A.J. Dianoux, *J. Phys.: Condens. Matter*, **6** (1994) 2169.

[12] K.D.M. Harris, S.P. Smart and M.D. Hollingsworth, *J. Chem. Soc. Faraday Trans.*, **87** (1991) 3423.

[13] F. Laves, N. Nicolaides and K.C. Peng, *Z. Krist.*, **121** (1965) 258.

[14] A.J.O. Rennie and K.D.M. Harris, *Proc. R. Soc. Lond. A*, **430** (1990) 615.

[15] A.J.O. Rennie and K.D.M. Harris, *J. Chem. Phys.*, **96** (1992) 7117.

[16] N.G. Parsonage and R.C. Pemberton, *Trans. Faraday Soc.*, **63** (1967) 311.

[17] A.J.O. Rennie and K.D.M. Harris, *Chem. Phys. Letts.*, **188** (1992) 1.

[18] M.D. Hollingsworth, K.D.M. Harris, S.P. Smart, J.C. Huffman and B.D. Santarsiero, manuscript in preparation.

[19] S.P. Smart, Ph.D. Thesis, University of St. Andrews, 1993.

[20] Y. Chatani, H. Anraku and Y. Taki, *Mol. Cryst. Liq. Cryst.*, **48** (1978) 219.

[21] F.H. Allen, O. Kennard, D.G. Watson, L. Brammer, A.G. Orpen and R. Taylor, *J. Chem. Soc. Perkin Trans. 2*, (1987) S1.

[22] K.D.M. Harris and J.M. Thomas, *J. Chem. Soc., Faraday Trans.*, **86** (1990) 1095.

[23] A.E. Aliev, E.J. MacLean, K.D.M. Harris, manuscript in preparation.

[24] M. Nishikawa, *Chem. Pharm. Bull.*, **11** (1963) 977.

[25] K. Fukushima, *J. Mol. Struct.*, **34** (1976) 67.

[26] A. Allen, V. Fawcett and D.A. Long, *J. Raman Spec.*, **4** (1976) 285.

[27] M.S. McKinnon and R.E. Wasylishen, *Chem. Phys. Lett.*, **130** (1986) 565.

[28] A.E. Aliev and K.D.M. Harris, *J. Am. Chem. Soc.*, **115** (1993) 6369.

[29] K. Müller, *Magn. Res. Chem.*, **30** (1992) 228.

[30] BIOSYM Technologies Inc., 8625 Scranton Road, San Diego, 92151 CA, U.S.A.

[31] H. Bertagnolli, T. Engelhardt and B. Lengeler, *Z. Phys. Chem. Neue Folge*, **155** (1987) 79.

[32] S. Uemura, A. Onoe and M. Okano, *Bull. Chem. Soc. Japan*, **47** (1974) 143.

[33] A. Dyer: *An Introduction to Zeolite Molecular Sieves*, Wiley, Chichester, 1988, p.1.

[34] A.E. Aliev, K.D.M. Harris and R.C. Mordi, *J. Chem. Soc. Faraday Trans.*, **90** (1994) 1323.

[35] A.R. George and K.D.M. Harris, *J. Mater. Chem.*, **4** (1994) 1731.

[36] K.D.M. Harris and M.D. Hollingsworth, *Proc. R. Soc. Lond. A*, **431** (1990) 245.

Chapter 6

Polymerisation of Guests Within the Tunnels of Perhydrotriphenylene Inclusion Compounds: Formation of Amidine Linked Polymers and Polyalkyleneamines

6.1 Introduction to Perhydrotriphenylene Inclusion Compounds

Perhydrotriphenylene is a tetracyclic hydrocarbon, of formula $C_{18}H_{30}$, which was first synthesised in the early 1960's [Fig. 6.1].

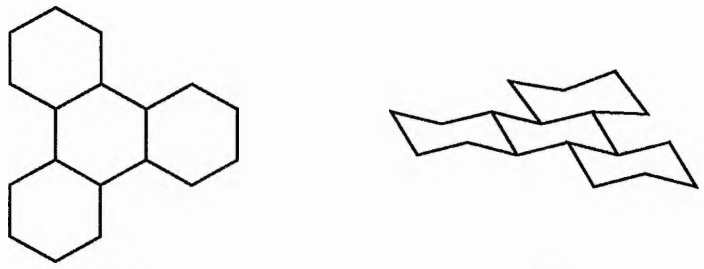

(a) (b)

Fig. 6.1: Diagram showing (a) the perhydrotriphenylene molecule (effectively three cyclohexane rings fused together), and (b) the *trans-anti-trans-anti-trans* isomer which is the most abundant form, and the isomer which forms the inclusion compounds discussed here.

Although perhydrotriphenylene was first synthesised as a low molecular weight model for optically active polymers, it has been more widely used as a solid state organic host, readily forming inclusion compounds with a wide range of guest molecules [1]. Perhydrotriphenylene occurs in ten different stereoisomeric forms, and it is just one of these isomers, *trans-anti-trans-anti-trans* perhydrotriphenylene [Fig 6.1(b)], which is able to form inclusion compounds. The *trans-anti-trans-anti-trans* isomer, which occurs in two enantiomorphic forms, is the most abundant and least soluble of the isomers, and so

can be readily separated from the other isomers. Henceforth, when referring to perhydrotriphenylene we will discuss only this isomer.

Perhydrotriphenylene readily forms inclusion compounds with a wide variety of solvents, and, consequently, inclusion compounds are easier to obtain than the pure crystalline phase of perhydrotriphenylene. Pure samples of perhydrotriphenylene have, however, been obtained by recrystallisation from methylethylketone [2] and 1-methylnaphthalene [3], [Space group: $P2_1/n$, $|a| = 18.315$ Å, $|b| = 15.319$ Å, $|c| = 5.298$ Å, $\beta = 95.53°$].

In contrast to other organic molecules which form tunnel inclusion compounds, such as urea and thiourea (discussed in the previous chapters), perhydrotriphenylene provides a relatively "flexible" tunnel environment into which guest molecules may be included. This flexibility enables a wide variety of different shapes and sizes of guest molecule to be accommodated, ranging from linear alkanes and cyclic compounds such as cyclohexane and toluene, to small molecules such as carbon tetrachloride. The cross sectional diameter of the tunnels is *ca.* 5.5 Å, though it varies according to the specific structural features of the guest molecule [2]. In the absence of guest molecules, the perhydrotriphenylene host structure is unstable and collapses to the pure crystalline phase of perhydrotriphenylene; this is similar to the behaviour of the host structure in urea inclusion compounds.

In the inclusion compounds of perhydrotriphenylene, although the general structure of the host remains tunnel-like, each different guest imposes subtly different structural properties on the perhydrotriphenylene host structure:

i) n-heptane/perhydrotriphenylene inclusion compound

For the n-heptane/perhydrotriphenylene inclusion compound, only the host substructure can be solved, and has space group $P6_3/m$ [$|a| = |b| = 14.40$ Å, $|c| = 4.78$ Å, $\gamma = 120°$] [2]. The host consists of stacks of the two different enantiomorphic forms of *trans-anti-trans-anti-trans* perhydrotriphenylene. Thus, the crystallographic mirror plane relates the different stacks of perhydrotriphenylene molecules [Fig. 6.2].

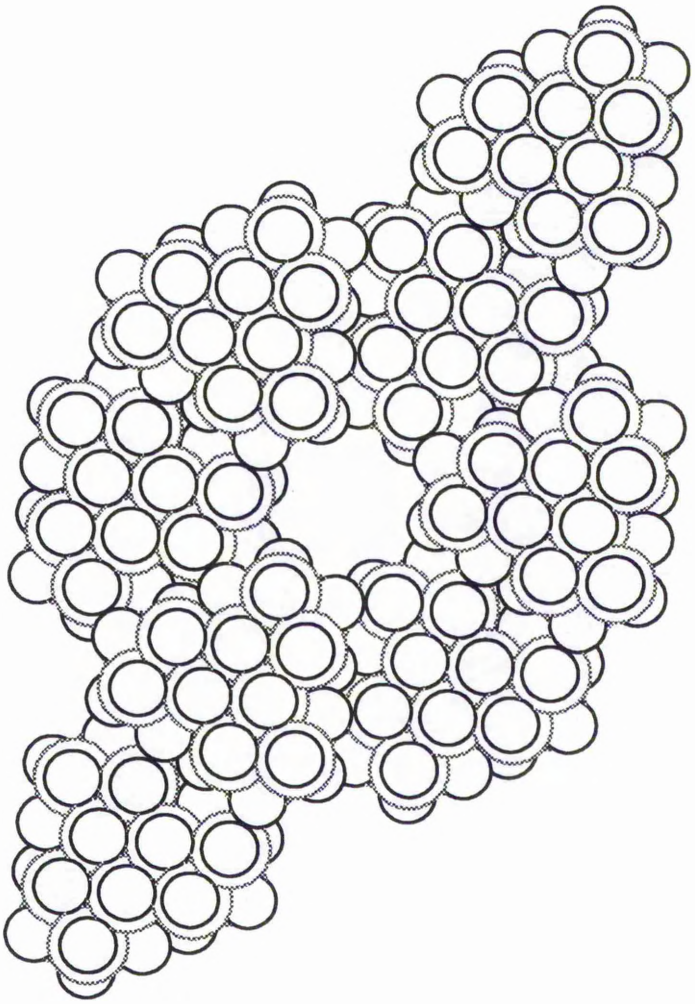

Fig. 6.2: Structure of the perhydrotriphenylene host structure (viewed down the *c*-axis) in the n-heptane/perhydrotriphenylene inclusion compound. The internal diameter of the tunnels is *ca.* 5.5 Å.

The long chain hydrocarbon guests are not located at specific positions within the host tunnel, but are observed as diffuse electron density along the tunnels. For n-heptane guests, a periodicity of 10.69 Å along the *c*-axis has been measured, suggesting that the host and guest substructures are incommensurate along the tunnel axis. The guest molecules are not observed due to being highly mobile and disordered in the tunnels of the perhydrotriphenylene. In contrast to n-alkane/urea inclusion compounds, in which

the guest molecules are known to be predominantly in an all-trans conformation [4], the guest molecules in the n-heptane/perhydrotriphenylene inclusion compound contain an extensive gauche conformation in order to best fit within the tunnel [5]. It has been shown that all-trans and skew(± 60°)-trans-skew(∓ 60°) conformations for the carbon chain best fit the internal diameter of the perhydrotriphenylene tunnel.

ii) $CHCl_3$/perhydrotriphenylene inclusion compound

The $CHCl_3$/perhydrotriphenylene inclusion compound has space group $P6_3/m$ [$|\boldsymbol{a}| = |\boldsymbol{b}| = 25.08$ Å, $|\boldsymbol{c}| = 4.78$ Å, $\gamma = 120°$] [2]. The similarities with the host structure in n-heptane/perhydrotriphenylene are clear, the difference being a three-fold increase in the size of the unit cell. This is, in part, as a consequence of the fixed location of the chloroform guest molecules at specific sites relative to the perhydrotriphenylene host structure. There are two crystallographically distinct $CHCl_3$ molecules within the structure; one is located on a threefold axis, and the other is disordered about a six-fold axis.

iii) Cyclohexane/perhydrotriphenylene inclusion compound

This inclusion compound has the rhombohedral space group $R\bar{3}$ [$|\boldsymbol{a}| = |\boldsymbol{b}| = 25.55$ Å, $|\boldsymbol{c}| = 43.02$ Å] [2]. Seven cyclohexane molecules are located in one period of the host structure along the tunnel. The length of the $\boldsymbol{c}$-axis is 9 times longer than that observed for i) and ii) above.

iv) Dioxan/perhydrotriphenylene inclusion compound

Like iii) above, this inclusion compound has space group $R\bar{3}$ but with a different cell [$|\boldsymbol{a}| = |\boldsymbol{b}| = 25.11$ Å, $|\boldsymbol{c}| = 28.68$ Å]. $|\boldsymbol{c}|$ is six times longer than that for the n-heptane/perhydrotriphenylene inclusion compound, and contains five dioxan molecules ($c_g = 5.69$ Å) in one repeat of the host substructure.

The greatest interest in perhydrotriphenylene inclusion compounds has been in the study of polymerisation reactions, with the potential for the formation of highly stereoregular polymers by polymerisation of guest molecules. Most notable, in this respect, is the polymerisation of 1,3-pentadiene to 1,4-*trans*-polypenta-1,3-diene

(initiated by γ-radiation), where the product polymer (obtained following dissolution of the host matrix) is the pure isotactic form [6–8]. The polymerisation proceeds *via* a free radical mechanism. Other polymers which have been included within the perhydrotriphenylene host structure include polyethylene, polyethylene oxide, 1,4-*trans*-polybutadiene and 1,4-polyisoprene. These inclusion compounds may be obtained either by inclusion of the preformed polymer or by reactions of suitable monomeric guests (e.g. ethene, butadiene, isoprene) inside the tunnels [6].

The perhydrotriphenylene host structure in these inclusion compounds is isomorphous with that in the n-heptane/perhydrotriphenylene inclusion compound. In the X-ray diffraction patterns for these inclusion compounds, discrete reflexions are not seen from the guest species, though diffuse scattering is observed. This has been attributed to dynamic disorder of the polymer chains within the tunnels, as for the n-heptane/perhydrotriphenylene inclusion compound [9].

The dynamic and conformational properties of the polymers when constrained within the perhydrotriphenylene host structure, are greatly different from those of the pure polymers in their amorphous or crystalline phases. For example, for 1,4-*trans*-polybutadiene in perhydrotriphenylene ^{2}H NMR experiments have shown that rapid diffusional motion occurs about the tunnel axis with correlation times $\tau_c \leq 10^{-7}$ s at room temperature and $\tau_c \leq 10^{-3}$ s at 160 K [10]. In pure 1,4-*trans*-polybutadiene, no motion occurs in the crystalline regions on the ^{2}H NMR timescale, whereas in the amorphous regions tetrahedral jumps occur ($\tau_c \leq 10^{-7}$ s). Reduced mobility of the polymer chain for 1,4-*trans*-polypenta-1,3-diene in perhydrotriphenylene is consistent with steric hindrance of the pendant methyl groups with the perhydrotriphenylene host tunnel [8,11].

For the 1,4-polyisoprene/perhydrotriphenylene inclusion compound, the isoprene monomers are able to flip round end-to-end in the tunnels of the host prior to polymerisation, which ensures regiospecificity of the polymer [12]. However, as polymerisation can be initiated in opposite directions within the same tunnel, about 12 % of head-to-head and tail-to-tail ordering is found.

The aims of the study undertaken here were twofold. We have investigated the potential for the formation of new linear polymers within the tunnels of the perhydrotriphenylene host structure. In the first case, the polymerisation of monomers which contain terminal amino and nitrile functional groups has been studied. Polymerisation of these monomers would give rise to the unusual, and relatively unstable, amidine bridging group. Second, the formation of linear polyalkyleneamines, via the reaction of ammonia with alkyl dihalides, has been studied.

6.2 Reactions of the 6-Aminocapronitrile/Perhydrotriphenylene Inclusion Compound

6.2.1 Background

Upon reaction between an amino group and a nitrile group, three possible bonding configurations can be envisaged [Fig. 6.3].

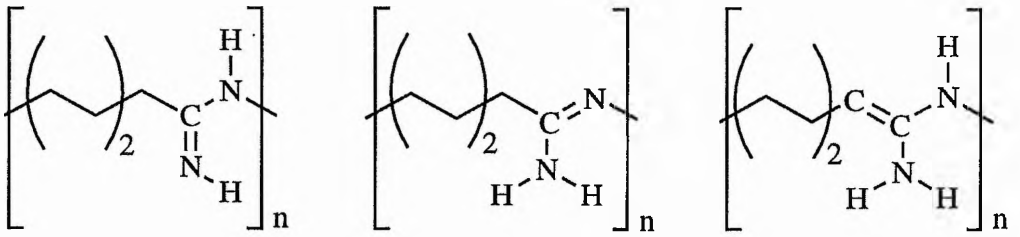

I II III

Fig. 6.3: Diagram of the three possible bonding configurations for the amidine group.

These linking groups can be readily distinguished by a combination of NMR spectroscopy and infrared spectroscopy, due to the characteristic shifts and frequencies of the functional groups present within each linkage. While configuration III can be identified due to the presence of peaks in the alkene region (110–140 ppm) of the ^{13}C NMR spectrum, the N-H band of the infrared spectrum needs to be considered closely in

order to distinguish I and II. The occurrence of two bands in this region (3500–3300 cm^{-1}) would indicate that the amine is primary (as in configuration II), whereas one weak band would suggest the presence of a secondary amine (configuration I). Additionally, for configuration I, the C=N-H group would be expected to show an additional band of medium strength in the region of 3400–3300 cm^{-1} for N-H stretch. [The position of this hydrogen in the ^{1}H NMR spectrum is variable, so it is not possible to use this information to assign the conformation.] Polymerisation to produce configuration I is perhaps the most favourable, as this involves the least rearrangement.

In order to rationalise the polymerisation of guests resulting in the formation of amidine linking groups, studies were carried out on the inclusion compound formed between 6-aminocapronitrile [$H_2N(CH_2)_5CN$] and perhydrotriphenylene.

Preliminary solid state ^{13}C NMR experiments had shown a peak at *ca.* 162 ppm after heating the 6-aminocapronitrile/perhydrotriphenylene inclusion compound to 50 °C – this peak is in the chemical shift region corresponding to a carbon-nitrogen double bond (C=N), as in the amidine linkages in I and II above. A change in colour from white to yellow was also observed [13].

The perhydrotriphenylene host structure promotes the positioning of the guest molecules in the desired steric orientation to enable the polymerisation to occur most favourably. The guest molecules are known from previous studies to favour a head to tail alignment (i.e. NH_2 adjacent to the CN of the next guest molecule in the tunnel) [Fig. 4] [13].

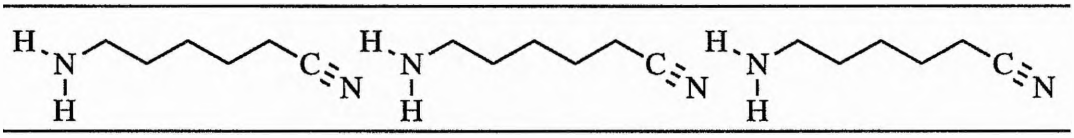

Fig. 6.4: A single tunnel of the perhydrotriphenylene host, showing the favoured head to tail alignment of the 6-aminocapronitrile guest molecules within the tunnel.

The walls of the perhydrotriphenylene tunnel provide a flexible environment in which the short guest molecules are able to reorientate themselves to achieve this ordered arrangement, in a similar manner to isoprene guest molecules [12].

6.2.2 Experimental

Perhydrotriphenylene was synthesised by the hydrogenation of dodecahydrotriphenylene (300 °C, 3000–4000 psi, 10% Pd/C catalyst) in n-heptane, and recrystallised from n-heptane. The product was sublimed (120 °C, 0.02 mmHg) to remove the n-heptane. The perhydrotriphenylene was characterised by powder diffraction and the purity was shown by gas chromatography to be > 99 %.

6-aminocapronitrile (Aldrich, 97 %) was purified by redistillation (57–58 °C, 0.07 mmHg) before use.

Crystals of 6-aminocapronitrile/perhydrotriphenylene were grown by dissolving perhydrotriphenylene in pure 6-aminocapronitrile at 115 °C and slowly cooling the solution to 0 °C. Similarly, crystals of perhydrotriphenylene with $X(CH_2)_rX$; X = Br, Cl, r = 4–6, were grown by dissolving the perhydrotriphenylene in the appropriate pure α,ω-dihaloalkane at 90 °C, and cooling the solution to room temperature. In both cases, the crystals formed were filtered off and dried between two sheets of lens paper (to remove as much free guest adhering to the crystal surfaces as possible).

Crystals of 6-aminocapronitrile/perhydrotriphenylene were heated (to induce polymerisation) on a home made hot stage microscope, allowing any visual changes to be easily observed.

Solution NMR spectra were recorded on a 400 MHz spectrometer. Solid state NMR spectra were recorded on a Bruker MSL-300 spectrometer. Infrared spectra were recorded for samples dispersed in KBr discs on a Galaxy 4020 Series FT-IR. Gas chromatograms were recorded on a Hewlett Packard 5810 Series II gas chromatograph.

6.2.3 X-Ray Diffraction

X-ray diffraction oscillation photographs, recorded for rotation of a single crystal about its tunnel axis, confirmed the formation of the 6-aminocapronitrile/perhydrotriphenylene inclusion compound. The features of the diffraction pattern were consistent with the known structure of the inclusion compounds with other linear guests such as n-heptane [Space group $P6_3/m$: $|\boldsymbol{a}_h| = |\boldsymbol{b}_h| = 14.4$ Å, $|\boldsymbol{c}_h| = 4.81$ Å].

No scattering, either diffuse or discrete, was observed from the guest, probably as a consequence of dynamic disorder of the guest molecules; it is probable oscillation photographs recorded at low temperature may allow X-ray diffraction maxima for the guest substructure to be observed.

6.2.4 Experimental Discussion

Single crystals of the 6-aminocapronitrile/perhydrotriphenylene inclusion compound were heated to 50 °C and 70 °C on a hot stage microscope. In both cases, there appeared to be some decomposition of the crystals (the clear faces of the crystals turning opaque) though the general morphology of the crystals remained needle shaped. Continued heating of the crystals to 125 °C resulted in the crystals melting – this is the melting point of pure perhydrotriphenylene. There was no change in the colour of the crystals. ^1H and ^{13}C solution NMR of the crystals after heating to 50 °C and 70 °C (dissolved in $CDCl_3$) showed no change in the chemical shifts from those observed for the unreacted crystals.

All solution state ^{13}C NMR spectra show three large peaks at 47.1 ppm, 30.1 ppm and 26.6 ppm, corresponding to CH, α-CH_2 and β-CH_2 of perhydrotriphenylene respectively. Peaks corresponding to the guest are seen at 119.6 ppm (<u>C</u>N), 41.8 ppm (<u>C</u>H_2-NH_2), 32.8 ppm (<u>C</u>H_2-CH_2-NH_2), 26.0 ppm (<u>C</u>H_2-CH_2-CH_2-NH_2), 25.3 ppm (<u>C</u>H_2-CH_2-CN) and 17.1 ppm (<u>C</u>H_2-CN).

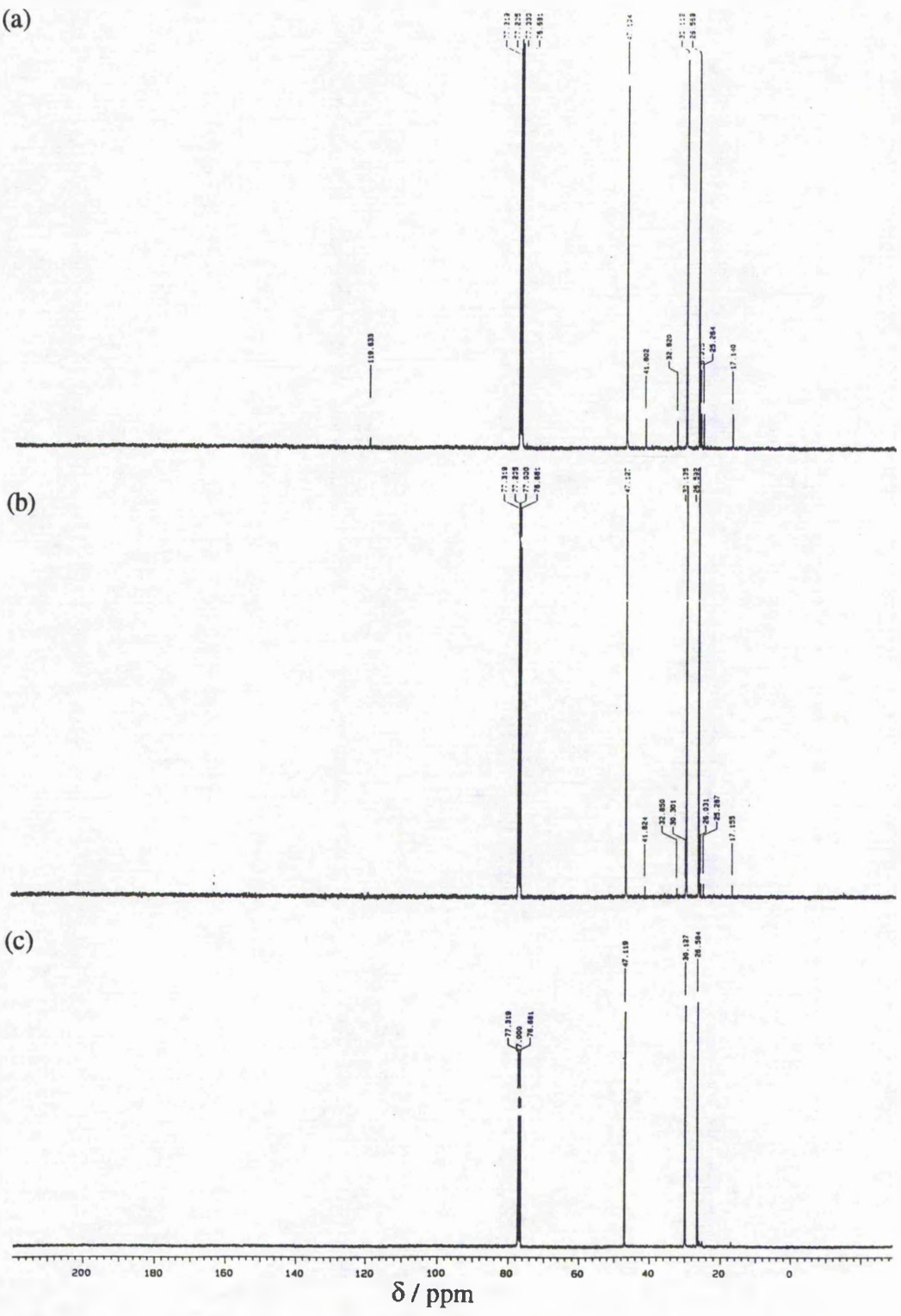

Spectra 6.1: Solution state ^{13}C NMR spectra for the inclusion compound formed between 6-aminocapronitrile and perhydrotriphenylene, dissolved in $CDCl_3$, recorded for: (a) crystals kept at room temperature, (b) crystals that had been heated to 50 °C, and (c) crystals that had been heated to 70 °C.

All solution state ^1H NMR spectra show four large peaks at 1.96 ppm, 1.70 ppm, 1.14 ppm and 0.68 ppm, corresponding to the hydrogens of perhydrotriphenylene. Well defined triplets are seen at 2.71 ppm ($C\underline{H}_2$-NH_2) and 2.35 ppm ($C\underline{H}_2$-CN). Note that the protons on the carbon α to the amine group are coupled only to the adjacent methylene protons – this indicates that there is rapid exchange of the protons on the nitrogen. The resonances for two other sets of methylene H atoms on the alkyl chain of the guest are found beneath the resonances due to the perhydrotriphenylene at 1.70 ppm and 1.14 ppm. The remaining CH_2 resonance and the NH_2 resonance (the position of which varies significantly depending on hydrogen bonding and solvent effects) give rise to the pair of peaks at *ca.* 1.4–1.5 ppm.

The peaks due to the guest were less intense for the material that had been heated to 50 °C than for the unreacted inclusion compound; this was attributed to removal of unincluded guest from the surfaces of the crystals upon heating to 50 °C [Spectra 6.1(a)–(c) & 2(a)–(c)]. For the sample that had been heated to 70 °C, the absence of peaks due to the guest indicates that substantial decomposition of the inclusion compound had occurred, with the guest removed from the tunnels. There was no evidence for a peak in the ^{13}C solution NMR spectra in the region of 160 ppm. Sensitivity in the spectra was a problem, with the peaks observed for the guest being very small in relation to those for the host. This is as a consequence of the fact that a large percentage of the sample (> 90 % by mass) is perhydrotriphenylene.

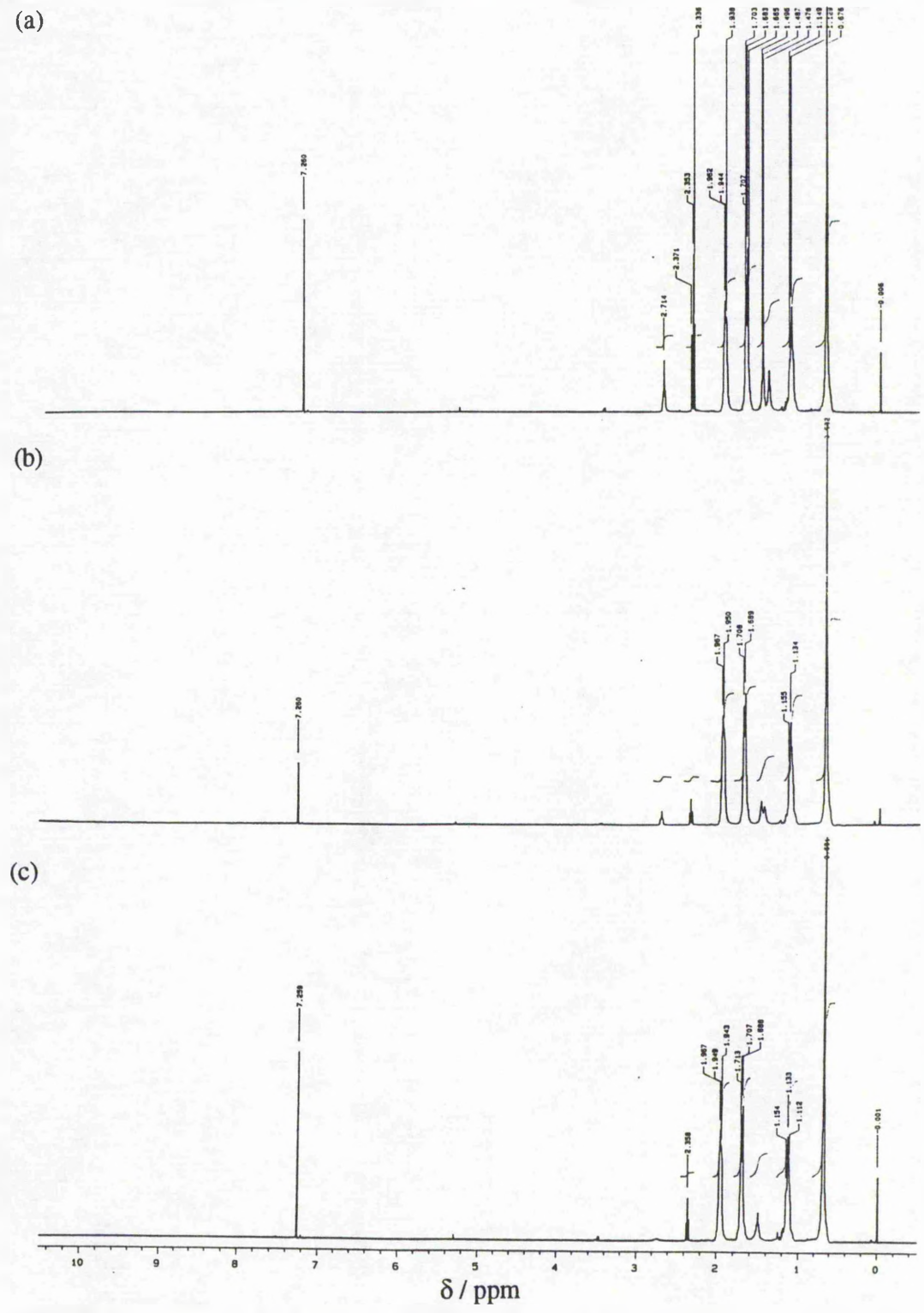

Spectra 6.2: Solution state ^{1}H NMR spectra for the inclusion compound formed between 6-aminocapronitrile and perhydrotriphenylene, dissolved in $CDCl_3$, recorded for: (a) crystals kept at room temperature, (b) crystals that had been heated to 50 °C, and (c) crystals that had been heated to 70 °C.

Infrared spectra were recorded for an unreacted sample of the 6-aminocapronitrile/perhydrotriphenylene inclusion compound and for samples of this inclusion compound that had been heated to 50 °C and 70 °C [Spectra 6.3(a)–(c)]. All spectra are dominated by intense C-H stretching modes in the region 2800–3000 cm^{-1}. In the spectra of both the unreacted inclusion compound and the sample heated to 50 °C, a small, weak band is observed at around 2244 cm^{-1}, corresponding to the CN stretching mode (this is absent from the spectrum of the sample heated to 70 °C). In the spectrum of the sample heated to 50 °C, an additional broad band appeared at around 3328 cm^{-1}, which is in the region of N-H stretching modes. There were no peaks in this region before heating, suggesting that this may be due to the N-H stretch of the C=N-H group in configuration I. Again, in all these spectra, these features were very weak compared to the C-H stretching band, rendering new bands difficult to detect.

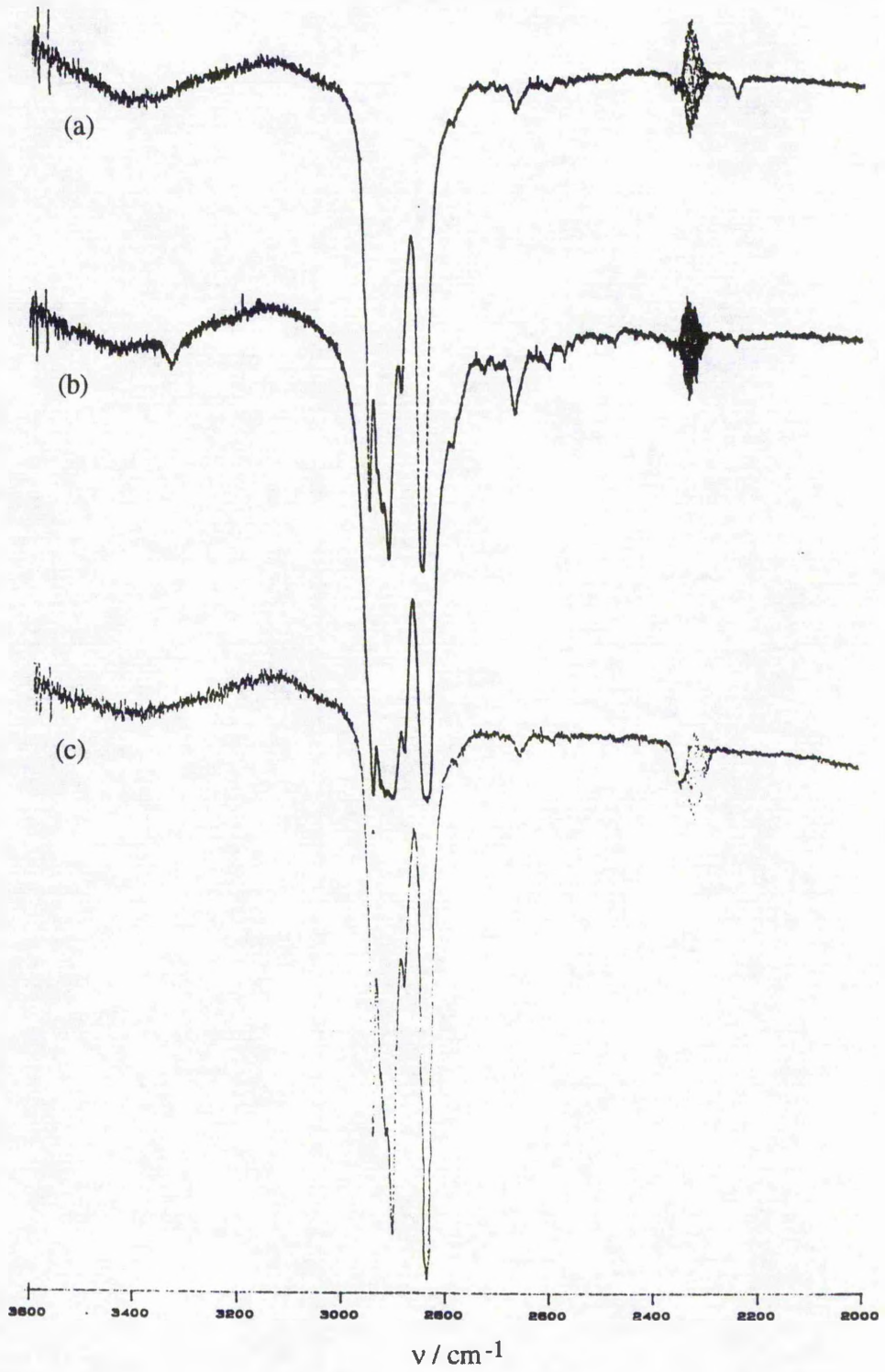

Spectra 6.3: Infrared spectra for the inclusion compound formed between 6-aminocapronitrile and perhydrotriphenylene, dispersed in KBr discs, for: (a) crystals kept at room temperature, (b) crystals that had been heated to 50 °C, and (c) crystals that had been heated to 70 °C. The spectra are shown over the range 3600–2000 cm^{-1}.

Solid state ^{13}C NMR spectra, recorded before and after heating the 6-aminocapronitrile/perhydrotriphenylene inclusion compound to 50 °C [Spectra 6.4(a) & (b)], show many of the same features as the solution ^{13}C NMR spectra. Peaks at 47.5 ppm, 31.0 ppm and 27.7 ppm, correspond to the perhydrotriphenylene. Peaks due to the guest are at 119.1 ppm (CN) and 17.4 ppm (CH_2-CN). Splitting of the nitrile peak as a consequence of residual dipolar interaction between ^{13}C and ^{14}N is observed. The peaks due to other carbons of the guest are obscured by the resonances from the perhydrotriphenylene. In addition to these peaks, an additional resonance is observed at 164.79 ppm. This is in the region expected for C=N, and indicates that some degree of polymerisation has occurred. However, this peak is also observed in the spectrum for the unreacted inclusion compound. This could be explained by either: (a) In the formation of the inclusion compound, heating of the solution to 120 °C may have resulted in some polymer forming prior to crystallisation or after the crystallisation process had started but while the solution was still warm – in this case, though, the band in the infrared spectrum at 3328 cm^{-1} would be expected to be observed for the unreacted material; (b) A period of several months elapsed between synthesis of the sample and recording the solid state ^{13}C NMR spectra, during which the sample was stored at room temperature. It may be that the reaction does occur at temperatures lower than 50 °C, but the rate of reaction is much slower.

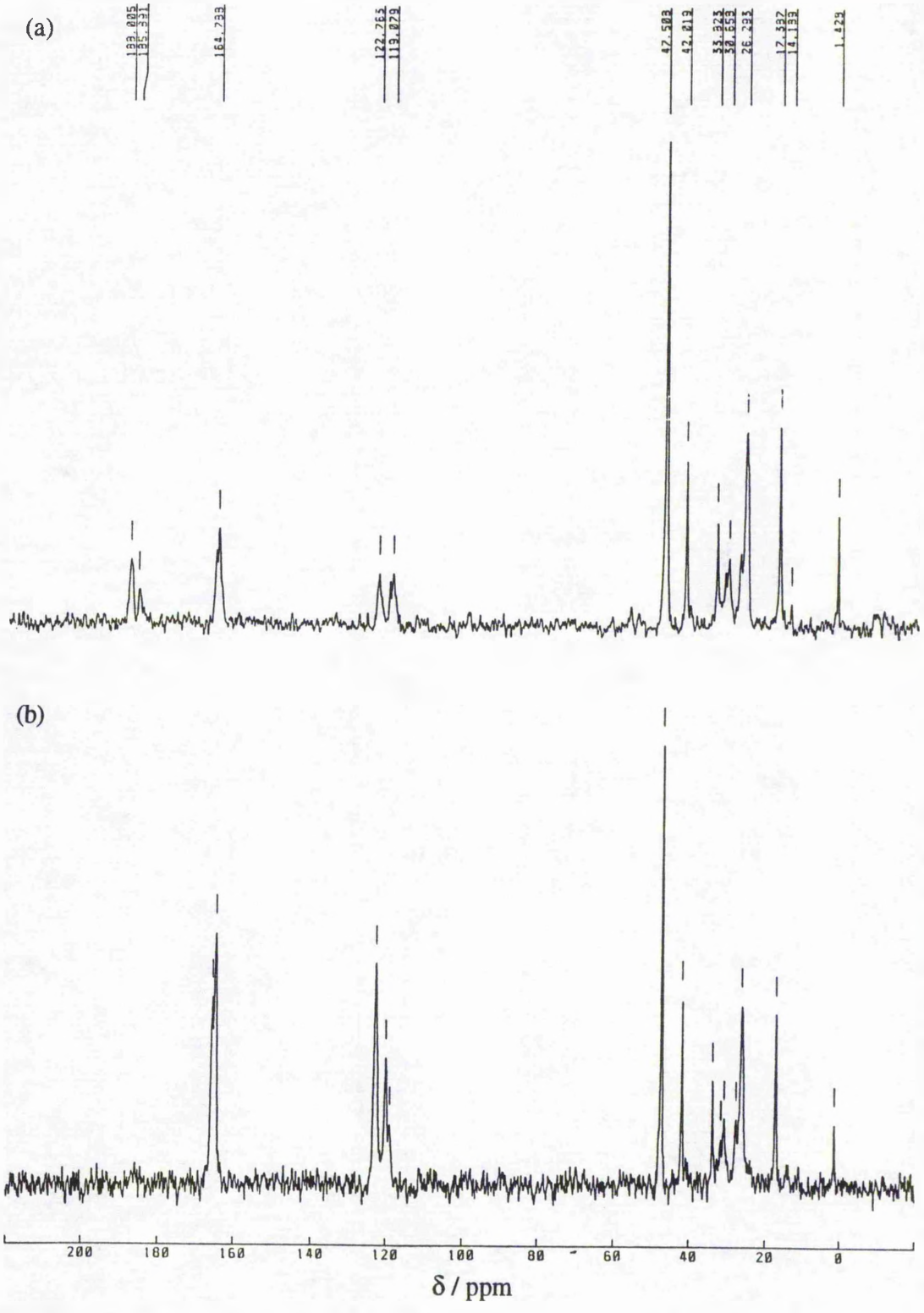

Spectra 6.4: Solid state ^{13}C NMR spectra for the inclusion compound formed between 6-aminocapronitrile and perhydrotriphenylene, recorded for: (a) crystals kept at room temperature, (b) crystals that had been heated to 50 °C.

6.3 Reaction of α,ω-Dihaloalkane/Perhydrotriphenylene Inclusion Compounds with NH_3

6.3.1 Background

It is well known that the reaction of alkyl halides with ammonia or amines results in the formation of alkylamines [14]. However, because secondary amines are more reactive than primary amines (and primary amines are more reactive than ammonia), full alkylation at the nitrogen occurs, and either tertiary amines or quaternary alkyl ammonium salts are formed [Fig. 6.5].

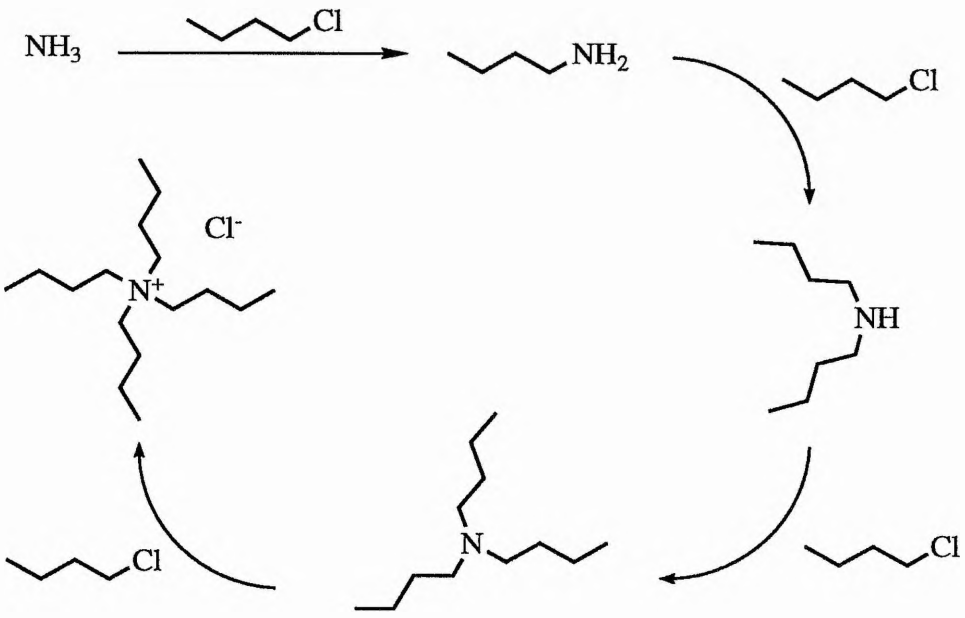

Fig. 6.5: The reaction of 1-chlorobutane with ammonia. The reaction proceeds, via the formation of primary and secondary amines, towards full alkylation around the nitrogen.

In the reaction of α,ω-dihaloalkanes with ammonia, the same reaction results in the formation of a cross-linked polymer, which contains no stereoregularity and consequently has non-uniform properties.

Linear unbranched polymers which contain nitrogen atoms spaced along the polymer chain at regular intervals are highly stable (to > 300 °C) and possess novel properties, such as water solubility. It is also possible to control the substitution of the remaining amine hydrogen, enabling the synthesis of functionalised derivatives of the polymer. In the studies undertaken here, the aim was to determine a simple method for synthesising these linear polyalkyleneamines.

Previously, the only unbranched polyalkyleneamine to be synthesised was polyethyleneamine, from the ring opening of aziridine [Fig. 6.6] [14].

Fig. 6.6: Ring opening reaction of aziridine to produce polyethyleneamine polymer.

It has not been possible to synthesise, in any significant yield, the polymers with longer alkyl chain spacers between the NH groups (e.g. polypropyleneamine). Perhydrotriphenylene inclusion compounds provide the environment within which it may be possible to synthesise these "longer" polymers. Because the tunnels in the perhydrotriphenylene host structure are uni-directional, cross-linking between polymer chains formed in adjacent tunnels is prohibited.

The inclusion of α,ω-dihaloalkane molecules within the perhydrotriphenylene host structure, and the subsequent diffusion of ammonia into the system, provides a possible mechanism through which the polymerisation may occur. The cross-sectional area of the tunnels is sufficiently large that ammonia can diffuse into the system. It has been found previously, in the case of the 11-fluoroundecanol/perhydrotriphenylene inclusion compound, that washing the crystals with water results in the water entering the tunnels to give a 1:1 molar ratio with the guest [15]. The ammonia molecule is of similar

size to water, and so it is expected that ammonia may also be able to diffuse into the tunnels.

In the experiments described here, both dibromoalkanes and dichloroalkanes have been studied. While bromoalkanes are more reactive to ammonia than chloroalkanes, they are not necessarily more suitable for the formation of alkyleneamine polymers. If the substitution of Br is too fast, it is possible that diamines may be formed before adjacent guests can react together.

6.3.2 Experimental and Discussion

Perhydrotriphenylene was synthesised as described previously (Section 6.2.2). Crystals of $X(CH_2)_rX$/perhydrotriphenylene; X = Br, Cl; r = 4–6, were grown by dissolving the perhydrotriphenylene in the appropriate pure α,ω-dihaloalkane at 90 °C, and cooling the solution slowly to room temperature. The crystals formed were filtered and dried between two sheets of lens paper (to remove as much free guest adhering to the crystal surfaces as possible).

To test the suitability of α,ω-dihaloalkane/perhydrotriphenylene inclusion compounds for producing linear alkyleneamine polymers, various sets of conditions and reactants were considered.

Both powdered samples of the inclusion compound and single crystals were studied. While using a powdered sample maximises the surface area and increase the probability of the ammonia diffusing into the tunnels compared to single crystals, the maximum length of the linear polymer chains that may be obtained is reduced.

In the initial experiments, a small molar excess of ammonium hydroxide [$NH_3.H_2O$] was added to samples of the α,ω-dihaloalkane/perhydrotriphenylene inclusion compound in a flask and shaken in an ultrasonic bath for *ca.* 3 hours at temperatures up to 40 °C.

The results are illustrated for 1,6-dibromohexane/perhydrotriphenylene in Spectra 6.5(a)–(b) & 6.6(a)–(b).

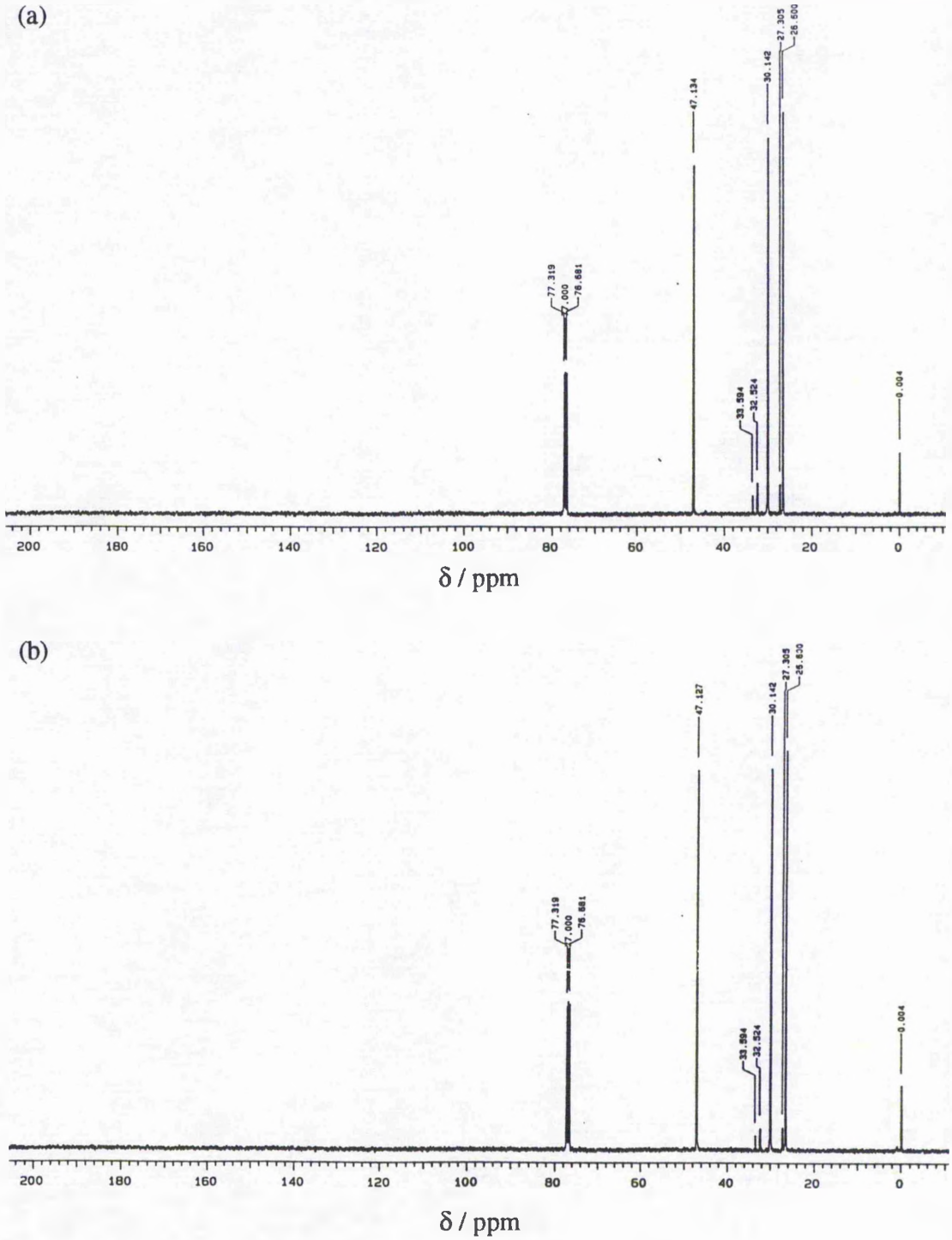

Spectra 6.5: Solution state ^{13}C NMR spectra (solvent $CDCl_3$) recorded for: (a) the 1,6-dibromohexane/perhydrotriphenylene inclusion compound, and (b) the 1,6-dibromohexane/perhydrotriphenylene inclusion compound after shaking with ammonium hydroxide and ethanol at 40 °C for 3 hours.

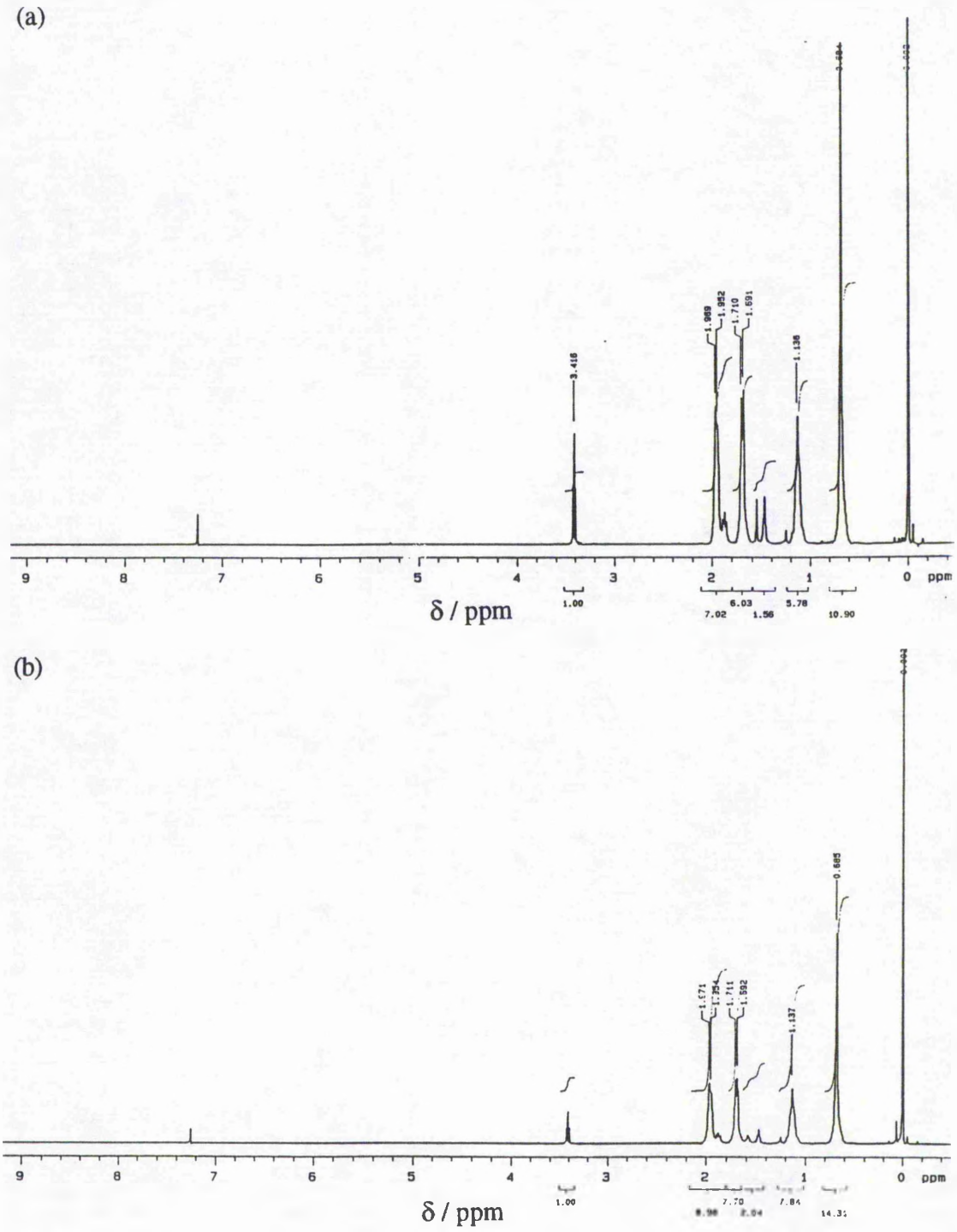

Spectra 6.6: Solution state ^{1}H NMR spectra (solvent $CDCl_3$) recorded for: (a) the 1,6-dibromohexane/perhydrotriphenylene inclusion compound, and (b) the 1,6-dibromohexane/perhydrotriphenylene inclusion compound after shaking with ammonium hydroxide and ethanol at 40 °C for 3 hours.

The solution ^{13}C NMR spectra (solvent $CDCl_3$) show the three large peaks at 47.1 ppm, 30.1 ppm and 26.6 ppm, corresponding to the perhydrotriphenylene. Peaks for the guest occur at 33.6 ppm ($\underline{C}H_2$-Br), 32.5 ppm ($\underline{C}H_2$-CH_2-Br) and 27.3 ppm ($\underline{C}H_2$-CH_2-CH_2-Br). In the ^1H NMR spectrum, the guest resonances occur at 3.42 ppm ($C\underline{H}_2$-Br; triplet), 1.88 ppm ($C\underline{H}_2$-CH_2-Br; multiplet) and 1.45 ppm ($C\underline{H}_2$-CH_2-CH_2-Br; multiplet). These results reveal that no reaction of the guest molecules has occurred for either the dibromoalkanes or dichloroalkanes.

In previous preparations of branched alkyleneamine polymers, ethanol had been frequently used as solvent for the reaction [14]. However, addition of ethanol to the reaction flask in our experiment did not lead to any reaction.

As an alternative source of nitrogen, liquid ammonia rather than ammonium hydroxide was tried. Excess liquid ammonia was added to a 95 % ethanol solution containing the 1,5-dibromopentane/perhydrotriphenylene inclusion compound at -40 °C (dry ice/acetone bath) in a sealed system. After a period of *ca.* 3–4 hours, the excess ammonia was removed and the ethanol solution filtered off. The crystals were clearly seen to have undergone a change in their morphology. Solution ^{13}C NMR showed that this solid was pure perhydrotriphenylene. There was no evidence for inclusion of ethanol within the perhydrotriphenylene.

On evaporating off the ethanol from the filtrate, a solid residue was left behind. Preliminary solution ^1H NMR of this solid (dissolved in d_6-dimethylsulphoxide) clearly shows that the peak at 3.42 ppm, due to $C\underline{H}_2$-Br (triplet) in the 1,5-dibromopentane, has disappeared, and a new triplet appears at 2.98 ppm [Spectra 6.7(a)–(b)]. This is in the region expected for the hydrogens of a methylene group adjacent to a protonated amine group ($C\underline{H}_2$-NR_3^+). The multiplet at 1.62 ppm may be assigned to $C\underline{H}_2$-CH_2-NR_3^+. It is not, however, possible to conclude from this whether the amine is secondary or tertiary and thus whether a cross-linked or linear polymer has been formed. Further ^1H and ^{13}C NMR studies of the deprotonated ammonium salt are required before the product can be fully characterised. Insufficient product was obtained from the reaction for an infrared spectrum to be recorded.

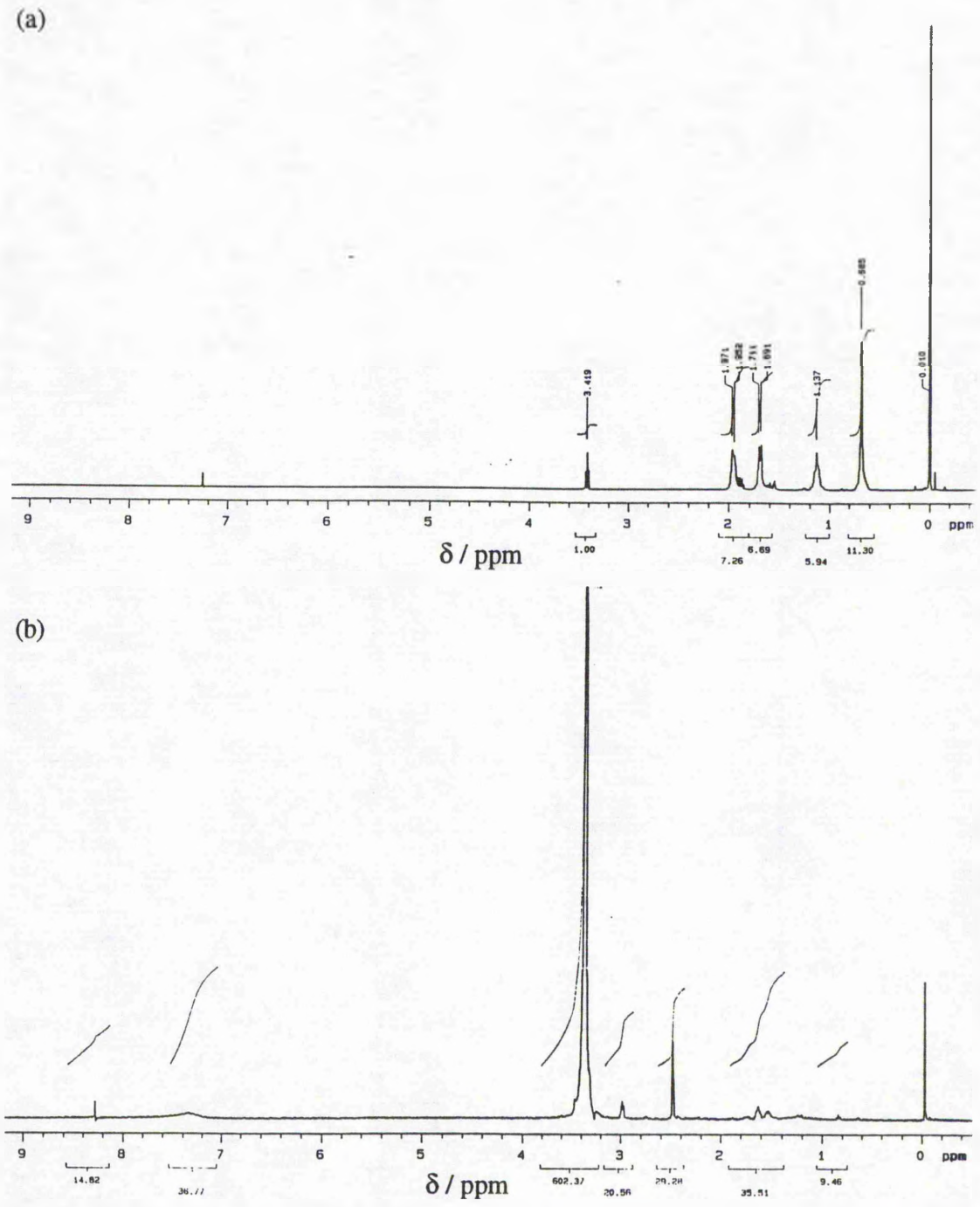

Spectra 6.7: Solution state ^1H NMR spectra recorded for: (a) the 1,5-dibromopentane/perhydrotriphenylene inclusion compound (solvent $CDCl_3$), and (b) the residue left from the ethanolic solution, after evaporation of the ethanol (solvent d_6-DMSO), from the reaction of the 1,5-dibromopentane/perhydrotriphenylene inclusion compound with liquid NH_3. [Spectrum (b) is dominated by impurity peaks due to water (3.4 ppm) and undeuterated DMSO (2.5 ppm) in the d_6-DMSO.]

It is not clear from these results whether the reaction occurred within the tunnels of the perhydrotriphenylene inclusion compound, or outside the inclusion compound.

If the polymer is found to be linear, this would suggest that the reaction occurred within the tunnels, followed by a decomposition of the inclusion compound, liberating the polymer into the ethanol solution. Alternatively, branching in the product would strongly imply that the inclusion compound decomposed prior to reaction with NH_3, and that the branched polymer is formed in the solution phase. It could be envisaged that linear polymer may further react in the solution phase, after decomposition of the perhydrotriphenylene host had occurred, in the presence of excess NH_3.

Further NMR studies, as indicated above, are vital before these questions can be answered.

6.4 Conclusion

From the combined evidence of infrared spectroscopy and solid and solution state ^{13}C NMR, several conclusions can be drawn about the formation of the amidine bridged polymer from 6-aminocapronitrile monomers, in the perhydrotriphenylene inclusion compound. On heating the 6-aminocapronitrile/perhydrotriphenylene inclusion compound to 50 °C, polymerisation of the guest molecules occurs with the generation of a linking group containing a carbon-nitrogen double bond. This excludes the formation of configuration III as the linking group. A change is also observed in the infrared spectrum with the appearance of a new single band in the N-H stretch region (3328 cm^{-1}); we suggest that this is the N-H stretch for the C=N-H group in configuration I (expected as a medium strength band at 3400–3300 cm^{-1}), as the primary amine (configuration II) would give rise to two bands. As mentioned before, the linkage in configuration I requires least rearrangement of the nitrile and amine groups.

The absence of a peak at *ca.* 162 ppm in the solution state ^{13}C NMR spectra suggests, however, that the polymer is too unstable to exist outside the confinement of the perhydrotriphenylene host tunnel structure – the polymer reverts to the 6-aminocapronitrile "monomer" units upon dissolution of the host matrix. Also, the

solution ^{13}C NMR and infrared spectra of the inclusion compound that had been heated to 70 °C show that the guest has been lost from the tunnels of the perhydrotriphenylene host structure.

The sensitivity of the techniques used has been a problem here in obtaining results on this system. Due to the fact that the vast majority of the sample is perhydrotriphenylene (> 90 %), the features of interest, in relation to polymerisation of the guest molecules, are relatively weak. In this respect, labelled compounds will provide an avenue for future work. In particular, ^{13}C or ^{14}N labelling of the nitrile group will facilitate the assignment of the mechanism for amidine polymer formation.

It has been demonstrated, from the preliminary experiments on the reaction of the α,ω-dihaloalkane/perhydrotriphenylene inclusion compound with NH_3, that there is potential for the formation of amines. Although it has not yet been possible to ascertain whether the reaction occurs inside or outwith the perhydrotriphenylene host structure, there is still considerable scope for tuning the reaction conditions (e.g. examining more closely the role of the ethanol). Even if the reaction does not produce the regular linear polymers that are the target of this work (e.g. if the ammonia is unable to diffuse into the tunnels) there is the possibility to use haloalkylamines [$X(CH_2)_nNH_2$; X = Br, Cl] as guest, with the host constraining the guest molecules to approach in the required orientation for reaction. For such guests handling in the pure state may be problematic – $X(CH_2)_4NH_2$ and $X(CH_2)_5NH_2$ readily cyclise to give pyrrolidine and piperidine respectively. In such cases, formation of tunnel inclusion compounds with perhydrotriphenylene could indeed be exploited as a means of "storing" such unstable guest molecules.

References

[1] M. Farina, in: *Inclusion Compounds, Vol. 2*, eds J.L. Atwood, J.E.D. Davies and D.D. MacNicol, Academic Press, London, 1984, p.69.

[2] G. Allegra, M. Farina, A. Immirzi, A. Colombo, U. Rossi, R. Broggi and G. Natta, *J. Chem. Soc. B*, (1967) 1020.

[3] R.L. Harlow and G.R. Desiraju, *Acta Cryst.*, **C46** (1990) 1054.

[4] H.L. Casal, *J. Phys. Chem.*, **94** (1990) 2232.

[5] G. Allegra, M. Farina, A. Colombo, G. Casagrande-Tettamanti, U. Rossi and G. Natta, *J. Chem. Soc. B*, (1967) 1028.

[6] M. Farina, G. Natta, G. Allegra and M. Loffelholz, *J. Polymer Sci. C*, **16** (1967) 2517.

[7] M. Farina, G. Di Silvestro and P. Sozzani, *Mol. Cryst. Liq. Cryst.*, **93** (1983) 169.

[8] S. Brückner, P. Sozzani, C. Boeffel, S. Destri and G. Di Silvestro, *Macromolecules*, **22** (1989) 607.

[9] P. Sozzani, F.A. Bovey and F.C.Schilling, *Macromolecules*, **24** (1991) 6764.

[10] P. Sozzani, F.A. Bovey and F.C.Schilling, *Macromolecules*, **22** (1989) 4225.

[11] A.E. Tonelli, *Macromolecules*, **23** (1990) 3129.

[12] F.C. Schilling, P. Sozzani and F.A. Bovey, *Macromolecules*, **24** (1991) 4369.

[13] M.D. Hollingsworth, unpublished results.

[14] *Encyclopedia of Polymer Science and Engineering, Vol. 1*, ed. J.I. Kroschwitz, Wiley, New York, 1985.

[15] M.D. Hollingsworth, H. Oumar-Mahamat, unpublished results.

Chapter 7

High-Resolution Solid State ^{13}C NMR Studies of Metallocenes as a Function of Magic Angle Sample Spinning Frequency

7.1 Solid State NMR Spectroscopy

Nuclear magnetic resonance (NMR) spectroscopy has been known for almost 50 years, first being observed in 1946. It has only really come to full fruition, however, since the 1970's and the advent of Fourier transform NMR, and is now recognised as one of the most powerful spectroscopic techniques [1].

While much of NMR spectroscopy is applied to the analysis of liquid samples, solid state NMR can probe properties of all types of solid, which may be difficult to investigate by other methods. For example, it is possible to gain a knowledge of the kinetics of motions (e.g. chemical exchange) occurring within a solid. In relation to crystallography, NMR can be used to determine the composition of the crystallographic asymmetric unit, and to supplement X-ray diffraction data by providing information on the positions of H atoms and detecting hydrogen bonding arrangements [1].

The basic theory behind solid state NMR is the same as that for solution state NMR. However, in order to obtain high resolution solid state NMR spectra there are several important problems, which do not apply to liquids, which must be overcome. These problems are discussed here with regard to ^{13}C NMR, but are valid for all dilute spin $\frac{1}{2}$ nuclei [2].

For dilute spin $\frac{1}{2}$ nuclei, there are many nuclear interactions which affect the properties of the nuclei in a magnetic field, of which the major ones are the direct and indirect dipole-dipole interactions between magnetic nuclei, and electron shielding, which alters the effective external magnetic field experienced at the nucleus. In solution NMR, these interactions are averaged by rapid molecular tumbling – the direct dipole-dipole

interaction is averaged to zero, the indirect dipole-dipole interaction to the scalar coupling constant (J), and the chemical shift anisotropy to the chemical shift (δ). However, in solids this is generally not the case, as the molecules are in a fixed (or spatially restricted) environment within the sample. In order to obtain high resolution solid state NMR spectra, similar to those for liquids, these interactions must be averaged by other methods. For dilute spin $\frac{1}{2}$ nuclei in solid samples, the two major contributions to NMR line-broadening arise from chemical shift anisotropy (CSA) and direct heteronuclear dipole-dipole interactions.

i) Chemical Shift Anisotropy

In a powdered solid, all orientations of a molecule relative to the external magnetic field (B_0) are present. Each of these orientations has a different chemical shift, and consequently the NMR spectrum obtained is a superposition of the resonances obtained from different crystallites [3], leading to a broad line powder pattern.

To remove this broadening an equivalent to the tumbling of molecules in liquids is required. This is achieved by a process known as magic angle sample spinning (MAS) [4,5]:

The chemical shift term for an *AX* system is given by:

$$\nu = \nu_A \pm \tfrac{1}{2}R(3\cos^2\theta - 1) \qquad \text{Eq. 7.1}$$

where ν_A is the Larmor frequency, R is the dipolar coupling constant, and θ is the orientation of the crystal with respect to the external magnetic field, and can take any value for a polycrystalline powder.

However, it can be shown that if the sample is rotated about an axis at an angle β to B_0 [Fig. 7.1], in the limit of sufficiently rapid rotation, the average value of $(3\cos^2\theta - 1)$ is given by:

$$\langle 3\cos^2\theta - 1 \rangle = \tfrac{1}{2}(3\cos^2\beta - 1)(3\cos^2\chi - 1) \qquad \text{Eq. 7.2}$$

where $\chi = \beta - \theta$. The angle β is under the control of the experimenter.

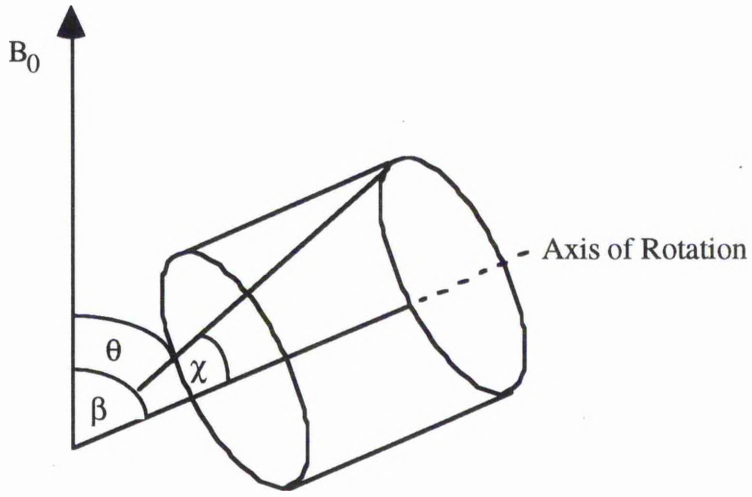

Fig. 7.1: Diagram of the geometric relationship for a sample rotating at an angle β to the magnetic field.

If $\beta = \cos^{-1}\left(1/\sqrt{3}\right) = 54°44'$, then $<3\cos^2\theta - 1> = 0$. Rotation of the sample (at frequency ν_r) about an axis inclined at this angle β with respect to the applied magnetic field, will transform an NMR line-broadened by CSA effects. For sufficiently rapid rotation, only a single line corresponding to the isotropic peak would be observed. The position (i.e. chemical shift) of the isotropic peak is independent of ν_r. In practice, it is not possible to attain these high spinning speeds, and consequently the line is split into a set of comparatively narrow equally spaced lines consisting of the isotropic peak and spinning sidebands. The spacing between adjacent lines is equal to the spinning frequency, ν_r.

ii) Heteronuclear Dipole-Dipole Interaction

For most organic solids with natural isotopic abundance, the only appreciable dipole-dipole interaction directly affecting the ^{13}C NMR spectrum is that between ^{13}C and ^{1}H [3]. Due to the fact that each nuclei is in a fixed environment within the solid, and that all orientations of molecules with respect to the external magnetic field are present, the

dipolar coupling is different for different molecular orientations resulting in broader lines in the spectrum. [As before, in solution rapid tumbling of the molecules in the sample ensures that the direct dipole-dipole interaction is averaged to zero]. The magnitude (Δ_{DD}) of this interaction (typically *ca.* 30 kHz for rigid organic solids) is usually significantly larger than the maximum experimentally attainable MAS frequencies, and, in general, substantial averaging of this interaction in order to give high-resolution spectra cannot be achieved using MAS. For this reason, high power ^1H decoupling is generally applied (in addition to MAS) during acquisition of the ^{13}C free induction decay in order to eliminate line-broadening due to the direct ^{13}C–^1H dipole-dipole interactions. [It should be noted that such high power ^1H decoupling will also eliminate splitting of ^{13}C spectral lines due to the indirect (electron-coupled) ^{13}C–^1H dipole-dipole interaction (which is rendered isotropic by MAS), and that the effects of direct ^{13}C–^{13}C dipole-dipole interactions in samples with natural abundance ^{13}C are generally insignificant].

There is an important distinction between the way in which the effects of CSA and direct dipole-dipole interactions are affected by MAS [4,6]. In the case of an NMR line-broadened by CSA, relatively slow MAS is generally sufficient to break up this line into the set of narrow, equally spaced lines discussed above (this arises even for $\nu_r << \Delta_{CSA}$, where Δ_{CSA} denotes the linewidth, due to CSA, for the static (i.e. $\nu_r = 0$) polycrystalline sample). For an NMR line-broadened by direct dipole-dipole interaction, on the other hand, significant line-narrowing will occur only when ν_r is in the region of (or greater than) the magnitude of the dipole-dipole interaction. As discussed by Maricq and Waugh [3], this difference arises from the fact that CSA gives rise to inhomogeneous broadening of the spectral line, whereas dipole-dipole interaction is a source of homogeneous broadening. It can be shown that the value of ν_r required to achieve effective line-narrowing is larger (relative to the linewidth of the static sample) in the case of homogeneous broadening. Furthermore, for a system in which there are sources of both homogeneous and inhomogeneous line-broadening, the resultant behaviour (with respect to the effect of MAS discussed above) is that of a homogeneously broadened system.

7.2 Solid State NMR of Metallocenes

In this chapter, we report high-resolution solid state ^{13}C NMR spectra of metallocenes [$(\eta_5\text{-}C_5H_5)M(\eta_5\text{-}C_5H_5)$; M = Fe, Ni, Ru] recorded as a function of magic angle sample spinning frequency. It is well known [7–9] that, at room temperature, there is substantial molecular motion in crystalline ferrocene. The existence of two solid phases of ferrocene, interconverted at 163.9 K, was demonstrated [10] *via* heat capacity measurements in the range 125–200 K. Reorientation of the cyclopentadienyl (C_5H_5) rings, which is thought [11–13] to involve a five-fold jump mechanism, occurs both in the low-temperature and high-temperature phases. A relationship between the correlation time for this motion and temperature has been established [11] for the high-temperature phase; the correlation time at 293 K is $\tau_c \approx 5 \times 10^{-12}$ s. The correlation time for ring reorientation in nickelocene at room temperature is essentially the same as that for ferrocene, whereas the correlation time for ring reorientation in ruthenocene is significantly longer ($\tau_c \approx 5 \times 10^{-10}$ s at 293 K) [11,12]. It has been suggested [8] that there may be some additional slower molecular motions in crystalline ferrocene at ambient temperature. All experiments reported in this study were carried out at (or close to) 293 K, and hence the correlation time for molecular motion for a given metallocene can be assumed to be constant for the set of results presented here.

In ^{13}C NMR spectroscopy of crystalline metallocenes, CSA and direct ^{13}C–^{1}H dipole-dipole interaction are important sources of line-broadening. Suwelack *et al* [14] have given a detailed theoretical and experimental consideration of the linewidth of the isotropic peak, recorded under MAS conditions, for a spin system that is broadened by CSA. One major result of their work was the demonstration that, by studying the variation of linewidth with temperature (and hence the variation of linewidth with correlation time), detailed information relating to slow molecular motions could be elucidated. It was also shown theoretically and experimentally (see Fig. 10 of ref. 14) that, at fixed temperature, the linewidth of the isotropic peak decreases as the MAS frequency (ν_r) is increased, approaching a limiting value at sufficiently large ν_r (see also relevant aspects of ref. 15).

In a second paper, Rothwell and Waugh [16] considered the linewidth of a spin system S, dipolar coupled to an unlike spin system I, under conditions of isotropic molecular motion and decoupling of the I spins. Again, it was shown that parameters relating to the molecular motion could be determined by studying the variation of linewidth as a function of temperature (and hence as a function of correlation time τ_c). Of more relevance to the work reported here, however, was the consideration of how the linewidth varies with decoupler field strength (denoted ω_1). It was shown (see Fig. 3 of ref. 16) that, in the limit of long correlation time (i.e. $\omega_1\tau_c >> 1$), the linewidth is proportional to ω_1^{-2}, whereas in the limit of short correlation time (i.e. $\omega_1\tau_c << 1$), the linewidth is independent of ω_1. Thus, for a sample at fixed temperature (and hence fixed τ_c), the linewidth would be expected either to decrease as the decoupler field strength is increased (in the long correlation limit of the sample of interest) or to be independent of the decoupler field strength (in the short correlation limit). The effects of anisotropic molecular motion on the measured spectrum were also discussed briefly in ref. 16, it being shown that the extent of the broadening effects observed are lessened due to only part of the total interaction between the decoupler field and the sample to be time dependent.

Here, we consider a situation in which both MAS frequency and decoupler field strength are important in controlling the linewidth of the isotropic peak. If the separate effects discussed above can be combined in a simple way, then it should be expected that: (a) at fixed temperature and fixed decoupler field strength, the linewidth should decrease with increasing MAS frequency (at least up to a limiting value, beyond which the linewidth should be effectively independent of the MAS frequency); and (b) at fixed temperature and fixed MAS frequency, the linewidth should either decrease or remain constant as the decoupler field strength is increased, depending on the relevant regime of the sample at the temperature of interest (i.e. whether it is in the long correlation limit or the short correlation limit, respectively).

We focus here on an investigation of how the linewidth of the isotropic peak of metallocenes varies with MAS frequency. It is shown that, for ferrocene and

ruthenocene at room temperature, the effects of MAS frequency and ^{1}H decoupler field strength on the ^{13}C NMR linewidth cannot be combined in this simple way, since the effective decoupler field strength is modulated by altering the MAS frequency. Nickelocene is paramagnetic, and for this reason it is not valid to consider nickelocene in the same way as ferrocene and ruthenocene in relation to the NMR properties discussed here.

7.3 Experimental

A polycrystalline sample of ferrocene was obtained by recrystallisation from hexane, and powder X-ray diffraction confirmed that it was a monophasic sample of the high-temperature phase. This sample of ferrocene, with natural isotopic abundances, is subsequently denoted ferrocene-h_{10} to distinguish it from the sample of perdeuterated ferrocene (ferrocene-d_{10}) discussed later. Samples of nickelocene and ruthenocene were used as received.

Finely ground samples of each metallocene were packed into zirconia rotors (4 mm external diameter) for use in the MAS NMR experiments. The same samples of metallocenes was used in all the NMR experiments reported here, and the zirconia rotors were not emptied and repacked at any stage during the series of experiments.

^{13}C NMR spectra were recorded at 125.758 MHz on a Bruker MSL500 spectrometer using a standard Bruker magic angle spinning probe (with double-bearing rotation mechanism). MAS frequencies of between *ca.* 1 kHz and 12 kHz could be attained using this probe, with stability typically better than *ca.* ± 10 Hz. All spectra were recorded at room temperature (293 ± 2 K).

Except where specifically indicated otherwise, the pulse sequence used to record the spectra involved a single ^{13}C 90° pulse, with high power ^{1}H decoupling applied during acquisition of the ^{13}C free induction decay. Typical experimental parameters were: ^{13}C 90° pulse length = 3.5 μs; recycle delay = 10 s. [Note that such spectra are normally recorded using the ^{13}C CPMAS method (which combines the cross polarisation (CP) and magic angle sample spinning (MAS) techniques together with high power ^{1}H

decoupling). Due to the short $T_1(^{13}C)$ for ferrocene at room temperature, and the extensive molecular motion in this system (which renders cross-polarisation comparatively inefficient), spectra recorded using the "single pulse" ^{13}C method on this sample had signal/noise ratios comparable to, or better than, those of spectra recorded using the ^{13}C CP-MAS method].

The ^1H decoupler field was set on resonance for the ^1H of ferrocene-h_{10}, and the decoupler field strength controlled *via* the Bruker software used. An accurate assessment of the decoupler field strength used in recording the ^{13}C spectrum was made by measuring (for adamantane) the length of the ^1H 90° pulse ($\tau_{90}(^1H)$), when using the same level of r.f. power applied to the ^1H channel as that used for the ^1H decoupling field in measuring the ^{13}C spectra. For the discussion of results, $\tau_{90}(^1H)$ has been converted to a decoupling frequency ν_1, with ν_1 obtained from:

$$\nu_1 = \frac{1}{4\,\tau_{90}(^1H)} \qquad \text{Eq. 7.3}$$

ν_1 is related to the decoupler field strength H_1 and to the parameter ω_1 (used in ref. 16) by the equations:

$$\nu_1 = \frac{\gamma(^1H)H_1}{2\,\pi} = \frac{\omega_1}{2\,\pi} \qquad \text{Eq. 7.4}$$

where γ is the magnetogyric ratio.

The linewidth of the isotropic peak in the ^{13}C NMR spectrum was measured as the full width at half maximum height; the experimental error in the measured linewidth is estimated to be less than *ca.* ± 5 Hz.

7.4 Results and Discussion

High resolution ^{13}C NMR spectra of ferrocene-h_{10} were recorded initially at two different settings (ν_1 = 64.9 kHz and 26.6 kHz) of the decoupler field strength, and at several MAS frequencies (ν_r) ranging from *ca.* 1 kHz to 11 kHz. The spectrum at $\nu_r \approx 5$

kHz was recorded at the start and again at the end of the series of experiments to confirm that no irreversible changes in the spectrum had occurred as a consequence of subjecting the sample to the high rotation rates. The variation of linewidth (Δ) of the isotropic peak as a function of ν_r is shown in Fig. 7.2. Clearly, at a given decoupler field strength, Δ increases as ν_r is increased, and this increase is approximately linear, particularly at the higher decoupler field strength. Furthermore, the gradient of this graph is greater for the lower decoupler field strength. At fixed ν_r, the linewidth Δ is, as expected, smaller at higher decoupler field strength, as shown in Fig. 7.2.

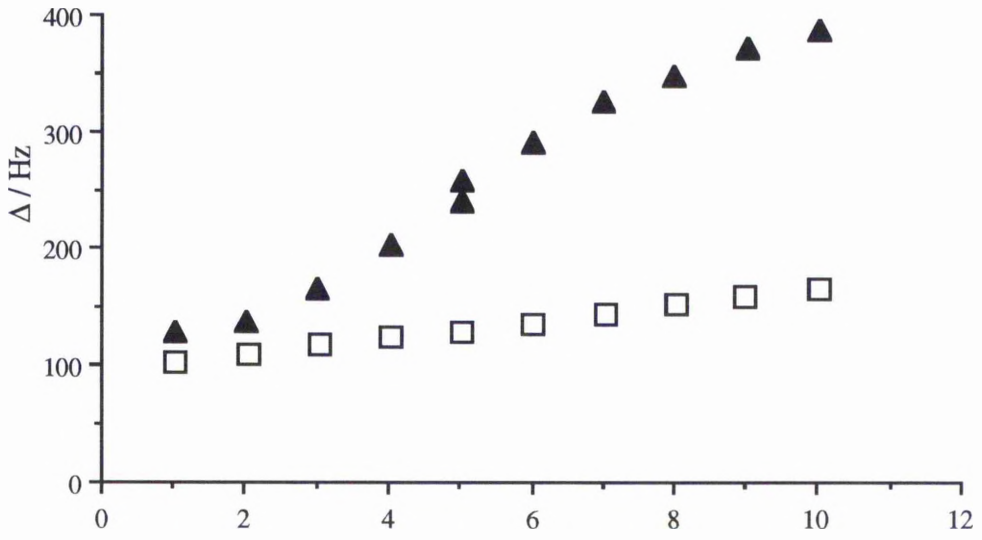

Fig. 7.2: Linewidth (Δ) of the isotropic peak in the ^{13}C NMR spectrum of ferrocene-h_{10} versus MAS frequency (ν_r). The spectra were recorded at ^{1}H decoupler field strengths corresponding to ν_1 = 64.9 kHz (❑) and ν_1 = 26.6 kHz (▲).

This observation that the linewidth of the isotropic peak for ferrocene-h_{10} at room temperature increases as the MAS frequency is increased contrasts markedly with the general comments in Section 7.2 that, under conventional conditions, Δ is expected to decrease, or remain constant, as ν_r is increased. It is proposed here that the observed increase in Δ with increasing ν_r for ferrocene-h_{10} is arising not because of a direct

influence of MAS on either the chemical shift anisotropy or the direct ^{13}C–^{1}H dipole-dipole interaction, but rather as a result of MAS indirectly modulating the efficiency of the ^{1}H decoupling (in such a way that the effective decoupler field strength is decreased, leading to line-broadening, as ν_r is increased). The following series of experiments confirms this hypothesis.

First, ^{13}C NMR spectra of ferrocene-h_{10} were recorded for a range of different decoupler field strengths (with ν_1 ranging from 20 kHz to 80 kHz) at fixed ν_r. The dependence of Δ on decoupler field strength from these experiments is shown in Fig. 7.3(a). As expected, Δ decreases as ν_1 is increased at fixed ν_r. Furthermore, in the limit of sufficiently high decoupler field strength (i.e. in the limit as $\nu_1 \rightarrow \infty$), it is clear that Δ becomes essentially independent of both ν_r and ν_1, with Δ converging to a limiting value (in the sense discussed by Alla and Lippmaa [15]) of *ca.* 100 Hz. It can be concluded from this fact that both values of ν_r (5.06 kHz and 9.05 kHz) used to record the data shown in Fig. 7.3(a) are sufficiently rapid to remove the ν_r-dependent sources of line-broadening due to CSA – i.e. at sufficiently high decoupler field strength, Δ is essentially independent of ν_r at these values of ν_r. Again, this is consistent with the opinion that, under the conditions of the experiments shown in Fig. 7.2, the property that is ν_r-dependent is the efficiency of the ^{1}H decoupling (and not the ability of MAS to remove the line-broadening effects due to CSA). The linear relationship between Δ and $(\nu_1)^{-2}$ evident from Fig. 7.3(b) (at least considering the data recorded at ν_r = 9.05 kHz) is consistent with the findings of ref. 16 for a system in the long correlation limit ($2\pi\nu_1\tau_c >> 1$). This point is considered further in Section 7.5.

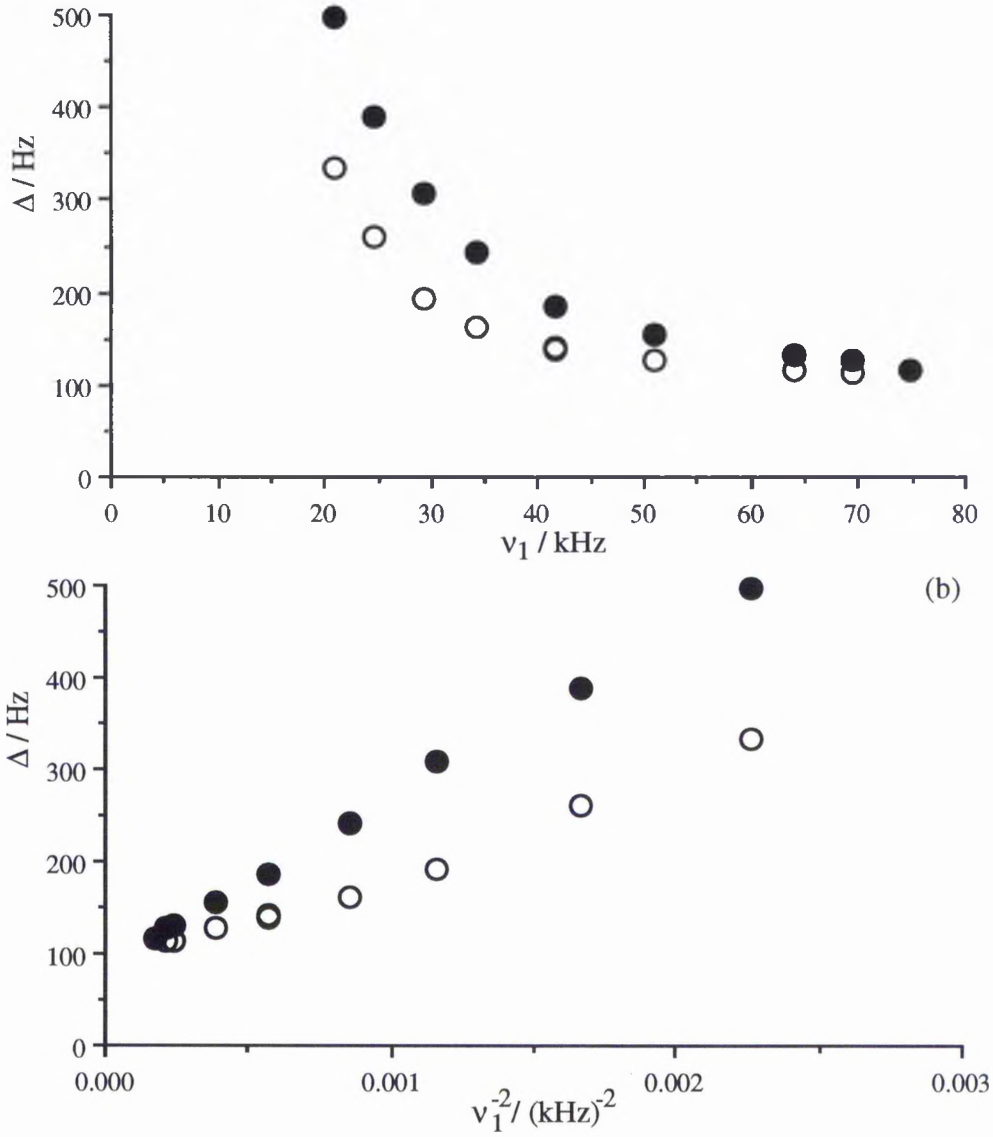

Fig. 7.3: Linewidth (Δ) of the isotropic peak in the ^{13}C NMR spectrum of ferrocene-h_{10} versus (a) ν_1 (as discussed in the text, ν_1 is a measure of the ^1H decoupler field strength), and (b) ν_1^{-2}. The spectra were recorded at MAS frequencies ν_r = 5.06 kHz (○) and ν_r = 9.05 kHz (●).

Second, ^{13}C NMR spectra of ferrocene-h_{10} were recorded as a function of ν_r, but with no decoupler field applied; the variation of Δ with ν_r in these experiments is shown in Fig. 7.4. Under these conditions, Δ decreases as ν_r is increased (as predicted from the discussion in Section 7.2 and from ref. 14), and reflects the direct effect of MAS on the

linewidth of the isotropic peak for a system that is subject to line-broadening by CSA and by direct ^{13}C–^{1}H dipole-dipole interaction. At the lowest value of ν_r studied (ν_r = 3 kHz), the value of Δ is *ca.* 592 Hz, and it is clear that slow MAS (in the absence of ^{1}H decoupling) is sufficient to substantially average the dipole-dipole interaction as well as CSA (see the comments in Section 7.1); this is as a consequence of the fact that the direct ^{13}C–^{1}H dipole-dipole interaction is already extensively averaged by molecular motion. The magnitude of the direct ^{13}C–^{1}H dipole-dipole interaction for ferrocene-h_{10} at room temperature has been estimated to be *ca.* 10 kHz, from measurement of the ^{13}C NMR spectrum recorded for the polycrystalline sample with no MAS and no ^{1}H decoupling; this is substantially smaller than typical values for conventional organic solids.

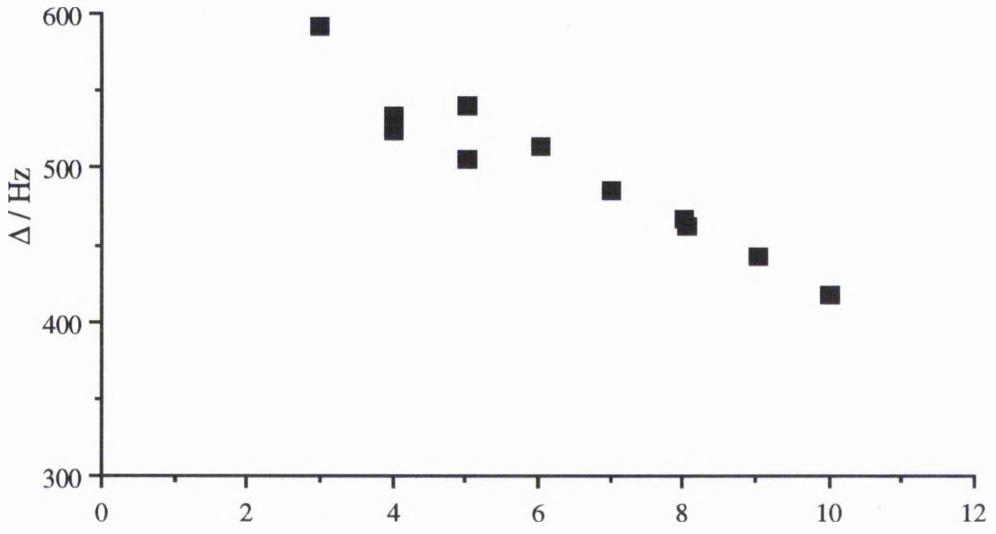

Fig. 7.4: Linewidth (Δ) of the isotropic peak in the ^{13}C NMR spectrum of ferrocene-h_{10} versus MAS frequency (ν_r), with no ^{1}H decoupling field applied.

Third, ^{13}C NMR spectra were recorded (using the "single pulse" ^{13}C method with no ^{1}H decoupler field applied) for ferrocene-d_{10} (^{2}H isotopic purity *ca.* 96.8 %) as a function of MAS frequency. Over the range $\nu_r \approx 1$ kHz – 12 kHz, the linewidth of the isotropic peak is independent of ν_r (see Fig. 7.5), and the value ($\Delta \approx 117$ Hz) is close to

the minimum (limiting) linewidth obtained in our experiments for ferrocene-h_{10}. [A similar value of this limiting linewidth has been reported in an independent investigation of ferrocene-d_{10} [17]]. In ^{13}C NMR spectroscopy of ferrocene-d_{10}, it can be assumed that the principal source of line-broadening is CSA and, furthermore, it can be assumed that the CSA should be substantially the same in ferrocene-d_{10} and ferrocene-h_{10}. The fact that Δ is essentially independent of ν_r for ferrocene-d_{10} therefore provides strong evidence to support the view that the variation of Δ with ν_r for ferrocene-h_{10} is not arising as a consequence of CSA being modulated by MAS. [Note that ^{13}C–^{2}H residual dipolar interaction [18] in ferrocene-d_{10} is assumed to be negligible given the high magnetic field strength used in our experiments and the rapid reorientation of the C_5D_5 rings at the temperature studied; the measured isotropic peak is clearly a single peak, rather than the 2:1 doublet that would arise if the ^{13}C–^{2}H residual dipolar interaction were appreciable].

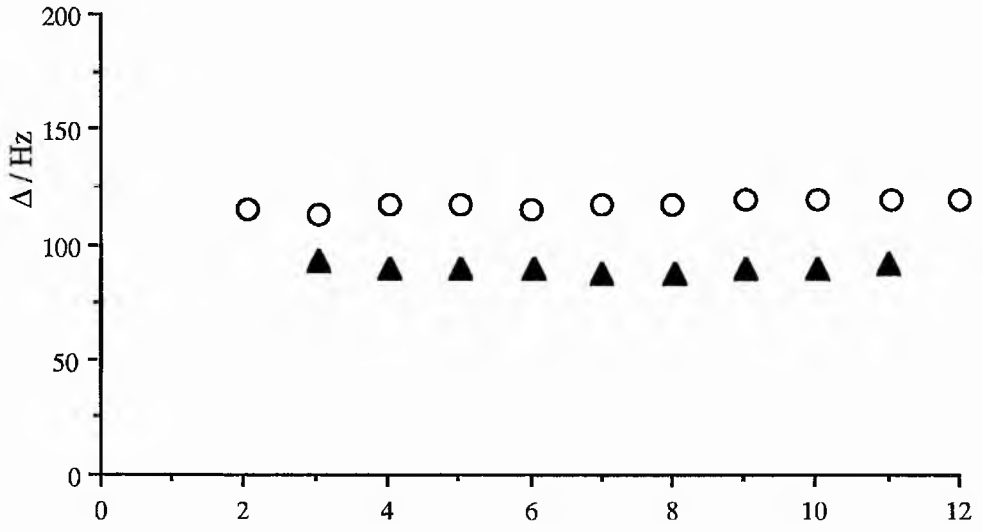

Fig. 7.5: Linewidth (Δ) versus MAS frequency (ν_r) for the isotropic peak in the ^{13}C NMR spectrum of ferrocene-d_{10} (○), and for the isotropic peak due to the CH_2 group of glycine (▲). Spectra for ferrocene-d_{10} were recorded with no ^{1}H decoupling field applied; the spectra for glycine were recorded with ^{1}H decoupler field strength $\nu_1 = 78.1$ kHz.

High-resolution ^{13}C NMR spectra of ruthenocene and nickelocene were also recorded as a function of MAS frequency in order to establish whether the behaviour observed for ferrocene is also exhibited by other structurally related systems. In Fig. 7.6, the relationships between Δ and ν_r for ruthenocene and ferrocene are compared, with all spectra recorded at the same ^1H decoupler field strength (ν_1 = 64.9 kHz).

It is clear that ruthenocene exhibits the same general trend as ferrocene, with Δ increasing as ν_r is increased, although the relationship for ruthenocene is apparently less linear than that for ferrocene. At the higher values of ν_r studied, the gradient $\partial\Delta/\partial\nu_r$ is larger for ruthenocene. These small differences in behaviour between ferrocene and ruthenocene presumably reflect small differences in the dynamic properties of these solids at 293 K (as suggested in ref. 12).

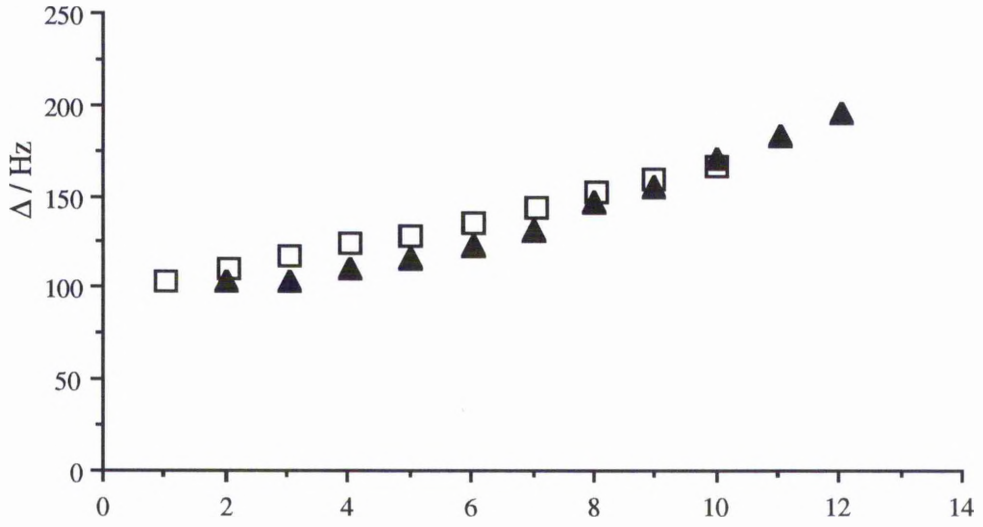

Fig. 7.6: Linewidth (Δ) versus MAS frequency (ν_r) for the isotropic peak in the ^{13}C NMR spectra of ferrocene (❑) and ruthenocene (▲), at fixed ^1H decoupler field strength corresponding to ν_1 = 64.9 kHz.

The linewidth in the ^{13}C NMR spectrum of nickelocene is substantially greater (Δ = 15.7 kHz at ν_r = 5 kHz) than that in spectra recorded for ferrocene and ruthenocene

under the same conditions. The linewidth for nickelocene was not significantly affected by increasing the MAS frequency, although there was a measurable decrease to $\Delta = 15.4$ kHz at $\nu_r = 11$ kHz. The very large ^{13}C NMR linewidth observed for nickelocene, even under conditions of MAS and high power ^{1}H decoupling, is due to the paramagnetic properties of this molecule (which contains two unpaired electrons). For this reason, it is not expected that the NMR properties of nickelocene will be comparable, in any way, to those of ferrocene and ruthenocene.

7.5 Conclusion

The increase in linewidth of the isotropic peak in the ^{13}C NMR spectra of ferrocene and ruthenocene as the MAS frequency is increased (at fixed temperature and fixed ^{1}H decoupler field strength) is due to an indirect effect in which the effective ^{1}H decoupler field strength is decreased as ν_r is increased. Considering the results of high-resolution ^{13}C NMR experiments for several crystalline organic solids carried out in our laboratory, it is clear that, for systems in which there is no appreciable molecular motion, Δ is essentially independent of ν_r. This result is illustrated in Fig. 7.5 for glycine (NH_2CH_2COOH).

As discussed in Section 7.2, it is well established that there is appreciable molecular motion in crystalline ferrocene at room temperature, and we propose that the reorientational motion of the ^{13}C–^{1}H vector is important in giving rise to the observed relationship between Δ and ν_r. Although the correlation time was constant (at fixed temperature) for the series of experiments reported here, the actual value of this correlation time is an important parameter, since it presumably sets the system into a regime in which the anomalous dependence of Δ on ν_r is observed. In view of the fact (see Section 7.2) that reorientation of the cyclopentadienyl rings in crystalline ferrocene at room temperature is occurring on a timescale of the order of 10^{-12} s – 10^{-11} s (and 10^{-10} s – 10^{-9} s for ruthenocene), it is not clear whether this dynamic process is responsible for influencing the value of Δ in our experiments; it might be expected that a motion occurring at a frequency comparable to ν_1 and/or ν_r (and thus in the approximate

frequency range 10^3 Hz – 10^6 Hz) would be required. Furthermore, the results of Fig. 7.3 suggest that, at fixed ν_r, the effect of decoupler field strength on the linewidth is being influenced by molecular motion in the long correlation limit; i.e. $\tau_c >> (2\pi\nu_1)^{-1} \approx 10^{-6}$ s [16].

A similar anomalous relationship between isotropic ^{13}C linewidth and temperature has been observed recently by Muller [19] in studies of thiourea inclusion compounds; in this case, linewidths for ^{13}C environments in the guest molecules (which undergo substantial molecular motion) have been observed to increase with increasing temperature, and again this effect has been attributed to an "interference" between the molecular motion and the efficiency of the ^1H decoupling. Here, we make no attempt to assign the dynamic process that is important in giving rise to the observed NMR phenomena for ferrocene-h_{10} and ruthenocene at room temperature. In ref. 8, from a discontinuity in the plot of correlation time against $\frac{1}{T}$ at the transition between the high and low temperature phases in ferrocene, it was concluded that the system could no longer be described by a single correlation time, and it may be that the slower motions in ferrocene alluded to here are influential in this regard.

In response to our study reported here [20,21], two subsequent publications have recently confirmed that the effect observed (of increasing linewidth with increasing ν_r) may indeed be attributed to a modulation of the heteronuclear decoupling field by rapid sample spinning [22,23]. In the first paper, Tekely *et al* [22] concluded, from experiments on adamantane, that a slowing down of flip-flop spin motion of protons with increasing ν_r was responsible for this modulation, while Nakai *et al* [23] demonstrated that for weak ^1H decoupling fields the linewidth passes through distinct local maxima where $\nu_1 = n\nu_r$ (n = 1,2), and attribute the effect to rotary-resonance ^{13}C–^1H recoupling (i.e. when the periods $\frac{1}{\nu_1}$ and $\frac{1}{\nu_r}$ match, a period is imposed upon the ^{13}C–^1H dipolar interactions which nullifies the decoupling field). The decoupling fields employed in Nakai's study (ν_1 = 6 to 18 kHz) are very weak compared to those utilised in our experiments (ν_1 = 26.6 kHz and ν_1 = 64.9 kHz). For the decoupling fields used in our study, the spinning speeds required for maxima in the linewidth to be observed are

beyond the maximum attainable limits of the spectrometer. However, the increase in the linewidth for ferrocene is in marked contrast to the constant linewidth observed for the CH_2 peak in the spectrum of glycine, from which it is clear that rotary-resonance ^{13}C–^{1}H recoupling alone cannot account for the changes occurring.

The results reported here have important implications in regard to recording high-resolution solid state ^{13}C NMR spectra [24,25] for systems that are subject to line-broadening by CSA and direct ^{13}C–^{1}H dipole-dipole interactions. It is clear that there are circumstances (as for ferrocene-h_{10} at room temperature), under which optimum resolution can be obtained by recording the spectrum at high decoupler field strength and low MAS frequency, rather than at high decoupler field strength and high MAS frequency (as might be assumed for conventional systems).

References

[1] R.K. Harris, *Chem. Brit.*, (1993) 601.

[2] R.K. Harris: *Nuclear Magnetic Resonance Spectroscopy*, Pitman, London, 1983, p.143.

[3] A.E. Derome and S. Bowden, *Chem. Rev.*, **91** (1991) 1307.

[4] E.R. Andrew, *Int. Rev. Phys. Chem.*, **1** (1981) 195.

[5] E.R. Andrew, *Phil. Trans. Roy. Soc. (Lond.) A*, **299** (1981) 505.

[6] M.M. Maricq and J.S. Waugh, *J. Chem. Phys.*, **70** (1979) 3300.

[7] D. Braga, *Chem. Rev.*, **92** (1992) 633.

[8] C.H. Holm and J.A. Ibers, *J. Chem. Phys.*, **30** (1959) 885.

[9] B.T.M. Willis, *Acta Cryst.*, **13** (1960) 1088.

[10] J.W. Edwards, G.L. Kington and R. Mason, *Trans. Faraday Soc.*, **56** (1960) 660.

[11] A.B. Gardner, J. Howard, T.C. Waddington, R.M. Richardson and J. Tomkinson, *Chem. Phys.*, **57** (1981) 453.

[12] A.J. Campbell, C.A. Fyfe, D. Harold-Smith and K.R. Jeffrey, *Mol. Cryst. Liq. Cryst.*, **36** (1976) 1.

[13] A. Kubo, R. Ikeda and D. Nakamura, *J. Chem. Soc. Faraday Trans. 2,* **82** (1986) 1543.

[14] D. Suwelack, W.P. Rothwell and J.S. Waugh, *J. Chem. Phys.,* **73** (1980) 2559.

[15] M. Alla and E. Lippmaa, *Chem. Phys. Lett.,* **87** (1982) 30.

[16] W.P. Rothwell and J.S. Waugh, *J. Chem. Phys.,* **74** (1981) 2721.

[17] S.J. Heyes, N.J. Clayden and C.M. Dobson, *J. Phys. Chem.*, **95** (1991) 1547.

[18] S.D. Swanson, S. Ganapathy and R.G. Bryant, *J. Mag. Res.*, **73** (1987) 239.

[19] K. Muller, *J. Phys. Chem.*, **96** (1992) 5733.

[20] I.J. Shannon, K.D.M. Harris and S. Arumugam, *Chem. Phys. Lett.,* **196** (1992) 588.

[21] I.J. Shannon, K.D.M. Harris and S. Arumugam, *Bull. Magn. Res.,* **14** (1992) 273.

[22] P. Tekely, P. Palmas and D. Canet, *J. Magn. Reson. A*, **107** (1994) 129.

[23] T. Nakai and C.A. McDowell, *Chem. Phys. Lett.*, **227** (1994) 639.

[24] A.N. Garroway, D.L. VanderHart and W.L. Earl, *Phil. Trans. Roy. Soc. (Lond.) A*, **299** (1981) 609.

[25] W.L. Earl, D.L. Van der Hart and A.N. Garroway, *J. Mag. Res.* **44** (1981) 361.

Appendix 1

Scientific Publications

As a result of the research described in the preceeding chapters, the following papers have been published:

1) I.J.Shannon, K.D.M. Harris, S. Arumugam, *Chem. Phys. Letts.*, **196** (1992) 588.
"High-resolution Solid State ^{13}C NMR Studies of Ferrocene as a Function of Magic Angle Sample Spinning Frequency".

2) I.J.Shannon, K.D.M. Harris, S. Arumugam, *Bull. Magn. Res.*, **14** (1992) 273.
"Variation of ^{13}C NMR Linewidths of Metallocenes as a Function of Magic Angle Sample Spinning Frequency".

3) I.J.Shannon, K.D.M. Harris, A.J.O. Rennie, M.B. Webster, *J. Chem. Soc. Faraday Trans.*, **89** (1993) 2023.
"Theoretical Prediction of the Guest Periodicity of Alkane/Urea Inclusion Compounds".

4) I.J. Shannon, K.D.M. Harris, A. Mahdyarfar, P. Johnston, R.W. Joyner, *J. Chem. Soc. Faraday Trans.*, **89** (1993) 3099.
"EXAFS Spectroscopic Studies of the Bromine Environment in the Crystalline Inclusion Compounds formed between Urea and α,ω-dibromoalkanes".

5) P.A. Schofield, I.J.Shannon, K.D.M. Harris, A.J.O. Rennie, *J. Chem. Soc. Chem. Comm.*, (1993) 1293.

"Structural Properties of the Chlorocyclohexane/Thiourea Inclusion Compound: Theoretical Predictions".

6) I.J. Shannon, N.M. Stainton, K.D.M. Harris, *J. Mater. Chem.*, **3** (1993) 1085.

"Structural Properties of Urea Inclusion Compounds Containing Carboxylic Acid Anhydride Guest Molecules: Anomalous Modes of Guest Molecule Ordering".